In vitro and Physiologically Based Pharmacokinetic models for pharmaceutical cocrystals

Irena Tomaszewska

Tomaszewska, Irena

Award date:
2013

Awarding institution:
University of Bath

In vitro and Physiologically Based Pharmacokinetic models for pharmaceutical cocrystals

Irena Tomaszewska

Thesis submitted for the degree of Doctor of Philosophy

University of Bath

Department of Pharmacy and Pharmacology

June 2013

COPYRIGHT

Acknowledgements

I would like to take this opportunity to thank a number of people who helped me in various ways during my Ph.D. study.

First and foremost, I express my deepest gratitude to my supervisor Dr Nikoletta Fotaki for making this study possible and providing invaluable support during the last four years. Thank you for fruitful discussions and great optimism.

Many thanks to my second supervisor Professor Robert Price for his support and involvement throughout the Ph.D. course.

Professor Abdul Basit and Professor Michael Threadgill are warmly thanked for their constructive criticism of this thesis.

The doctoral research was made possible by financial support from the University of Bath that sponsored my studentship. I want to thank the entire staff at the Pharmacy and Pharmacology department for making it a pleasant workplace.

I thank Dr Karen Edler for allowing the use of the surface tension meter in her lab. Dr Hanne Kinnunen for her kind help with particle size analysis and Christopher Vernall for training on the differential scanning calorimeter.

Prosonix Ltd for providing cocrystals which were the subject of investigation during this Ph.D. program and Lipoid GmbH for kindly donating egg – lecithin.

Simcyp Ltd for providing license for Simcyp® software.

I particularly thank office mates Dr Natalie Belsey, Dr Liz O'Donovan, Dr Ann Thitilertdecha, Dr Quan Yang, Dr Luis Nogueiras Nieto, Wing Sin Chiu, Jin Zhang, Chiau Ming Long and Luis Rodrigo Contreras Rojas for their friendship and creating a cheerful and friendly working environment.

I am very grateful to Dr Natalie Belsey for her attention to detail during proof – reading of my thesis.

I would like to particularly thank Chiau Ming Long, who joined the department a few months after me. My Ph.D. experience would not have been as rewarding, enriching and fun without him. Your friendship is priceless.

I would like to thank my friend Magda Nasieniak for being a great listener and guide. Thank you for your motivation and time spent on watching movies, burning and gaining calories and every minute spent on the phone.

I wish to thank my family and family in-law for encouragement during the last years.

I was born prematurely during six and a half months of pregnancy, having no chances to survive doctors said to my parents that even if I survive I will never function properly. Here I am, many years after completing a Ph.D. not in my native language. I would like to thank my parents for their courage of my upbringing and never doubting in me.

The completion of my thesis would not have been possible without the unconditional love of my husband Marcin Tomaszewski. I am graceful to him for his understanding, patience and sacrifice, which will always inspire me.

Publications (peer – reviewed journals)

Tomaszewska, I., Karki, S., Shur, J., Price, R. and Fotaki, N., 2013. Accepted. Pharmaceutical characterisation and evaluation of cocrystals: Importance of in vitro dissolution conditions and type of coformer. *International Journal of Pharmaceutics.*

Conference contributions

Poster presentations

Tomaszewska, I. and Fotaki, N., 2012. Development of a PBPK model for a poorly soluble drug: importance of in vitro solubility and dissolution data. *In*: *UK-PharmSci Meeting, 2012*, 2012-09-12 - 2012-09-14, Nottingham.

Tomaszewska, I., Price, R. and Fotaki, N., 2012. Investigation of the mechanism of dissolution from pharmaceutical cocrystals and implications for oral administration. *AAPS Annual Meeting and Exposition, 2012, Chicago.*

Tomaszewska, I., Price, R. and Fotaki, N., 2011. Pharmaceutical cocrystals: effect of media and coformer on dissolution. *AAPS Journal*, 13 (S2).

Tomaszewska, I., Price, R. and Fotaki, N., 2011. Dissolution method development for pharmaceutical cocrystals. *In*: *PharmSci APSGB Meeting*, Nottingham.

Oral presentations

Development of a PBPK model for a poorly soluble drug: importance of in vitro solubility and dissolution data, *In*: *UK-PharmSci Meeting, 2012*, 2012-09-12, Nottingham.

Table of Contents

List of figures

List of tables

Abbreviations

2D	Two - dimensional
ACAT	Advanced Compartmental Absorption and Transit
ADME	Absorption, Distribution, Metabolism and Excretion
ADAM	Advanced drug absorption and metabolism
AIC	Akaike Information Criterion
ANOVA	Analysis of Variance
API	Active pharmaceutical ingredient
AUC	Area under the curve
β	Shape parameter
β	Buffer capacity
BCS	Biopharmaceutics classification system
BDM	Biorelevant dissolution media
CAT	Compartmental Absorption and Transit
CBZ	Carbamazepine
CCF	Cocrystal former
c_i	Molar concentration of the ion
C_{max}	Maximum plasma concentration
CMC	Critical micelle concentration
C_s	Saturation solubility
CSD	Cambridge Structural Database
C(t)	Input response
CV	Coefficient of variation
δ	Unit impulse
D	Diffusion coefficient constant
D_{10}	Distribution width 10% of particles have size less than
D_{50}	Distribution width 50% of particles have size less than
D_{90}	Distribution width 90% of particles have size less than
DAD	Diode array detector
DH	Dihydrate
DLM	Diffusion layer model
DMSO	Dimethyl sulfoxide
DSC	Differential scanning calorimetry
ER	Extended-release
EUC	European Patent Convention
f_1	Difference factor
f_2	Similarity factor
$F_a(T)$ ***or FD***	Fraction of the dose absorbed
FaSSCoF	Fasted State Simulated State Colonic Fluid

FaSSGF	Fasted State Simulated Gastric Fluid
FaSSIF	Fasted State Simulated Intestinal Fluid
FDA	Food and Drug Administration
GE	Gastric Emptying
GI	Gastointestinal
GIT	Gastointestinal tract
GRAS	Generally recognized as safe
h	Diffusion layer thickness
HCF	Human colonic fluid
HIF	Human intestinal fluid
HPLC	High Performance Liquid Chromatography
I	Ionic strength
IDR	Intrinsic dissolution rate
IND	Indomethacin
In vitro	*Latin*. in glass
In vivo	*Latin*. within the living
IP	Intellectual property
IR	Immediate-release
IVIVC	*In vitro-in vivo* correlation
J_{AB}	Flux of compound across the cell membrane
k_0	Zero- order release/dissolution constant
k_1	First-order release/dissolution constant
k_a	Absorption rate constant
K_a	Dissociation constant
k_e	Elimination rate constant
α	Time scale parameter
LAG	Liquid assisted grinding
LOD	Limit of detection
LOQ	Limit of quantification
MCC	Microcrystalline cellulose
MDCK	Madin-Darby Canine Kidney
MDT	Mean dissolution time
MGM	Modified gastric media
MIM-I	Modified media I (Na-SIF+0.2% SLS)
MIM-II	Modified media II (blank FaSSIF+0.1% SLS)
MMC	Migrating motor complex
MR	Modified-release
MRT	Mean residence time
MSD	Merck Sharp & Dohme Limited

n	Number of replicates
n	Number of the dissolution time points
N/A	Not applicable
NDA	New drug Application
NIC	Nicotinamide
NSAID	Nonsteroidal anti-inflammatory drug
PAMPA	Parallel artificial membrane permeability assay
PBPK	Physiologically Based Pharmacokinetic
PE	Predictability error
P_{eff}	Human effective permeability
pK_a	Dissociation constant
PK	Pharmacokinetic
PR	Prolonged-release
prec.	Precipitated
PSD	Particle size distribution
PVT	Performance Verification Test
PXRD	Powder X-ray diffraction
r	Time varying particle radius
R	Segment radius
R^2	Goodness of fit
QC	Quality control
Re	Reynolds number
R_i	The percentage dissolved of the reference profile at the *i* time
RH	Relative humidity
RSD	Relative Standard Deviation
S	Surface area
SAC	Saccharin
SCoF	Simulated Colonic Fluid
SD	Standard Deviation
SEM	Scanning Electron Microscopy
sd	Spray-drying
SGC	Soft Gelatin Capsule
SGF	Simulated Gastric Fluid
SIF	Simulated Intestinal Fluid
sim	Simulated using
SLS	Sodium lauryl sulphate
SMPD	Sulfamethoxypyridazine
S/N	Serial number
sp	Sample powder

ss	Sonic-slurry
ST	Surface tension
SUPAC	Scale-up post approval changes
TFA	Trifluoroacetic acid
T_i	The percentage dissolved of the test profile at the *i* time
TRIS	Tris(hydroxymethyl)aminomethane
T_{max}	Time to reach maximum plasma concentration
TMP	Thrimethroprim
UK	United Kingdom
UMAX	Ultrasound mediated amorphous to crystalline transition
US	United States
USP	United States Pharmacopoeia
USP apparatus 1	Basket dissolution apparatus
USP apparatus 2	Paddle dissolution apparatus
USP apparatus 3	Reciprocating cylinder apparatus
USP apparatus 4	Flow-through cell apparatus
USP apparatus 5	Paddle over disk apparatus
USP apparatus 6	Cylinder apparatus
USP apparatus 7	Reciprocating holder apparatus
V	Volume
vs.	Versus
WF	Wang Flanagan
W_t	Amount of the drug dissolved in time *t*
W_{max}	Maximal amount of drug dissolved
X_d	Amount of drug dissolved
z_i	Charge number of ion

Table of Units

°C	Degrees Celsius
ΔpH	change of pH
cm	Centimetre
cm^3	Centimetre cube
g	Grams
h	Hour
kg	Kilograms
L	Litres
mg	Milligrams
min	Minutes
mL	Millilitres
mm	Millimetre
mM (mmoL)	Millimole
mN/m	MilliNewton/metre
mOsmo	milliOsmoles
N	Normality
rpm	Rotation per minute
µg	Microgram
µm	Micrometre
µM	Micromolar
%	Percent
w/v	weight by volume

Abstract

About 30% of commercial and developmental drugs exhibit poor solubility and thus poor bioavailability. Strategies that enhance solubility of such compounds have become more popular. Cocrystallisation is one of these strategies, so characterisation of *in vitro* performance of cocrystals is essential. Conventional dissolution systems (USP apparatus 1 and USP apparatus 2) are often not suitable for testing poorly soluble drugs due to failure in providing sink conditions and inability to change the media during the experiment. This project involves designing appropriate dissolution methods that will help understand the mechanism of dissolution of cocrystals. Successful dissolution methods were used to test marketed formulations of Carbamazepine (CBZ) (IR and PR Tegretol® tablets) and Indomethacin (IND) (IR Indocid® capsules). Flow-through cell (USP 4) apparatus proved to be more suitable to test poorly soluble formulations than basket (USP 1) apparatus. Formulations and their cocrystals were tested in four combinations of media: compendial (SGF/SIF), modified I (MGM/MIM-I), modified (MGM/MIM-II) and biorelevant media (FaSSGF/FaSSIF-V2). USP apparatus 4 allowed capturing and quantifying the precipitation of IND samples upon the media change. All Indomethacin formulations exhibited precipitation; however, this occurred into the smaller extent in biorelevant media. The greatest enhancement in CBZ dissolution was observed for Saccharin cocrystals of CBZ. On the other hand, Nicotinamide cocrystal of IND improved dissolution of IND greater than Saccharin cocrystal. Dissolution profiles with physicochemical and pharmacokinetic parameters were used to develop a Physiologically Based Pharmacokinetic (PBPK) model using *in silico* program Simcyp®. Successful models were then used to predict *in vivo* performance of cocrystals. Successful PBPK models were developed for IR and PR formulations of Tegretol® tablets and IR Indocid® capsules using dissolution data tested in biorelevant media using dissolution USP apparatus 4. It was found that *in vivo* absorption of CBZ from cocrystals did not increase dramatically. An overall 2 % increment was observed when compared against the CBZ_{sp} sample. However, the rate of absorption for CBZ-SAC_{ss} samples was significantly faster than the rate of CBZ_{sp} absorption. API and cocrystals of IND completely absorbed within 3 hours and IND-NIC_{ss} cocrystal were found to absorb slightly faster than the other cocrystals. Absorption was 8% higher at 1 h in comparison to IND. However, overall the improvement was not statistically significant. In summary, this research demonstrates that selection of appropriate medium and apparatus is essential to build a successful PBPK model.

1 Cocrystals

1.1 Introduction

Pharmaceutical sector encounters many challenges in discovering and developing new active substances. The challenging aspects in development of a new active pharmaceutical ingredient (API) are often associated with selection of an active form, manufacture or storage. Some solids are unstable due to different polymorphic states; some APIs are poorly soluble and therefore poorly bioavailable. According to the Biopharmaceutics classification system (BCS), drugs that exhibit poor solubility and high permeability belong to BCS class II (1), which is currently estimated to account for about 30% of both commercial and developmental drugs (2, 3). Increasing solubility can significantly enhance the oral absorption of class II drugs and consequently result in increased number of more bioavailable medications on the market. The traditional approaches (*i.e*. micronisation, salt formation, and polymorphism) that are used to improve solubility often fail to produce adequate enhancement of bioavailability (4). For instance, the dissolution enhancement reported for different polymorphs of Carbamazepine (CBZ) was not observed *in vivo* due to solution - mediated transformation from a more soluble anhydrous form to a less soluble but more stable dihydrate form of CBZ (5). Over the last decade, cocrystals have emerged as a promising approach to modify physicochemical properties, resulting in improvement of stability, solubility and dissolution and possibly, providing better bioavailability. Moreover, pharmaceutical cocrystals might offer advantages over the API that may help overcome a range of limitations (*i.e*. stability) encountered with traditional approaches (6). Cocrystals are solid-chemistry materials of which physicochemical properties have been extensively studied. The prototype cocrystal, Quinhydrone, was studied by Friedrich and Wöhler in 1844 (7). However, cocrystals' biopharmaceutical properties are under – studied.

The next sections will define cocrystal-related terminology and provide detailed descriptions of their potential applications, chemistry and advantages. As Carbamazepine and Indomethacin (IND) cocrystals were studied in this project, designated sections will be devoted to the review of these specific drugs and their cocrystals.

1.2 Definition

To discuss cocrystals, it is crucial to understand what they are. They have also been referred to as *co-crystal* (8), *molecular complex* (8, 9) or *multi-component molecular crystals* (10). The definition of the cocrystal concept was the subject of debate in journal articles and presentations at conferences (8, 9, 11-15). The arguments varied from the use of hyphenation (*i.e.*, cocrystal *versus* co-crystal) to the nature of components and interactions between them. The first issue was resolved using *The Columbia Guide to Standard American English*, which states that *co-* prefix should be attached to the base word without a space or hyphen (16). The second part of the discussion was more chemistry related and evolved gradually. Initially, Dunitz defined cocrystal as a multi-component complex of two or more molecular species (8). Then Aakeröy and Salmon expanded the term by highlighting that cocrystal should be composed of components that are solids at ambient temperature when in their pure form (17). The latest part of the debate focused on the characterisation of interactions between components. The definition suggested by Almarsson and Zaworotko indicated that at least two components of cocrystal should interact by hydrogen bonding as well as possibly by other noncovalent and non-ionic interactions (12). Three years afterwards, Lara-Ochoa and Espinosa-Pérez emphasised the importance of these interactions in lattice stabilisation (18). They have reported that two cocrystal components can be bonded using π-π aromatic interactions and van der Waals forces, π – π stacking interactions and halogen binding (18). In other words, cocrystals are crystalline solids generated from API and cocrystal formers (CCF) (19, 20). Cocrystal former has been reported often as *coformer* (21), *ligand* (22, 23, 24) *or guest* (25, 26). Many organic compounds have been screened for the best coformer characteristics including acetone, dimethyl sulfoxide (DMSO) or acetic acid. When a cocrystal is intended for a pharmaceutical application, the scale of potential coformer is limited due to toxicity issues. Therefore, compounds that are non-toxic and generally recognized as safe are strongly recommended by Food and Drug Administration (27). However, not all GRAS compounds can be used in pharmaceutical dosage forms. Some GRAS compounds are only approved to be used as flavourings at part per million levels, which would not be sufficient to engineer the cocrystal. Nicotinamide, Saccharin and Acetic acid are so far the most successful GRAS compounds used as coformers in cocrystals (28).

1.3 Chemistry of cocrystals

Hydrogen bonds seem to play an important role in cocrystal formation (29). Etter and co-workers emphasised the importance of the hydrogen bond donors and acceptors of two components that may form a cocrystal and have published guidelines to aid design of cocrystals (30). According to these instructions, all proton donors and acceptors participate in hydrogen bonding. Also, six-membered ring intramolecular hydrogen bonds are formed in preference to intermolecular hydrogen bonds (31, 32).

The term *supramolecular synthon* was introduced and defined by Desiraju (29) as "structural units within supermolecules which can be formed and/or assembled by known conceivable synthetic operations involving intermolecular interaction". There are two types of synthons possible depending on types of functional groups that form this synthon: homosynthons are formed from carboxylic acids and amides, while heterosynthons contain pyridine – carboxylic acid functional groups (Figure 1).

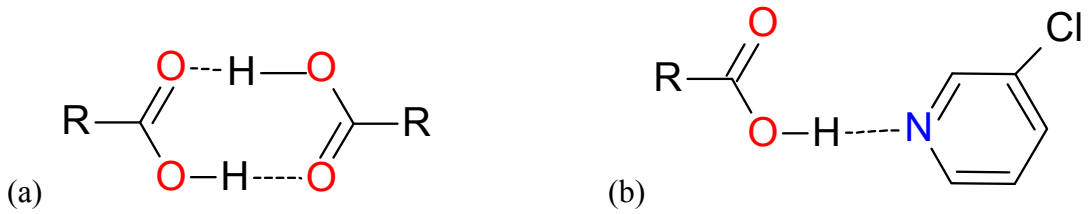

Figure 1. Homosython (a) and heterosynthon (b) motifs observed in cocrystal structures. Redrawn from (12).

Typical examples of such supramolecular synthons include amide-amide dimers, carboxylic acid- carboxylic acid dimers and carboxylic acid-amide dimers (Figure 2). The heterosynthons are preferred for cocrystal formation probably due to enthalpic advantages. The energy gain in heterosynthons is greater than in homosynthons. Analysis of the Cambridge Structural Database (CSD) revealed that 97% of cocrystals would be formed between carboxylic acid – aromatic nitrogen heterosynthons, in contrast to 3% of cocrystals formed between carboxylic acid – carboxylic acid homosynthons (33). This indicates that heterosynthons dominate cocrystal formation (12, 15, 33, 34).

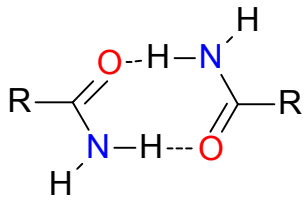

(a) amide – amide homosynthon

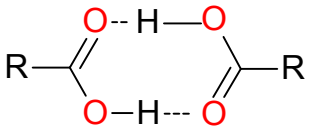

(b) acid – acid homosynthon

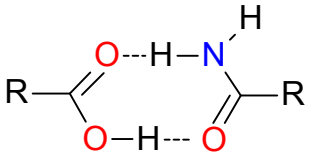

(c) acid – amide heterosynthon

Figure 2. Schematic illustrations of supramolecular hydrogen – bonded synthons occuring in cocrystals. Hydrogen bonds are shown as dotted lines. Redrawn from (12).

1.4 Hydrates, solvates and salts *versus* cocrystals

It is important to define what distinguishes cocrystals from other solubility enhancement strategies such as solvates, hydrates and salts. Hydrates and solvates are also multi-component crystals; however, in the case of hydrates, one component is water, while, in solvates, one component is an organic compound used as a solvent (11). Salt formation is a widely implemented and convenient method used for improving solubility of poorly soluble compounds. However, only ionic APIs can be used for salt formation. On the other hand, cocrystals can be formed with neutral or ionic forms of an API (35). Nonetheless, not all APIs and coformers can create cocrystals. Therefore, it is important to understand the rules which govern salt and cocrystal formation. Salt formation is an acid – base reaction, involving the transfer of protons (little or no proton transfer occurs during cocrystal formation) (Figure 3). Thus, the dissociation constants (14) of the acid and base are important parameters that define whether or not salt formation occurs (14).

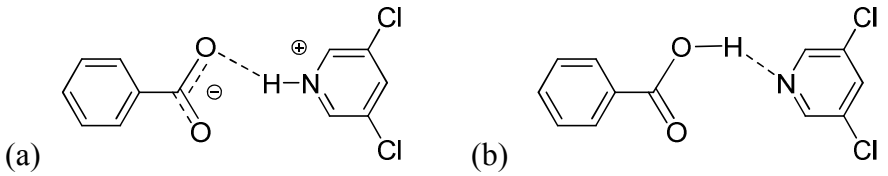

Figure 3. Illustrations of a) Salt and b) Cocrystal between N – heterocycle and carboxylic acid. Redrawn from (11).

The difference in pKa between the acid and base must be greater than 2 or 3 pKa units to form a salt that is stable in water (14). Moreover, Bhogala *et al*. noted that ΔpK_a less than 0 will always result in cocrystal formation (36). Although, when ΔpK_a range varies from 0 to 2, no prediction is achievable. These types of products can be either salts or cocrystals or cannot be assigned to either group. However, it has been reported by Aakeröy *et al.* that the exact location of protons may be subjected to temperature conditions (11).

1.5 Applications

It is worth noting that cocrystals have been the subject of research for the past 165 years (7). However, the debate about pharmaceutical cocrystals started in 2003 (8). Cocrystals have been used in a wide variety of industries, including chemical processing, photographic film formulation, propellant, electronic (37), paper and textile (38). Table 1 lists some examples of pharmaceutical cocrystals reported in the literature.

Table 1. Examples of pharmaceutical cocrystals.

Cocrystal	**References**
4,4'-Bipyridine – Pimelic acid (1:1)	(39)
AMG517 – Sorbic acid	(40)
Benzoic acid – isonicotinamide (2:1)	(41)
Caffeine – Oxalic acid (2:1)	(42)
Caffeine – Maleic acid (2:1)	(43)
Caffeine – Malonic acid (2:1)	(43)
Caffeine – Glutaric acid (1:1)	(43-44)
Carbamazepine –Benzoquinone (2:1)	(45)
Carbamazepine –Bipyridine (2:1)	(45)
Carbamazepine – Saccharin (1:1)	(45, 46)
Carbamazepine – Nicotinamide (1:1)	(45, 47)
Carbamazepine – Terephthalaldehyde (2:1)	(45)
Celecoxib – Nicotinamide (1:1)	(48)
Exemestane – Maleic acid	(49)
Fluoxetine hydrochloride – Benzoic acid (1:1)	(13)
Fluoxetine hydrochloride – Succinic acid (2:1)	(13)
Fluoxetine hydrochloride – Fumaric acid (2:1)	(13)
Indomethacin – Saccharin	(50)
Itraconazole – 1,4-dicarboxylic acids	(51)
Magestrol acetate – Saccharin (1:1)	(50)
Melamine – Cyanuric acid (1:1)	(52)
Monophosphate salt - phosphoric acid (1:1)	(53)
Norfloxacin – isonicotinamide (1:1)	(54)
Piracetam – Gentisic acid (1:1)	(55)
Piroxicam – Saccharin (1:1)	(56)
Sildenafil – Acetylsalicylic acid (1:1)	(57)
Sulfamethazine – Anthranilic acid	(57)
Sulfamethazine – Aspirin (1:1)	(57)
Sulfamethazine – Benzoic acid (1:1)	(57)
Theophylline – Oxalic acid	(58, 59)
Theophylline – Malonic acid	(59)
Theophylline – Maleic acid	(59)
Theophylline – Glutaric acid	(59)
Trimethroprim – Sulfamethoxypyridazine (1:1)	(60)

1.6 Methods of preparation

Cocrystals can be prepared by a wide range of methods including solution cocrystallisation (61, 62), cogrinding also known as dry grinding (63), solvent evaporation (64), sonic-slurrying (65), spray-drying (66) and ultrasound mediated amorphous to crystalline transition (UMAX) (67, 68). Cocrystals that were studied in this project were prepared by sonic-slurrying, spray-drying and UMAX methods.

1.6.1 Sonic-slurrying technique

A slurry is prepared by adding appropriate amounts of API and coformer into the jacketed vessel containing organic solvent (e.g. ethyl acetate). The slurry is then stirred using a magnetic stirrer at specified conditions (temperature, duration of stirring, speed of stirring). Slurry is then filtered and dried under vacuum overnight (65).

1.6.2 Spray-drying technique

The spray-drying process coverts a liquid into a powder and it is composed of the following four stages. The first phase consists of atomisation of the feed into a spray. Then spray-air contact occurs followed by the drying stage. The final step involves separation of the dried product from the drying gas (66).

1.6.3 UMAX technique

UMAX process encompasses the following three stages: the first stage involves judicious spray-drying of an API and coformer solution. The second stage consists of collecting the unstable amorphous or part-amorphous spray-dried particles in a non-solvent, and applying power ultrasound to particles to effect crystallization. The final stage is known as solid isolation and occurs preferably by spray-drying (67, 68).

1.7 Biopharmaceutical characteristics of cocrystals

1.7.1 Stability studies

It has been reported that cocrystals greatly improve stability (13). Many cocrystals, including Caffeine-Oxalic acid cocrystal, Caffeine-Maleic acid cocrystal and Caffeine-Glutaric acid cocrystal as well as Theophylline cocrystals with Glutaric acid, Maleic and Malonic acids transformed to the hydrate form after exposure to 98% RH (43, 69). It was noted that the strongest acid used (Oxalic acid) formed the most stable cocrystal, while the weakest acid (Glutaric acid) produced the least stable cocrystal (43). Also, Carbamazepine-Saccharin and Carbamazepine-Nicotinamide cocrystals were observed to be stable until exposure to 98% RH (70). Moreover, minimal (< 0.05%) water uptake was reported for Indomethacin-Saccharin cocrystal up to 95% RH (50). Few studies investigated long-term stability (53, 69). For instance, Monophosphate salt with Phosphoric acid showed physical stability after 8 weeks of storage at 40 °C/ 75% RH (53).

1.7.2 Solubility studies

It has been claimed that cocrystals enhance solubility of poorly soluble compounds. Great enhancement in solubility of cocrystals in organic solvents has been noted (71). In order to understand the behavior of cocrystal *in vivo*, testing solubility in aqueous media was essential. Basovoju *et al*. reported the case when Norfloxacin – Isonicotinamide cocrystal improved solubility three times in comparison to the solubility of the parent compound (54). Also, Cheney *et al.* successfully prepared pharmaceutical cocrystal made of two active components: Meloxicam and Aspirin. Aspirin in this case played a coformer role. This cocrystal resulted in significant solubility enhancement (0.22g/mL) in phosphate buffer pH 7.4 at 37 °C, when compared with solubility of Meloxicam (0.005g/mL) (72). There were some exceptions, through where the enhancement in solubility did not occur. For instance, Rahman *et al.* reported no significant improvement in equilibrium solubility between CBZ and Carbamazepine – Nicotinamide cocrystal tested in four different media: water, HCl (pH 1.2), acetate buffer (pH 4.5) and 0.2 M phosphate buffer (pH 6.8) at 25 and 37 °C (73). In contrast to pH, the temperature had a significant effect on solubility of CBZ and CBZ-NIC cocrystal. Insensitivity of CBZ to pH changes can be explained by the fact that CBZ behaves like neutral drug in physiological pH range (pH 1.2 – 7.5). A Lamotrigine – Nicotinamide cocrystal also did not improve the solubility of Lamotrigine in water and HCl (pH 1.2) (74). It

was concluded that the cocrystal is a single molecular entity in the solid state and, upon contact with water, hydrogen bonding dissociates into individual components (59, 73). The cocrystal cannot improve the solubility over a mixture of the individual components because solubility is an equilibrium thermodynamic property.

1.7.3 Dissolution studies

Dissolution enhancement has been reported using a range of dissolution methods and apparatus. It has been observed by Remenar and co-workers that dissolution (0.1M HCl, 25 °C, methodology not specified) of Itraconazole from cocrystals of Itraconazole with Succinic acid, Malic acid and Tartaric acid was similar to the dissolution of amorphous Itraconazole from commercial product Sporanox®. Moreover, cocrystals resulted in four to twenty fold higher concentrations in comparison to its crystalline form (75).

Shiraki *et al*. showed that the intrinsic dissolution rate (IDR) of Megestrol acetate – Saccharin cocrystal (2.53 ± 0.91 μg/cm^2/min) is three to four times greater than the intrinsic dissolution rate of its parent compound (0.66 ± 0.33 μg/cm^2/min) (49). This enhancement was also observed during dissolution studies (USP 2, 50 rpm) performed in 100 mL vessels filled with 50 mL of Fasted State Simulated Intestinal Fluids (FaSSIF) (Figure 4). Supersaturation of fine (average particle size: 15 μm) Megestrol acetate – Saccharin cocrystal occurred within 15 minutes, after which the cocrystal started transforming to the parent compound. Larger particles of cocrystal did not exhibit supersaturation.

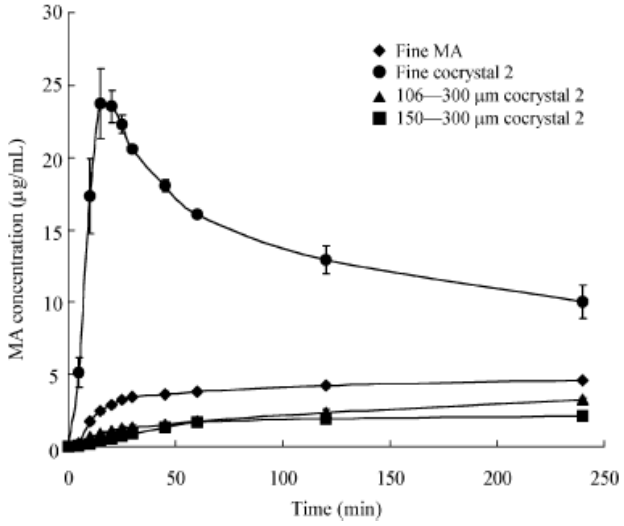

Figure 4. Dissolution profile of cocrystal 2 (Megestrol acetate – Saccharin) (n=4) in FaSSIF using USP 2 (50rpm, 50 mL). Reprinted with permission from (49).

On the other hand, dissolution studies of Carbamazepine – Saccharin cocrystal with six different particle size fractions ranging from 53 µm to 1000 µm in SGF with 1% Triton X (pH 2) (USP 2, 100 rpm, 900 mL) showed slower dissolution rates of Carbamazepine from samples with particle size > 500 µm (46).

Lu and Rohani have presented the case of Theophylline – Nicotinamide cocrystal which proved that not only an enhancement in dissolution (50 mL, water, 25 °C) is an important advantage of cocrystallisation, but sometimes the benefit of producing more stable product should be sufficient (76) (Figure 5). Theophylline tends to convert from its more soluble anhydrous form to a stable but less soluble hydrate state during processing and dissolution. Theophylline – Nicotinamide cocrystal resulted in a more stable material that inhibited the conversion to the hydrate state (59).

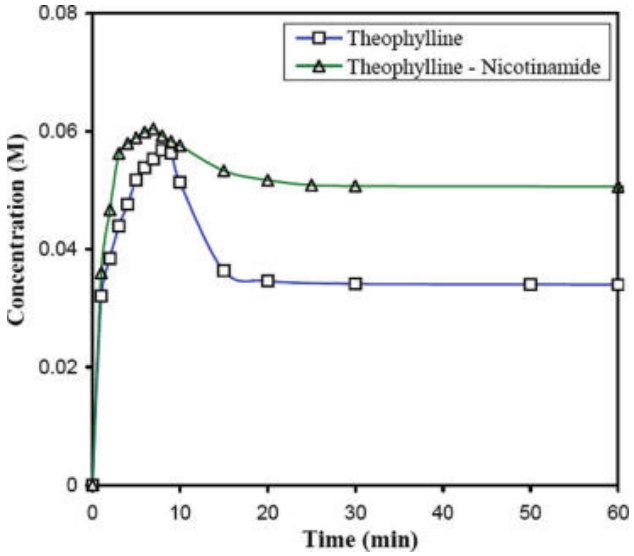

Figure 5. Dissolution of Theophylline and Theophylline – Nicotinamide cocrystal in water. Reprinted with permission from (76).

1.7.4 Bioavailability studies

It was important to investigate if the enhancement of solubility and dissolution of cocrystals can lead to improvement of *in vivo* performance. So far, none of the cocrystals were tested in humans. All available *in vivo* data were performed using various animal species. Suspension (1 mg/kg) of Meloxicam – Aspirin cocrystal administered via oral gavage in rats (n = 5) resulted in an oral bioavailability of 69%, compared with 16% for Meloxicam (72). Moreover, AMG517 – Sorbic acid cocrystals proved not only to significantly increase solubility of AMG517 but also to enhance eight times C_{max} of AMG517 in rats (40). Also, cocrystal of

Glutaric acid with sodium channel blocker that showed an eighteen times increase in its intrinsic dissolution rate, resulted in a three-fold increase in exposure over the parent compound in a canine pharmacokinetic study (69) (Figure 6).

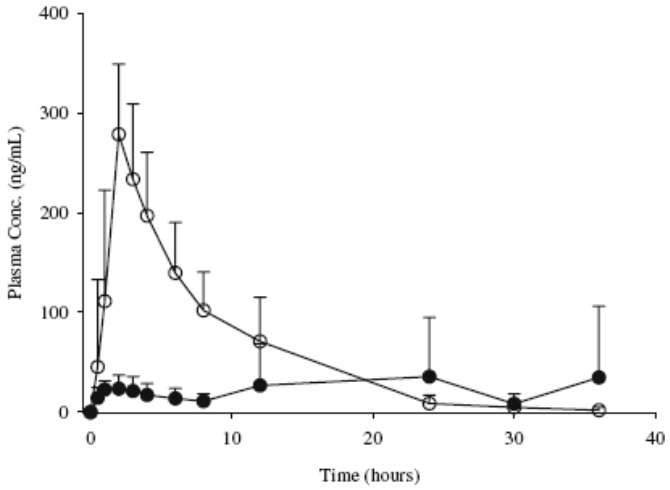

Figure 6. Mean plasma concentration (+SD) *versus* time profiles after administration of 50 mg/kg of API (●) and cocrystal of glutaric acid (○) in dogs (n=6). Reprinted with permission from (69).

Jung *et al*. examined bioavailability of orally administered capsules of IND-SAC cocrystals in beagle dogs (77) (Figure 7). The *in-vivo* bioavailability of IND in dogs was significantly higher ($p < 0.05$) than that of physical blend of IND and SAC, but exhibited similar ($p > 0.05$) performance to a commercial formulation of IND (Idomee®, Sweden). Indomee® is a highly optimised formulation that has been marketed for a long time and hence would be expected to have good bioavailability (77).

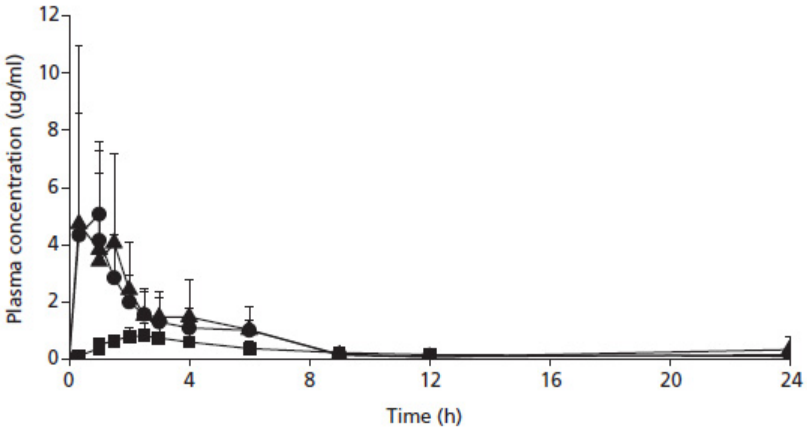

Figure 7. Plasma concentration - *versus* time profiles for indomethacin after oral administration of various formulations in dogs: ● IND – SAC cocrystal; ■ Physical mixture of IND and SAC; and ▲Indomee® capsules. Error bars show standard deviations. Reprinted with permission from (77).

Despite the limited number of examples, cocrystals proved successful in increasing the bioavailability of poorly soluble drugs in animal studies.

1.8 Cocrystals studied

1.8.1 Carbamazepine and its cocrystals

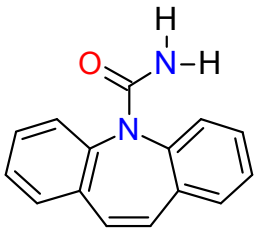

Figure 8. Structure of Carbamazepine.

Carbamazepine is a well-known drug used for epilepsy and trigeminal neuralgia (Figure 8). It is classified as a BCS class II compound due to its high permeability and low solubility in aqueous media (anhydrous: 0.38 mg/mL; dihydrate: 0.13 mg/mL at 25 °C) (78). It exhibits in four anhydrous polymorphs: monoclinic (III), triclinic (I), trigonal (II) forms and a dihydrate (DH) form (79, 80). The monoclinic form (MP~174 °C) is the most thermodynamically stable at ambient conditions (80). It was reported that the intrinsic dissolution rate of the metastable monoclinic polymorph was greatest (67.4 µg/cm^2/min) when compared to the triclinic (I) (61.8 µg/cm^2/min) and dihydrate form (DH) (41.8 µg/cm^2/min) (80). However, this form tends to convert to the least soluble dihydrate (DH) form, faster than the stable triclinic form (I) (MP~190 °C) (79, 81). This trend was in agreement with *in vivo* studies (46). Commercial formulations of CBZ, Tegretol® tablets are formulated with the anhydrous monoclinic form. From a supramolecular perspective, CBZ is a simple molecule with one hydrogen bond. It is a weak acid with pK_a value of 11.83, thus during *in vitro* and *in vivo* dissolution in physiological pH range (1.2 – 7.5) CBZ does not lose a proton to form the corresponding anion, so the compound is unionised (82).

Saccharin (MP~229.47 °C) is a potent sweetener that is often used as taste-masking agent to improve patient compliance (56). It is an ionizable compound (pKa = 1.8-2.2) (83) with aqueous solubility of around 3.45 mg/mL (74). In the cocrystal, Saccharin acts as both a hydrogen bond donor and acceptor. SAC forms an N – H ··· O hydrogen bond to the CBZ carboxyl, and the Saccharin sulfonyl group forms an S = O ··· H – N hydrogen bond with CBZ (Figure 9).

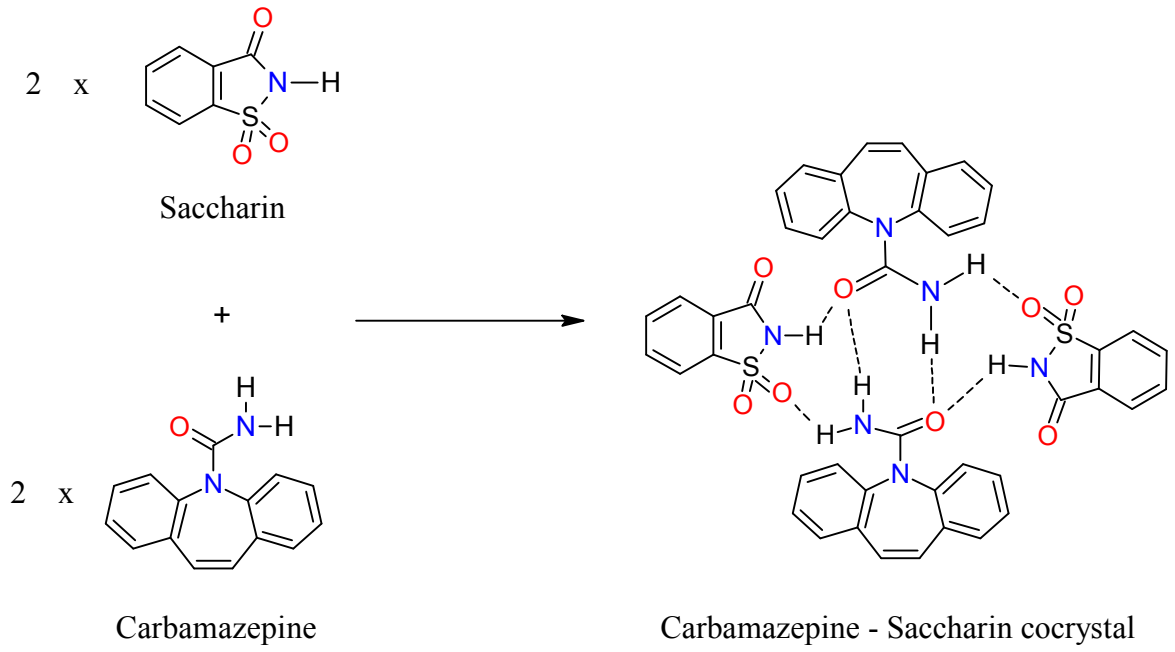

Figure 9. Formation of CBZ-SAC cocrystal. Redrawn from (46).

The Carbamazepine-Saccharin (CBZ-SAC; 1:1) cocrystal has been extensively studied (45, 46, 84). The presence of two distinct morphologies - plates and needles (polymorphs, CBZ-SAC I (MP~166.8 °C) and CBZ-SAC II (MP~173 °C) have been revealed by optical microscopy (84) (Figure 10). According to this study, form II of CBZ-SAC heterosynthon is formed differently, by a hydrogen bond between N – H of SAC with carboxyl group of CBZ and hydrogen bond between N – H group of SAC with the carboxyl group of CBZ.

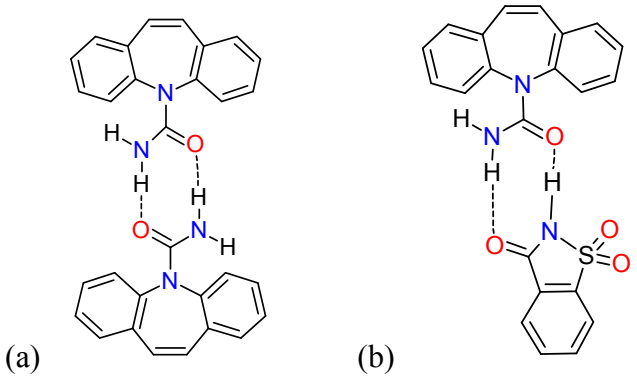

Figure 10. Illustration of (a) the homosynthon between two CBZ molecules in CBZ-SAC I and (b) the heterosynthon between a CBZ and SAC molecule in CBZ-SAC II. Redrawn from (84).

Nicotinamide (NIC, pyridine-3-carboxylic acid amide) is also known as vitamin B_3 and is very potent hydrotropic agent used to increase the aqueous solubility of many drugs (85). It is an ionisable compound (pKa = 3.35) (86) with high aqueous solubility of around 1000 mg/mL (74). Hathwar *et al*. produced Nicotinamide – Salicylic acid cocrystal, in which the nitrogen

atom in the pyridine ring of Nicotinamide can form heterosynthons with salicylic acid, resulting in an amide – pyridine, an acid – pyridine or hydroxyl – pyridine hydrogen motif (86). However, the possibility of formation of homosynthons between amide – amide and pyridine – pyridine moieties was also reported (87).

Carbamazepine – Nicotinamide exhibits three polymorphs, named CBZ-NIC-I, CBZ-NIC-II and CBZ-NIC-PN (47, 84). Raman spectroscopy has revealed that the latter converts to CBZ-NIC-I in the temperature range 124 – 128 °C (84). NIC is non-covalently bonded to CBZ through C = O ··· H – H hydrogen bonds. Crystal packing reveals π···π interactions between the CBZ and NIC rings (45) (Figure 11). The hydrotropic effect of NIC has been claimed to be mainly due to its ability to destroy water structure and/or to form complexes with certain drugs on the basis of p-electron donor–acceptor and hydrogen bonding (88-90).

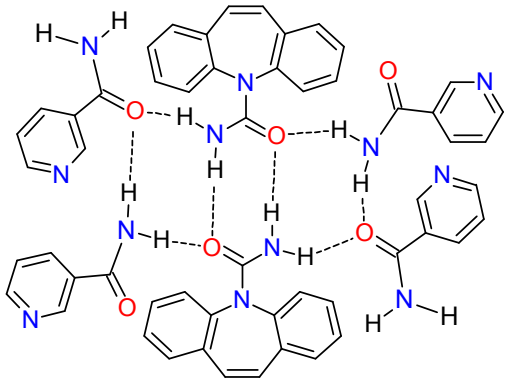

Figure 11. Carbamazepine – Nicotinamide cocrystal. Redrawn from (45).

1.8.2 Indomethacin and its cocrystals

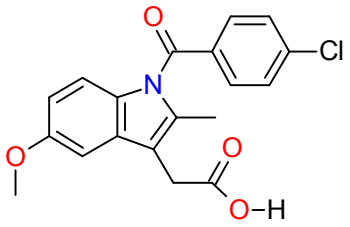

Figure 12. Structure of Indomethacin.

Indomethacin is a nonsteroidal drug with anti-inflammatory (NSAID), antipyretic and analgesic properties (Figure 12). It is widely prescribed for patients with moderate to severe rheumatoid arthritis, ankylosing spondylitis, osteoarthritis and acute arthritis (91). It is well known to cause gastrointestinal disturbances. Indomethacin is a poorly soluble BCS class II drug. Indomethacin exists in two polymorphic forms, termed a-form (α) (MP~ 154.5-155.5 °C) and c-form (γ or g-form) (MP~160.82 °C), and an amorphous form (92). C-form is thermodynamically stable at room temperature but is practically insoluble in water (2.5-4 mg/mL) (93). Indomethacin – Saccharin cocrystal (MP~184.20 °C) is characterised by specific carboxylic acid and imide dimer synthons interconnected by weak hydrogen bonds (50) (Figure 13).

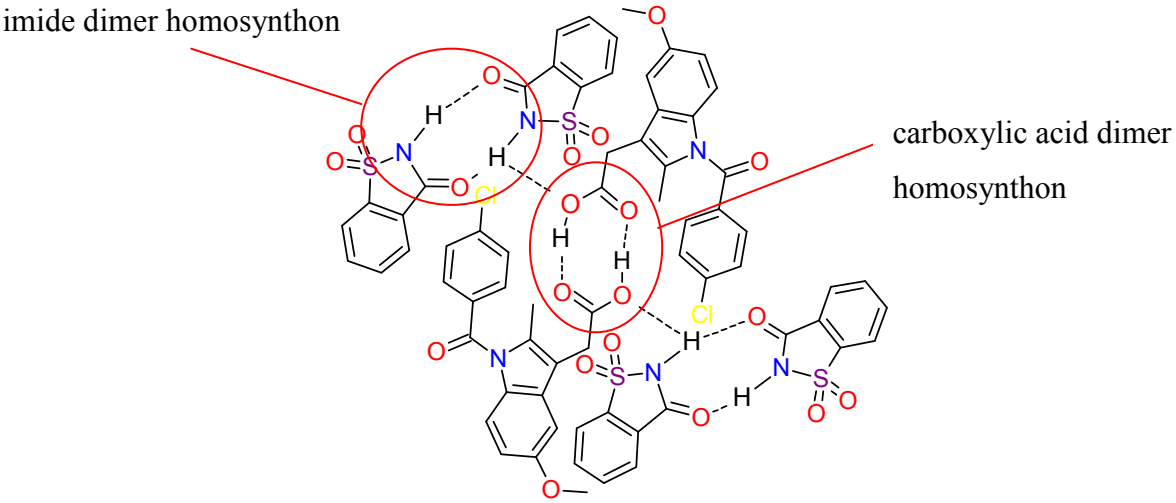

Figure 13. Indomethacin – Saccharin cocrystal. Redrawn from (50).

Alhalaweh and Velaga successfully prepared IND-NIC (1:1) cocrystals using spray-drying and solvent evaporation methods (66). Cocrystals exhibited an amorphous state for a short

period of time and then crystallised to cocrystal upon storage. The same group of scientists prepared IND-SAC (1:1) and IND-NIC (1:1) cocrystals using grinding method (71). Solubility of these cocrystals was tested in various organic solvents including methanol, ethanol and ethyl acetate. It was found that IND-NIC cocrystals were more soluble than the IND-SAC cocrystals in all media.

2 *In vitro* dissolution testing

2.1 Introduction

Over the last half century, dissolution became a very important tool in the pharmaceutical industry. Simply defined, dissolution is the process by which a solid enters into a solution in the presence of solvent (94). The dissolution rate may be defined as the amount of drug substance that goes in solution per unit time under standardized conditions of liquid/solid interface, temperature and solvent composition. This section will describe the types of dissolution systems officially approved by pharmacopoeias and the applications of the *in vitro* dissolution testing. Two dissolution systems: basket (USP apparatus 1) and flow-through cell (USP apparatus 4) will be closely characterised in terms of their advantages and disadvantages, as well as hydrodynamics and their potential applications. A short review of existing dissolution media is also included in this chapter together with statistical approaches of comparing *in vitro* dissolution profiles.

2.2 Dissolution theories

Dissolution process is controlled by the affinity between the solid substance and the solvent and consists of two consecutive steps. The first step involves the liberation of molecules from the solid phase to the liquid layer near the solid surface. Followed by the transport of solutes from solid – liquid interface into the bulk solution. The dissolution of the solid substance is generally modelled based upon the significance of these two transport stages (95). The most common dissolution theories will be described in the following section.

2.2.1 Diffusion layer model (DLM)

The diffusion layer model was originally proposed by Nerst and Brunner in 1904 (96). The model assumes that a diffusion layer of thickness h is surrounding the surface of a dissolving particle. The transport at the solid-liquid interface is assumed to be instantaneous, providing equilibrium at the interface. Concentration at the surface is the saturated solubility of the substance (97). The solute molecule that diffuses through the film layer reaches liquid – solvent interface. Rapid mixing provides uniform bulk concentration (C). Fick's first law was applied to model the diffusion process through the liquid film. This law relates flux of a solute to its concentration gradient (Equation 1):

$$J = -D\frac{dC}{dx} \quad \text{(Equation 1)}$$

where J is the amount of substance passing perpendicularly through a unit surface area per unit time. D is the diffusion coefficient, and dC/dx is the concentration gradient, which represents a driving force for diffusion. At steady state this equation can be expressed as (Equation 2):

$$J = -D\frac{C - C_S}{h} \quad \text{(Equation 2)}$$

where C is the bulk concentration, Cs is the saturation concentration, and h is the thickness of the stagnant diffusion layer. Thus, dissolution rate, which is directly proportional to the flux of solutes across the diffusion layer can be characterised by equations:

$$V\frac{dC}{dt} = SJ \quad \text{(Equation 3)}$$

$$\frac{dC}{dt} = \frac{SD(C_S - C)}{Vh} \quad \text{(Equation 4)}$$

where S is the total surface area of particles, and V is the volume of dissolution medium. C_s-C represents the concentration gradient within the stagnant diffusion layer with thickness h. This equation is known as Nerst-Brunner equation.

2.2.2 Interfacial Barrier model

In contrast to DLM, the interfacial barrier model assumes that the reaction at the solid surface is significantly slower than the diffusion across the interface (98). Thus, no equilibrium exists at the surface, and liberation of solutes at the solid-liquid interface controls the overall rate of the transport process. This model can describe dissolution rate using Equation 5.

$$G = k_i(C_S - C) \quad \text{(Equation 5)}$$

where G is the dissolution rate per unit area, k_i is the interfacial transport coefficient.

2.2.3 Danckwerts' model

Assuming that the solid surface reaction is instantaneous, the Danckwerts' model suggests that the transport of solute is achieved by the macroscopic packets that reach the solid surface, absorb solutes at the surface (according to law of diffusion) and deliver them to the bulk solution (99). The packet is then replaced with the new packet of solvent. According to this theory dissolution can be characterised by Equation 6:

$$\frac{dm}{dt} = S(\gamma D)^{1/2} - (Cs - C) \qquad \text{(Equation 6)}$$

where *m* is the mass of dissolved substances and γ is the interfacial tension.

2.3 Applications of *in vitro* dissolution testing

The importance of *in vitro* dissolution testing has been recognized by the pharmaceutical industry since the early 1930s (100). Dissolution testing has been included in the United States Pharmacopoeia (USP <711>, <724>) since 1970 and from that time onwards plays an important role as a quality control (QC) tool (97). Initially, the aim of dissolution was to differentiate between acceptable and unacceptable batches during the manufacture process (101). Formulators treat the dissolution test as a valuable tool that is able to show the effect of certain excipients on manufacture variables. Dissolution is still a critical test that determines the effect of aging of the product on stability (102, 103). For instance, dissolution testing was used to proved that type of packaging and storage conditions significantly affected the stability of Prednisone tablets (104). Moreover, dissolution serves as an *in vitro* surrogate for *in vivo* bioequivalence studies by development of *in vivo – in vitro* correlation (IVIVC) and can support a biowaiver for formulation based on the biopharmaceutics classification system (BCS) (97, 105-107). This approach minimises the number of human studies required for drug approval. This is because a biowaiver allows the use of dissolution curves in place of a bioequivalent study to prove equivalence of formulation or process.

2.4 The dissolution apparatus

There are seven dissolution systems officially approved by United States Pharmacopeia (USP <711>) that can be used to test several types of formulations (Table 2) (108).

Table 2. List of the dissolution apparatuses and their applications (109).

Dissolution Apparatus	**Formulations that can be tested**
USP apparatus 1 (basket) USP <711>	Coated tablets Uncoated tablets Delayed release Extended release
USP apparatus 2 (paddle) USP <711>	Conventional Enteric coated Extended release
USP apparatus 3 (reciprocating cylinder) USP <711>	Modified release dosage form Bead type
USP apparatus 4 (flow-through cell) USP <711>	Modified release (poorly soluble drugs, suppositories, soft gelatin, bead type)
USP apparatus 5 (paddle over disk) USP <724>	Transdermal
USP apparatus 6 (cylinder) USP <724>	Transdermal
USP apparatus 7 (reciprocating holder) USP <724>	Non disintegrating modified release dosage form Transdermal

2.4.1 USP apparatus 1

2.4.1.1 Operation mode

The apparatus 1 was made an official regulatory test by USP in 1970 (110). The rotating basket device is simple, robust and adequately standardised (Figure 14). It can be also automated which makes it useful for routine experiments. The rotating basket apparatus consists of a cylindrical basket held by a motor shaft. The basket holds the sample (tablet, capsule, *etc.*) and rotates in a cylindrical, round bottomed vessel, which is usually made of glass and contains the dissolution medium. The entire vessel is immersed in a constant temperature bath set at 37±0.5 °C. The position of the basket (25±2 mm) is specified by the USP (109). USP apparatus 1 is used for dosage forms that tend to float or disintegrate slowly (*i.e.* capsules, tablets). The system can accommodate from 500 to 1000 mL of medium using the standard size vessel. The volume of the media is particularly important for poorly soluble drugs that require large amounts of medium in order to maintain sink conditions. It is possible but very uncommon to accommodate 4 or 5 L vessels (111). On the other hand, small dosage formulations can be tested in non – compendial 100 – 250 mL vessels (112-114). The vessel is filled with a fixed volume of media to which formulation is exposed throughout the experiment. There are several disadvantages of this system. The media change procedure within a single run that cannot be easily performed, and it is difficult to mimic the change in luminal conditions during transit from stomach to the intestine (115).

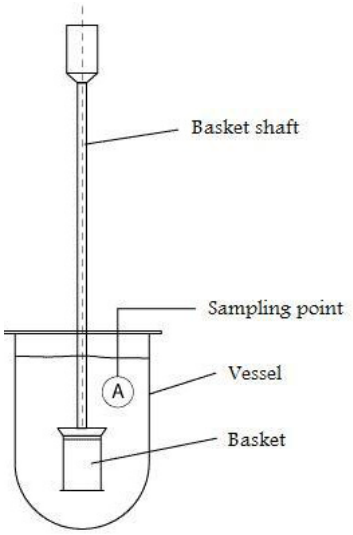

Figure 14. Diagram of rotating basket apparatus (USP apparatus 1).

2.4.1.2 Hydrodynamics

In vivo hydrodynamics is often reflected using a non-dimensional parameter, Reynolds number (*Re*), which provides an estimate of the ratio of flow acceleration to frictional force in the flow around a dosage form (116, 117). Abrahamsson *et al*. have reported that hydrodynamics in the gastrointestinal (GI) tract varies from *Re* 0.1 to 30, whereas *Re* values in USP apparatus 2 are around 2000 (118-120). Reynolds number for USP apparatus 1 has not been reported, but we can assume that it is greater than those reported for USP apparatus 2 However, D'Arcy *et al.* compared the hydrodynamics of both of these systems in terms of fluid velocities (121). According to this study, a similar magnitude of velocities was observed inside the basket as at the base of the vessel of the paddle apparatus at the same rotation speed, although slightly lower. It is important to note that this research did not consider the mesh size of the basket and presence of the spring clips which hold the basket. This has been reported elsewhere (122).

Agitation speed is an important factor when developing a dissolution test. Paddle agitation speed can change the hydrodynamics of the dissolution medium significantly. Too fast speed may not be able to discriminate between the batches, while too slow may not disperse the solute well (123). For instance, prednisone tablets are fast disintegrating. If the agitation is below 100 rpm, the tablet sinks to the bottom of the vessel and disintegrates within less than five minutes (124). Insufficient speed leads to coning of the formulation in the central area of the vessel. This traps the drug in the cone and releases it slowly by diffusion. Sometimes increasing the speed can solve this problem. There are also special peak vessels available which unable cone formation.

2.4.2 USP apparatus 4

2.4.2.1 Operation mode

The flow-through cell apparatus consists of a pump that forces the medium through the cell that holds the test sample (Figure 15).

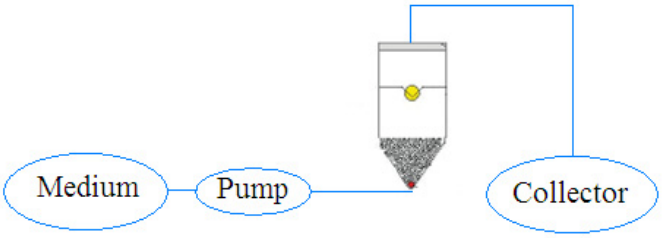

Figure 15. Diagram of the USP apparatus 4.

The dissolution part of USP apparatus 4 consists of seven cells that are assembled in a row as one compartment (Sontax® model) or individually (Erweka® model). Two types of cells are available for orally administered dosage forms: a large cell (22.6 mm i.d.) and a small cell (11.3 mm i.d.). The flow-through cell has three parts: the lower cone, the middle cylindrical portion and the filter head on the top. Dissolution medium enters the cone on the bottom and flows up to the cell. The lower cone houses a 5 mm glass bead which protects the inlet tube and prevents backflow (125). Positioning of the dosage form in the middle cylinder is a key factor that affects its dissolution (126). Various types of cells are available that are suitable for a range of formulations such as powders, tablets, suppositories, ointments *etc*. Often 1 mm glass beads are used. Before reaching the cells, medium is pumped through heat exchangers which are placed in an electronically regulated thermostatted bath, assuring a test temperature of 37 °C. Additionally, the water from the water bath is raised up and surrounds the cell positioned in the jacket tube allowing maintained constant temperature. After passing through the cell, the eluents are filtered within the filter heads and then either collected or transferred directly to the spectrophotometer for analysis. The filter head is generally equipped with a glass microfiber filter. Depending on the sample, filters of different pore sizes can be used. A combination of two filters with glass wool may be used separated in order to improve filtration quality (127). Piston pump is generally used to pump the medium. Different flow rates can be applied, varying from 2-50 mL/min with typical flow rates of 4, 8 and 16 mL/min. Flow rates between 4 and 8ml/min have been proposed for tests that simulate fasted and fed state conditions (128-130). Duration of the dissolution test and flow rates used are designed to balance between GI fluid volumes and the physiological residence times in the GI lumen, and to compensate not only for radial loss (absorption) of the drug but also for the water re-absorption (131). USP apparatus 4 can work in two configurations either as an open or closed system. The former allows always fresh media to be pumped from a reservoir through the cell in a continuous flow; whereas the latter recycles fixed volume of the same medium.

2.4.2.2 Applications

The flow-through cell dissolution apparatus was designed and developed in 1957 (132) but it was not included into USP as an official dissolution method until 1990 (119, 128). Flow-through cell dissolution methods for three formulations were included in the FDA database (133). All the formulations are injectable suspensions of Methylprednisolone acetate, Betamethasone acetate and Betamethasone sodium phosphate. Recently, official monograph for 200 mg and 400 mg Rufinamide tablets was included in US Pharmacopoeia (134). It is designated for the testing of poorly soluble drug products, granules, powders and some special dosage units such as suspension, implants, injectable formulations and suppositories (135). It has been also reported that USP apparatus 4 has been successfully used for evaluating the disintegration of cross-linked gelatin capsules of Amoxicillin (136). Moreover, Zolnik *et al.* effectively used the USP apparatus 4 to monitor the release of Dexamethasone from microspheres over a 30 day period (137). The design of flow-through cell dissolution apparatus is more physiologically relevant than design of basket and paddle dissolution apparatus. Often biorelevant dissolution leads to the successful development of an IVIVC. For instance, Emara *et al*. have developed successful IVIVC for two Vincamine Prolonged Release (PR) formulations using dissolution data obtained using open USP apparatus 4 (138). Formulations were exposed to four different compendial media for certain duration of time: pH of 1.2 (1 h)/ pH 4.5 (1 h)/ pH 6.8 (2 h) and pH 7.5 (1 h). A flow rate of 8 mL/min was maintained throughout the run. *In vitro* dissolution data were then directly correlated with *in vivo* absorption data obtained from 16 healthy human volunteers.

2.4.2.3 Advantages

In contrast to USP apparatus 1 closed dissolution system, USP apparatus 4 allows media/or flow rate changes as well as maintenance of sink conditions (126, 127, 131). The former is particularly important, for example, for enteric coated dosage forms, as well for some pH-dependent solubility formulations that have a tendency to precipitate. Maintenance of sink conditions is particularly important when poorly soluble drugs are tested (119). Flow-through cell apparatus is able to work with unlimited amounts of solvent (open system) which helps to overcome this problem. On the other hand, closed system can be very beneficial when testing formulations with low drug loading that may have sensitivity issues in USP apparatus 1.

USP apparatus 4 allows testing of suppositories (139), powders and implants and lipid soft gelatin capsules (SGC) (140) in specially designed cells, which would be challenging or

impossible using dissolution USP apparatus 2. For instance, Hu *et al.* investigated the release of a free base of a secondary amine from lipid SGC using USP apparatus 2 and USP 4 systems (140). Due to filtration and sampling issues of oil droplets, it was impossible to use USP apparatus 2; and USP apparatus 4 equipped with a standard cell. The improved results were obtained when specialised SGC flow-through cells (known also as suppositories cells) were used.

2.4.2.4 Disadvantages

One major disadvantage of the USP apparatus 4 is filter blockage/clogging that has been reported, especially when testing powders or large formulations (127, 130). Due to the fact that the standard cell is made of high-grade acrylic glass, testing formulations in hydro-ethanolic media is not possible (*Personal communication with Erweka Ltd; 06-05-2013*).

2.4.2.5 Hydrodynamics

So far, USP apparatus 4 provides the most physiological hydrodynamic conditions (*Re* < 30) (120). Linear flow velocity of the dissolution medium is the major parameter which characterizes the hydrodynamic *agitation* of the dissolution medium (130). It has been reported that the average axial velocity is about 1.5 cm/min under fasted state and 1.3 cm/min under fed state conditions (130). These values correspond to flow rates below 2 mL/ min in small cells (11.3 mm) and below 8 mL/min in a large cell (22.6 mm) of USP apparatus 4 (130) (Table 3). Generally, higher than *in vivo* flow rates are used to compensate for the resulting high total fluid volume (130)

Table 3. Correlation between the linear flow velocity and volumetric flow provided in USP apparatus 4 cells (130)

Cell diameter (mm)	**11.3**	**22.6**	**Volumetric flow (mL/min)**
Area (cm)	1	4	
Linear flow velocity (cm/min)	2	0.5	2
	4	1	4
	8	2	8
	16	4	16
	32	8	32

Interestingly, faster flow rates do not affect the release of drug from the matrix tablets (141). This is due to the fact that release from this dosage form depends not only on the transport through the diffusion layer but also on the drug release mechanism.

The hydrodynamics in the cell can be controlled by the presence or absence of glass beads. There are two types: laminar, when glass beads are placed in the cone part of the cell and turbulent in the case when the cell is set up without small glass beads. Generally, tablets and hard gelatin capsules, powder and granulates are tested under laminar flow; whereas turbulent flow offers benefits for testing suppositories and SGC (142). Recently, Kakhi argued that fully laminar conditions are unlikely achievable and as a consequence suggested replacing existing terminology of laminar and turbulent flow with packed and open columns, respectively (Figure 16) (143).

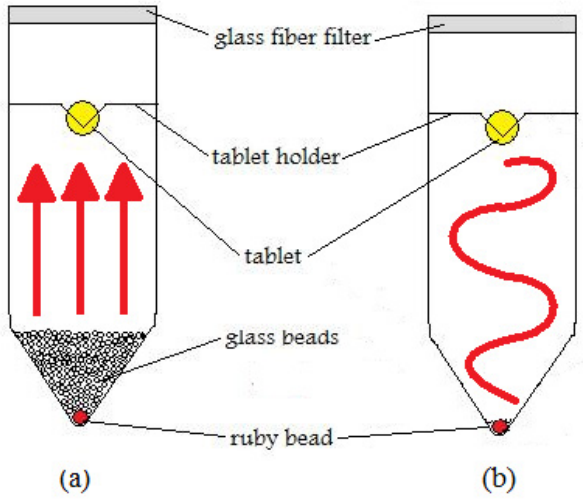

Figure 16. Schematic of (a) packed and (b) open column (143).

It was reported by Zhang *et al*. that the release rate from erodible tablets was not influenced by different flow rates ranged between 7 to 21 mL/min (144). Whereas, discriminative dissolution profiles were observed when turbulent flow pattern was applied (126). Shiko *et al.* argues that the local values of *Re* (Reynolds number) did not exceed 200, thus the turbulent flow term should not be used even in the more aggressive conditions in the USP apparatus 4 (145). It was also suggested by this group that 1mm glass beads should be used to provide less chaotic and asymmetric flow in the cell.

Swedish scientists from five different pharmaceutical laboratories made an attempt to compare results generated for dissolution of USP Prednisone calibrator tablets using flow-through cell apparatus and USP 2 paddle apparatus (146). They have reported that similar

dissolution profiles were observed when tablets were tested in 12 mm cells at the flow rate of 9 mL/min; and in 22.6 mm cells at a flow rate of 32 mL/min. This is due to the similarities of the linear flow rate of the medium in these two cells at these flow rates. A correlation was found that the dissolution profile obtained using flow-through 12 mm cell at 16 mL/min falls within the range between the dissolution profiles obtained using USP apparatus 2 at 50 and 100 rpm. On the other hand, they found that the USP 2 dissolution method provided more consistent data for Prednisone tablets between the laboratories than the USP 4 dissolution method. For instance, variability in dissolution of Prednisone tablets (n = 30) using a 12 mm cell at 16 mL/min was reported to be 17 % after 30 min testing. For the USP 2 dissolution method, the corresponding values were 6 % and 11 % at 50 and 100 rpm, respectively (146). However, it has been reported that the hydrodynamics in 12 mm cells is more variable than in 22.6 mm cells. Therefore, the variability in dissolution rate could be related to the type of cell selected. It is important to note that Prednisone tablets are official calibrator formulations for USP apparatus 2 only and that there are no official calibrator formulations for USP apparatus 4 (127). Eaton *et al*. reported Salicylic acid tablets to be suitable for Performance Verification Test (PVT) of USP apparatus 4 (147).

2.5 The dissolution medium

Many studies have been conducted to understand the *in vivo* drug release, in order to develop more physiologically relevant media that can predict *in vivo* dissolution (148-150). Various media have been proposed for simulating gastric and intestinal contents. Some media are simple and simulate mainly pH and ionic content of the GI tract (compendial media) while others are more complex in composition and are designed to mimic osmolality, buffer capacity and surface tension (biorelevant media) of individual GI segments.

2.5.1 Compendial media

There are three most commonly used compendial media that simulate gastric, intestinal and colonic environments (Table 4). Compendial media mainly simulate the pH and ionic environment of gastric and intestinal environments but do not simulate the *in vivo* performance accurately. Simple Simulated Gastric Fluid (SGF) consists of an aqueous hydrochloric acid solution with a pH of 1.2. There are two versions of these media proposed in United States Pharmacopeia: one contains pepsin (3.2 mg/mL) that characterizes conditions in the stomach and one without it (108). Small intestinal conditions are represented by

Simulated Intestinal Fluid (SIF) which is composed of phosphate ions providing a pH of 6.8. This medium can also be present with or without pancreatin (108). It has been reported that addition of pepsin and pancreatin improves dissolution of hard gelatin capsules that exhibit cross – linking (151).

Table 4. Composition of compendial media.

	SGF (108)	SIF (108)
Sodium chloride (mM)	34.2	-
Hydrochloric acid (mM)	70.96	-
Potassium dihydrogen orthophosphate (mM)	-	49.96
Sodium hydroxide (mM)	-	15.4
pH	1.2	6.8

2.5.2 Biorelevant media

2.5.2.1 Stomach

Over the last decade, biorelevant dissolution media (BDM) have been proposed in order to simulate fasted and fed physiological conditions of the GI tract. Biorelevant media that simulate fasted conditions were subject of this review. The Fasted State Simulated Gastric Fluid (FaSSGF) (Table 5) was developed by Vertzoni *et al*. to reflect the actual gastric composition in the fasting state according to published physiological data (152). This medium contains physiologically relevant amounts of pepsin and bile salts generating a surface tension close to that found *in vivo*.

Table 5. Composition of the Fasted State Simulated Gastric Fluids (152).

Fasted State Simulated Gastric Fluids (152)	
Sodium taurocholate (µM)	80
Lecithin (µM)	20
Pepsin (mg/ mL)	0.1
Sodium chloride (mM)	32.4
Hydrochloric acid *qs*	pH 1.6
pH	1.6
Osmolality (mOsmoL/kg)	120.7±2.5
Surface tension (mN/m)	42.6

2.5.2.2 Small intestine

In 1998, Dressman and co-workers developed Fasted State Simulated Intestinal Fluid (FaSSIF) to simulate fasting conditions in the small intestine (153). This medium has shown to provide a more accurate simulation of pharmacokinetic profiles than SIF (154, 155). The differences in the composition were due to the presence of mixed micelles formed by addition of bile salts (sodium taurocholate) and lecithin and the changes in surface tension, pH and osmolality values. These changes helped to simulate better physiological environment in the GI tract (Table 6). The FaSSIF – V2 media prior to addition of bile salts and lecithin is referred to as blank FaSSIF –V2.

Table 6. Composition of medium simulating fasted conditions of small intestine (153).

FaSSIF	
Sodium taurocholate (mM)	3
Lecithin (mM)	0.75
Dibasic sodium phosphate (mM)	28.65
Sodium hydroxide (mM)	8.7
Sodium chloride (mM)	105.85
pH	6.5
Osmolality (mOsmoL/kg)	270 ± 10
Buffer capacity (mmoL/L/ΔpH)	12

As further data on characterisation of *in vivo* gastrointestinal contents were published, the composition of FaSSIF was revised and updated (Table 7). Jantratid *et al.*, have modified the composition of FaSSIF by reducing the amounts of lecithin from 0.75 mM in FaSSIF to 0.2 mM in FaSSIF-V2 (156). The ratio of mixed micelles formed of sodium taurocholate to lecithin was changed in these media from 4:1 to 15:1, respectively. Moreover, maleate buffer was used instead of phosphate buffer. These changes resulted in a decrease in osmolality values of FaSSIF-V2. It is worth noting that the surface tension of both FaSSIF and FaSSIF-V2 are much higher than the surface tension of human intestinal fluids (HIF) (54 vs. 33.6 mN/m) (150).

Table 7. Composition of the medium to simulate the contents of the small intestine in the fasted state (157).

	FaSSIF-V_2 (157)
Sodium taurocholate (mM)	3
Lecithin (mM)	0.2
Glyceryl monooleate (mM)	-
Maleic acid (mM)	19.12
Sodium hydroxide (mM)	34.8
Sodium chloride (mM)	68.62
pH	6.5
Osmolality (mOsmoL/kg)	180±10
Buffer capacity (mmoL/L/ΔpH)	10
Surface tension (mN/m)	54

2.5.2.3 Large intestine

Fotaki *et al.* proposed Simulated Colonic Fluids (SCoF) that mimics the pH and buffer capacity of the colonic environment (158). In 2010, Vertzoni *et al*. proposed the composition of Fasted State Simulated Colonic Fluid (FaSSCoF) that were designed to reflect fluids collected from the ascending colon in healthy adults (Table 8) (159). It has been reported that FaSSCoF more closely predict solubility of poorly soluble compounds in human colonic fluids (HCF) than plain buffers (159). However, none of the media contain colonic bacteria as it is challenging to simulate anaerobic environment (149).

Table 8. Composition of media simulating conditions in colon.

	SCoF (158)	FaSSCoF (159)
TRIS (g)	-	5.5
Maleic acid (g)	-	8.8
0.5N Sodium hydroxide (176)	-	240
Sodium hydroxide (mM)	157	-
Ox bile salt extract (g)	-	0.113
Phosphatidylcholine (g)	-	0.222
Palmitic acid (g)	-	0.026
Dichloromethane (177)	-	6
Bovine serum albumin (g)	-	3
Acetic acid (mM)	170	-
pH	5.8	7.8

2.6 Comparison of dissolution profiles

Characterization of dissolution profile is recommended in cases described in Table 9. Numerous mathematical approaches for the comparison of dissolution profiles have been described in the literature (160-169).

Table 9. Areas where characterization of dissolution profiles is recommended (165).

Recommended case
Establishing the Quality of ER drug products
Defining dissolution specifications for generic formulations
Waiving bioequivalence requirements for lower strengths of an IR formulation
Point-to-point *in vitro-in vivo* correlations
Predicting the entire *in vivo* plasma profile based on dissolution data
Establishing IR and MR products sameness after level 2 and 3 post approval changes

2.6.1 Model-independent methods

There are two commonly used indices: the difference factor (f_1), the similarity factor (f_2) (160). The difference factor f_1 is the sum of the absolute values of the vertical distance between the test and the reference mean values at each dissolution time point and is defined by the following equation:

$$f_1 = 100\left[\frac{\sum_{i=1}^{n}|R_i - T_i|}{\sum_{i=1}^{n} R_i}\right] \qquad \text{(Equation 7)}$$

Where R_i and T_i are the percentage dissolved of the reference and test profiles at the i time point, respectively. When f_1 is equal to zero this indicates that two profiles are identical.
Additionally, f_1 can be modified in order to quantify areas between two profiles and then is known as $f_{1,\,area}$ (Equation 8) (167).

$$f_{1,area} = \frac{\int_0^{\tau}|R_i - T_i|dt}{\int_0^{\tau} R_i dt} \qquad \text{(Equation 8)}$$

Where τ represents time intervals between sampling time points.

The similarity factor f_2 measures the similarity in the percentage dissolution between two profiles and is defined by the following equation:

$$f_2 = 50\log\left[100\left(1/\sqrt{1+\frac{1}{n}\sum_{i=1}^{n}\left(R_i - T_i\right)^2}\right)\right] \qquad \text{(Equation 9)}$$

Where n is the number of the time points considered in comparison. The similarity factor fits the result between 0 and 100 with 100 to indicate that the two profiles are identical. The FDA suggests that the two dissolution profiles are similar when f_2 is between 50 and 100 (160-162, 164-167).

When data have low variability (%CV < 15), mean profiles can be used. Coefficient of variation (CV) should not then exceed more than 20% at early time points and no more than 10% at other time points (101). Number of replicates plays an important role in the selection of an appropriate index. For instance, all three indices can be used for data sets with only three replicates; however, confidence intervals must be determined (167). At least four equally spaced data points should be used for both indices, and only one after 85% dissolution of the test of reference (whichever occurs first) should be used (170). The main advantages of these indices are that they are easy to compute and result in a single number that describe the comparison of two dissolution profiles (169). However, several disadvantages have been identified such as shape of the curve, unequal spacing between the sampling points.

2.6.2 Dissolution kinetics

Over the last two decades different models have been proposed to aid characterization of dissolution profiles. These models are able to characterize parameters that for instance can define shape, plateau and kinetics of dissolution (166). Zero-order, first-order and 3-parameter Weibull function will be described in the following section.

2.6.2.1 Zero-order kinetics

Zero-order kinetics is often used to describe dissolution of modified release dosage forms such as matrix tablets or osmotic systems that do not disintegrate and release the drug slowly (166).

$$W_t = k_0 t \qquad \text{(Equation 10)}$$

Where W_t is the amount of drug dissolved in time t and k_0 is the zero – order release/dissolution constant. The formulations that follow zero-order kinetics release constant amount of drug per unit of time. The plot of % cumulative of drug dissolved *versus* time results in a straight line. This is an ideal method of drug release in order to achieve a pharmacological prolonged action (171).

2.6.2.2 First-order kinetics

Many water soluble drugs follow first-order kinetics described below (166).

$$W_t = W_{\max}(1 - e^{-k_1 t}) \qquad \text{(Equation 11)}$$

Where W_{max} is maximal amount of drug dissolved and k_1 is the first-order release/dissolution constant.

2.6.2.3 Weibull distribution function

The Weibull function is very useful models for describing drug dissolution data (169). It can be successfully applied to most of dissolution curves. It combines the advantages of both first-order and log-normal presentation (172). The Weibull function can be written in several ways. The Equation 12 describes the 3-parameters Weibull used in this thesis:

$$W_t = W_{\max} * \left(1 - e^{-\frac{(t \wedge \beta)}{\alpha}}\right) \qquad \text{(Equation 12)}$$

where W_{max} is the maximal percentage of the drug dissolved, α is the time scale parameter, which provides information about the rate of the process (173). Scale parameter (α) represents the time interval necessary to dissolve or release 63.2% of the drug. β is the shape parameter (when $\beta = 1$ the curve is exponential; $\beta > 1$ the curve is S-shaped with upward curvature followed by a turning point; $\beta < 1$ parabolic with a higher initial slope. Applying the Weibull equation to highly variable data or to not well characterized dissolution curves (limited number of dissolution points) can lead to over-parameterization of Weibull model (173).

3 Oral drug absorption and *in vitro – in vivo* correlations (IVIVC)

3.1 Factors affecting oral absorption

Gastrointestinal absorption of drugs is a complex process and is affected by many factors that fall into three categories (174). The first category represents physicochemical parameters of the drug such as pK_a, solubility, stability, diffusivity and lipophilicity. The second category consists of physiological factors of the GI tract such as gastrointestinal pH, gastric emptying, active transport and efflux, small and large intestinal transit time as well as gut metabolism. The last category comprises of formulation related factors such as drug particle size, crystal form, surface area and type of dosage form (tablet, capsule, solution, suspension *etc*.) (175). This review will focus on a description of the absorption limiting factors after oral administration.

3.1.1 Physicochemical parameters

Solubility and intestinal permeability are important physicochemical parameters that affect the rate and extent of absorption of an oral drug product. Moreover, these two factors also closely interrelate with many other influential factors, such as lipophilicity, hydrophilicity and molecular size (175).

3.1.1.1 Solubility

The pH-dependent solubility and stability of a drug plays an important role in its absorption. In order to permeate across the biological membrane, drug must be in a solubilised, stable and unionised form (175). Differences in regional pH can affect solubilisation or provide an environment for degradation of the drug (176). This is why understanding the ionization properties of a drug candidate are essential for the absorption potential. Most of drugs are weakly acidic or weakly basic compounds that cannot be ionized completely in aqueous media. Dissolution of ionised drugs is greatly dependent on the pH of the medium. The Henderson – Hasselback equation describes the relationship between pH and drug ionization for weak acids and weak bases (177):

Weak acids: $$anti\log(pH - pK_a) = \frac{[ionized]}{[un-ionized]}$$ (Equation 13)

$$\%un-ionized = \frac{100}{1 + anti\log(pH - pK_a)}$$ (Equation 14)

Weak base:

$$anti\log(pK_a - pH) = \frac{[ionized]}{[un-ionized]}$$ (Equation 15)

$$\%un-ionized = \frac{100}{1 + anti\log(pK_a - pH)}$$ (Equation 16)

According to Equation 13, weak acids solubilise in basic pH, when the drug exists in an ionized form, and hardly solubilise in an acidic environment while remaining in the un-ionized form (178). On the other hand, weakly basic compounds exist in their ionised form in lower pH, where they solubilise better and tend to have a minimal dissolution in higher pH (Equation 15). In the case of poorly soluble weak acids such as Indomethacin, dissolution in the stomach will be negligible. However, the small intestine with its high pH offers a better environment to Indomethacin, resulting in greater dissolution. Thus, for weak acids, the longer exposure to acidic environment is disadvantageous, thus gastric emptying is the absorption rate – limiting step. On the other hand, poorly soluble weak bases dissolve more readily in the stomach than in the intestine. This can result in supersaturation as the drug moves from acidic to basic conditions. Upon the movement to basic pH, the degree of ionisation and equilibrium solubility are reduced causing supersaturation of the drug (179).

3.1.1.2 Permeability

Permeability of the drug through an intestinal membrane is an important factor in achieving desirable bioavailability of a drug after oral administration. There are two types of transport across the intestinal membrane. The first, describes the passive diffusion across lipid membrane often referred to as transcellular absorption (180). The second is known as paracellular absorption and is described as diffusion through the aqueous pores at the tight junctions between the cells (181). The ability of drug to diffuse across the lipid core of the membrane depends on the physicochemical properties of the compound such as lipophilicity.

Lipophilic compounds permeate through the intestinal membrane more readily than poorly lipophilic compounds. This explains why transcellular transport is the predominant pathway for more lipophilic drugs (182). On the other hand, paracellular transport is favoured by hydrophilic compounds.

3.1.2 Physiological parameters

The absorption process depends on a large number of factors that are related to the physiology of the GI tract, such as composition of the GI fluids, gastric emptying, transit time across intestinal segments, and passage of the drug across the membrane *etc* (183).

3.1.2.1 Composition of the GI fluids

3.1.2.1.1 Stomach

Gastrointestinal fluid is a complex mixture of various components that originate from various sources within the GI tract. Stomach content is composed of saliva, gastric secretions, dietary food and liquid, and refluxed fluids from the duodenum (184). Major components of the gastric fluids include hydrogen ion concentration, which are responsible for the acidic environment; pepsin, an enzyme that aids digestion; lipase, which aids the release from lipid-based dosage forms (185-187); and bile salts that decrease the surface tension of the fluids, which enhances solubility (Table 10). Also, bile salts combined with lipids form micelles, improving the solubility of poorly soluble drugs (188). Quantification of these components *in vivo* is very challenging due to inter-individual variability. For instance, Kalantzi *et al*. reported stomach pepsin levels during the fasted state in a range from 0.11 to 0.22 mg/mL, whereas other researchers have found them to vary between 0.1 to 1.3 mg/mL (186,187, 189). This may be due to the type of analytical method used. Some of the reported research was carried out over four decades ago, when the sample collection, treatment and quantification methods may have been less advanced.

Table 10. Concentrations of components present in stomach during fasted and fed states.

Components	State	Reported range
Pepsin	Fasted state	0.11 – 0.22 mg/mL (189) 0.1 – 1.3 mg/mL (186,187)
	Fed state	0.26 – 1.72 mg/mL (187)
Hydrogen ions	Fasted state	0.01 – 0.1 M (pH 1 – 2) (184)
	Fed state	0.0000001 M – 0.001 M (pH 3 – 7) (184)
Lipase	Fasted state	0.1 mg/mL (152)
	Fed state	11.4 – 43.9 U/mL (188)
Bile salts	Fasted state	0.08 – 0.275 mM (152, 189)
	Fed state	0.06 mM (190)
Bicarbonate	Fasted state	7 – 20 mequiv/L (191, 192)

3.1.2.1.2 Small intestine

The upper small intestine fluids are composed of the chyme from the stomach as well as secretions from different parts of body including the liver (bile salts, phospholipids, bicarbonate, and cholesterol), the pancreas (bicarbonates, proteases) and the wall of the small intestine (bicarbonates, sodium, chlorides, water). Its composition is affected by fluid segmentation, absorption of fluid into the wall and transit down the intestinal tract (Table 11). The wide range of the data reported in Table 11, could be attributed to the use of different sampling and analysis techniques as well as various equipment used. Some of the data were reported as far back as 1973.

Table 11. Concentrations of components present in the small intestine during fasted and fed states.

Components	State	Reported range
Lipolytic products (*i.e.* monoglycerides)	Fasted state	0 – 1.8 mg/mL (193)
	Fed state	0.5 – 100 mg/mL (188, 193)
Phospholipids	Fasted state	0.03 – 0.6 mM (193, 194)
	Fed state	0.8 – 2.4 mM (123)
Bile salts (ileum)	Fasted state	2 – 10 mM (195)
	Fed state	0.2 – 30 mM (196)
Bicarbonates	Fasted state	in the duodenum and jejunum 2 – 30 mM (197, 198) in the ileum 30 – 75 mM (198, 199)

3.1.2.1.3 Large intestine

The large intestine is about 152 cm in length and average 6.3 cm in diameter. It is divided into four principal regions: caecum, colon, rectum and anal canal. The absorption of water is an important function of the large intestine. In addition, absorption of vitamin K, biotin and vitamin B_5 occurs in the colon (200). Despite the fact that transit through the lower part of the GI tract is claimed to last for 24 hours, the colonic environment only the ascending part of colon has fluid to facilitate dissolution (200). Composition of colonic fluids is affected by feeding (Table 12).

Table 12. Concentrations of components present in the colon during fasted and fed states.

Parameters	**State**	**Reported range (149)**
Proteins	Fasted state	9.7 ± 4.6 mg/mL
Carbohydrates	Fasted state	8.1 ± 8.6 mg/mL
	Fed state	14.0 ± 7.4 mg/mL
Acetate levels	Fasted state	20.8 ± 11.6 mM
	Fed state	35.9 ± 14.0 mM
Short chain fatty acids	Fasted state	30.9 ± 15.4 mM
	Fed state	48.1 ± 21.7 mM
Bile acids	Fasted state	115.2 ± 119.3 µM
	Fed state	587.4 ± 412.8 µM
Palmitic acid	Fasted state	49.6 ± 43.7 µM
	Fed state	103.8 ± 112.1 µM
Linoleic acid	Fasted state	37.4 ± 29.6 µM
	Fed state	47.8 ± 30.0 µM
Oleic acid	Fasted state	32.8 ± 36.7 µM
	Fed state	73.4 ± 81.7 µM
Phosphatidylcholine	Fasted state	362 ± 210 µM
	Fed state	539 ± 393 µM

3.1.2.2 Characteristics of GI fluids

Parameters such as the pH, buffer capacity, osmolality, surface tension, volume and temperature of the gastrointestinal fluids affect the *in vivo* performance of the pharmaceutical oral dosage forms (Table 13). For instance, different levels of buffer capacity can affect the dissolution rate of ionisable drugs (201). The general trend is that the higher the buffer capacity, the more the buffer will influence pH changes at the drug – fluid interface (184, 202). The pH of the fluid, the pK_a of the individual components of the buffer and its concentration affect buffer capacity the most. Osmolality proved to affect drug release and excipients performance (156). For instance, common ion effect can result in slower dissolution (156, 203). Surface tension may affect dissolution by influencing wetting properties of the formulation (185), with a lower surface tension leading to enhanced wetting. Bile salts such as sodium taurocholate and phospholipids that are present in GI fluids affect the contact angle of the drug and lower the surface tension. The volume of the fluids in the gastrointestinal tract affects the concentration of solubilised drug which often may limit the absorption. The temperature is probably the most stable of all parameters in human body. The only time when the temperature can fluctuate is generally during exercise (204). Temperature can also affect the diffusion coefficient of the drug and the solubility of the API and the formulation.

Table 13. Parameters affecting *in vivo* performance of dosage forms.

Parameters	**State**	**Reported range**
pH	Fasted state	Stomach 1 – 8 (205, 206) 1.2 – 3.5 (183) 1.5 – 3 (207)
		Duodenum 6.1 – 7.0 (193)
		Jejunum 4.4 – 8.1 (208, 209)
		Ileum 6.5 – 8 (210, 211)
		Colon 7.8 (149)
	Fed state	Stomach 6 -7 (208) 2 – 5 (207) 2.7 - 6.4 (148, 208)
		Duodenum 3.1 – 6.7 (208)
		Jejunum 5.2 – 6.0 (212)
		Ileum 6.8 – 8.0 (213)

		Colon 6.0 (149)
Osmolality	Fasted state	Stomach 29 – 276 mOsm/kg (214, 215)
		Upper small intestine 124 – 278 mOsm/kg (204, 216)
		Colon 81 mOsm/kg (217)
	Fed state	Stomach 559 mOsm/kg 30 min after meal (148) 217 mOsm/kg 210 min after meal (148)
		Small intestine 250 – 367 mOsm/kg (204)
		Colon 99 – 349 mOsm/kg (149)
Surface tension	Fasted state	Stomach 41 – 46 mN/m (148)
		Upper small intestine 28 – 46 mN/m (193, 218)
		Colon 42.7 mN/m (217)
	Fed state	Stomach 30 – 31 mN/m (148)
		Upper small intestine 27 – 37 mN/m (193, 218)

3.1.3 Gastric motility

3.1.3.1 Migrating motor complex (MMC)

The MMC occurs during fasting state and it is divided into different phases: basal (Phase I), pre-burst (Phase II), burst (Phase III) and transition (Phase IV) intervals (183). Phase I is characterized by a lack of secretory, electrical and contractile activity which lasts from 30 to 60 minutes. In Phase II contractile motions increase in frequency and exhibits intermittent action for 20 to 40 minutes. During this phase bile enters duodenum and mucus is discharged. Phase III continues mucus discharge and is characterised by intense, regular contractions known as housekeeper waves, which sweep off undigested food and last 10 to 20 minutes. Finally, Phase IV is the transition period between Phase I and Phase III and lasts up to five minutes (183).

3.1.3.2 Gastric emptying time

Gastric emptying (GE) is influenced by various physiological and pathological factors, drug delivery system properties, and most of all, by food intake (183). Emptying of the stomach under fasting and fed conditions is subject to MMC, during which the short lasting intense contractions (Phase III) cause the emptying of the stomach content (184). Gastric emptying is a highly variable parameter that is not only varied between the subjects (inter – variability) but also within the same subject (intra – variability) on different days (219). It was found that

formulation characteristic can significantly affect GE time. In the case of the non-disintegrating tablets, different tablet size affects gastric emptying time (220, 221). For instance, Khosla and Davis observed that the shortest gastric emptying time for 7 mm tablets (116 ± 19 min), followed by 11 mm tablets (128 ± 17 min) and 13 mm tablets (171 ± 13 min) (221). On the other hand, the same studies performed using floating systems indicated no statistically significant difference in GE time among different dosage form sizes (221).

3.1.3.3 Transit time

Yu *et al*. have examined small intestine transit times of over 400 volunteers and reported the mean transit time of 3.3 hours (174). They also determined that the seven compartment transit model best described the small intestine passage (Figure 17). The first half of the first compartment represents the duodenum, the second half of this compartment together with the second and third compartment represent the jejunum, and the rest of the compartments represent the ileum. The corresponding transit times in the duodenum, jejunum, and ileum are 14, 71 and 114 min, respectively (174). To complete the model, two additional compartments are taken into account to represent the stomach and colon, making a total of nine compartments.

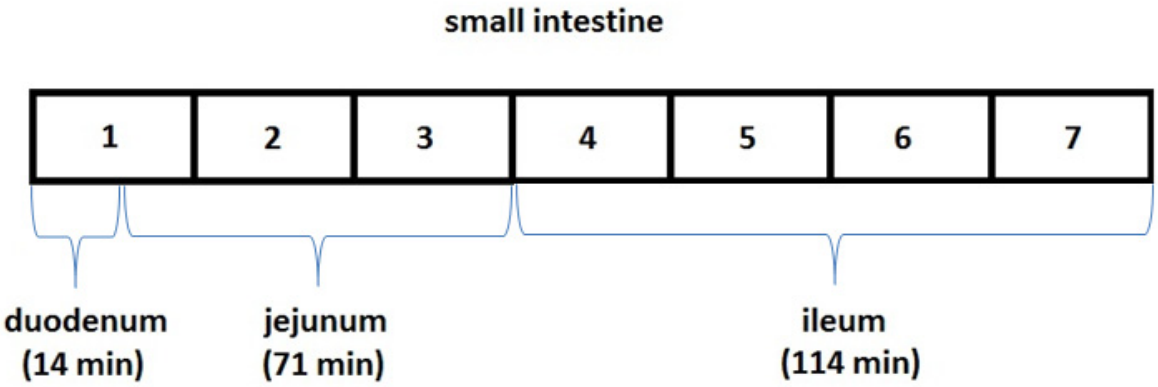

Figure 17. Schematic diagram of 7 – compartments model (174).

3.1.4 Formulation parameters

Physicochemical, physiological and formulation parameters strongly influence each other. For instance, different dosage forms are characterised by different transit times across the segments of the GI tract (Table 14) (183).

Table 14. . Small intestine transit time reported for different dosage forms in fasted state (184)

Formulation	Time (min)
coated pellets	90-324
pellets	132-154
tablets	54-372

Generally, absorption from oral solution is a rapid and complete process when compared with other orally administered dosage forms. Poorly soluble drug can be formulated as a suspension in order to improve bioavailability. Capsules and tablets can provide similar dissolution performance; however its behaviour strongly depend on many variables such compression forces, excipients choice, surface area, particle sizes *etc*. Various excipients can be used to in order to produce desired dissolution profiles. For instance, disintegrants such as lactose helps to break the tablet apart. Wetting agents such as SLS can be added to the formulation to aid the penetration of water into the tablets. Immediate – release formulations are designed to be absorbed quickly, whereas prolonged – release formulations are intended to release larger dose (than IR) for a much longer time. Despite that larger dose is introduced at once, controlled mechanism allows to release amounts below toxic level.

3.2 IVIVC

Development of a pharmaceutical dosage form requires a good understanding of the *in vitro* and *in vivo* performance of the formulation. Correlating *in vitro* drug data with *in vivo* drug performance still remains a challenge. The following sections will focus on development of IVIVC and its applications.

3.2.1 Definitions

The USP and the FDA proposed definitions of IVIVC:

3.2.1.1 USP definition

The establishment of a rational relationship between a biological property, or a parameter derived from a biological property produced by a dosage form, and a physicochemical property or characteristic of the same dosage form (222).

3.2.1.2 FDA definition

IVIVC is a predictive mathematical model describing the relationship between an in vitro property of a dosage form and a relevant in vivo response. Generally, the in vivo property is the rate or extent of drug dissolution or release while the in vivo response is the plasma drug concentration or amount of drug absorbed (223).

3.2.2 Levels of IVIVC

FDA has defined four correlation levels (A, B, C and Multiple C) which reflect the type of the correlation. Each level correlates to different types of parameters. For the purpose of this thesis Level A correlation will be described in details.

Level A correlation

This level represents a point-to-point relationship between *in vitro* dissolution and the *in vivo* input rate of the drug from the dosage form (223). Generally, percent of the drug absorbed (or cumulative amount absorbed) may be calculated using model-dependent techniques such as Wagner-Nelson method for one-compartmental model drugs (224) or Loo-Riegelman method for two-compartmental model drugs (225) or by model-independent numerical deconvolution (226). Good understanding of the drug's pharmacokinetics is essential for appropriate use of

deconvolution techniques. Level A correlation describes a direct relationship between *in vivo* data such that the measurement of *in vitro* dissolution rate alone is sufficient to determine *in vivo* performance of this dosage form (227). Visualization of the dissolution and absorption profiles together, which assesses the degree of superimposition, is an important part in development of Level A correlation (228). Failure to superimpose them may not warranty the successful correlation; however, further attempts can be made by developing a dissolution method, which will mimic the *in vivo* performance closely. Sometimes the profiles are superimposed but a lag time can be observed. In this case, more quantitative correlations such as linear regression need to be explored (229, 230). The aim of an IVIVC should be establishing a relationship between *in vivo* behavior of a formulation and *in vitro* performance of the same formulation, which would allow *in vitro* data to be used as a surrogate for *in vivo* performance (227, 231). Level A is the most useful and informative from the regulatory point of view. It can be used to predict entire *in vivo* performance from the *in vitro* data. Once IVIVC is successfully developed, the validation of the model is required. According to FDA guidelines, two types of validation approaches are available: internal and external (223). The former, is accomplished by measuring predictability error (*%PE*) of data that has been employed for development of this certain IVIVC model. The latter uses different sets of data to test how well the developed IVIVC is able to predict additional data sets based on *%PE* calculation (Equation 17) (223, 232). Internal predictability should be applied where IVIVC was developed using two or three formulations with different release rates (223). External predictability should be adopted when two formulations with different release rates were used for IVIVC development (227). External validation is recognized as a better tool than internal validation. *% PE* below 10 % indicates good predictability of C_{max} and *AUC* values (230).

$$\%\ PE = [(Observed\ value - Predicted\ value)/Observed\ value] \times 100 \quad \text{(Equation 17)}$$

It is worth noting that Level A IVIVC can also be obtained through convolution techniques, in which the *in vitro* dissolution profile is used to generate the corresponding plasma concentration profile. This profile is further compared with observed plasma concentration profiles (230).

3.2.3 Applications

IVIVC can be used for several purposes. During the formulation development process, alterations are introduced that involve *i.e*. composition, manufacture or equipment changes. Generally, these types of changes require additional clinical trials to prove bioequivalence of new product with the original formulation. However, in this case, if IVIVC is successfully developed it can be used to replace human studies. IVIVC serves as surrogate for *in vivo* bioavailability and to grant a biowaiver. It also aids to set dissolution specifications. IVIVC is an excellent tool in quality control (QC) to monitor certain scale-up and post-approval changes (SUPAC) (223, 227).

IVIVC is established for modified release (233-237) dosage forms where the drug release is a rate limiting step during the absorption process (227). Attempts at the development of IVIVC for immediate-release (IR) were also made (238-240). Development of IVIVC for IR formulation is more challenging. There is no official regulatory guidance for development of IVIVC for IR dosage forms. Normally, IVIVC is expected for highly permeable drugs, as in this case absorption is not limited by the permeability. Also, dissolution must be the rate-limiting step. For instance, IVIVC for IR formulation of highly water soluble drug (BCS class I or class III) may not be possible, because dissolution occurs too fast and gastric emptying or membrane permeation is usually the rate – limiting step (241).

Biopharmaceutical Classification System (BSC) became a very useful tool that helps to categorize drugs according to their intestinal permeability and solubility characteristics as well as allowing estimation of IVIVC (242). Generally, BCS classifies drugs into four categories (Figure 18).

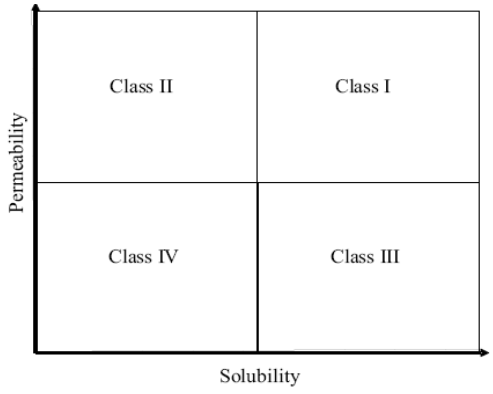

Figure 18. Biopharmaceutical classification of drugs (1).

Compounds with high solubility and permeability values belong to Class I, whereas those characterized by low solubility and high permeability fit in Class II. Class III and Class IV includes drugs with low permeability but high and low solubility, respectively. The BCS classification is used to predict *in vivo* performance of dosage forms based on their permeability and solubility characteristics (1). It is adopted by many regulatory bodies as a tool that allows grant biowaivers for IR formulations with wide therapeutic windows. BCS assists also in prediction if IVIVC is expected (Table 15) (227).

Table 15. BCS and expected IVIVC for IR products (241).

Class	**I**	**II**	**III**	**IV**
Solubility	High	Low	High	Low
Permeability	High	High	Low	Low
IVIVC	Correlation (if dissolution is rate – limiting step)	IVIVC expected	Little or no IVIVC	Little or no IVIVC

According to Table 15, IVIVC is usually expected for IR formulations that belong to Class I (if dissolution is slower than absorption) and Class II compounds (241).

3.3 Development of IVIVC

3.3.1 Traditional IVIVC

3.3.1.1 Model-dependent method

3.3.1.1.1 Wagner-Nelson method

In the absence of intravenous or oral solution data, the apparent *in vivo* cumulative absorption profile can be deconvoluted from data obtained from orally administered dosage forms using model-dependent Wagner-Nelson deconvolution technique (224, 243). This approach is derived from a one-compartmental model and the mass balance (Equation 18):

$$X_a = X_t + X_e \qquad \text{(Equation 18)}$$

Where X_a, X_t and X_e are amounts of drug absorbed, in the "body", and eliminated at time *t,* respectively (244).

In order to calculate the amount of drug absorbed up to time T, $(X_a)_T$ the equation has to be further derived as follows:

$$(X_a)_T = VC_T + kV\int_0^T Ctdt \qquad \text{(Equation 18)}$$

Where V is the volume of the central compartment, C_T is concentration of the drug in the central compartment at time T and k is the first-order elimination rate constant. In IVIVC terms, this equation is often expressed in terms of fraction (F) of the dose (D) absorbed (Equation 20). Fraction of the dose absorbed is then compared with fraction released *in vitro* (227).

$$F_a(T) = \frac{(X_a)_T}{(X_a)\infty} = \frac{C + k\int_0^T Ctdt}{k\int_0^\infty Ctdt} \qquad \text{(Equation 19)}$$

$F_a(T)$ or FD is the fraction of the bioavailable drug absorbed at time T.

Equation 20 is frequently applied to extravascular data in the case of absence of intravenous data in IVIVC modeling. According to the above formula, the apparent *in vivo* fraction absorbed can be estimated from terminal phase elimination rate constant k and partial AUC (232).

Deconvoluted data are then either superimposed with the fraction released profile or linear regression between fraction absorbed and fraction released is applied to establish the correlation. Correlated data can be validated using external or internal predictability error.

3.3.1.2 Model-independent method

3.3.1.2.1 Numerical deconvolution

For cases when clinical data for intravenous or oral solution formulations are available, numerical deconvolution can be applied in order to develop an IVIVC. Softwares such as PCDCON generate deconvoluted profiles (245). Deconvolution involves estimating the rate at which a drug dissolves *in vivo* using the observed *in vivo* (either IR or ER) data, which contains information on dissolution, absorption, distribution, metabolism and excretion of the

drug and reference *in vivo* observed data (which does not involve dissolution). Mathematically, deconvolution can be expressed using convolution integral (227):

$$C(t) = C_{\delta}(t) * f(t) = \int_0^t C_{\delta}(t-u) f(u) du \qquad \text{(Equation 20)}$$

Where *C(t)* is called input response and defines function for any measurable quantity that is a direct result of input (*i.e*. plasma concentration from orally administered drug) (227, 244). δ is unit impulse, which determines unit dose of any amplitude and zero duration such that integral of $\delta(t)$ is equal one. This function describes distribution and elimination phases, respectively. Thus, $C_{\delta}(t)$ is a function known as unit impulse response that describes the cumulative effects of response changes, following all previous drug input $f(t_{0\ to\ t})$ at time *t*. Unit impulse dose can be illustrated by concentration at time *t* following unit i.v. bolus dose (245). Input rate *f(t)* is a function that determines the rate at which drug is absorbed.

As input rate *f(t)* is unknown, Equation 21 requires conversion in order to be able to perform deconvolution:

$$f(t) = \frac{C(t)}{C_{\delta}(t)} \qquad \text{(Equation 21)}$$

The deconvolution result can be also expressed in terms of cumulative input $X_{in}(t)$:

$$X_{in}(t) = \int_0^t f(u) du \qquad \text{(Equation 22)}$$

Where *f* defines drug absorption rate and X_{in} cumulative amount absorbed.

PCDCON software uses inverse Laplace transform, which means that Equation 20 is reversed (Equation 24) (244). Once deconvoluted *in vivo* data are obtained, the attempt of establishing an IVIVC can be undertaken.

$$F_a(T) = \frac{k\int_0^{\infty} Ctdt}{C + k\int_0^{T} Ctdt} \qquad \text{(Equation 23)}$$

A deconvolution – based IVIVC is also known as two stage approach as involves estimation of the *in vivo* release/absorption profile from plasma concentration data using deconvolution technique (232). The deconvoluted profile is then assessed and validated by comparing the

predicted with observed plasma profiles. A simple linear model (Equation 25) with intercept (a) and slope (b) can be applied to define IVIVC:

$$\text{fraction absorbed}_{invivo} = a + b^{*} \text{ fraction dissolved}_{invitro} \qquad \text{(Equation 24)}$$

A slope closer to 1 indicates 1:1 correlation and a negative intercept implies that the *in vivo* process is slower than *in vitro* dissolution (or otherwise depending on the selection of axis). In the cases when *in vitro* and *in vivo* profiles exhibit different rates and/or difference in the starting of a phenomenon or difference in the lag time, various scaling factor can be applied to achieve 1:1 correlation (249). For instance, a Levy plot is one type of scaling technique (247). This plot is generated by fitting the time at which certain amount (*i.e*. 5, 10, 15 mg *etc.*) of the drug dissolved *in vitro* on the X-axis against the time to absorb the same amount of drug *in vivo.* This allows assessing the time scale and shifting differences between *in vitro* dissolution and *in vivo* absorption (227). A straight line will be observed if a similar process is observed between *in vivo* and in *vitro data*. Otherwise, turning point in the Levy plot can be observed (246). Turning point indicates at which time point the data start to diverge.

If dissolution performance is independent of dissolution conditions such as pH, surfactants, enzymes and ionic strength, then the result for a single formulation may be sufficient. Otherwise, at least two formulations with release rate differing by 10% should be tested (223).

It is important to select adequate bioavailability studies for the development of IVIVC. Crossover studies involving 6 to 36 subjects are preferred. Parallel studies or cross-study may be acceptable (223). The reference product for developing an IVIVC should be an intravenous solution or aqueous oral solution under fasted conditions. In the absence of intravenous solution or aqueous oral solution, IR formulations can be used.

3.3.2 PBPK models

Physiologically based pharmacokinetics (PBPK) models are comprised of mathematical models that integrate anatomical and physiological parameters of humans or animals, physicochemical properties of drug substances, and formulation properties of drug products to predict absorption, distribution, metabolism and excretion (ADME) of compounds *in vivo* (248-250).

3.3.3 Absorption models

Several physiologically based mathematical models have been described in the literature, some of which have become commercially available, such as GastroPlus™, PK-Sim® and Simcyp®.

3.3.3.1 CAT and ACAT

Yu and Amidon developed a compartmental absorption and transit (251) model to simulate the rate and extent of drug absorption. Initial CAT model was further developed to the Advanced CAT (ACAT) to take into account parameters such as dissolution rate, the solubility pH-dependence, controlled release, absorption in stomach and colon, gut and liver metabolism and degradation *etc.* (Table 16) (249). This theory is implemented in GastroPlus™ software.

Table 16. Detailed characteristics of the GI tract (184).

Section	Average length (cm)	Diameter (cm)	pH	Villi present	Transit time (h)
Oral cavity	15-20	10	5.2-6.8	Absent	Short
Esophagus	25	2.5	5-6	Absent	Very short
Stomach	20	15	1.2-3.5	Absent	0.25-3
Duodenum	25	5	4.6-6.0	scarcely present	0.23
Jejunum	300	5	6.3-7.3	abundantly present	1.18
Ileum	300	2.5 -5	7.6	abundantly present	1.9
Caecum	10-30	7	7.0-8.0	scarcely present	short
Colon	150	5	6.1-7.3	absent	variable

3.3.3.2 ADAM model

Advanced Dissolution, Absorption and Metabolism (252) model is implemented in Simcyp® software. According to the ADAM model, the GI tract is divided into nine segments from the stomach through the intestine to the colon (250, 252). Each segment has its specific characteristics in terms of pH, length, transit time *etc*. the model assumes that absorption from the stomach is minor (249). The ADAM model allows entering either raw dissolution data previously obtained experimentally or predicts dissolution based on various solubility values (pH profile, intrinsic solubility, values at certain pH) and particle size values (mean or distribution). One of the differences between the GastroPlus™ and the Simcyp® is the way

how dissolution data are predicted. The ADAM model uses the Wang-Flanagan model (253) (Equation 26), as opposed to the Noyes-Whitney equation (97, 254). When raw dissolution data are inserted into the ADAM model the effect of pH on solubility and supersaturation are not modelled implicitly (250).

$$\frac{dX}{dt} = -4\pi r^2(t) D\left(\frac{1}{r(t)} + \frac{1}{h}\right)\left(C_s - \frac{X_d}{V(t)}\right) \qquad \text{-}h = r \text{ of } r < 30\mu\text{m}; \text{ (Equation 25)}$$

$h = 30$ for $r > 30$ μm

Where dX/dt is the dissolution rate; r is time – varying particle radius; D is diffusion coefficient constant; h is diffusion layer thickness; C_s is the saturated concentration (solubility) at the interface between the solid and the solution; X_d is the amount of dissolved drug; V is fluid volume related to the segments in the GIT.

Simcyp® has several prediction tools built-in that help to estimate some parameters such as permeability, intrinsic solubility, diffusion coefficient, fraction of drug unbound to protein and many others. For instance, permeability value can be predicted from various studies such as cell monolayers (Caco-2, MDCK), artificial membranes (PAMPA) or just using physicochemical properties (255). Equation 27 is used to calculate the flux (J_{AB}) of compounds across the cell membrane (250).

$$J_{AB} = P_{eff,man} S(C_A - C_B) \qquad \text{(Equation 26)}$$

Where $P_{eff,\ man}$ (cm/h) is the effective permeability; S is the surface area available for absorption; C_A and C_B are compound concentrations on the apical and basolateral sides, respectively.

The relationship between measured values of human permeability in the jejunum for a range of drugs and the permeability values obtained experimentally *in vitro* allows estimation of $P_{eff,\ man}$ value. Based on the assumption that the absorption rate constant (k_a) in each segment is proportional to $P_{eff,\ man}$ values can be calculated using (174) Equation 28:

$$k_a = \frac{2P_{eff,man}}{R} \qquad \text{(Equation 27)}$$

Where R (cm) is the segment radius.

3.3.4 Applications

Originally, computational tools were used to support toxicology, safety and risk assessments at the early stage of drug discovery and development (256). Nowadays, computational techniques are used for other purposes such as absorption modelling at the early stage of drug discovery to aid with assessing a drug's potential for absorption as well as in the drug development stage to design dosage formulation and evaluate its behaviour *in vivo* (257). It allows shortening the time prior to new drug application (NDA) submission and reduces the number of experimental procedures required for compound selection and development (258, 259). PBPK models proved to be successful predictive tools in oncology and antibiotics areas as they allow the simulation of plasma concentration – time profiles within the targeted organ (260, 261). More often, PBPK modelling is used to obtain mechanistic insights into drug behaviour by characterising its pharmacokinetics and drug – drug interactions (262). Ability to select different populations allows predicting drug pharmacokinetics of paediatric formulations (263, 264). This feature allows predicting drug pharmacokinetics under different physiological and pathological conditions such as food effect, pregnancy, liver cirrhosis and others (265-267). PBPK can also monitor not only a parent drug but also its metabolite (268, 269). It can be clearly seen that PBPK is becoming more popular in the pharmaceutical field.

Aims and objectives

The general objective of this work was to develop an appropriate dissolution method that will allow the prediction of *in vivo* performance of pharmaceutical cocrystals.

In order to predict *in vivo* performance of cocrystals, the specific objectives of this work were to:

- characterise APIs and cocrystals in terms of their solubility and particle-size distribution,
- develop biorelevant dissolution methods to test commercial, API and cocrystal formulations,
- collect physicochemical and pharmacokinetic parameters for selected marketed formulations,
- develop IVIVC using both: traditional approaches such as deconvolution techniques and more sophisticated *in silico* tools such as PBPK modelling,
- predict *in vivo* performance of cocrystals using the developed PBPK models.

On the basis of the results of this work, it should be possible to assess if investigated pharmaceutical cocrystals enhance *in vivo* performance of selected poorly soluble compounds.

4 Experimental Part

4.1 Materials

Chemicals, samples and formulations used are listed in Table 17 and Table 19, respectively.

Table 17. List of chemicals used.

Material/Chemical name	Batch no./Lot no./Grade	Manufacturer/Supplier
Acetic acid ≥99.7%	09214CJ, SZBB2210V	Sigma-Aldrich (UK)
Bovine serum albumin (96%)	62828	Fisher Scientific (UK)
Dichloromethane	1020198	Fisher Scientific (UK)
Ethanol HPLC grade	SZBB0170V	Sigma-Aldrich (UK)
Hydrochloric acid (37%)	0925336	Fisher Scientific (UK)
Lecithin	563098-01/936	Lipoid (Germany)
Maleic acid	0065974, 1137140	Fisher Chemical (UK)
Methanol (HPLC grade)	Various	Fisher Scientific (UK)
Microcrystalline cellulose	Avicel PH 302/ 200/105	FMC BioPolymer (Belgium)
Nicotinamide	051M1837V	Sigma-Aldrich (UK)
Orthophosphoric acid	1001564	Fisher Scientific (UK)
Ox bile salt extract	LP0055	Oxoid (UK)
Palmitic acid	A0290542	Across Organics (UK)
Pepsin, from porcine gastric mucosa	030M1571V	Sigma-Aldrich (UK)
Potassium phosphate monobasic	091341A, 103498 080M0041	Fisher Scientific (UK). Sigma
Saccharin 98+%	A0259796	Acros Organics (UK)
Sodium acetate trihydrate	1142730	Fisher Chemical (UK)

Sodium chloride	0758662 BCBG4549V	Fisher Scientific (UK). Sigma-Aldrich
Sodium dihydrogen orthophosphate dihydrate	1133834	Fisher Chemical (UK)
Sodium dodecyl sulphate ≥99%	098K0067	Sigma-Aldrich (UK)
Sodium hydroxide	BCBC7310V	Sigma-Aldrich (UK)
Sodium taurocholate	2011040152	Prodotti Chimici E Alimentari S.P.A. (Italy)
Trifluoroacetic acid	BCBB2269	Sigma-Aldrich (UK)
Tris (hydrozymethyl)-aminomethane (TRIS)	A020562001	Acros Organics (UK)

Filters used and other materials are listed in Table 18 and Table 20.

Table 18. List of filters used.

Material	Grade	Manufacturer/Supplier	Application
Glass microfiber filters	GF/D (ø24 mm, 2.7 µm)	Whatman®, UK	Dissolution using USP Apparatus 4
Glass microfiber filters	GF/F (ø24 mm, 0.7 µm)	Whatman®, UK	Dissolution using USP Apparatus 4
Cellulose nitrate membrane filters	(ø13 mm, 0.45 µm)	Whatman®, Germany	Precipitation, and solubility studies; Dissolution studies using USP 1
Cellulose filters	Qualitative standard grade (ø 110mm)	Fisher Scientific, UK	Blend uniformity

Table 19. List of samples and formulations used.

Material/Chemical name	Batch no./Lot no./Grade	Manufacture/Supplier
Tegretol® PR tablets (400 mg)	U0281	Novartis Ltd (UK)
Tegretol® IR tablets (200 mg)	U0552	Geigy (UK)
Carbamazepine Standard (99% w/w), CBZ_{sp} (sp: sample powder)	A0272746	Acros Organics/Prosonix (UK)
CBZ-SAC_{ss} (ss: sonic slurry method)	PXLB 028-98C1 PXLB 045-60C1	Prosonix (UK)
CBZ-SAC_{umax} (umax: umax method)	PXLB 0280-98C1	Prosonix (UK)
CBZ-NIC_{ss} (ss: sonic slurry method)	PXLB 031-043-6-S PXLB 045-58C1	Prosonix (UK)
Indocid® capsules (25 mg)	K5895	MSD (Australia)
Indomethacin Standard (≥99% w/w), IND_{sp} (sp: sample powder)	1000573578	Sigma-Aldrich/ Prosonix (UK)
IND-SAC_{sd} (sd: spray-drying method)	PXLB 028-91A	Prosonix (UK)
IND-SAC_{ss} (ss: sonic slurry method)	N/A	Prosonix (UK)
IND-SAC_{umax} (umax: umax method)	028-102C1	Prosonix (UK)
IND-NIC_{ss} (ss: sonic slurry method)	N/A	Prosonix (UK)

N/A – not applicable

Table 20. List of materials used.

Material	Supplier	Applications
Centrifuge tubes	Corning Inc. New York, US	Solubility studies
Swinny stainless steel 13 mm filter holders	Millipore, Billerica, US	For filtration during solubility and USP 1 dissolution studies
Sampling cannulae for 500 mL	Varian, CA, US	For dissolution using USP 1 studies
Glasss syringe 5 mL with Luer -Lock	Fortuna® Optima®, Poulten & Graf Ltd, Essex, UK	For dissolution using USP 1 studies
Sieve 425µm		

4.2 Apparatus

A Vankel rotating basket dissolution system (model 10-1200, Edison, NJ, US) and an Erweka® flow-through dissolution tester (model DFZ720, Erweka GmbH, Heusenstamm, Germany) equipped with Ø 22.6 mm cells and connected to an Erweka® Piston Pump (model HKP720) were used.

The HPLC system consisted of an Agilent 1100 Quat pump, an Agilent 1100 DAD spectrophotometer, an Agilent 1100 ALS autosampler and ChemStation® software (Agilent Technologies, Santa Clara, US).

For Carbamazepine studies a Zorbax® Eclipse XDB C18, 5 µm, 250x4.6 mm (Agilent Technologies, US) column was used. For the detection of Indomethacin, Saccharin and Nicotinamide a Zorbax® SB-C18, 3.5 µm, 150x4.5 mm (Agilent Technologies, US) column was used.

Laser light diffraction (Helos, Sympatec, Clausthal-Zellerfeld, Germany), wet dispersing system (Cuvette®, Sympatec, Clausthal-Zellerfeld, Germany) and Windox 5.0 software (Sympatec, Clausthal-Zellerfeld, Germany) were used for particle-size distribution experiments.

A shaking water bath (model Grant SS40-2, Grant Instruments, Cambridge, UK) was used for solubility studies.

The thermal behaviour of solid phases was studied using differential scanning calorimetry (DSC) (TA Instruments 2920, New Castle, US).

A rotary evaporator (Buchi R-114, Buchi, Switzerland) equipped with water bath (Buchi B-480, Buchi, Switzerland) and vacuum pump (Vacuubrand CVC 2II, Vacuubrand GMBH, Germany) were used for the preparation of biorelevant media.

A Hydrus pH meter (model 300, Fisher Scientific, UK) was used for adjustment of the pH of the media used for solubility and dissolution studies.

Turbula blender (Willy A. Bachofen AG, Basel, Switzerland) was used for preparation of physical blends.

A Sigma 701 tensionmeter (Biolin Scientific, Sweden) equipped with Titronic Universal Burette was used to measure surface tension of modified media.

A Sartorius balance (AG Gottingen, Germany) was used for all weighing.

Vortex rotamixer (Hook & Tucker Instruments, England) was used for mixing samples before transferring to HPLC vials.

Various sizes of Finnpipette tips (Fisherbrand, UK) (1-5 mL: S/N 9066708; 100-1000 µL: S/N 9097462; 20-200 µL: S/N 9113779) were used for sample preparations involving standard preparations, treatment of precipitated samples and buffer capacity studies.

Ultrapure water was obtained from a NANOpure® DIamond UF and UV/UF Water Barnstead System (Thermo Scientific, Dubuque, US).

Heating Magnetic Stirrer (Fisher Scientific, UK) was used for buffer capacity studies.

4.3 Software

Excel 2007 (Microsoft, US) was used to process all data solubility, dissolution and IVIVC data.

DDSolver Excel add-in was used for analysis of dissolution kinetics.

Simcyp Population-based ADAM Simulator (SimCYP®, Sheffield, UK) was used for the development of PBPK models.

Graph Pad Prism 5.02 (GraphPad Inc.) was used for comparison of solubility data.

PCDCON® 1.1 Deconvolution Utility (by Gillespie) was used for numerical deconvolution of plasma concentration data after oral administration of Indomethacin.

xyExtract Graph Digitizer V5.1 (by Wilton P.Silva, 2011) was used for extracting data from 2D graphs.

4.4 Methods

4.4.1 Preparation of cocrystals

All cocrystals were produced and provided by Prosonix Ltd using three different preparation techniques: sonic slurrying (ss), spray-drying (sd) (61, 66) and ultrasound mediated amorphous to crystalline transition (umax). The author of this thesis was not involved in cocrystal production process.

Sonic-slurrying technique

CBZ-SAC, CBZ-NIC, IND-SAC and IND-NIC cocrystals were prepared with the sonic-slurrying method (65). Slurry was prepared by adding appropriate amounts of API and coformer into the jacketed vessel containing organic solvent (ethyl acetate). Slurry was then stirred at 60 rpm using a magnetic stirrer for one hour at 15 °C. Obtained slurry was then filtered and dried under vacuum overnight.

Spray-drying technique

Spray-drying technique was used to prepare Saccharin cocrystal of Indomethacin. The technique was briefly described in section 1.6.2.

UMAX technique

UMAX method was used to prepare Saccharin cocrystals of Carbamazepine and Indomethacin. Short description of UMAX process was included in section 1.6.3.

4.4.2 Cocrystals sample preparation

4.4.2.1 Preparation of capsules for dissolution studies using USP apparatus 1

CBZ, CBZ-NIC_{ss}, CBZ-SAC_{ss} and CBZ-SAC_{umax} were weighed and filled into standard gelatin capsules (size 0). Amounts equivalent to 200 mg of CBZ were used in all cases (Table 21). Calculations of the amount of CBZ in the cocrystal form were made based on the molar mass (Appendix 1).

Table 21. Amount of CBZ cocrystals used in dissolution testing.

Cocrystal [drug-coformer]	Ratio of CBZ : coformer	Amount of CBZ [mg]	Amount of coformer in 0.847mmol [mg]	Amount of cocrystal [mg]*
CBZ-SAC_{ss} CBZ-SAC_{umax}	1:1	200	155	355
CBZ-NIC_{ss}	1:1	200	103	303

*amount of cocrystal that corresponds to 200 mg of CBZ on a molar basis (Appendix 1)

4.4.2.2 Preparation of samples for solubility and dissolution studies using USP apparatus 4

Carbamazepine (CBZ) case

4.4.2.2.1 Preparation of samples to assess effect of MCC on dissolution

In order to reduce static charges of the CBZ cocrystal material to enable weighing and further encapsulation, blending with microcrystalline cellulose was essential. MCC is also present in commercial forms of CBZ, Tegretol®. Thus, it was important to assess if MCC has any effect on the dissolution performance of Carbamazepine. Three grades of MCC characterised by different particle size were selected for these studies (Table 22).

Table 22. Characteristics of different MCC grades.

Product grade	Nominal particle size [µm]	Moisture [%]	Loose bulk density [g/cc]
PH-105	20	< 5.0	0.20 – 0.30
PH-302	100	3.0 to 5.0	0.35 – 0.46
PH-200	180	2.0 to 5.0	0.29 – 0.36

One batch for each MCC grade was prepared. Carbamazepine was sieved through a 425µm stainless steel sieve (Pascal Eng Ltd., Sussex, UK) prior to weighing. Equivalent amounts to 2.00 g of CBZ were weighed and placed between two layers of 300 mg MCC in a plastic vial. Samples were blended for 45 minutes using a Turbula blender at 46 rpm/min.

4.4.2.2.2 Preparation of cocrystal samples for dissolution studies

Based on the previous study MCC grade with particle size of 100 µm (PH-302) was selected for further studies. Carbamazepine cocrystal (CBZ-SAC_{ss}, CBZ-SAC_{umax} and CBZ-NIC_{ss}) samples were then blended with MCC according to the method described in section 4.4.2.2.1 (*Preparation of samples to assess effect of MCC on dissolution*).

4.4.2.2.3 Blend uniformity test

For each blend, ten samples equivalent to 20 mg of CBZ were collected from different fractions of the blend and were dissolved in 60 mL of methanol and then 40 mL of water was added. MCC that did not dissolve in the organic solvents was filtered through qualitative filter paper. All CBZ fully dissolved in this amount of methanol. Filtrate was analyzed by HPLC and the percentage of relative standard deviation (%RSD) of the area was calculated (Appendix 2). %RSD below 2% indicated that the blending procedure produced a homogenous blend. After blending with MCC, the name of the formulations remained the same as follows: CBZ, CBZ-SAC_{ss}, CBZ-SAC_{umax} and CBZ-NIC_{ss}.

Indomethacin (IND) case

Equivalent amounts to 25 mg of IND were used for dissolution studies of all IND-SAC_{ss}, IND-SAC_{umax} and IND-NIC_{ss} cocrystals (Table 23). Calculations of the amount of IND in the cocrystal form were made based on the molar mass (Appendix 3).

Table 23. Amount of IND cocrystals used in dissolution testing.

Cocrystal [drug-coformer]	Ratio of IND : coformer	Amount of IND [mg]	Amount of coformer in 0.0699mmol [mg]	Amount of cocrystal [mg]
IND-SAC_{ss} IND-SAC_{sd} IND-SAC_{umax}	1:1	25	12.79	37.79
IND-NIC_{ss}	1:1	25	8.53	33.53

*amount of cocrystal that corresponds to 25 mg of IND on a molar basis (Appendix 3)

4.4.2.3 Preparation of physical blends for dissolution studies using USP apparatus 4

The mechanism of cocrystal dissolution was characterized against the physical blends of adequate API's and coformers. Physical blends were prepared using blending procedure. API's (CBZ and IND) and coformers (SAC and NIC) were sieved through a 425 µm stainless steel sieve prior to weighing. Equivalent amounts of API and coformers to that present in the cocrystals were weighed (Table 24). API was always placed between two layers of coformer in a plastic vial. Samples were blended for 45 minutes using a Turbula blender at 46 rpm/min.

Table 24. Amounts of components used for preparation of physical blends.

Amounts of components used		
	SAC	**NIC**
CBZ [2 g]	1.50 g (2 x 0.75g)	1.30 g (2 x 0.65g)
IND [2.5 g]	1.28 g (2 x 0.64g)	0.85 g (2 x 0.43g)

Obtained this way physical blends were then placed between two layers of MCC (2 x 0.3g) and were blended using the same blending protocol.

4.4.2.3.1 Blend uniformity

For each blend, ten samples equivalent to 20 mg of CBZ and 20 mg of IND were collected from different fractions of the blend and dissolved in 60 mL of methanol and then 40 mL of water (for CBZ) or 70 mL of ethanol and 30 mL of water (for IND). All components fully dissolved and 1.5 mL samples were transferred to HPLC vials for analysis. % RSD of the area of ten replicates was calculated (Appendix 4). %RSD below 2% indicated that the blending procedure produced a homogenous blend. Physical blends in this study are referred to as CBZ--SAC, CBZ--NIC, IND--SAC and IND--NIC.

4.4.3 Media composition

Three different types of media were selected for *in vitro* studies: compendial (SGF, SIF, SCoF), modified (MGM: SGF+0.01%SLS, MIM-I: Na-SIF+0.2%SLS, MIM-II: blank FaSSIF+0.1%SLS) and biorelevant media (FaSSGF, FaSSIF-V2, FaSSCoF).

4.4.3.1 Compendial media

SGF (108), SIF (108) and SCoF (158) media were prepared according to the composition as presented in Table 4 and Table 8.

4.4.3.2 Modified media

Surface tension is an important property of characterise human gastrointestinal fluids for solubility and dissolution of drugs. Typical surface tension values in the fasted state stomach range between 35 – 45 mN/m (270). This is due to the presence of surface active agents such as lecithin and lysolecithin (271). According to Solvang and Finholt, the levels of these surfactants *in vivo* are below critical micelle concentration (CMC) (272). Several authors developed gastric media that were modified by addition of artificial surfactants such as sodium lauryl sulphate (SLS) or Triton X-100 in order to achieve a surface tension close to that of human fluids (273). In this project SGF+ 0.01% SLS (MGM) was used based on studies performed by Fotaki and Long (274).

Kalantzi *et al*. reported a surface tension value of human intestinal fluids (HIF) of 33.6 mN/m (150); biorelevant media (FaSSIF, FaSSIF –V2), which thus far seems to offer the most similar environment to the intestinal conditions, reported a surface tension of 54 mN/m (157). Biorelevant media contain mixed micelles, which concentrations were recorded to be above CMC. One aim of this project focused on the development of simple media modified by addition of simple surfactants (SIF; blank FaSSIF) would produce media with surface tension comparable to HIF.

4.4.3.2.1 Surface tension (ST) studies

Du Nouy ring method was used to determine the CMC from surface tension (ST) studies of SIF and blank FaSSIF-V2 (*Compendial media* section 2.5.1 and *Biorelevant media* section 2.5.2) by addition of SLS (99% pure) using a built – in automatic titrator. Accurate amount of SLS was titrated dropwise (up to a total concentration of 3% SLS) into buffer, and surface tension was measured after each addition of surfactant. The 99% pure SLS was used as previous reports had shown that SLS purity could affect the CMC and dissolution of drugs used in the study (275). Due to the precipitation of potassium from the phosphate salt (SIF) with lauryl sulphate from SLS, potassium salts were replaced with sodium phosphate salts (Na-SIF) (276).

Additionally, ionic strengths of Na-SIF and blank FaSSIF-V2 were calculated using following equation:

$$I = \frac{1}{2}\sum_{i=1}^{n} c_i z_i^{\,2} \qquad \text{(Equation 28)}$$

Where I is ionic strength, c_i is the molar concentration of the ion and z_i is the charge number of that ion (277).

4.4.3.2.2 Buffer capacity (β)

For an aqueous solution, the buffer capacity is defined in terms of the concentration of acid or base that must be added to influence pH by one pH unit (277). Buffer capacity of Na-SIF and Na-SIF+0.2%SLS (MIM-I) was determined according to the USP 29, in which a potentiometric titration method is described (278). The buffer capacity was estimated by dropwise addition of 1N NaOH or 1M HCl measuring the volume required to change the pH by one unit, under constant agitation. 0.2 mL of 1M HCl or 1N NaOH was added using a pipette to 100 mL of buffer (Na-SIF, MIM-I) within 1 minute intervals during which solution was stirred at constant rate on the stirrer plate using a magnetic stirrer bar. The pH was measured and recorded using a pH probe immersed in the solution. Buffer capacity was then calculated using equation (279):

$$\beta = 2.3C\frac{Ka\left[H_3O^+\right]}{\left(Ka + \left[H_3O^+\right]\right)^2} \qquad \text{(Equation 29)}$$

Where β is the buffer capacity, C is the total buffer concentration *i.e.* the sum of the molar concentrations of acid and salt, K_a is dissociation constant and $[H_3O^+]$ is the molar concentration of the hydronium ion.

4.4.4 Biorelevant media

FaSSGF (152), FaSSIF-V2 (157) and FaSSCoF (159) media were prepared according to the composition as presented in Table 5, Table 7 and Table 8 (*Biorelevant media* section 2.5.2).

4.4.5 Particle-size distribution (PSD)

The particle-size distribution of the batches of CBZ, IND powder and their cocrystals was measured by laser light diffraction (HELOS, Sympatec, Clausthal-Zellerfeld, Germany) using a wet dispersing system (CUVETTE, Sympatec, Clausthal-Zellerfeld, Germany). In case of CBZ, powder samples (50 mg) were suspended in 5mL of dispersion media, comprising of cyclohexane and 0.1% w/v lecithin. The suspension was sonicated for 10 minutes at 25 °C prior to analysis. In the case of IND, powder samples (50 mg) were suspended in SGF and sonicated for 10 min at 25 ºC. The suspended powder materials were then introduced into a 50 mL quartz-glass cuvette containing a solution of 0.1% w/v lecithin in cyclohexane (CBZ) or SGF (IND) and stirred with a magnetic bar at 1000 rpm for 2 min before sizing. Particle sizing was triggered when the optical concentration was greater or equal to 5%, and measurements were performed in triplicate. The cumulative undersize particle diameters were calculated using Windox 5.0 software (Sym patec, Clausthal-Zellerfeld, Germany).

4.4.6 Differential Scanning Calorimetry (DSC)

A differential scanning calorimeter (DSC, 2190, TA Instruments, Surry, UK) was used to perform thermal analysis on the CBZ and IND (as received), and their cocrystal samples, after initial calibration with indium. Powder samples (n = 3) of approximately 5-10 mg were accurately weighed in aluminium pans, ensuring a total covering of the base by pressing down the samples and then hermetically sealed. The temperature was equilibrated to 50°C before heating at a rate of 10 °C/min to 350 °C under dry nitrogen purge (0.30 L/min).

4.4.7 Development and validation of chromatographic methods

HPLC methods used to quantify CBZ, IND, SAC and NIC in samples from solubility and dissolution studies are presented in Table 25. The HPLC method used for the analysis of CBZ is a modification of the method of Vertzoni *et al*. (280)**.** Analysis of IND was conducted using a modified method of Al Za'abi, *et al.* (281) (Table 25). For quantification of coformers from dissolution studies of cocrystals and physical blends in biorelevant media, gradient methods were developed (Table 26). NIC and SAC peaks tend to elute in the first 4 minutes of the separation; therefore some interference between them and components of FaSSGF occurred.

Table 25. Summary of HPLC methods for detection of CBZ, IND, SAC and NIC.

	CBZ	IND	SAC	NIC
Column name	Zorbax® Eclipse	Zorbax®	Zorbax®	Zorbax®
Column type	XDB-C18	SB-C18	SB-C18	SB-C18
Column size [mm]; pore size [µm]	250x4.6; 5 µm	150x4.5; 3.5 µm	150x4.5; 3.5 µm	150x4.5; 3.5 µm
Column temp. [ºC]	20	23	23	23
Flow rate [mL/min]	1	1	1	1
Injection volume [µL]	50	100	100	100
Mobile phase [%v/v]	MeOH:H_2O 60:40	MeOH:H_2O:H_3PO_4 70:29.5:0.5	MeOH:H_2O+ 0.1 % TFA gradient	MeOH:H_2O+ 0.1 % TFA gradient
Wavelength [nm]	240	270	270	270
Run time [min]	9	10	18	18
Retention time [min]	6.6	7.8	3.8	1.9

Table 26. Gradient used for detection of SAC and NIC.

SAC gradient method			NIC gradient method		
Time[min]	**MeOH**	**Water+0.1 % TFA**	**Time[min]**	**MeOH**	**Water+0.1 % TFA**
0	30	70	0	30	70
3	30	70	2	30	70
5	30	70	4	70	30
7	90	10	6	90	10
11	90	10	10	90	10
13	60	40	13	50	50
15	30	70	15	30	70
18	30	70	18	30	70

4.4.7.1 Standard curve preparation for all media.

Prior to each experiment, a calibration curve was performed in order to observe any changes to the formulation, sample, medium or system (Table 27). Adequate amounts of stock solution was transferred into a volumetric flask and diluted up to volume with adequate medium in order to achieve the desired standard concentration.

Table 27. Summary of standard curve conditions.

	Stock solution conc. [µg/mL]	Stock solution solvents	Standards conc. range [µg/mL]	Standard conc. [µg/mL]
CBZ	2000	methanol (60):water (40)	10-200	10, 20, 30, 40, 50, 75, 100, 125, 150, 175 and 200
IND	500	Ethanol	0.5-50	pH 1.2-1.6: 0.5, 0.75, 1, 2.5, 5, 7.5 and 10 pH 6.5-6.8: 1, 2.5, 5, 10, 20, 30, 40 and 50
SAC	500	Water	2.5-50	2.5, 5, 10, 20, 30, 40 and 50
NIC	500	Water	5-50	5, 10, 20, 30, 40 and 50

Linearity and Range

The linearity of each assay method was evaluated by six point standard curves using concentrations presented in Table 28. Calibration curves for CBZ and IND were constructed over a 6 weeks period to determine the variability of the slope and intercept. Due to the limited number of experiments that required NIC and SAC quantification, three replicates of each standard were made on one day to assess linearity. Mean (± SD) regression equations were constructed using linear regression analysis. The goodness of fit was reported in terms of R^2 value.

Table 28. Standards selected for linearity.

	Standards conc. range [µg/mL]	Selected concentrations [ug/mL]
CBZ	10-200	10, 50, 75, 100, 150 and 200
IND	0.5-50	Acidic cond. 0.5, 0.75, 1, 2.5, 5 and 10
		Basic cond. 1, 5, 10, 20, 40 and 50
SAC	2.5-50	2.5, 5, 10, 20, 50 and 75
NIC	5-50	5, 10, 20, 30, 40 and 50

Precision

Working standards of each concentration (CBZ: 50 µg/mL in SIF; IND: 50 µg/mL in SIF; SAC: 50 µg/mL in FaSSGF and NIC: 50 µg/mL in FaSSGF) for each method were injected ten times under the same conditions during a short time period (1 day). Intra – day precision was assessed based on the %RSD of area of replicates.

Limit of detection (LOD) and quantification (LOQ)

The sensitivity of all assays either in SIF or FaSSGF was evaluated by determining the limit of quantification (LOQ) which is defined as the lowest concentration of the calibration curve. Limit of detection (LOD) is defined as the lowest concentration that can be distinguished from the noise level. The LOQ and LOD values are defined as follows:

$$LOQ = \frac{10S_{y/x}}{b} \quad \text{(Equation 30)}$$

$$LOD = \frac{3.3S_{y/x}}{b} \quad \text{(Equation 31)}$$

Where b is the slope and $S_{y/x}$ is the residual standard deviation of the regression line calculated using working standards.

4.4.8 Solubility studies

Solubility over time studies

Solubility over time of IND and two of its cocrystal (IND-SAC_{ss} and IND-NIC_{ss}) was measured in SIF (pH 6.8) and FaSSIF-V2 (pH 6.5). An excess (40 mg) of sample and 10 mL of medium transferred into centrifuge tubes. Capped tubes were then placed in a tray within a shaking water bath (37 ˚C) and were shaken at 200 strokes/min. Samples were analysed at various time: 5, 10, 20, 30, 40, 50, 60, 90, 120, 180, 240 and 1440 minutes using HPLC. Concentration values were plotted against the time.

Saturation solubility studies

The pH-profile solubilities were measured in triplicate using the shake-flask method (282). Various media were used to cover the physiologically relevant pH ranges from 1.2 to 6.8 (Table 29). Medium (10 mL) and excess (40 mg) of CBZ, IND and their cocrystal samples were transferred into centrifuge tubes. Capped tubes were then placed in a tray within a shaking water bath (37 ˚C) and were shaken at 200 strokes/min for 24 h. After equilibrium was reached, the supernatant solution was filtered using syringes fitted with 13 mm stainless steel swinny filter holders equipped with cellulose nitrate membrane filters (0.45 μm). Samples after dilution were analysed by HPLC using methods described in section 4.4.7.

Table 29. Media selected for pH-profile solubility studies.

Medium	pH
SGF	1.2
FaSSGF	1.6
Acetate buffer	4.5
FaSSIF-V2	6.5
SIF	6.8

4.4.9 *In vitro* dissolution studies

Dissolution studies were performed using two different dissolution systems: basket dissolution apparatus (USP apparatus 1) and flow-through cell dissolution apparatus (USP apparatus 4).

4.4.10 Basket dissolution apparatus (USP apparatus 1)

Protocol for the dissolution tests of capsules with USP apparatus 1:

Dissolution media	SGF and SIF
Dissolution medium volume	500 mL
Temperature	37±0.5 °C
Basket rotating at	100 rpm
Sample volume	5 mL
Sampling location	Half-way between the top of the medium and the top of the basket
Sampling times	CBZ: 10, 20, 30, 45, 60, 90, 120, 180, 240, 300 and 360 min. IND: 10, 20, 30, 45 and 60 min.
Formulation tested	Indocid® capsules, Tegretol® tablets Encapsulated CBZ_{sp} Encapsulated CBZ-SAC_{ss} Encapsulated CBZ-NIC_{ss}

Experiments were run in triplicate

Sampling procedure for the dissolution tests.

Samples were removed using a 5 mL Fortuna Optima® syringe fitted with a stainless cannula to facilitate representative sampling. The drawn sample volume was replaced with the same volume of blank dissolution medium, which was kept in a separate vessel at a temperature of 37±0.5 °C. Each sample was filtered through a Whatman® cellulose nitrate membrane filter 0.45 μm placed in filter swinny holder and, after discarding the first 1 mL, an appropriate volume of the filtrate was injected into the HPLC system.

4.4.11 Flow-through cell dissolution apparatus (USP apparatus 4)

Protocol for the tests of all CBZ and IND formulations.

According to the USP 24 specifications a 5 mm–size glass bead was positioned in the tip of the cell (22.6 mm-size), 1.7 g of 1 mm–size glass beads were added. In the case of all CBZ formulations, a Whatman® glass fiber filter (GF/F: 0.7 μm pore size, 24 mm diameter) was placed on the top of the cell. For IND formulations an additional Whatman® glass fiber filter (GF/D: 2.7 μm pore size, 24 mm diameter) separated from the GF/F filter by 0.1 g of the glass wool was used. For the dissolution experiments of Tegretol®, the tablets were mounted on a holder (Figure 19a)**,** while the Indocid® capsule was placed on the top of the glass beads and the tablet holder was reversely mounted to prevent sticking of the capsule to the filter head (Figure 19b). For the dissolution experiments of all APIs and cocrystals samples, the samples were placed between 1.7 g and 6.3 g of the glass beads (Figure 19c).

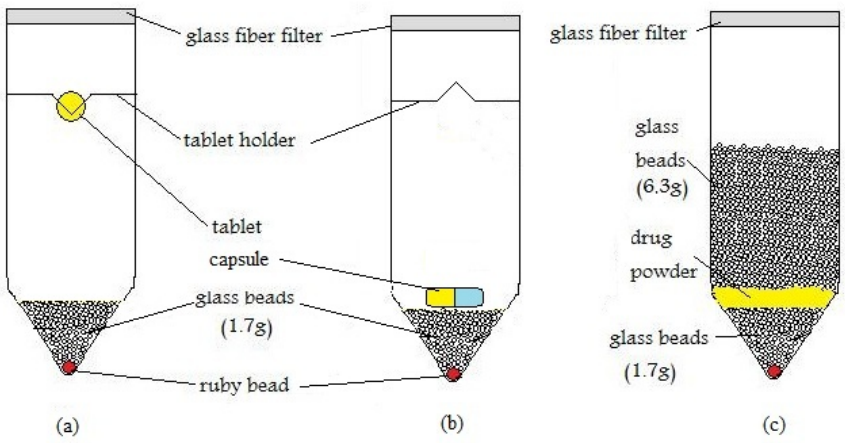

Figure 19. Schematic diagram of the conditions used for the dissolution experiments with the flow-through cell apparatus.

The experiments were performed in compendial, modified and biorelevant media (*The dissolution medium* in section 2.5) with sequential changes of the media and flow rates according to Table 30.

Table 30. The periods during which formulations were exposed to the various media and the flow rate that each medium was pumped through the cell.

Type of medium	Medium	Period (min)	Flow rate (mL/min)*
Compendial media	SGF	0-60	8
	SIF	60-240	4
Modified gastric media (MGM) / Modified intestinal media (MIM-I)	SGF+0.01%SLS	0-60	8
	Na-SIF+0.2%SLS	60-240	4
Modified gastric media (MGM) / Modified intestinal media (MIM-II)	SGF+0.01%SLS	0-60	8
	blankFaSSIF-V2 +0.1%SLS	60-240	4
Biorelevant media	FaSSGF	0-60	8
	FASSIF-V2	60-240	4

*The flow rate is defined by steps in the piston pump. Their relation is given by the equation: y=0.0157x+0.7842 (y: flow rate, x: steps).

Sampling times every 10 min up to 240 min

Temperature: 37±0.5 °C.

Experiments were run in triplicate

4.4.11.1 Sampling procedure

The samples were collected in volumetric cylinders, and after appropriate dilution (where necessary) a sufficient volume was injected into the HPLC system.

4.4.11.1.1 Treatment of precipitated IND samples

Indomethacin is a weak acid which upon the media change tends to precipitate so additional treatment of the sample is essential. The treatment of the sample took place immediately after collection, as the rate of precipitation strongly depends on the time. Firstly, the fraction of sample-collected at 70 minutes was withdrawn using a 5 mL Fortuna Optima® syringe, then 13 mm stainless steel swinny filter holders equipped with cellulose nitrate membrane filters (0.45 μm, Whatman) were used to discard 1 mL of sample and then transfer the remaining volume to a HPLC vial (referred to as filtered sample). Secondly, 5 mL of the

precipitated sample was dissolved in 5 mL of ethanol (referred to as diluted sample) then stirred firmly and transferred to a HPLC vial. Obtained data were then used for calculations of % of sample and dose precipitated.

4.4.11.1.2 Calculation of % of sample precipitated

Concentrations of both filtered and diluted samples were calculated and then % of the sample that precipitated at 70 minutes in each cell was calculated accordingly to the equation:

$$\%_{\text{prec.70min}} \text{ of the sample} = 100 * \frac{\left[diluted_{sample} - filtered_{sample}\right]}{\left[diluted_{sample}\right]} \qquad \text{(Equation 32)}$$

4.4.11.1.3 Interpretation of non-cumulative data

Dissolution profiles of all IND formulations were also presented in non-cumulative way. Amount dissolved [mg] were calculated based on the volume of the sample collected between each time intervals *i.e*. 10 to 20 minutes, 20 to 30 minutes *etc*. The amounts dissolved were then plotted against the time intervals creating *stairs* like profile.

4.4.11.1.4 Calculation of % of dose precipitated

Concentrations of both filtered and diluted samples were calculated and the amount dissolved [mg] was calculated based on the volume of the sample collected between 60 to 70 minutes. The difference between the amount of sample dissolved and filtered is then further used to calculate percentage of the dose precipitated:

$$\%_{\text{prec.70min}} \text{ of dose} = \frac{\left(Amount_{diluted} - Amount_{filtered}\right) * 100\%}{Dose} \qquad \text{(Equation 33)}$$

Mean and SD values of % dose and % that calculated were then plotted on bar charts for each formulation across all dissolution media.

4.4.12 Release of CBZ from 400 mg PR Tegretol® tablets

Release profile of CBZ from 400 mg PR Tegretol tablets was determined using USP apparatus 4. Tablets were positioned in the cell using cell set up described in Figure 19a. Three experiments were performed using specifications summarized in Table 31.

Table 31. Dissolution specifications for 400 mg PR Tegretol®

Experiment no.	Media used	Time of exposure [h]	Selected flow rates [mL/min]
1	SGF/SIF/SCoF	1/4/2	8/4/4
2	FaSSGF/FaSSIF-V2/SCoF	1/4/2	8/4/4
3	FaSSGF/FaSSIF-V2/FaSSCoF	1/4/2	8/4/4

4.4.13 Effect of MCC on dissolution of Carbamazepine

It was essential to ensure that MCC would not affect the dissolution performance of Carbamazepine. Therefore, three batches of Carbamazepine containing different grades of MCC (PH105, PH302 and PH 200) that were previously blended were analysed using USP apparatus 4 dissolution methods for powder samples. MCC grades had similar sensitivity to moisture but various particle size (20 – 180 µm). Amounts equivalent to 25 mg of Carbamazepine (n = 3) were tested using USP apparatus 4 for one hour in SGF (pH 1.2) at 8 mL/min following one hour exposure to SIF (pH 6.8) at 4 mL/min. Samples were collected every 10 minutes.

4.4.14 Treatment of *in vivo* data

Plasma concentration-time profiles for a single administration of one 200 mg IR Tegretol® tablet were extracted from fasted state studies performed by Meyer *et al*. (283). Clinical studies involved twenty four healthy, non-smoking male volunteers ranging in age from 21 to 35 and weighing 61-93 kg. Two sets of clinical studies were found for PR Tegretol® tablets. Kovacević *et al*. tested the drug during open label, randomized cross-over studies on a group of twenty four healthy volunteers of both sexes, whose age ranged between 20-52 and body weight 50-96 kg (82). Volunteers received a single administration of one 400 mg dose. Data were also compared with that obtained by Larkin *et al*., who tested single administration of one 400 mg PR Tegretol® tablet during double-blind cross over studies where eight healthy subjects (7 males; 1 female) participated with an age range of 25 to 47 (284). All *in vivo* data were extracted as mean values using xyExtract Graph Digitizer.

For the IND case, plasma concentration-time profile for IR Indocid® capsules were extracted from fasted state studies performed by (285). Clinical studies involved fourteen healthy male volunteers. Mean and SD values for this clinical study were reported.

4.4.15 *In vitro-in vivo* correlations

Traditionally, IVIVC was developed by correlating dissolution data with fraction absorbed obtained through either model-independent or model-dependent approaches (227). The former model involves numerical deconvolution using pharmacokinetic softwares such as PCDCON®. The latter approach is based on algebraic equation such as Wagner-Nelson. Nowadays, the development of IVIVC with the help of *in silico* tools through Physiologically Based Pharmacokinetic (PBPK) models (*i.e*. Simcyp®) is becoming more popular.

4.4.15.1 Model-independent approach

Numerical deconvolution of Indomethacin data was performed using the software programme PCDCON® (271). Mean plasma concentration time profile following intravenous administration (285) was used as impulse response (Appendix 5). Unit impulse response was calculated based on the dose for intravenous IND formulation, which was 25 mg. Mean plasma concentration time profile after oral administration of Indocid® capsule was used as input response function (Appendix 5). Both profiles were then fitted to an interpolating cubic spline function and then deconvoluted. Data were generated for 4 hours using step size 0.04 and were presented as cumulative amount of IND absorbed. 10 minutes intervals were used for the calculation of the *in vivo* cumulative fraction absorbed; therefore, the number of calculated points for 4 hours of deconvolution was set to 25. Deconvoluted this way *in vivo* drug absorption profile was presented as a fraction of IND absorbed and correlated with fraction of IND dissolved *in vitro* dissolution experiments using USP apparatus 1 and USP apparatus 4.

Scaling factor such a Levy plot was applied this way that on the X-axis, the time to have certain amount dissolved (*i.e* 5, 10, 15 mg *etc.*) was marked, and on the Y-axis, the time to reach similar amount of the drug absorbed was pointed. It was not possible to obtain linear correlation; therefore, time shifting was applied. The time shifting was illustrated by the time to observe turning point on the generated plot. This time can be further used to shift the slower process (absorption or dissolution) in order to correlate with faster process (absorption or dissolution).

4.4.15.2 Model-dependent approach

Carbamazepine case

Wagner-Nelson model

An intravenous formulation of Carbamazepine is not available; therefore application of numerical deconvolution method is not possible. In this instance, plasma concentration time profiles after oral administration can be deconvoluted using Wagner-Nelson model (224). The observed mean *in vivo* plasma CBZ concentration time profile was deconvoluted to its *in vivo* absorption time profile assuming a one-compartmental open body model. As CBZ follows two-compartmental model Wagner-Nelson method was applied with caution assuming that it follows one-compartmental model.

The area under the curve ($AUC_{0\text{-}168h}$) was calculated by the trapezoidal rule. The elimination rate constant (*ke*) was estimated from the terminal slope (based on the last three time points) of the logarithmic plasma CBZ concentration time profile, which was further used for calculating area under the curve from zero to infinity ($AUC_{0\text{-}\infty}$). Amount of CBZ absorbed at a time *t* (A_t) was then calculated as a sum of plasma concentration at a certain time and $AUC_{0\text{-}\infty}$. Based on this calculation, the total amount of CBZ absorbed can be determined, which then can be used to produce a graph of cumulative fraction absorbed. Due to the facts that sink conditions were not provided and only 50 % of the CBZ was dissolved in experiments using USP apparatus 1. This data were normalised as 100%. The relationship between fractions of CBZ dissolved *in vitro* and fraction of CBZ absorbed *in vivo* was examined by plotting the fraction of drug dissolved at 0.5, 1, 2, 3 and 4 hours *versus* fraction of the drug absorbed at equivalent time intervals. Linear regression analysis was then applied (Excel 2007).

4.4.15.3 PBPK model

4.4.15.3.1 Carbamazepine case

The Simcyp® population-based ADME simulator was used to simulate the plasma concentration – time profiles of 200 mg IR and 400 mg of PR Tegretol® tablets. Parameters used for developing a minimal PBPK model of Carbamazepine are presented in Table 32.

Table 32. Summary of CBZ parameters inserted into the Simcyp® software.

Parameter	Value/unit
Molecular weight [g/mol]	236.27
Log P	2.45 (286)
pK_a	11.83
dose [mg]	IR 200 PR 400
Human jejunal permeability (P_{eff})	$4.3x10^{-4}$cm/s (287)
f_u	0.25 (288)
Main plasma binding protein	Human serum albumin (HSA)
Clearance after oral dosage [L/h]	1.01 (%CV 27.27) (289)
Volume of distribution [L/kg]	0.96 [%CV 9.38] (290)

The simulations for single dose of both IR and PR formulations were performed using time – based simulations according to the trial design which corresponds to clinical studies, including the number of participants (24 subjects), age range, gender range and dose regimen. Sim-Healthy volunteer population was used and gastric emptying time was set up to 1 hour which was in agreement with media change during dissolution studies. The rate and extent of oral absorption of CBZ was simulated using the fasted human ADAM model, which describes the gastrointestinal tract as segments based on their anatomical and physiological characteristics. The ADAM model incorporates two types of dissolution data: (1) predicted dissolution data based on Wang-Flanagan (WF) equation based on solubility and particle-size distribution data obtained experimentally and (2) raw data obtained from the *in vitro* experiments. All of these data were obtained previously. Therefore, simulations of both Tegretol® tablets were performed using both approaches according to the schedule presented in Table 33.

.

Table 33. Schedule for simulations of Tegretol® IR and PR formulations.

Approach		Media
1) Predicted dissolution data using solubility and particle size data	Solubility pH profile (IR)	Compendial media
		Biorelevant media
2) Experimentally determined dissolution data	USP apparatus 1 (IR)	SGF and SIF
	USP apparatus 4 (IR & PR)	SGF/SIF (IR) MGM/MIM-I (IR) MGM/MIM-II (IR) FaSSGF/FaSSIF-V2 (IR & PR)

Level A point-to-point correlations between observed and predicted plasma concentration over time profiles were established. Both of the models were compared with the observed data using difference factor f_1. To better understand the absorption process of CBZ, data were presented as regional fraction of the Tegretol® dose absorbed and cumulative fraction of CBZ absorbed.

In addition, parameter sensitivity was performed to analyse the effect of selected parameters such as *logP*, clearance, volume of distribution *etc* on the predicted C_{max}, T_{max} and AUC values. Sensitivity analysis was performed for IR formulation under fasted conditions. During this analysis, one parameter was changed gradually within a realistic range.

4.4.15.3.2 Indomethacin case

The rate and extent of oral absorption of Indomethacin from 25 mg Indocid® capsules was simulated using the fasted human ADAM model in Simcyp®. Basic physicochemical properties such as lipophilicity, solubility and molecular weight were required for simulations. These values along with pharmacokinetics parameters were taken from scientific literature and are summarised in Table 34.

Table 34. Summary of IND parameters inserted into the Simcyp® software.

Parameter	Value/unit
Molecular weight [g/mol]	357.787
Log P	4.27 (291)
pK_a	4.42 (292)
dose [mg]	25
Human jejunal permeability (P_{eff})	21.146 x10^{-4}cm/s [based on Caco-2 255.66x 10E^{-06} cm/s]
f_u	0.04 (293)
Main plasma binding protein	Human serum albumin (HSA)
Clearance after oral dosage [L/h]	6.541 [%CV 18.12]
Volume of distribution [L/kg]	0.12

If human P_{eff} is not available *in vitro* permeability models such as MDCK II and LLC-PK_1 or Caco-2 can be used to predict the P_{eff}. The Simcyp® uses six reference compound assays to generate the relationship between $P_{app,\ Caco\text{-}2}$ to $P_{eff,\ man.}$ Human effective jejunal permeability (P_{eff}) was estimated to be 255.66 x 10^{-6} cm/s based on high Caco-2 permeability, which was converted to an estimated P_{eff} in human of 21.15 x 10^{-4} cm/s using the permeability predictor. Gastric emptying time was set up to the default value of 0.4 h. The simulations for single dose of Indocid® formulation were performed using time-based simulations according to the trial design which corresponds to clinical study, including the number of participants (14 subjects), age range, gender range and dose regimen. A Sim-Healthy volunteer population was used. The ADAM model incorporates two types of dissolution data: (1) predicted dissolution data using the Wang-Flanagan (WF) equation based on solubility and particle-size distribution data obtained experimentally and (2) raw data obtained from the *in vitro* experiments. All of these data were obtained previously. Therefore, simulations of both Tegretol® tablets were performed using both approaches according to the schedule presented in Table 35.

Table 35. Schedule for simulations of Indocid® IR capsules.

Approach		Media
1) Predicted dissolution data using solubility and particle size data	Solubility pH profile	Compendial media
		Biorelevant media
2) Experimentally determined dissolution data	USP apparatus 1	SGF and SIF
	USP apparatus 4	SGF/SIF MGM/MIM-I MGM/MIM-II FaSSGF/FaSSIF-V2

Level A point-to-point correlation between observed and predicted plasma concentration over time profiles were established. Simulated profiles were compared with the observed profile using difference factor f_1. In order to better understand the absorption process of IND, data were presented as a regional fraction of the Indocid® dose absorbed and cumulative fraction of IND absorbed. In addition, parameter sensitivity was performed to analyse the effect of selected parameters such as *logP*, clearance, volume of distribution *etc* on the predicted C_{max}, T_{max} and AUC values.

4.4.15.4 Predictions of *in vivo* performance of cocrystals based on PBPK models

The developed PBPK IR Tegretol® and Indocid® models were implemented for the prediction of *in vivo* performance of pharmaceutical cocrystals of CBZ and IND, respectively. Predicted plasma concentration time profile of CBZ_{sp} and IND_{sp} were used as a reference profiles against which *in vivo* performance of cocrystals were compared. Due to software limitations, it was not possible to indicate that the CBZ_{sp} and cocrystal formulations that were tested were present in a powder form. Thus, these data were inserted into the dissolution window in the formulation section designated for IR solid formulations. Mean values of percentage of CBZ dissolved with SD were inserted as a whole dissolution profile, which was characterised by linear interpolation of eighteen dissolution time points fairly distributed up to 4 h (0.17; 0.33; 0.50; 0.67; 0.83; 1.00; 1.17; 1.33; 1.50; 1.67; 1.83; 2.00; 2.33; 2.67; 3; 3.33; 3.67 and 4.00 h). Predicted cumulative fractions absorbed from each cocrystal were compared with that of

CBZ_{sp}. Regional fraction absorbed and cumulative fraction absorbed profiles were also useful to aid the discussion.

4.4.15.5 Statistical Analysis

Comparison of solubility data

Solubility data for all IND and CBZ formulations in different media were processed using GraphPad Prism software. Mean, standard deviations and standard errors of the mean were calculated. Two-Way ANOVA repeated measurements were performed for solubility concentrations for either selected medium or selected formulations ($p < 0.05$). The Bonferroni post-test was employed to perform pairwise multiple comparisons of all groups at a significance level of $p < 0.05$. Significant figures were presented to three significant digits. The same analysis was applied to compare mean values of simulated AUC, C_{max}, and T_{max} parameters for Tegretol® IR PBPK model.

Dissolution profile comparisons

Dissolution profile comparisons were performed with the use of $f_{1,area}$ assuming the dissolution profile of the CBZ_{sp} and IND_{sp} samples as the reference profiles. Evaluation of $f_{1,area}$ was considered up to the time corresponding to the first experimental datum after 85% of the plateau level of the reference data set. In cases where this datum point was not observed within 5 h of experiment, $f_{1,area}$ was evaluated up to 4 h, to reflect the maximum physiologically reasonable small intestinal residence period. Since the coefficient of variation of data points at every sampling time was in all cases less than 15%, $f_{1,area}$ was evaluated from mean data sets. In the present study, a 15% average difference of a test from a reference data set ($f_{1,area}$= 0.15) was set as the limit for identifying differences between the samples

Plasma concentration profile comparisons

The difference between mean simulated and mean observed plasma profiles was determined using difference factor f_1 (*Comparison of dissolution profiles* section 2.6). The observed plasma concentration time data were used as a reference data set. Predicted profiles were compared in this manner that the equivalent time points to reference profiles were selected for comparison. Entire profiles were taken into account. 15% average difference of a test from a reference data set ($f_{1,area}$= 0.15) was set as the limit for identifying differences between the profiles.

Dissolution kinetics

Zero-order, first-order with W_{max} and 3-parameters Weibull functions were applied to all dissolution profiles using the Excel add-in (DDSolver). The dissolution kinetics was applied to individual dissolution profiles and Mean with SD values were summarized in the tables. Dissolution data modeling library contained all essential equations (*Dissolution kinetics* section 2.6.2). The software requires the input of the time and its unit as well as % dissolved data. Additional tab in Excel were produced with the summary of all the data and their best - fit parameters. *AIC* and R^2 values were used to express the goodness of fit.

Kinetic of absorption (k_a) of CBZ, IND and their cocrystals were calculated from cumulative fraction absorbed over time profile using first-order equation.

5 Results and discussion

5.1 Blend uniformity

Samples (n = 10) equivalent to 20 mg of CBZ were analysed by HPLC and their areas were converted into concentrations and were further interpreted in terms of mean, SD and %RSD values and are presented in Table 36. Values of %RSD < 2 indicated that blending protocol described in section 4.4.2.2 produced homogenous blends.

Table 36. Blend uniformity data for CBZ and its cocrystals blended with MCC.

	Concentration [µg/mL]			
Sample no	**CBZ-MCC**	**CBZ-SAC$_{ss}$-MCC**	**CBZ-SAC$_{umax}$-MCC**	**CBZ-NIC$_{ss}$-MCC**
Mean	19.49	18.96	19.18	18.97
SD	0.24	0.22	0.08	0.25
%RSD	**1.26**	**1.16**	**0.44**	**1.29**

Samples (n = 10) equivalent to 20 mg of CBZ or IND were analysed by HPLC and their of mean, SD and %RSD values and are presented in Table 37. Values of %RSD < 2 indicated that blending protocol described in section 4.4.2.2 produced homogenous blends. Data in Table 37 demonstrates that physical blends of CBZ--SAC, CBZ--NIC, IND--SAC and IND--NIC were blended homogenously.

Table 37. Blend uniformity data for physical blends of CBZ and IND with SAC and NIC.

	Concentration [µg/mL]			
Sample no	**CBZ--SAC**	**CBZ--NIC**	**IND--SAC**	**IND--NIC**
Mean	19.30	22.11	25.97	25.84
SD	0.30	0.19	0.43	0.38
%RSD	**1.56**	**0.84**	**1.65**	**1.47**

5.2 Modified media composition

5.2.1 Surface tension (ST) studies

Kalantzi *et al*. reported that the surface tension of human intestinal fluid (33.6 mN/m) is significantly reduced in comparison to surface tension of water (72 mN/m) (150). The value in the fed state is even lower than in the fasted state (28 *versus* 33.6 mN/m), corresponding to the higher levels of bile salts present in the fed state. Preparation of biorelevant media may be time- and cost-consuming; therefore attempts at developing modified compendial media that mimic surface tension of human intestinal fluids were made in this study. Modified media may be useful not only for research purposes but as a tool for routine QC tests providing sink conditions for poorly soluble drugs. Figure 20 illustrates the effect of the addition of SLS to the medium (SIF and blank FaSSIF-V2) on the surface tension measurements.

It is important to note that the micelles created using SLS are single-type micelles, whereas, in biorelevant media and in HIF, mixed micelles are present (294). The mixed micelles can increase drug solubilisation more effectively than single micelles. Simplification of the biorelevant media by replacement of mixed micelles with single micelles produced by SLS was previously attempted. For instance, Taupitz and Klein investigated blank FaSSIF media containing SLS varying from 0.1 to 1.5% (295). They concluded that these media can be particularly useful for developing predictive and discriminative methods in QC and early stages of formulation development of poorly soluble drugs (295).

CMC can be defined as the concentration of surfactant above which micelles are formed (296). At concentrations greater than the CMC value, the surface tension of the medium does not decrease with an increase in surfactant concentration. The surface tension of media prepared with SLS was influenced by the species present in the media. The larger the amounts of the ions present in the media, the greater its ionic strength. Blank FaSSIF-V2 has greater ionic strength (0.12 M) than Na-SIF (0.07 M), which is in agreement with the observation that buffer with greater ionic strength, will result in lower CMC but larger micellar size (297-299). This is due to the presence of electrolytes, which reduce the forces of electrostatic repulsion between the charged head groups at the micelle surface, thus allowing the micelle to grow (297). It is important to note that purity of the SLS will affect surface tension measurements. Crison *et al*. reported 10% difference in the intrinsic dissolution rate of CBZ when tested in two different grades of SLS purity: 95 and 99% (275).

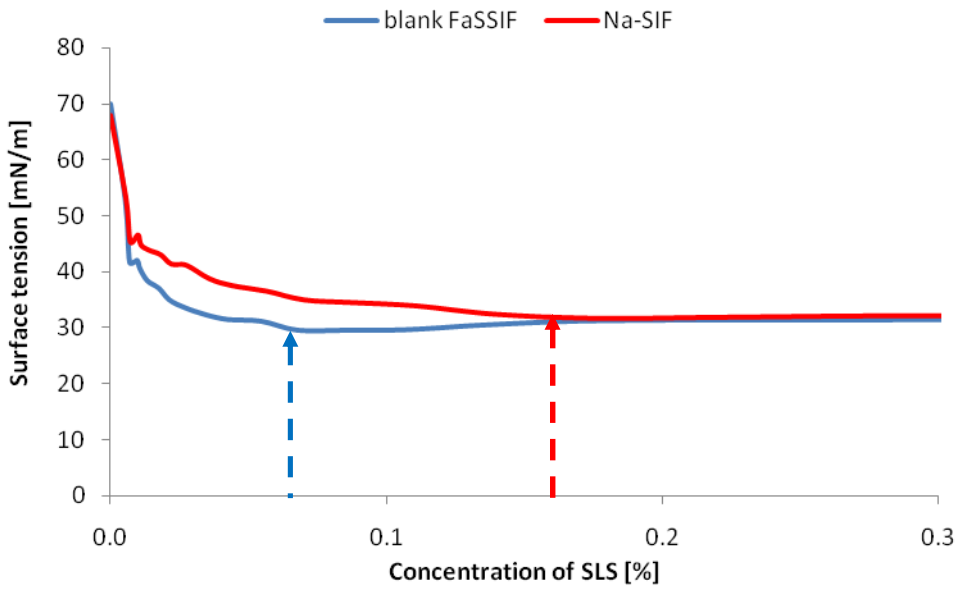

Figure 20. Surface tensions of SIF and blank FaSSIF during SLS titration. [Arrows indicate CMC]

Less surfactant was required in order to reach critical micelle concentration (CMC) of blank FaSSIF-V2. A CMC value of 0.0061 moles/L corresponding to 0.1751% of SLS has been obtained at a surface tension of 31.578 mN/m in SIF, whereas a CMC value of 0.0023 moles/L calculated to be equivalent to 0.00678% of SLS was determined in blank FaSSIF-V2. After the addition of surfactant, both media resulted in surface tensions close to physiological values (33.6 mN/m). They were named MIM-I (Na-SIF + 0.2% SLS) and MIM-II (blank FaSSIF-V2 + 0.1% SLS). Due to the fact that concentrations of natural surfactants that are present *in vivo* are above CMC, amounts of SLS that were further used in MIM-I and MIM-II were rounded up to 0.2 and 0.1%, respectively. The final composition of modified media is presented in Table 38.

Table 38. Composition of modified media (per 1L).

Components (units)	**MGM**	**MIM-I**	**MIM-II**
Sodium chloride (mM)	34.2	-	68.62
Hydrochloric acid (80, 323)	7	-	-
Sodium phosphate monobasic (mM)	-	49.95	-
Maleic acid (mM)	-	-	19.12
Sodium hydroxide (mM)	-	22.4	34.8
SLS (mM)	0.35	6.94 (0.2%)	3.47 (0.1%)
Water	Up to volume	Up to volume	Up to volume
pH	1.2	6.8	6.5
Volume (L)	1	1	1

5.2.2 Buffer capacity studies

The eexperimentally determined buffer capacity of Na-SIF (20 mmoL/L/pH) proved to be similar to the buffer capacity of SIF reported previously (18 mmoL/L/pH) (300). Zoeller and Klein claimed that buffer capacity of blank FaSSIF along with its pH and osmolality are not influenced by the presence of surfactant tested (299). This is also the case for Na-SIF containing SLS as surfactant, for which the buffer capacity value of 18 mmoL/L/pH has been determined.

Buffer capacity is important for the performance of ionisable compounds and excipients (*i.e*. enteric coating) (301), as their solubility strongly depends on the pH of the medium. Failure to provide buffer capacity (*i.e*. water) allows random, uncontrollable changes of pH. HIF contain bicarbonates which are natural species responsible for providing buffer capacity in human GI fluids. It is challenging to reproduce the same conditions *in vitro* due to the increasing pH of bicarbonate buffers as a consequence of the loss of CO_2 from solution (302). However, several scientists successfully characterised the dissolution of various formulations such as enteric coated tablets and modified-release and ionizable drugs using bicarbonate buffers (303-305). Moreover, Garbacz *et al*. developed the device called Physio-stat that helps maintain and regulate the pH of bicarbonate buffers (306).

Buffer capacity of HIF in the fasted state has been reported to be 5.6 mmoL/L/pH, which is in agreement with previously reported by Moreno *et al*. (4-13 mmoL/L/pH) (307). Up to date biorelevant media attempts to mimic HIF closely. Although its buffer capacity is higher than HIF (FaSSIF: 12 mmoL/L/pH; FaSSIF-V2: 10 mmoL/L/pH this is still within the reported range of 4-13 mmoL/L/pH.

5.3 Particle size studies

5.3.1 Carbamazepine case

The particle-size distribution (PSD) of CBZ and its cocrystals were determined (Figure 21). The mean and standard deviation values are shown in Table 39. Particle-size distribution profiles of all formulations are presented in Appendix 6.

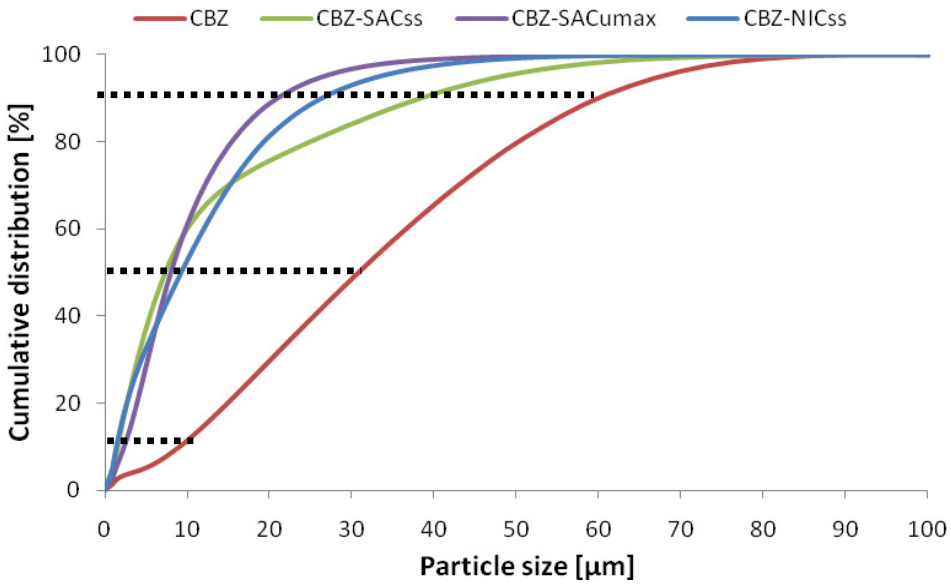

Figure 21. Cumulative PSD of CBZ and its cocrystals.

Table 39. Particle size of CBZ and its cocrystals.

	D_{10} ± SD	D_{50} ± SD	D_{90} ± SD
CBZ	9.08 ± 0.08 µm	30.86 ± 0.34 µm	60.09 ± 0.94 µm
CBZ-SAC$_{ss}$	1.56 ± 0.08 µm	7.38 ± 0.57 µm	38.42 ± 1.18 µm
CBZ-SAC$_{umax}$	2.34 ± 0.04 µm	8.05 ± 0.15 µm	20.99 ± 0.25 µm
CBZ-NIC$_{ss}$	1.42 ± 0.12 µm	9.27 ± 0.81 µm	26.51 ± 0.88 µm

As can be seen from Figure 21 and Table 39, the median particle size (D_{50}) of CBZ was at least up to three times higher when comparing with its cocrystals. This indicates that both of the techniques: sonic-slurrying and UMAX that were used to obtain cocrystals could be used

to micronise an API to a certain extent. Reduction of particle size via micronisation results in an increased surface area which according to the Noyes-Whitney equation may enhance the dissolution (257). All cocrystals demonstrated to have similar D_{10} (1.4-2.3 μm) and median particle size values around 7-9 μm, which consequently could generate similar dissolution profiles. The scanning electron microscopy (SEM) pictures of CBZ-SAC_{ss} and CBZ-NIC_{ss} cocrystals reveal that based on visual observation these two cocrystals are different (Figure 22) (65). Spherical particles of CBZ-SAC_{ss} tend to create small agglomerates, while CBZ-NIC_{ss} cocrystals have needle-like shape with much longer dimensions. This could indicate that the laser diffraction is not the most appropriate technique to analyse these cocrystals. The findings based on laser diffraction do not discriminate between the particle sizes, which could be due to breaking needle - like CBZ-NIC_{ss} particles during the sonication stage. According to the method described in section 4.4.5, all samples were sonicated prior to analysis in order to obtain primary particle size. Sonication is a very invasive technique that separates agglomerated particles apart, allowing measurement of their primary size. Too long a sonication process can break more fragile particles, resulting in a misleading interpretation. If this remark will be reliable, CBZ-SAC_{ss} will result in faster dissolution profile due to smaller particle size observed on SEM pictures.

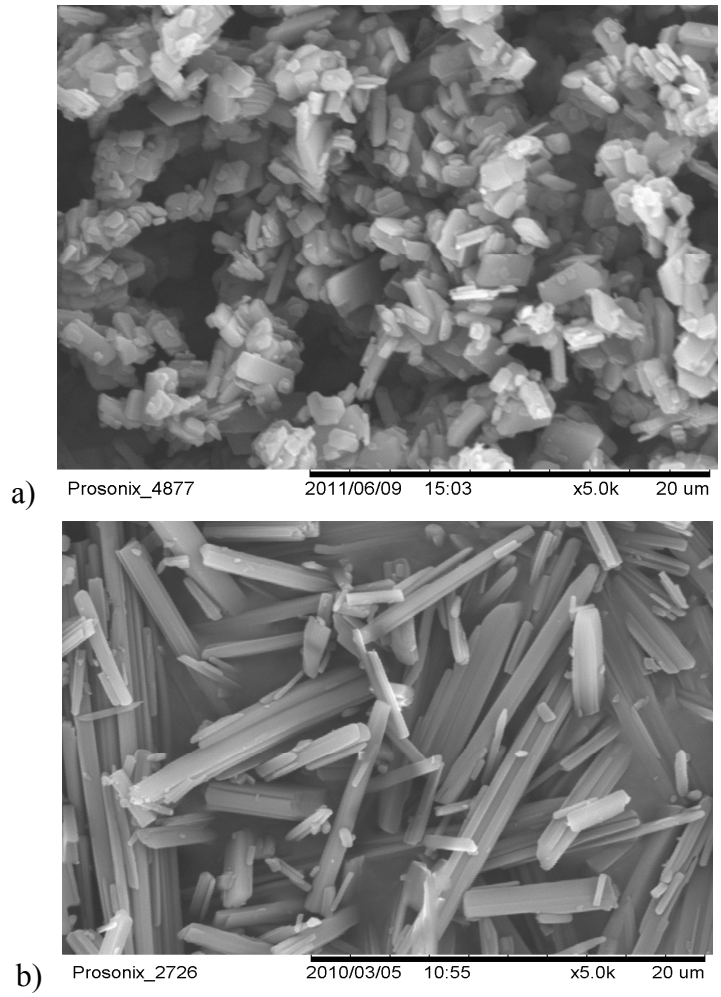

Figure 22. SEM images of a) CBZ-SAC_{ss} and b) CBZ-NIC_{ss} cocrystals (65).

5.3.2 Indomethacin case

The particle-size distribution of IND and its cocrystals was determined (Figure 23). The mean and standard deviation values are shown in Table 40. The particle-size distribution profiles of all formulations are presented in Appendix 6. Particle-size distribution of IND and its cocrystals was determined using the wet dispersion method. The median diameter (D_{50}: 9.30 μm) indicates that the cocrystals with the smallest particle size were produced using sonic-slurrying technique during preparation of CBZ-NIC_{ss}. These particles are over two and a half fold smaller than those characterising IND_{sp} (D_{50}: 24.86 μm). On the other hand, cocrystals made by UMAX technology demonstrate the largest PSD (D_{50}: 32.27 μm), which is even greater than the median value of IND_{sp}. This could be due to the fact that UMAX process consists of three stages, two of which involve spray-drying. IND-SAC samples after first spray-drying step resulted in similar particle size that IND_{sp}. However, a second spay-drying process increased the particle size further (D_{50}: 32.27 μm).

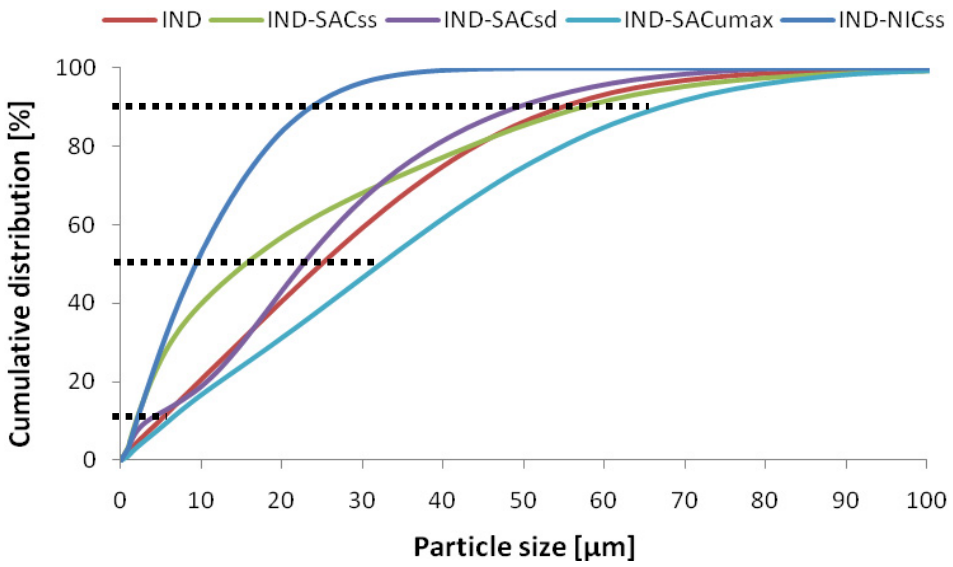

Figure 23. Cumulative PSD of IND and its cocrystals.

Table 40. Particle size of CBZ and its cocrystals.

	D_{10} ± SD	D_{50} ± SD	D_{90} ± SD
IND	4.74 ± 0.04 µm	24.86 ± 0.13 µm	55.21 ± 0.74 µm
IND-SAC$_{ss}$	1.89 ± 0.01 µm	15.40 ± 0.14 µm	57.45 ± 0.62 µm
IND-SAC$_{sd}$	3.27 ± 0.09 µm	22.63 ± 0.28 µm	49.59 ± 1.36 µm
IND-SAC$_{umax}$	5.89 ± 0.10 µm	32.27 ± 1.81 µm	67.34 ± 3.63 µm
IND-NIC$_{ss}$	1.95 ± 0.04 µm	9.30 ± 0.05 µm	23.71 ± 0.41 µm

5.4 Differential Scanning Calorimetry

DSC studies were performed to confirm the cocrystal nature of the samples that were used in solubility and dissolution studies. DSC thermograms of the CBZ and its cocrystals are presented in Figure 24. The CBZ$_{sp}$ showed an endotherm at ~160 ºC followed by another endotherm at ~192 ºC. These thermal events could be explained by the polymorphic transformation of form III (MP~174 ºC) to form I (MP~190 ºC) (73). This has been previously reported in the literature (73). Interestingly, commercial formulation of CBZ, Tegretol® tablets is formulated with the anhydrous monoclinic form (85). Both CBZ-SAC$_{ss}$

and CBZ-SAC$_{umax}$ cocrystals exhibited a melting point of ~176 ºC (Figure 24 and Figure 25), which is in agreement with reported melting point range 172-177.5 ºC (308) for CBZ-SAC form I (312). This value is lower than its pure components SAC (MP~212-229 ºC) (308) and CBZ form I (MP~192 ºC) (73). Similarly, NIC has been reported to have a sharp melting endothermic peak at ~113-130 ºC (73), while CBZ-NIC cocrystals showed a sharp melting peak at ~162 ºC, which is similar to values found in the literature (73) (Figure 25). Cocrystals have a melting point lower than for pure Carbamazepine. All data confirmed that samples that were further used for dissolution and solubility studies were cocrystals.

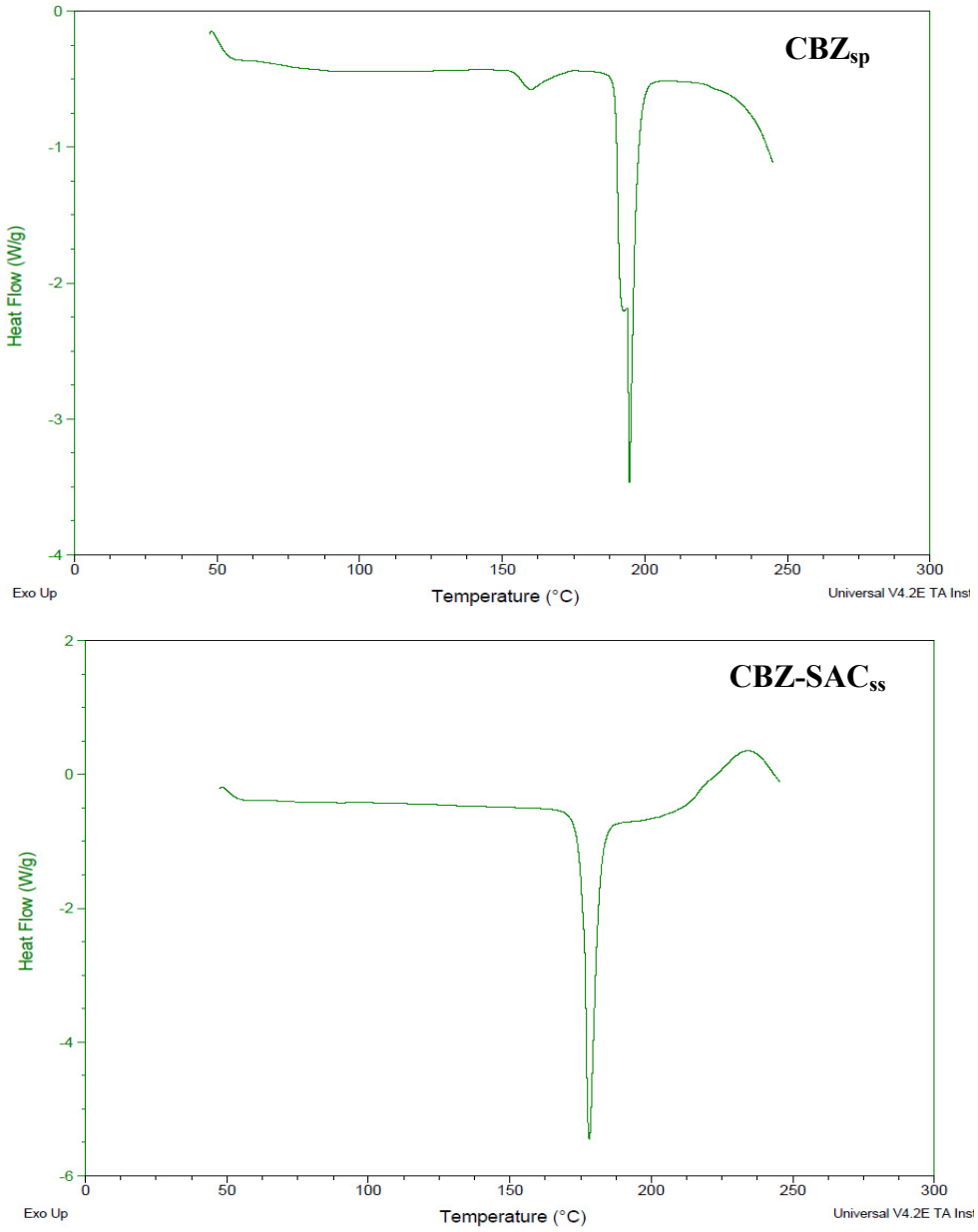

Figure 24. DSC thermograms of CBZ$_{sp}$ and CBZ-SAC$_{ss}$.

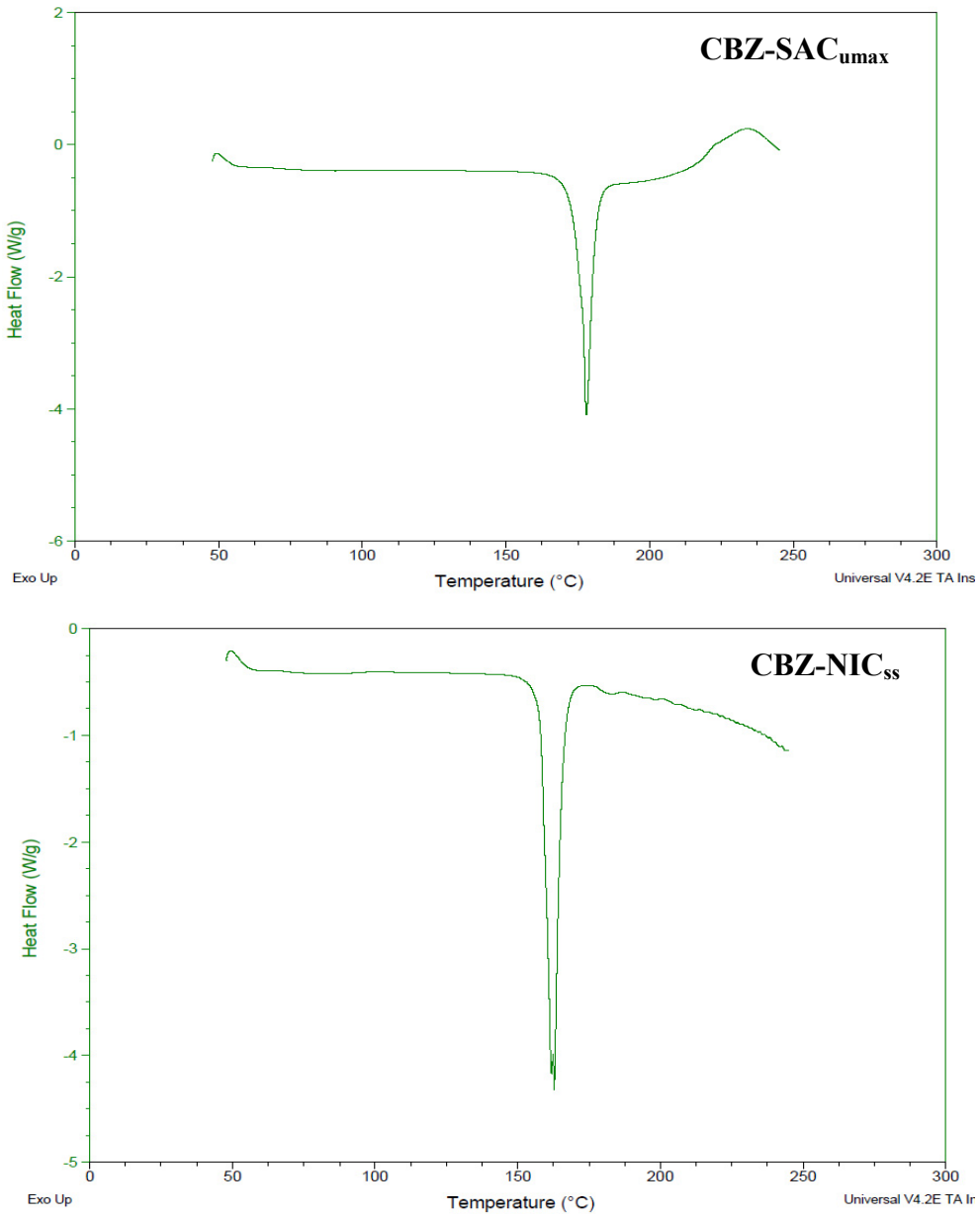

Figure 25. DSC thermograms of CBZ-SAC_{umax} and CBZ-NIC_{ss}.

DSC thermograms of pure components of IND and its cocrystals prepared by various methods are shown in Figure 26, Figure 27 and Figure 28. The thermogram of IND_{sp} exhibited a melting peak at ~162 ºC, which is in agreement with literature (Figure 26) (77, 89). IND-SAC cocrystals that were prepared by either sonic-slurrying, UMAX or spray-drying methods were found to have melting peaks at ~185 ºC, which confirmed the presence of cocrystal forms (Figure 26 and Figure 27) (50, 77). Cocrystal of IND-NIC_{ss} exhibited a melting point at ~128 ºC (Figure 28) (71). DSC methods confirmed the presence of cocrystal forms.

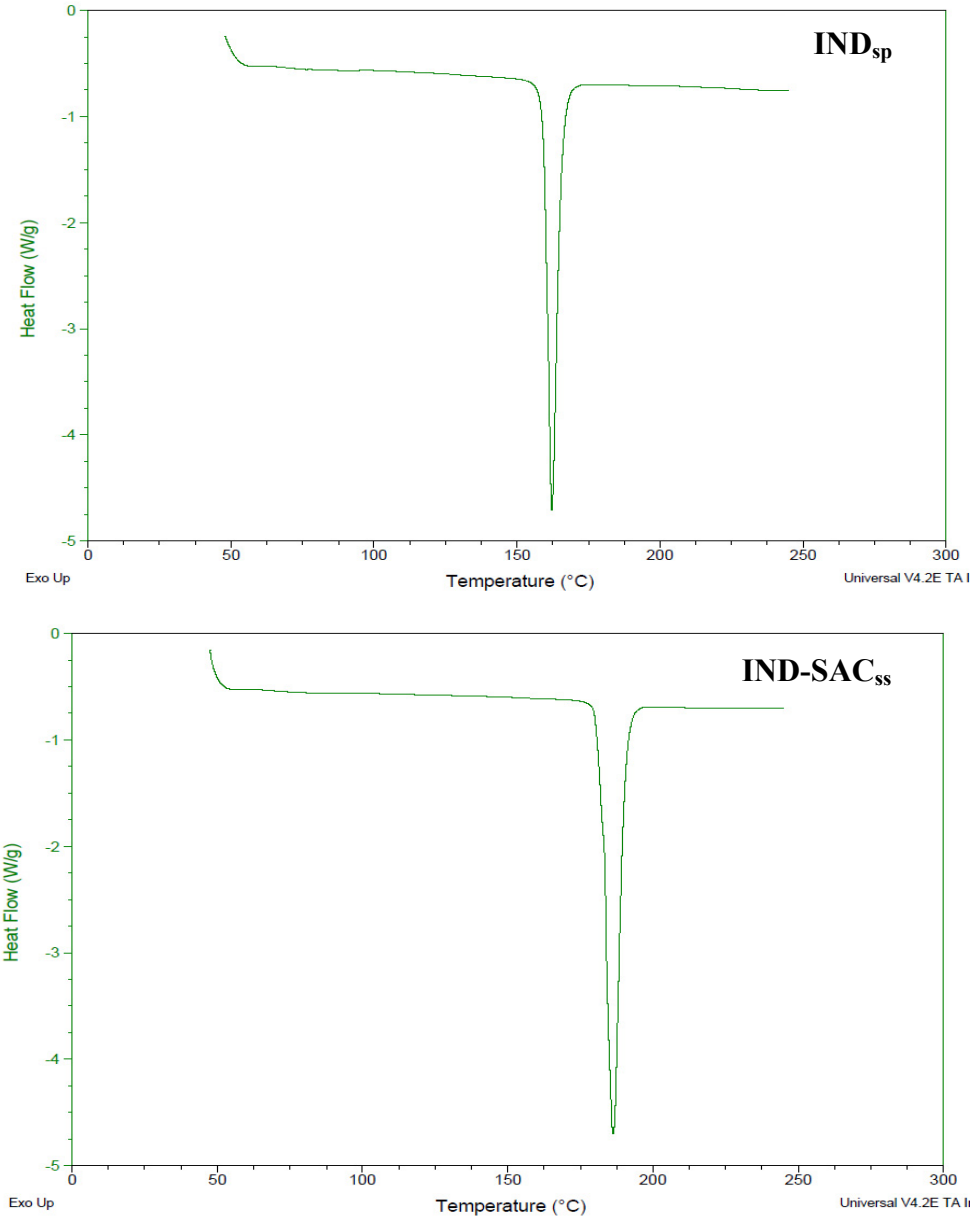

Figure 26. DSC thermograms of IND_{sp} and $IND\text{-}SAC_{ss}$.

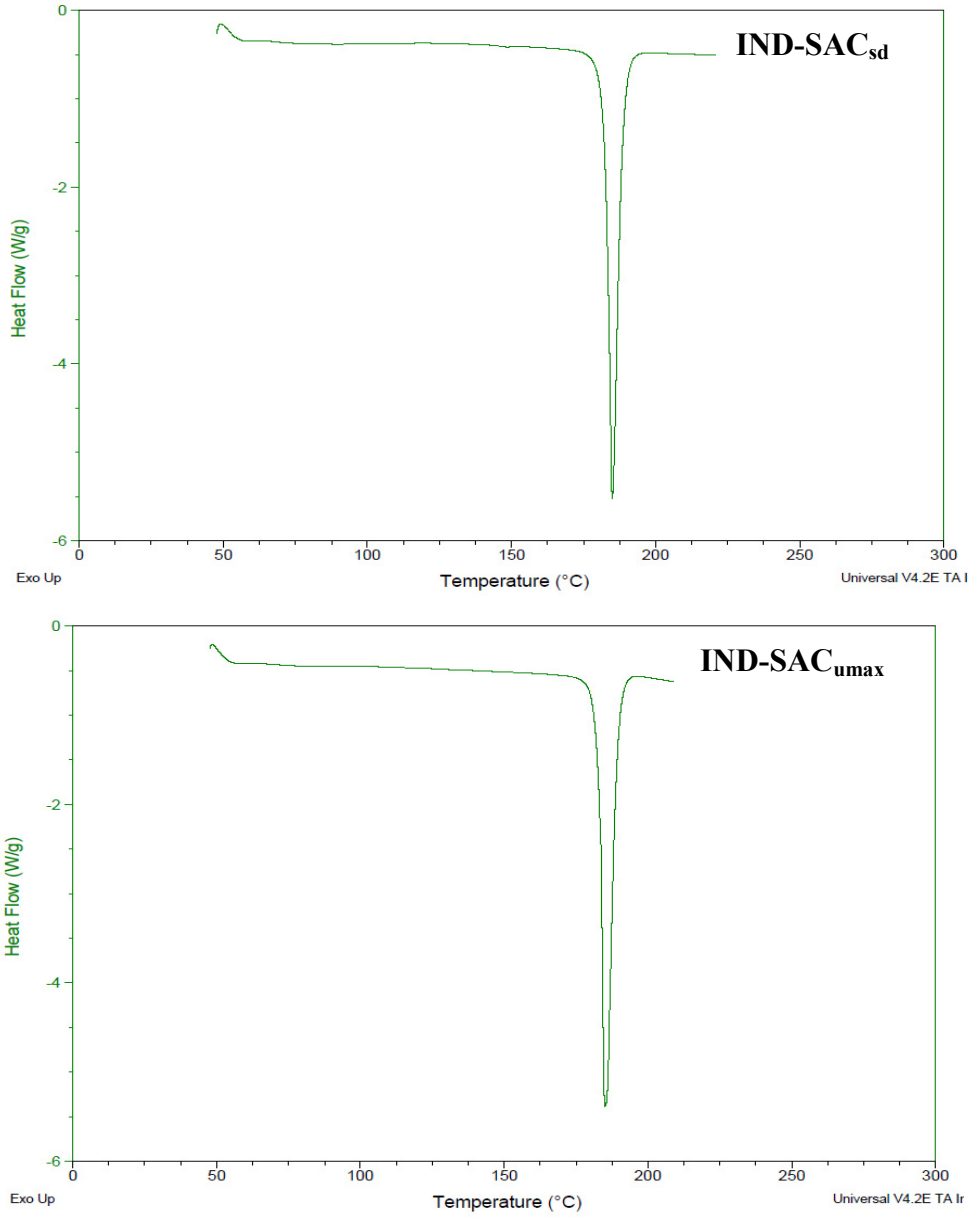

Figure 27. DSC **t**hermograms of IND-SAC$_{sd}$ and IND-SAC$_{umax}$.

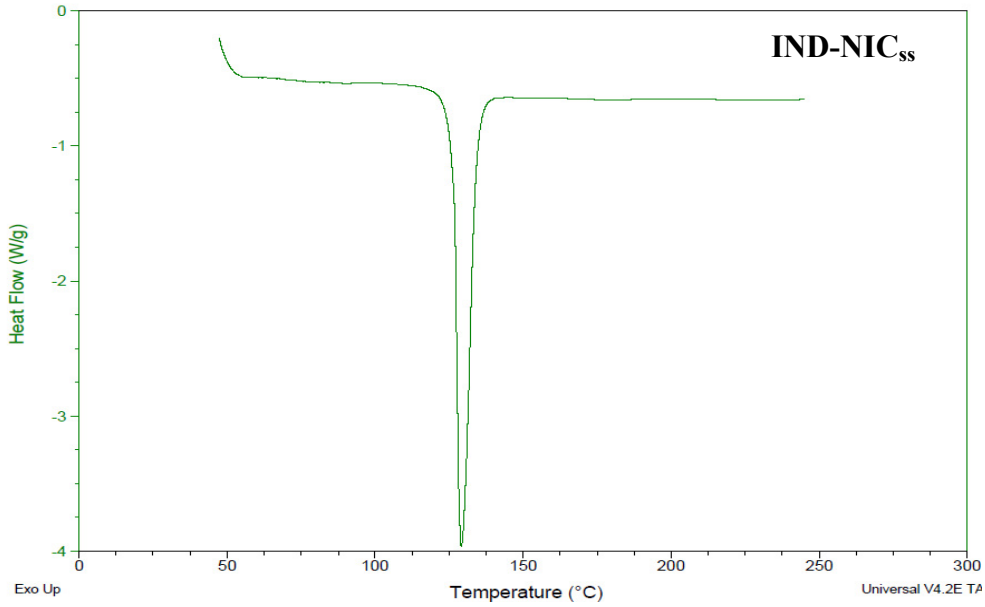

Figure 28. DSC thermograms of IND-NIC_{ss}.

5.5 Validation of chromatographic methods

Adequate volumes of all solutions were injected into the system; sample chromatograms are presented in Figure 29. Retention time for CBZ and IND were 6.6 and 7.8 minutes, respectively.

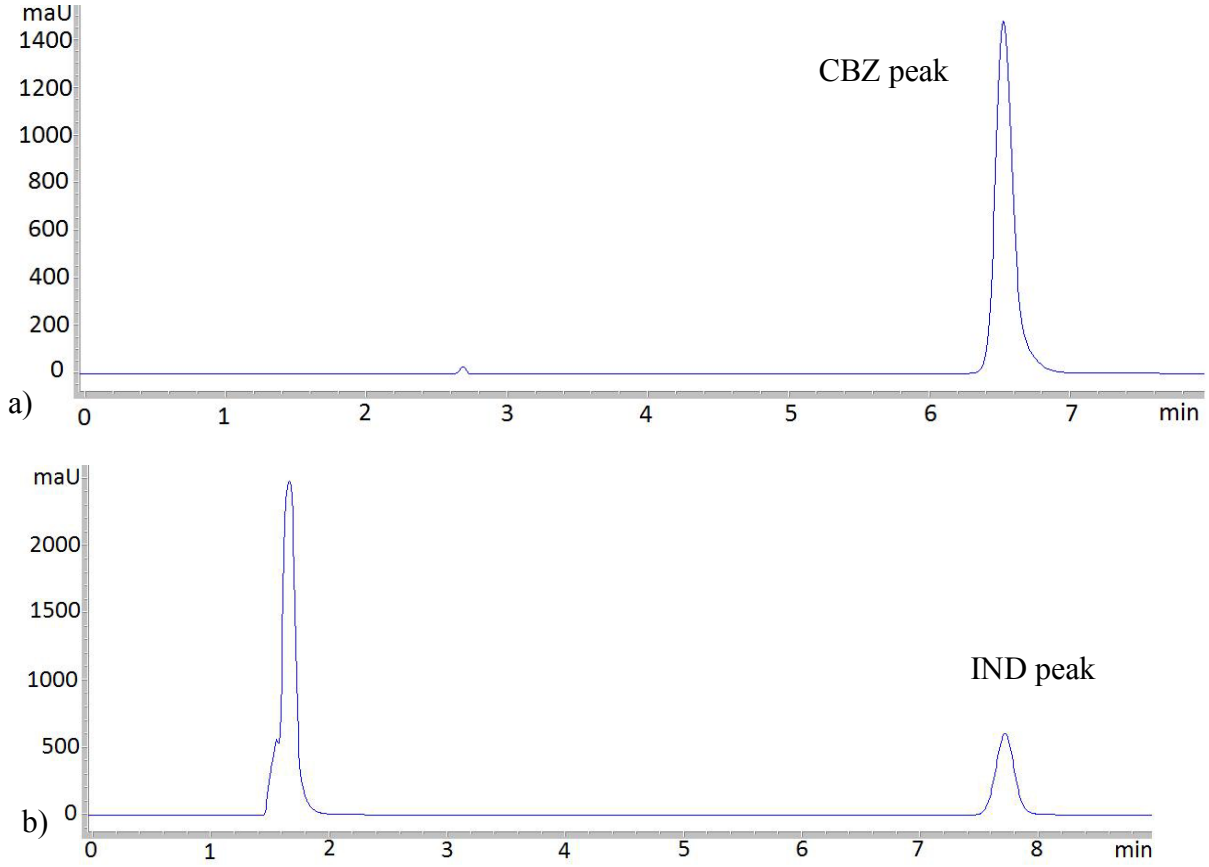

Figure 29. Chromatograms of represented samples: a) CBZ in FaSSGF and b) IND in FaSSIF-V2.

HPLC methods were developed to quantify the concentration of coformer dissolved from cocrystal. Retention times for SAC and NIC peaks were 3.8 and 1.9 minutes, respectively (Figure 30). The peaks appeared in the early onset of chromatograms and there was no interference between coformers' peaks and components of FaSSGF.

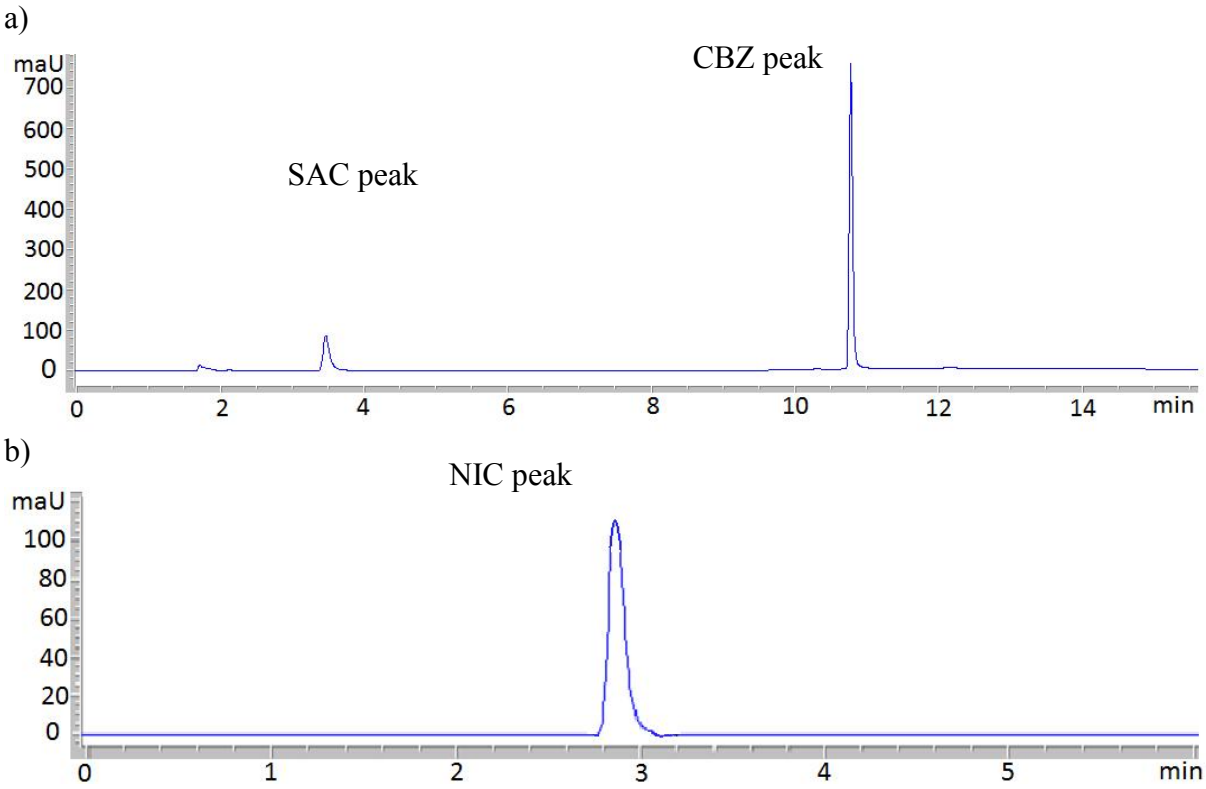

Figure 30. Chromatograms of different samples: a) SAC in FaSSGF and b) NIC in FaSSGF**.**

Linearity and range

Linear calibration curves for CBZ and IND were obtained throughout the concentration ranges studied (Table 41). Linearity criteria imposed a correlation coefficient (R^2) close to one.

Table 41. Linearity and correlation variance for calibration curves.

Media	CBZ		IND	
	Linear regression equation	R^2	**Linear regression equation**	R^2
SGF	y = 159.03x + 11.418	1.00	y = 180.30x + 9.81	1.00
SIF	y = 159.67x + 247.81	1.00	y = 219.83x – 53.11	1.00
MGM	y = 159.08x + 245.49	1.00	y = 217.57x – 1.72	1.00
MIM-I	y = 158.92x + 390.13	1.00	y = 236.00x – 3.49	1.00
MIM-II	y = 159.41x + 285.07	1.00	y = 239.67x – 60.75	1.00
FaSSGF	y = 158.13x +459.83	1.00	y = 195.92x – 10.01	1.00
FaSSIF-V2	y = 158.07 + 278.42	1.00	y = 233.43x – 59.07	1.00

Standard calibration curves of SAC and NIC in FaSSGF reflected good linearity (R^2 =1) in the concentration range studied. The linear regression of SAC and NIC in FaSSGF produced equations y = 39.32x – 9.92 and y = 154.43x + 51.42, respectively.

Precision, Limit of Quantification (LOQ) and Limit of detection (LOD)

The precision of the HPLC methods was examined in 50 µg/ mL standards prepared in either SIF or FaSSGF media. Results showed that intra – day relative standard deviation were less than 1% (Table 42). The LOQ for CBZ, IND, SAC and NIC was found to be 5.32, 0.44, 2.34 and 3.99 µg/ mL, respectively.

Table 42. Summary of precision, LOQ and LOD values.

	CBZ	IND	SAC	NIC
Precison [% RSD]	0.59	0.66	0.98	0.48
LOQ [µg/ mL]	5.32	0.44	2.34	3.99
LOD [µg/ mL]	1.60	0.13	0.70	1.20

5.6 Solubility Studies

5.6.1 Carbamazepine case

The solubility results for the CBZ_{sp} and its cocrystals are shown in Figure 31.

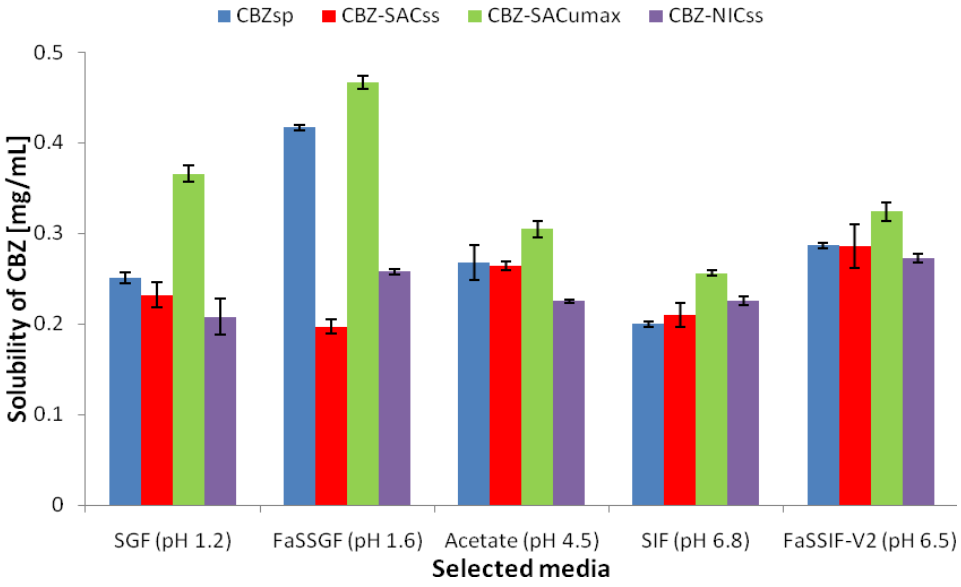

Figure 31. Solubility values (± SD) of CBZ_{sp} in different media.

There is a statistically significant ($p < 0.05$) enhancement in solubility for all CBZ formulations tested in FaSSGF in comparison to compendial SGF. Although, it can be noted that CBZ-SAC_{ss} is slightly less soluble in FaSSGF than in SGF, according to ANOVA this result is not of statistical significance ($p = 1$) (Appendix 7). It has been reported that CBZ behaves as a neutral compound at physiological pH (pK_a = 11.83) (82). Despite that biorelevant media simulating intestinal conditions (FaSSIF-V2) enhance the solubility of all CBZ formulations when compared to compendial SIF, the media simulating gastric conditions provided greater enhancement of solubility than those simulating intestinal conditions. As can be noted from Figure 31, the cocrystals made by sonic-slurry (CBZ-SAC_{ss} and CBZ-NIC_{ss}) did not enhance the solubility of CBZ. Some enhancement was observed for CBZ-SAC cocrystals made by UMAX technology.

Similar results were reported for solubility studies of CBZ, CBZ-SAC and CBZ-NIC cocrystals that were performed for 72 hours at 37 °C (74). Both cocrystals were prepared by cooling crystallisation technique (Table 43). These cocrystals did not enhance the solubility but they proved to be more stable than CBZ against transformation to dihydrate form (72, 308).

Table 43. Solubility data of CBZ (73, 308).

	Solubility of CBZ [mg/mL]		
	HCl buffer (pH 1.2)	**Acetate buffer (pH 4.5)**	**Phosphate buffer (pH 6.8)**
CBZ	0.243 ± 0.026	0.243 ± 0.014	0.238 ± 0.023
CBZ-SAC	0.246 ± 0.013	0.250 ± 0.004	0.235 ± 0.011
CBZ-NIC	0.236 ± 0.008	0.237 ± 0.002	0.234 ± 0.010

5.6.2 Indomethacin case

5.6.2.1 Solubility over time studies

Solubility profiles of IND and its SAC and NIC cocrystals (made by sonic-slurry method) over time were determined (Figure 32 and Figure 33). There was no visible indication of the spring and parachute effect. Some of the researchers claim that *spring and parachute* concept can be explain the phenomena by which cocrystals enhance solubility and dissolution (309). According to this concept, cocrystal dissociate to amorphous or noncrystalline drug clusters (*the spring*), which transform via fast-dissolving metastable polymorphs to the insoluble

crystalline modification to give high solubility for cocrystals and optimal drug concentration (*the parachute*) in the aqueous medium (309). Spring and parachute effect can last from few minutes to hours. So there is a risk of omitting the solubility enhancement when measuring saturation solubility at the equilibrium

The initial solubility values were measured at five minutes. Thus, there is a possibility that the spring and parachute phenomena might have occurred before five minutes. The high variability in concentrations at different time points was due to the fact that the solubility equilibrium has not been reached yet. There were no samples collected between 240 and 1440 minutes, neither after 1440 minutes. Based on these data, it is difficult to make the decision on the definite equilibrium time points. 24 hour (1440 minutes) time point was treated as solubility equilibrium, as it was noticed that in samples which were left longer than 24 hours, needle-shaped crystals were observed. This could indicate that anhydrous form of Carbamazepine transformed to less soluble dihydrate form. However, this was not investigated further.

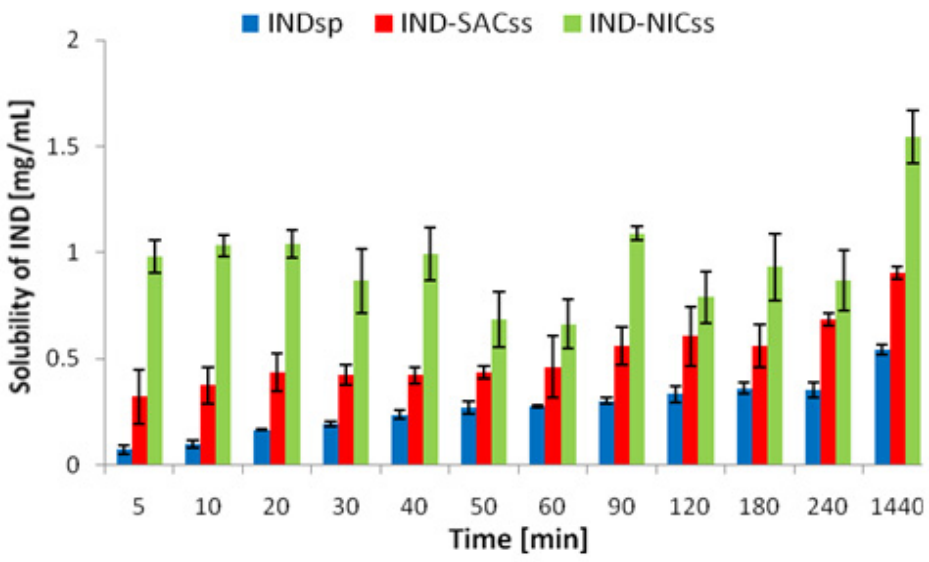

Figure 32. Solubility of IND values (± SD) over the time in SIF.

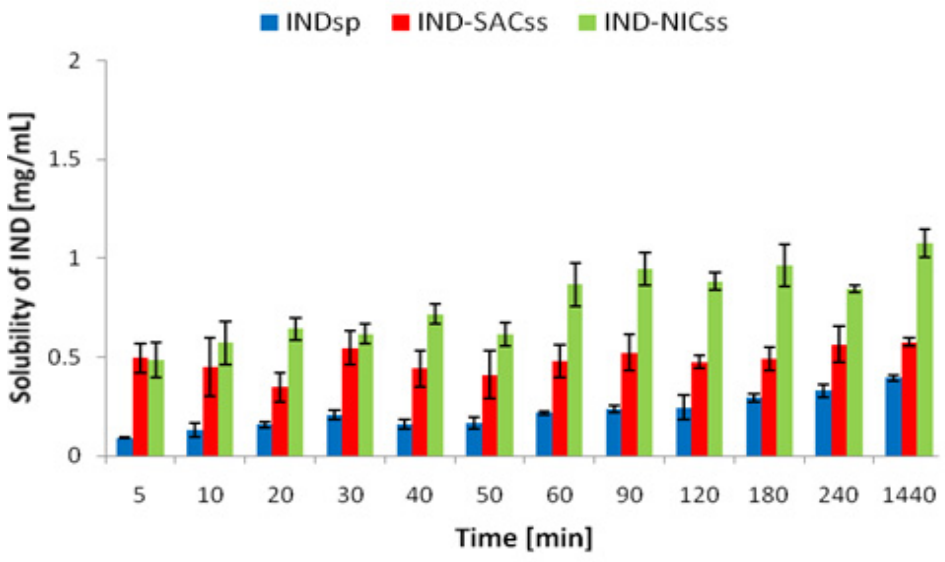

Figure 33. Solubility of IND values (± SD) over the time in FaSSIF-V2.

5.6.2.2 Saturation solubility studies

Due to the fact that IND has pH-dependent solubility (pKa 4.42) the solubility data are presented on two separate graphs to ease the observation. IND has a very low solubility when the compound is in its un-ionised form at pH < 3.4 (Figure 34). Despite that IND and its cocrystals are poorly soluble in acidic conditions (SGF and FaSSGF) (< 0.03 mg/mL), 2 to 10 folds enhancement in solubility can be observed when solubility of IND is measured from its cocrystal form. Higher solubility values observed in acetate buffer pH 4.5 are due to the fact that at this pH IND is 50% in its ionised form. When the pH exceed pH 5.4 (one unit above pK_a) the IND is fully ionised and reaches maximum solubility (Figure 35). Interestingly, solubility of all IND formulations is lower in FaSSIF than in SIF despite the presence of bile salts. Despite the decrease in solubility in the presence of bile salts, there is still a clear trend visible, that cocrystallisation with Nicotinamide enhances the solubility of IND the most (up to three times).

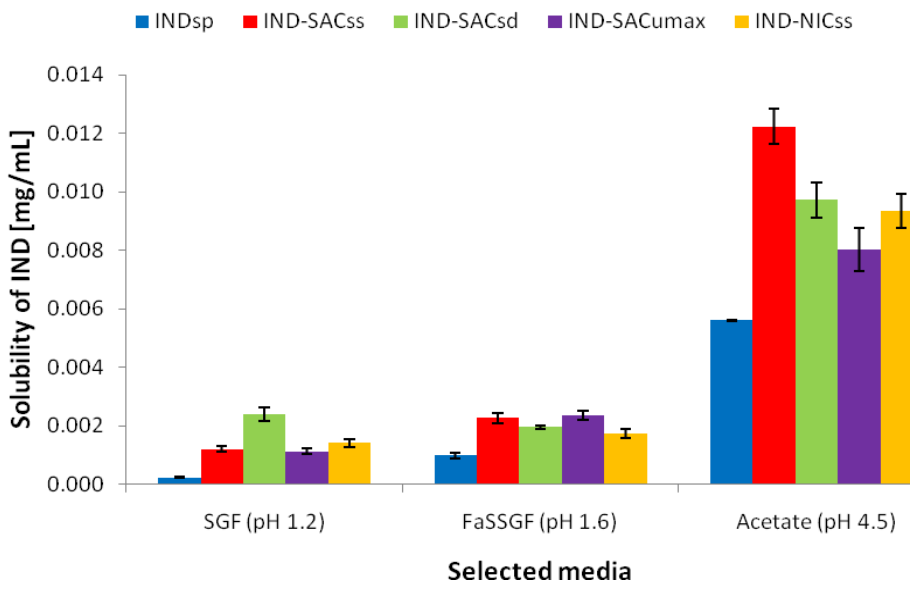

Figure 34. Solubility values (± SD) of IND in SGF, FaSSGF-V2 and acetate media.

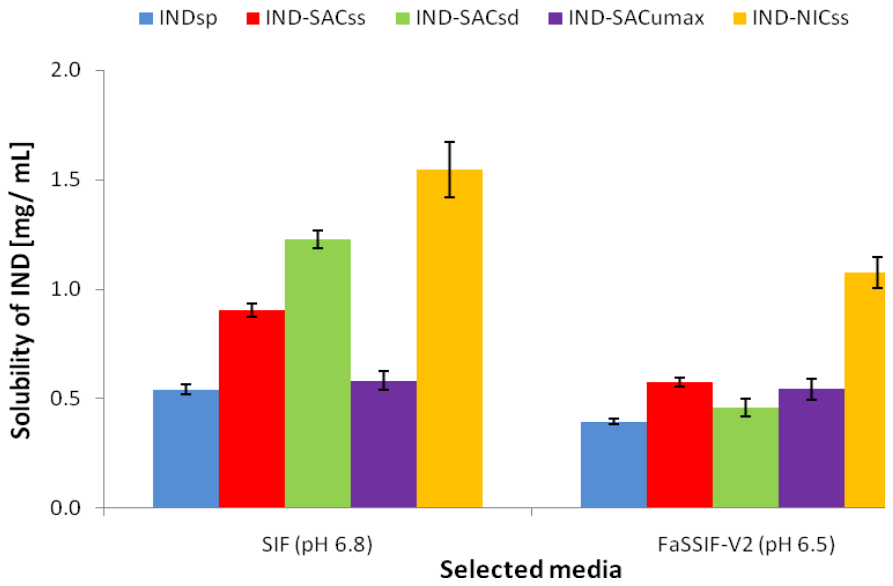

Figure 35. Solubility values (± SD) of IND in SIF and FaSSIF-V2.

Nokhodchi reported slightly higher saturated solubility of IND in SGF (0.004 mg/mL) and SIF (0.768 mg/mL) (310). The discrepancies could be due to differences in methodology (25°C, 72 h). Solubility of IND cocrystals was well studied in organic solvents (71) but up to now little was known about the solubility of IND cocrystals in compendial and biorelevant media.

5.7 *In vitro* dissolution studies

Initial experiments were performed using USP apparatus 1. Dissolution profiles of all of the formulations of CBZ and IND tested using USP Apparatus 4 were tested in four different sets of media: compendia SGF/SIF, modified MGM/MIM-I and MGM/MIM-II and biorelevant FaSSGF/FaSSIF-V2. Data collected for each formulation were interpreted, compiled and presented as cumulative percentage dissolved *versus* time.

5.7.1 Carbamazepine case

5.7.1.1 Dissolution studies using USP apparatus 1

Dissolution of CBZ from Tegretol® tablets in SGF was incomplete using the USP apparatus 1 (Figure 36). Only 50% of the drug dissolved after four hours of experiment. This is due to the fact that 500 mL of medium in USP apparatus 1 did not provide sink conditions for 200 mg of poorly soluble drug. The volume of 500 mL of medium was selected to be more physiologically relevant than 900 mL. In order to provide at least three times sink condition, dissolution should be performed using 3 L of medium. Dissolution of CBZ from Tegretol® tablets was much faster than those from CBZ_{sp} capsules due to the presence of various excipients such as diluents and disintegrants in the Tegretol® formulation. The dissolution of both CBZ-SAC_{ss} and CBZ-NIC_{ss} cocrystals capsules was much slower than the performance of CBZ_{sp} capsules and Tegretol® tablets. This can be explained by the over-compaction of cocrystal powder in size 0 capsule. The compaction forces were greater in CBZ-NIC_{ss} capsules, as in order to fill in equivalent to 200 mg of CBZ, 303 mg of CBZ-NIC_{ss} needs to be packed in size 0 capsule. It was observed that it was more challenging to fill the capsule with 303 mg of CBZ-NIC_{ss} cocrystal than with 355 mg of CBZ-SAC_{ss} sample. This is potentially due to the differences in powder density of these two samples (Table 44) (308, 73).

Table 44. Summary of cocrystal powder densities values found in literature (73, 308).

	CBZ (74)	CBZ-SAC (312)	CBZ-NIC (74)
True density [g/cm^3]	1.381	1.441	1.337
Bulk density [g/cm^3]	0.452	0.592	0.174
Tapped density [g/cm^3]	0.782	0.790	0.292

According to the tapped density values (Table 44), it would be much harder to compress CBZ-NIC (the lowest tapped density) powder than CBZ and CBZ-SAC cocrystal into the same size of capsule. The lowest tapped density value of 0.292 g/cm^3 indicates that CBZ-NIC cocrystals have a shape of needles. These findings are in agreement with SEM findings (65).

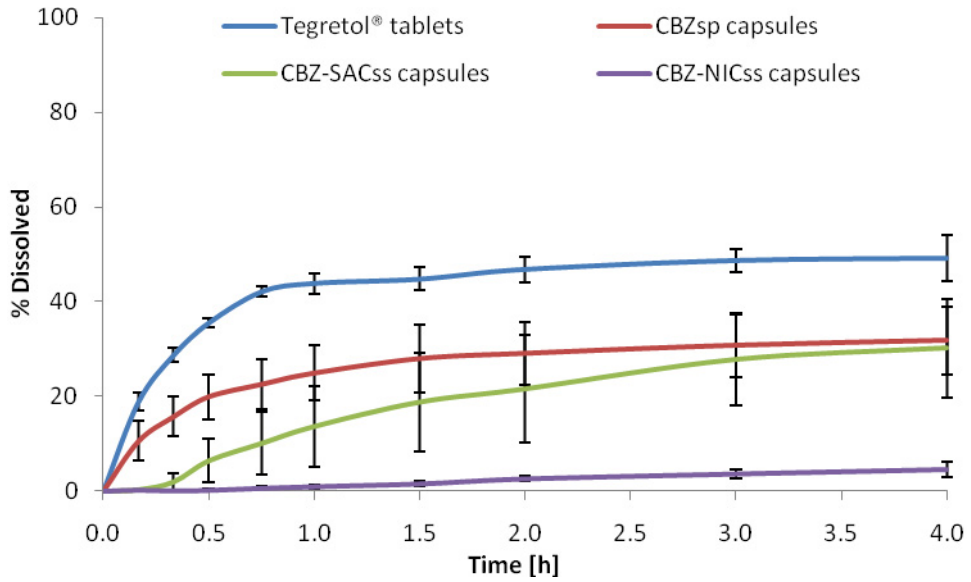

Figure 36. Mean % dissolved (± SD) of different CBZ formulations in SGF using USP apparatus 1.

Similar dissolution behaviour of CBZ was observed for Tegretol® tablets and CBZ capsules tested in SIF using the USP apparatus 1 (Figure 37). Similarity between profiles in SGF and SIF (Tegretol® in SGF *vs* SIF; $f_{1,\,area}$: 0.09; CBZ_{sp} in SGF *vs* SIF; $f_{1,\,area}$: 0.13) is attributed to the solubility of CBZ in both media (SGF: 0.251 mg/mL; SIF: 0.250 mg/mL). Failure of providing sink conditions and problematic encapsulation of samples makes continuation of dissolution studies using USP apparatus 1 debatable. Further studies were performed using USP apparatus 4 dissolution system, which allows testing powder samples and provides sink condition for poorly soluble CBZ formulations.

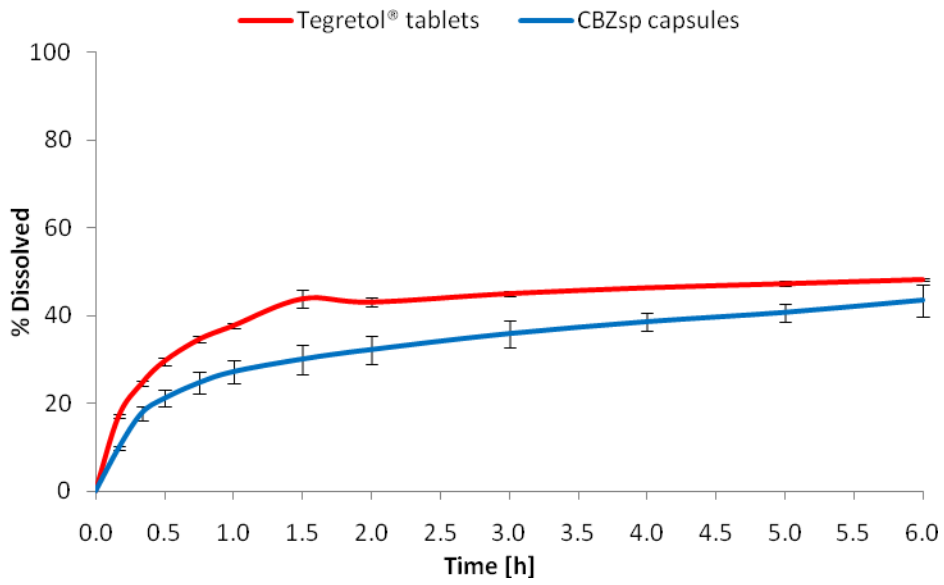

Figure 37. Mean % dissolved (± SD) of different CBZ formulations in SIF using USP apparatus 1.

Various dissolution profiles have been reported for 200 mg Tegretol® tablets (315). Due to the fact that different specifications were used to obtain that data (USP apparatus type, rpm, media type and volume) further direct comparison of data was not achievable.

Dissolution of CBZ-SAC cocrystals (made by cooling crystalisation) tested using USP apparatus 2 has been reported (100 rpm, 37 °C) (308). CBZ-SAC sample was sieved into different particle size (50, 150, 300, 500 and 1000 µm) and encapsulated into a gelatin capsule. In order to provide sink conditions, formulations were tested in 900 mL of SGF containing Triton – X as a surfactant. Results indicated that CBZ-SAC cocrystal samples with the particle size smaller than 150 µm demonstrated the fastest dissolution profiles due to increased surface area. Dissolution performance of cocrystal was strongly dependent on the particle size of the cocrystal tested.

5.7.1.2 Dissolution studies using USP apparatus 4

5.7.1.2.1 Effect of MCC on CBZ dissolution

As CBZ cocrystals samples exhibit static properties, the decision of adding MCC to all CBZ (CBZ_{sp}, CBZ-SAC $_{(ss\ and\ umax)}$ and CBZ-NIC_{ss}) samples was made. MCC is the major diluent in CBZ commercial formulation Tegretol®. Different grades of MCC were investigated varying in particle size from 20 µm (PH 105), 100 µm (PH 302), to 180 µm (PH 200). Approximately 70% of the CBZ was dissolved from CBZ-MCC formulations within two

hours of the experiment (Figure 38). According to $f_{1,\ area}$ (Table 45) there was no statistical difference between dissolution profiles after blending with any grade of MCC when compared with the CBZ dissolution profile. For further studies, all CBZ samples were blended with the medium size of MCC (PH 302). Small variability (%CV < 7.2) was observed for the dissolution of these formulations.

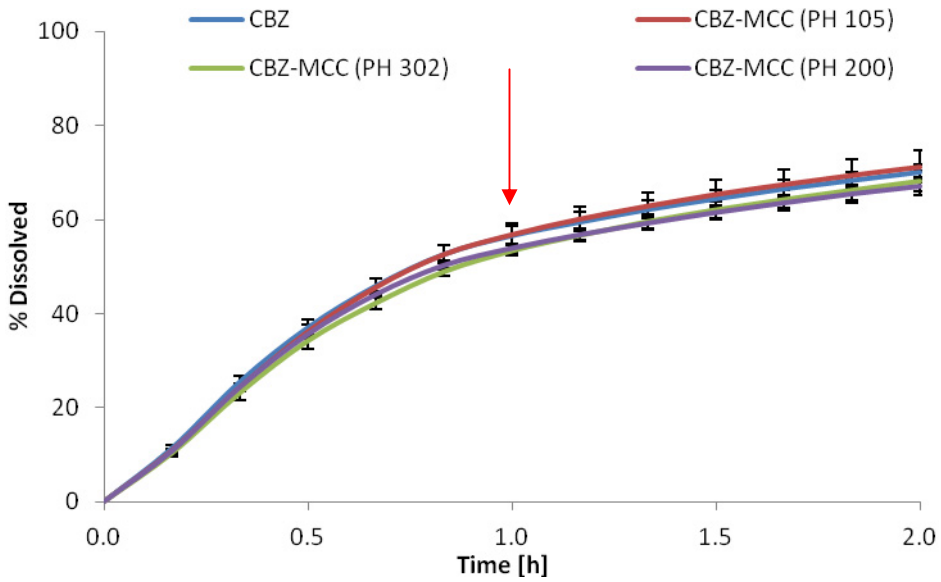

Figure 38. Mean % dissolved (± SD) of CBZ from different CBZ_{sp}-MCC formulations in SGF (8mL/min; 1h) and SIF (4mL/min; 1hr) using USP apparatus 4. [Red arrow indicates media change].

Table 45. Summary of $f_{1,\ area}$ values comparing dissolution profiles of CBZ_{sp}-MCC in various media.

CBZ (as reference)	**CBZ-MCC grade**		
	PH-105	**PH-200**	**PH-302**
$f_{1,\ area}$	0.01	0.05	0.05

Despite that all CBZ samples (CBZ_{sp}, CBZ-SAC_{ss}, CBZ-SAC_{umax}, CBZ-NIC_{ss}) were blended with MCC (PH-302) for further studies, nomenclature remained unchanged.

5.7.1.2.2 Dissolution studies of commercial formulations

Carbamazepine commercial formulations available in UK are known under its brand name Tegretol® and have been manufactured by Novartis since 1965. Tegretol® is available for oral administration as chewable tablets of 100 mg and 200 mg, liquid of 100 mg/ 5mL, immediate release tablets of 100 mg, 200 mg and 400 mg and prolonged release tablets of 200 mg and 400 mg (formerly known as Tegretol® retard). It is also available for rectal administration as suppositories of 125 mg and 250 mg. Dissolution profiles of CBZ from 200 mg Tegretol® IR tablets and 400 mg Prolonged Release Tegretol® tablets were tested using USP apparatus 4.

5.7.1.2.2.1 Tegretol® IR tablets

Dissolution profiles of Tegretol® IR formulations in various media are presented in Figure 39. Based on the $f_{1,\ area}$ values (Table 46) dissolution profiles in both modified and biorelevant media are significantly different when compared with compendial media (SGF/SIF). The greatest increment by 1.5 fold occurred in biorelevant media ($f_{1,\ area}$: 1.46) due to the presence of bile salts. It is known that biorelevant media contain mixed micelles as opposed to single type of SLS micelles present in modified media (299). Distinctive nature of the micelles has different effect on the dissolution of poorly soluble compounds. The mixed surfactant systems (ionic & non-ionic) show synergetic behaviour and thus the total quantity of surfactant required for the same performance is smaller (312).

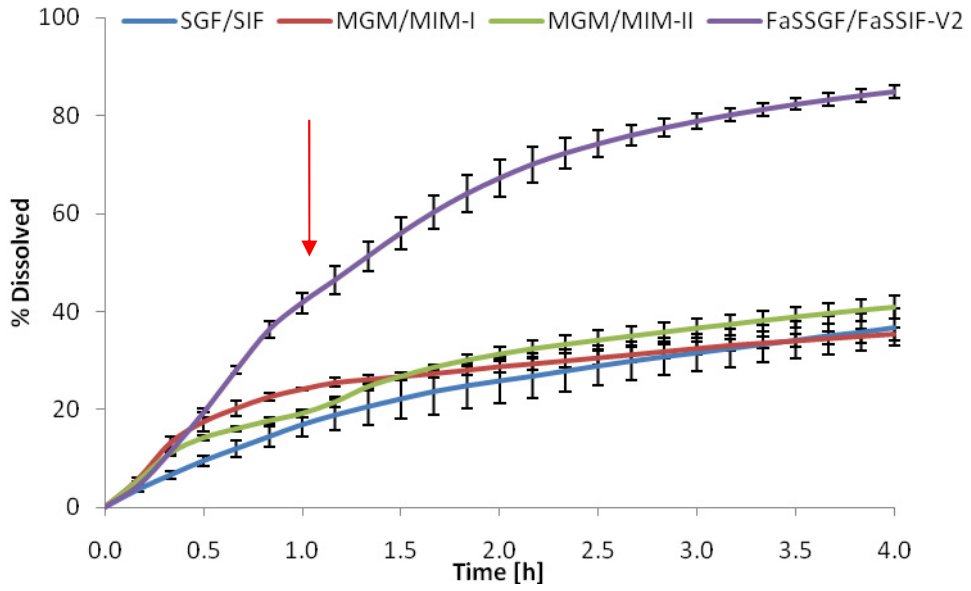

Figure 39. Mean % dissolved (± SD) of CBZ from 200 mg Tegretol® IR tablets in various media using USP apparatus 4. [Red arrow indicates media change].

Table 46. Summary of $f_{1,\ area}$ values comparing dissolution profiles of CBZ from 200mg Tegretol® tablets in various media.

SGF/SIF (as reference)	Tegretol® tablets		
	MGM/MIM-I	**MGM/MIM-II**	**FaSSGF/FaSSIF-V2**
$f_{1,\ area}$	0.15	0.18	1.46

Recently, Medina *et al*. published dissolution studies of Tegretol® IR formulation using USP apparatus 4 (313). It has been reported that 80% of CBZ was released from the tablet within 60 minutes. Although different flow rate (16 mL/min) and media (1% SLS) were used during this investigation.

According to the *AIC* and R^2 values which both indicate the best model and its goodness of fit, the dissolution kinetics of CBZ from 200 mg Tegretol® IR tablets can be best described using 3-parameter Weibull function (Table 47). Based on β parameter that reflects the shape of the dissolution curve, three of the dissolution profiles (in compendial and both of modified media) have a parabolic shape ($\beta < 1$), whereas dissolution profile in biorelevant media is more characterised by S-shape ($\beta > 1$). Weibull function is purely mathematical equation that does not have any physiological meaning.

All dissolution profiles obtained for 200 mg Tegretol® IR tablets follows first-order kinetics. The presence of the surfactant in the media does not change the kinetics (Table 47).

Table 47. Dissolution kinetic parameters (± SD) of 200 mg Tegretol® IR tablets.

Parameters	Zero-order kinetics			
	SGF/SIF	**MGM/MIM-I**	**MGM/MIM-II**	**FaSSGF/FaSSIF-V2**
$k_0 [h^{-1}]$	10.70 ± 1.50	11.39 ± 0.39	12.49 ± 0.58	26.51 ± 0.60
R^2	0.84 ± 0.08	0.17 ± 0.19	0.71 ± 0.08	0.79 ± 0.05
AIC	151.71 ± 18.01	186.33 ± 2.80	171.61 ± 3.23	205.98 ± 7.01
First-order kinetics				
W_{max} [%]	42.16 ± 4.27	33.40 ± 2.12	43.45 ± 4.83	96.99 ± 3.25
$k_1 [h^{-1}]$	0.49 ± 0.13	1.26 ± 0.20	0.65 ± 0.10	0.56 ± 0.07
R^2	1.00 ± 0.00	0.97 ± 0.02	0.99 ± 0.00	0.99 ± 0.00
AIC	55.52 ± 13.71	97. 95 ± 15.45	83.46 ± 5.99	117 ± 20.03
3-parameter Weibull function				
W_{max} [%]	67.60 ± 43.47	37.10 ± 2.03	50.30 ± 4.02	87.52 ± 4.20
α [h]	4.01 ± 3.71	1.03 ± 0.14	1.88 ± 0.21	1.61 ± 0.22
β	0.89 ± 0.14	0.73 ± 0.10	0.82 ± 0.07	1.25 ± 0.13
R^2	1.00 ± 0.00	0.99 ± 0.01	1.00 ± 0.00	1.00 ± 0.00
AIC	36.89 ± 23.07	83.82 ± 15.18	65.72 ± 19.52	74.63 ± 7.69

5.7.1.2.2.2 Tegretol® PR tablets

Prolonged and extended release formulations tend to benefit from partial absorption from the colon. Thus, exposure to media that simulate colonic environment is essential. Release rate of CBZ from 400 mg Tegretol® PR formulation was tested in either compendial media (SGF/SIF/SCoF), biorelevant media (FaSSGF/FaSSIF-V2/FaSSCoF) or mixed biorelevant/compendial media (FaSSGF/FaSSIF-V2/SCoF) (Figure 40). CBZ from prolonged release formulation of Tegretol® dissolved in a well-controlled manner, regardless the type of

medium selected for the experiment. There is no significant difference ($f_{1,\ area}$: 0.11) between the dissolution profile in compendial media (SGF/SIF/SCoF) and in FaSSGF/FaSSIF-V2/SCoF (Table 48). Interestingly, no significant difference ($f_{1,\ area}$: 0.05) was observed between two dissolution profiles that both used biorelevant media for the first five hours and then used either SCoF or FaSSCoF as media.

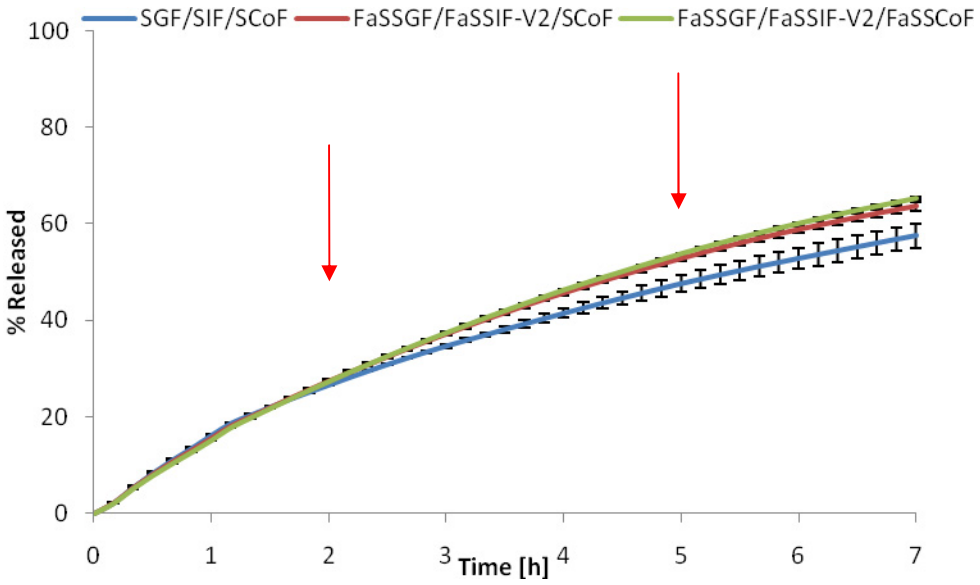

Figure 40. Mean % dissolved (± SD) of CBZ from 400 mg Tegretol® PR tablets in various media using USP apparatus 4. [Red arrows indicate media change].

Table 48. Summary of $f_{1,\ area}$ values comparing dissolution profiles of CBZ from 400mg Tegretol® tablets in various media.

	Tegretol® PR tablets	
SGF/SIF/SCoF (as reference)	**FaSSGF/FaSSIF-V2/SCoF**	**FaSSGF/FaSSIF-V2**
$f_{1,\ area}$	0.09	0.11

According to Table 49 release of CBZ from 400 mg Tegretol® PR tablets can be best described by first-order kinetics, dissolution constant indicates that the dissolution profile in biorelevant media ($k_1 = 0.18$) is slightly faster than in compendial media ($k_1 = 0.24$).

Table 49. Dissolution kinetic parameters (± SD) of 400 mg Tegretol® PR tablets**.**

Parameters	**Zero-order kinetics**		
	SGF/SIF/SCoF	**FaSSGF/FaSSIF-V2/SCoF**	**FaSSGF/FaSSIF-V2/FaSSCoF**
$k_0 [h^{-1}]$	9.47 ± 0.31	10.42 ± 0.12	10.60 ± 0.03
R^2	0.88 ± 0.03	0.93 ± 0.01	0.94 ± 0.00
AIC	308.74 ± 6.20	301.77 ± 2.48	296.78 ± 2.18
First-order kinetics			
W_{max} [%]	69.92 ± 6.65	86.06 ± 2.56	92.29 ± 1.94
$k_1 [h^{-1}]$	0.24 ± 0.03	0.19 ± 0.01	0.18 ± 0.01
R^2	1.00 ± 0.00	1.00 ± 0.00	1.00 ± 0.00
AIC	150.71 ± 2.27	67.82 ± 9.74	42.33 ± 3.56
3-parameter Weibull function			
W_{max} [%]	93.80 ± 14.84	94. 51 ± 1.96	97.87 ± 2.11
α [h]	5.44 ± 0.99	5.63 ± 0.17	5.98 ± 0.19
β	0.84 ± 0.01	0.95 ± 0.01	0.97 ± 0.00
R^2	1.00 ± 0.00	1.00 ± 0.00	1.00 ± 0.00
AIC	100.19 ± 3.47	32.27 ± 6.32	24.38 ± 7.98

5.7.1.2.3 CBZ_{sp} and pharmaceutical cocrystals

Carbamazepine cocrystals were tested under the same conditions as Tegretol® commercial formulations. CBZ_{sp} samples were used as a control formulation.

5.7.1.2.3.1 CBZ_{sp} samples

Dissolution profiles of CBZ_{sp} samples in different media are presented in Figure 41. Dissolution of CBZ_{sp} in compendial media (SGF/SIF) was initially faster (until first hour) than in all the other media and then slowed down after the media change and resulted in overall first-order kinetics (Table 51). On the other hand, dissolution profiles obtained in media containing surfactants or bile salts can be closely characterised using overall zero-order kinetics (Table 51). This demonstrates that the dissolution kinetics has been altered by the presence of surfactant. $f_{1,\ area}$ allows distinguishing between the profiles (Table 50). There was statistically significant difference ($f_{1,\ area}$: 0.32) in the dissolution profile of CBZ_{sp} in MGM/MIM-I when compared with its performance in compendial media.

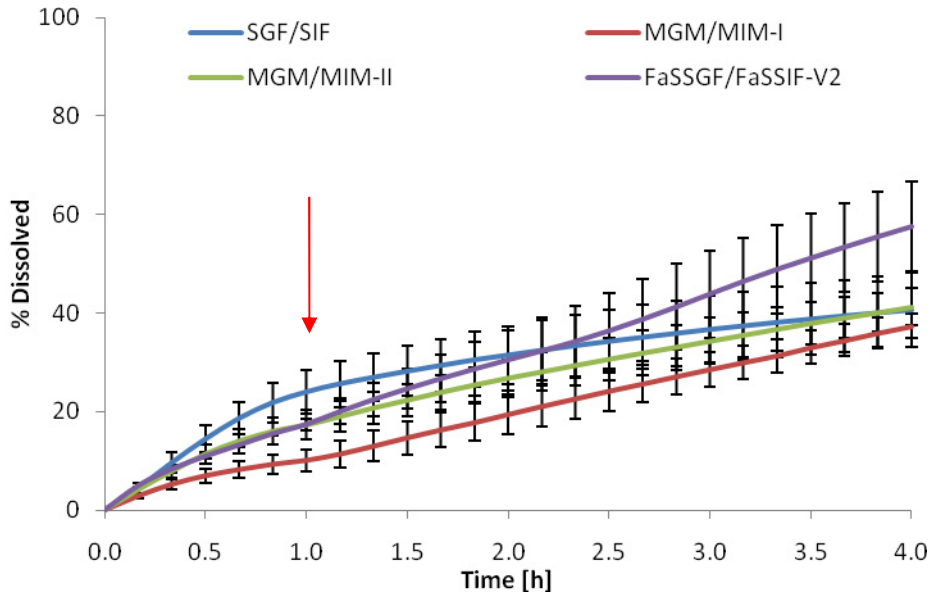

Figure 41. Mean % dissolved (± SD) of CBZ_{sp} in various media using USP apparatus 4. [Red arrow indicates media change].

Table 50. Summary of $f_{1,\ area}$ values comparing dissolution profiles of CBZ_{sp} in various media.

SGF/SIF (as reference)	CBZ_{sp}		
	MGM/MIM-I	**MGM/MIM-II**	**FaSSGF/FaSSIF-V2**
$f_{1,\ area}$	0.32	0.12	0.19

Table 51. Dissolution kinetic parameters (± SD) of CBZ_{sp} profiles.

Parameters	**Zero-order kinetic**			
	SGF/SIF	**MGM/MIM-I**	**MGM/MIM-II**	**FaSSGF/FaSSIF-V2**
$k_0\ [h^{-1}]$	12.664 ± 2.33	8.13 ± 2.68	11.68 ±1.47	14.80 ± 2.66
R^2	0.59 ± 0.09	0.98 ± 0.01	0.88 ± 0.04	0.98 ± 0.02
AIC	179.61 ± 10.46	92.88 ± 18.22	149.90 ± 13.13	119.26 ± 12.13
First-order kinetics				
$W_{max}\ [\%]$	40.59 ± 7.73	-	49.49 ± 1.64	-
$k_1\ [h^{-1}]$	0.83 ± 0.10	-	0.41 ± 0.07	-
R^2	0.99 ± 0.00	-	0.99 ± 0.00	-
AIC	81.91 ± 6.13	-	86.14 ± 9.65	-
3-parameter Weibull function				
$W_{max}\ [\%]$	43.79 ± 8.77	-	-	-
α *[h]*	1.37 ± 0.18	-	-	-
β	0.86 ± 0.01	-	-	-
R^2	0.99 ± 0.00	-	-	-
AIC	73.91 ± 3.68	-	-	-

5.7.1.2.3.2 CBZ-SAC$_{ss}$ samples

Dissolution profiles of CBZ-SAC$_{ss}$ cocrystal samples tested in various media are presented in Figure 42. According to Figure 42, micelles that are present in both modified as well as biorelevant media significantly enhance the dissolution of CBZ-SAC$_{ss}$ (Table 52). The performance of CBZ-SAC$_{ss}$ in MGM/MIM-I was similar to that in biorelevant media ($f_{1,\ area}$: 0.04). All the dissolution profiles follow first-order dissolution kinetics (Table 53).

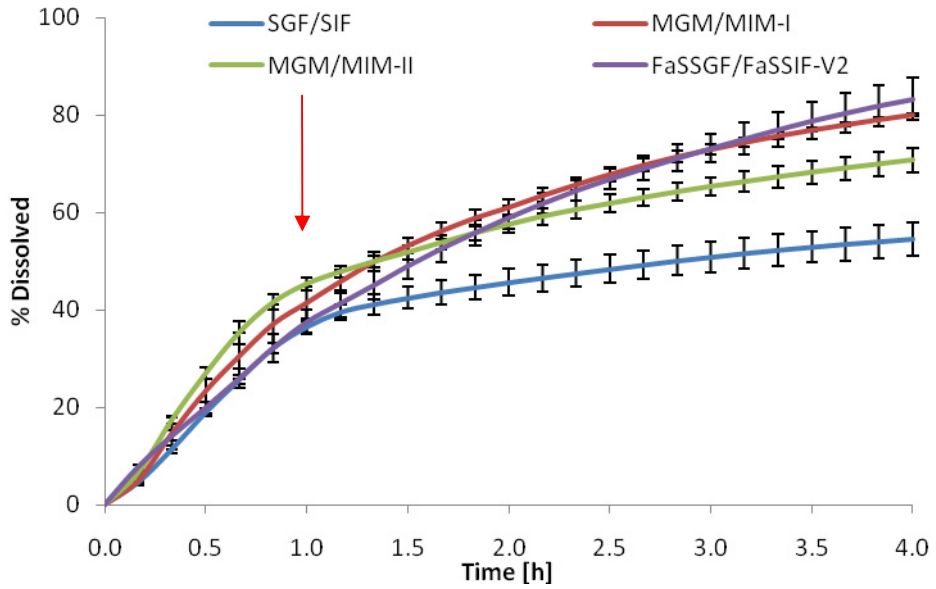

Figure 42. Mean % dissolved (± SD) of CBZ from CBZ-SAC$_{ss}$ in various media using USP apparatus 4. [Red arrow indicates media change].

Table 52. Summary of $f_{1,\ area}$ values comparing dissolution profiles of CBZ-SAC$_{ss}$ in various media.

SGF/SIF (as reference)	CBZ-SAC$_{ss}$		
	MGM/MIM-I	MGM/MIM-II	FaSSGF/FaSSIF-V2
$f_{1,\ area}$	0.35	0.28	0.32

According to 3-parameters Weibull function, dissolution of CBZ from CBZ-SAC$_{ss}$ in MGM/MIM-II and biorelevant media has more parabolic ($\beta < 1$) shape, whereas dissolution profiles in compendial and MGM/MIM-II has sigmoidal shape ($\beta > 1$).

Table 53. Dissolution kinetic parameters (± SD) of CBZ-SAC_{ss} profiles.

Parameters	Zero-order kinetics			
	SGF/SIF	**MGM/MIM-I**	**MGM/MIM-II**	**FaSSGF/FaSSIF-V2**
$k_0 [h^{-1}]$	17.70 ± 1.05	24.78 ± 0.42	22.63 ± 0.65	24.68 ± 0.90
R^2	0.46 ± 0.04	0.74 ± 0.08	0.48 ± 0.07	0.85 ± 0.07
AIC	203.89 ± 1.73	205.37 ± 6.15	214.17 ± 2.65	191.85 ± 9.83
First-order kinetics				
W_{max} [%]	54.43 ± 29.36	86.54 ± 3.29	70.01 ± 2.85	99.84 ± 12.24
$k_1 [h^{-1}]$	0.97 ± 29.37	0.64 ± 0.10	0.95 ± 0.08	0.47 ± 0.12
R^2	0.99 ± 0.00	1.00 ± 0.00	0.99 ± 0.00	1.00 ± 0.00
AIC	107.59 ± 58.40	97.54 ± 9.38	112.41 ± 4.81	44.82 ± 8.91
3-parameter Weibull function				
W_{max} [%]	52.97 ± 3.57	85.50 ± 7.28	71.63 ± 3.97	104.23 ± 16.18
α [h]	0.97 ± 0.05	1.57 ± 0.32	1.11 ± 0.12	2.34 ± 0.63
β	1.12 ± 0.04	1.02 ± 46.30	0.94 ± 0.03	0.97 ± 0.02
R^2	0.99 ± 0.00	1.00 ± 0.00	0.99 ± 0.00	1.00 ± 0.00
AIC	105.60 ± 0.91	91.74 ± 50.09	112.32 ± 6.67	36.94 ± 15.87

5.7.1.2.3.3 CBZ-SAC_{umax} samples

Dissolution performance of CBZ-SAC_{umax} cocrystals was determined in various media and shown in Figure 43. Dissolution profiles in all media were much faster than in compendial media (Table 54). It seems that cocrystals produced by UMAX technique were more affected by sodium lauryl sulphate (SLS) surfactant present in modified media (MGM/MIM-I and MGM/MIM-I). It is also worth noting that dissolution profiles of all CBZ formulations in SGF and FaSSGF (up to the first hour) were similar. In this case dissolution of CBZ from

CBZ-SAC$_{umax}$ in MGM is much faster than in SGF and FaSSGF. Based on the *AIC* and R^2 values (Table 55), dissolution of CBZ from CBZ-SAC cocrystals made by UMAX methods follows first-order kinetics and kinetic pattern is not affected by the presence of single or mixed micelles. The presence of both types of micelles enhances drug solubilisation.

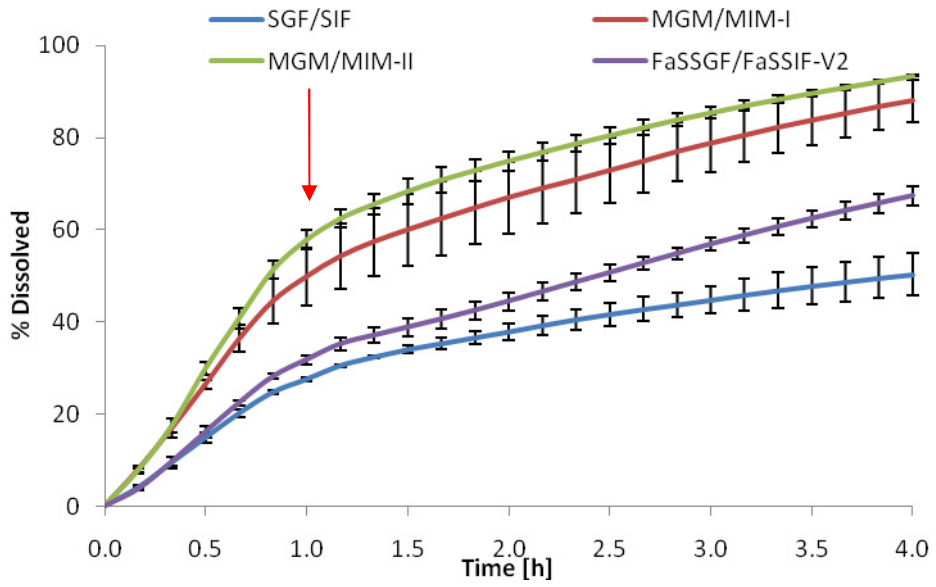

Figure 43. Mean % dissolved (± SD) of CBZ from CBZ-SAC$_{umax}$ in various media using USP apparatus 4. [Red arrow indicates media change].

Table 54. Summary of $f_{1,\,area}$ values comparing dissolution profiles of CBZ-SAC$_{umax}$ in various media.

SGF/SIF (as reference)	**CBZ-SAC$_{umax}$**		
	MGM/MIM-I	**MGM/MIM-II**	**FaSSGF/FaSSIF-V2**
$f_{1,\,area}$	0.76	0.94	0.22

Table 55. Dissolution kinetic parameters (± SD) of CBZ-SAC_{umax} profiles.

Parameters	Zero-order kinetics			
	SGF/SIF	**MGM/MIM-I**	**MGM/MIM-II**	**FaSSGF/FaSSIF-V2**
$k_0 [h^{-1}]$	15.43 ± 0.99	27.09 ± 2.22	29.56 ± 0.38	19.36 ± 0.57
R^2	0.68 ± 0.12	0.68 ± 0.06	0.58 ± 0.07	0.86 ± 0.02
AIC	184.92 ± 4.49	214.19 ± 9.07	224.65 ± 3.70	181.02 ± 3.40
First-order kinetics				
W_{max} [%]	52.30 ± 6.78	90.18 ± 4.29	94.04 ± 1.56	76.87 ± 3.40
$k_1 [h^{-1}]$	0.71 ± 0.15	0.72 ± 0.08	0.85 ± 0.08	0.47 ± 0.03
R^2	0.99 ± 0.00	0.99 ± 0.00	0.99 ± 0.00	0.99 ± 0.00
AIC	88.46 ± 8.91	128.51	129.16 ± 7.60	116.80 ± 1.78
3-parameter Weibull function				
W_{max} [%]	53.91 ± 7.76	96.52 ± 5.72	92.71 ± 2.70	102.84 ± 21.34
α [h]	1.50 ± 0.33	1.45 ± 0.26	1.16 ± 0.13	3.03 ± 0.81
β	0.95 ± 0.04	0.96 ± 0.18	1.05 ± 0.06	0.85 ± 0.09
R^2	0.99 ± 0.00	0.99 ± 0.00	0.99 ± 0.00	0.99 ± 0.00
AIC	88.17 ± 12.35	118.13 ± 14.81	129.69 ± 6.88	111.50 ± 4.52

5.7.1.2.3.4 CBZ-NIC_{ss} samples

Dissolution profiles of CBZ from CBZ-NIC_{ss} cocrystals in different media tested using USP apparatus 4 are presented in Figure 44. Dissolution of CBZ from CBZ-NIC_{ss} cocrystal in both modified and biorelevant media follows zero-order kinetics (Table 57), while samples tested in modified media had sigmoidal shape curves ("S" curve), as a consequence of extensive enhancement of dissolution in modified media. This enhancement could be attributed to the solubilisation properties of NIC. Nicotinamide is a well known hydrotrope, that is able to

solubilise hydrophobic compounds in aqueous solution (314). However, the amounts of NIC released from CBZ-NIC_{ss} cocrystal were insufficient to provide solubilisation effect. Hence, the presence of SLS in the media assured the synergetic effect. Generally, Weibull function can be used to characterise dissolution kinetics of sigmoidal shape profiles. Unfortunately, fittings resulted in insufficient parameters. For instance W_{max} exceeded extensively 100% despite the attempt of setting it to optimal 100%.

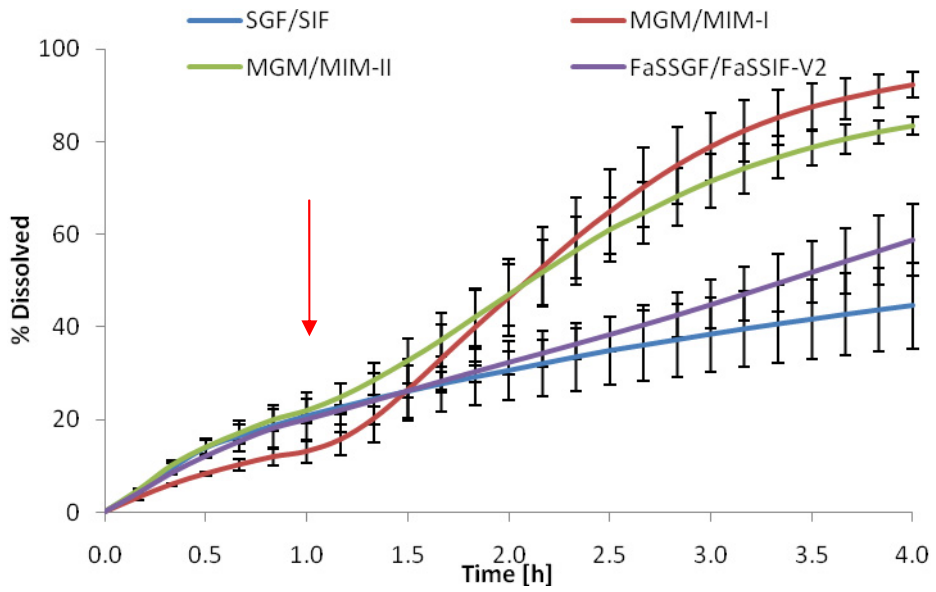

Figure 44. Mean % dissolved (± SD) of CBZ from CBZ-NIC_{ss} in various media using USP apparatus 4. [Red arrow indicates media change].

Table 56. Summary of $f_{1,\,area}$ values comparing dissolution profiles of CBZ-NIC_{ss} in various media.

SGF/SIF (as reference)	CBZ-NICss		
	MGM/MIM-I	MGM/MIM-II	FaSSGF/FaSSIF-V2
$f_{1,\,area}$	0.75	0.61	0.14

Table 57. Dissolution kinetic parameters (± SD) of CBZ-NIC_{ss} profiles.

Parameters	Zero-order kinetics			
	SGF/SIF	**MGM/MIM-I**	**MGM/MIM-II**	**FaSSGF/FaSSIF-V2**
$k_0 [h^{-1}]$	13.05 ± 2.24	24.17 ± 1.76	22.74 ± 1.40	15.30 ± 1.38
R^2	0.82 ± 0.01	0.96 ± 0.01	0.98 ± 0.01	0.97 ± 0.02
AIC	164.00 ± 9.21	176.89 ± 2.91	137.38 ± 17.86	132.63 ± 9.49
First-order kinetics				
W_{max} [%]	49.32 ± 9.88	-	-	-
$k_1 [h^{-1}]$	0.51 ± 0.03	-	-	-
R^2	0.99 ± 0.00	-	-	-
AIC	89.65 ± 5.98	-	-	-
3-parameter Weibull function				
W_{max} [%]	-	96.96 ± 3.74	-	-
α [h]	-	8.20 ± 1.11	-	-
β	-	2.26 ± 0.01	-	-
R^2	-	1.00 ± 0.00	-	-
AIC	-	125.27 ± 4.94	-	-

5.7.1.2.4 Effect of type of coformer

Dissolution profiles of CBZ_{sp}, CBZ-SAC_{ss} and CBZ-NIC_{ss} in biorelevant media were studied in order to verify the effect of the coformer type on the enhancement of dissolution (Figure 45). CBZ-SAC_{ss} cocrystal demonstrated a significant enhancement of dissolution of CBZ ($f_{1, area}$: 0.75).

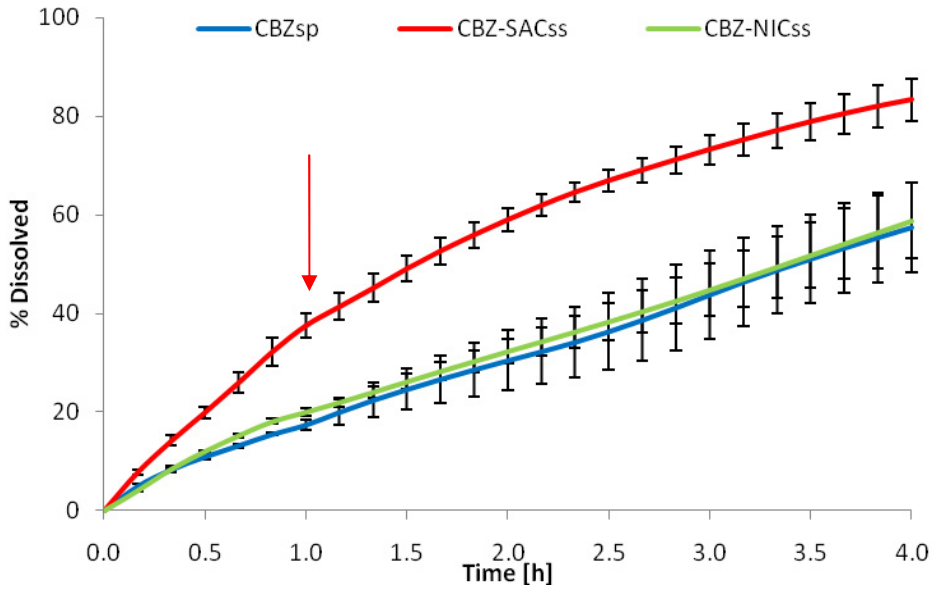

Figure 45. Mean % dissolved (± SD) of CBZ from cocrystals made by sonic-slurrying method and tested in biorelevant media using USP apparatus 4. CBZ_{sp} samples were used as control. [Red arrow indicates media change].

Interestingly, the formulation of CBZ-NIC_{ss} had no statistically significant effect on dissolution of CBZ ($f_{1,\ area}$: 0.05). NIC due to its hydrotropic properties should have a synergetic effect with mixed micelles from biorelevant media and enhance dissolution of CBZ. There may be a few potential justifications. It could be that in comparison to high doses of CBZ (200 mg), the amount of NIC (103 mg) in cocrystal might not be sufficient to produce micelles. Also, NIC which is a highly soluble compound (1000 mg/mL) (74) could dissolve very quickly during the initial sample collection time, thus the synergetic effect could never be triggered. CBZ-SAC cocrystal made by sonic-slurrying method resulted in significant enhancement in CBZ dissolution ($f_{1,\ area}$: 0.75).

5.7.1.2.5 Effect of method of preparation

Dissolution profiles of CBZ-SAC_{ss} and CBZ-SAC_{umax} in biorelevant media were compared against dissolution of CBZ_{sp} samples in order to assess which cocrystallisation method resulted in the highest improvement of dissolution (Figure 46). $f_{1,\ area}$ values indicate that both SAC cocrystals significantly improved dissolution of poorly soluble CBZ. SAC cocrystals made by sonic-slurrying method resulted in two-fold higher dissolution ($f_{1,\ area}$: 0.75) than cocrystals made using UMAX technology ($f_{1,\ area}$: 0.37) when compared against dissolution of CBZ_{sp} samples. It can be clearly noted from Figure 46, that cocrystallisation reduces the

variability (%CV: CBZ_{sp} < 22%; $CBZ\text{-}SAC_{ss}$ < 14%; $CBZ\text{-}SAC_{umax}$ < 11%) between individual dissolution curves.

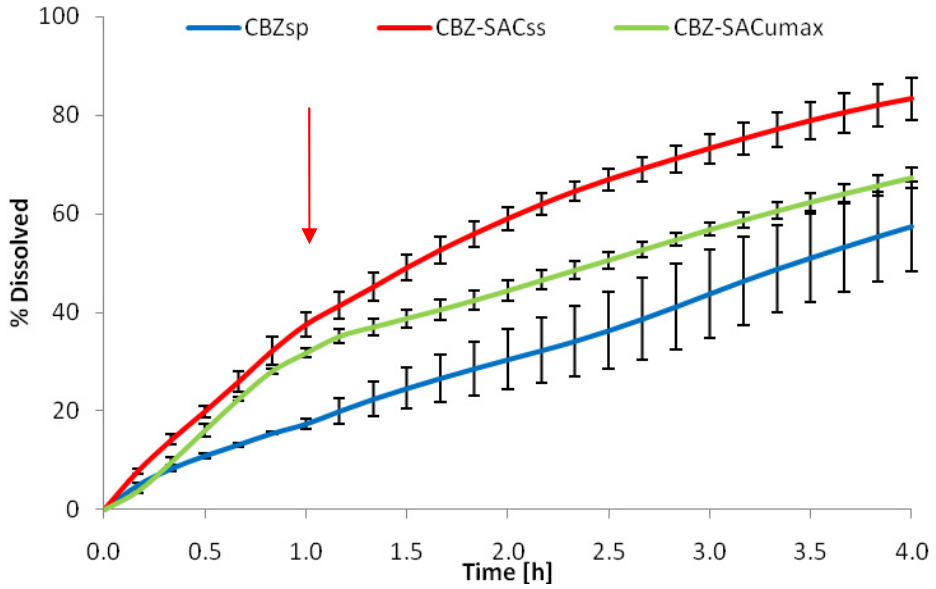

Figure 46. Mean % dissolved (± SD) of CBZ from CBZ-SAC cocrystals made by different cocrystallisation methods and tested in biorelevant media using USP apparatus 4. CBZ_{sp} samples were used as a control. [Red arrow indicates media change].

5.7.1.2.6 Effect of cocrystal and its mechanism of dissolution

5.7.1.2.6.1 Saccharin types of CBZ cocrystals

The aim of this study was to evaluate if the improvement in dissolution rate of CBZ was due to the cocrystal formation. Dissolution of CBZ from a physical blend made of CBZ and SAC tested in biorelevant media was compared to the dissolution of CBZ from CBZ-SAC cocrystals (Figure 47). It was found that physical blends of CBZ and SAC (CBZ--SAC) significantly enhanced dissolution of CBZ (Table 58). Nevertheless, CBZ-SAC cocrystal made by sonic-slurrying method enhances dissolution of CBZ the most ($f_{1,\ area}$: 0.75). $f_{1,\ area}$ between blend (CBZ--SAC) and $CBZ\text{-}SAC_{umax}$ cocrystal indicate that dissolution performance of this cocrystal is as good as the blend ($f_{1,\ area}$: 0.09). Thus, only cocrystallisation by sonic-slurrying proved to make a complex compound that enhanced dissolution better than the physical mixture of the two components.

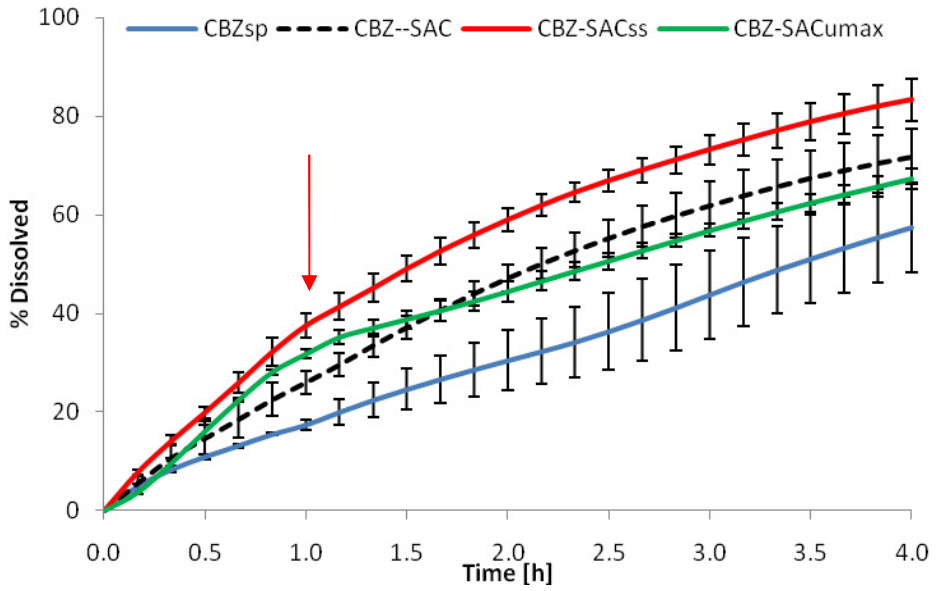

Figure 47. Mean % dissolved (± SD) of CBZ from different CBZ-SAC formulations in biorelevant media. Dissolution of CBZ_{sp} was used as a control. [Red arrow indicates media change].

Table 58. Summary of $f_{1,\ area}$ values comparing dissolution profiles of different CBZ-SAC formulations in biorelevant media.

CBZ_{sp} (as reference)	FaSSGF/FaSSIF-V2		
	CBZ—SAC	CBZ-SAC_{ss}	CBZ-SAC_{umax}
$f_{1,\ area}$	0.42	0.75	0.34

Gao *et al*. reported that cocrystallisation of BCS class III drug; Adefovir dipivoxil with Saccharin greatly enhanced the dissolution of Adefovir dipivoxil when compared with its physical mixture and API (315). Dissolution studies were performed in 500 mL of either 0.1M HCl, water or phosphate buffer pH 6.8 at 50 rpm using USP 2 dissolution apparatus. The data in 0.1M HCl were inconclusive as API is highly soluble in this pH and all drug dissolved within 5 minutes. Dissolution of cocrystal in pH 6.8 was significantly faster that it's API (f_1: 223.06). According to difference factor (f_1: 10.74) there was not a statistically significant difference between dissolution profiles of API and physical blend in this buffer (315). It was concluded that the enhancement in dissolution was due to the fact that cocrystallisation with Saccharin changed crystal packing and arrangement, which favoured the dissolution of Adefovir dipivoxil.

Further investigation, during which the dissolution of SAC from cocrystals was measured simultaneously with dissolution of CBZ, showed that SAC from CBZ-SAC_{ss} cocrystal was dissolving at a slower rate than SAC from the physical blend (Figure 48), despite the fact that both SAC dissolved within the first 90 minutes of the experiment. This could be attributed to the fact that, upon contact with water, weak hydrogen bonds between hydrophobic CBZ and the highly soluble coformer SAC in cocrystal break down immediately.

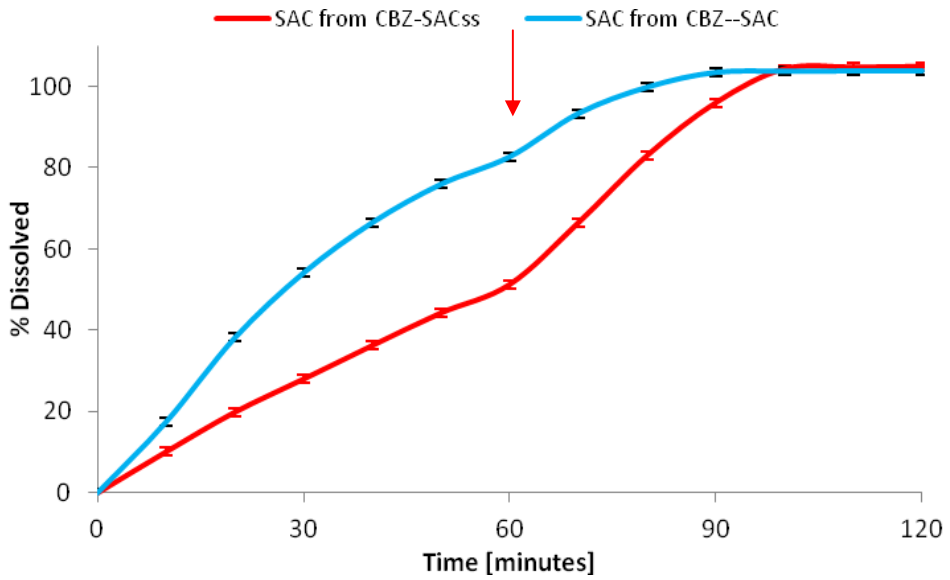

Figure 48. Mean % dissolved (± SD) of SAC from CBZ-SAC_{ss} cocrystal and physical blend formulations. [Red arrow indicates media change].

Dissolution of SAC from the cocrystal form follows a zero-order kinetics pattern (in both media separately) and it is slower than that from the physical blend (first-order kinetics observed in both media). The observed differences on dissolution can be related to the solubility properties of the coformer used (SAC- 3.45 mg/mL). The larger undissolved amounts of SAC from the cocrystal were available for water to dissolve (controlled and continuous access of the dissolution medium around the drug molecule) and thus allowing water to penetrate between poorly soluble CBZ at the same time, leading to dissolution enhancement of CBZ (Figure 48).

The findings that the same ratio of API and coformer formed as cocrystal or physical blend can lead to different dissolution performance leads to the conclusion that crystal packing and arrangement in these two formulations are different and play an important role in enhancement of dissolution of poorly soluble compounds by cocrystallisation.

5.7.1.2.6.2 Nicotinamide type of CBZ cocrystals

Dissolution of CBZ from CBZ-NIC$_{ss}$ cocrystal and physical blend (CBZ--NIC) in biorelevant media was studied using USP apparatus 4 and compared against the CBZ$_{sp}$ sample (Figure 49). The dissolution performance of CBZ-NIC$_{ss}$ did not result in any changes ($f_{1,\ area}$: 0.05) compared to CBZ$_{sp}$ dissolution characteristics. On the other hand, the physical blend of CBZ and NIC resulted in significantly slower ($f_{1,\ area}$: 0.32) dissolution than those of CBZ$_{sp}$.

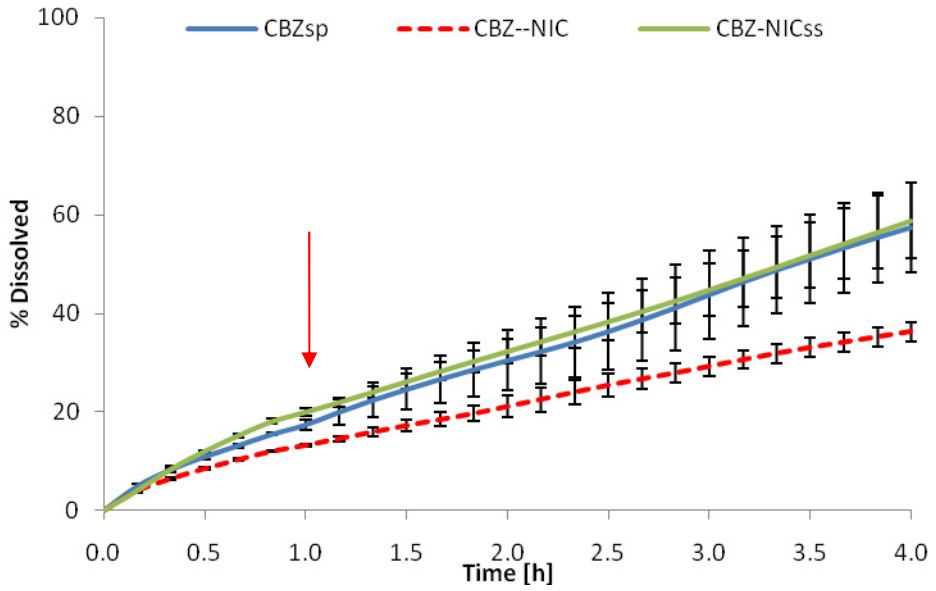

Figure 49. Mean % dissolved (± SD) of CBZ from different CBZ-NIC formulations in biorelevant media. Dissolution of CBZ was used as a control. [Red arrow indicates media change].

This could be attributed to a different arrangement of CBZ and NIC in the blend in comparison to the cocrystal lattice arrangement. The hydrophobic part of NIC could repel the water, resulting in higher hydrophobicity which consequently would decrease solubility of CBZ. Another reason for it could be the particle size of the physical blend, which is probably greater than CBZ itself.

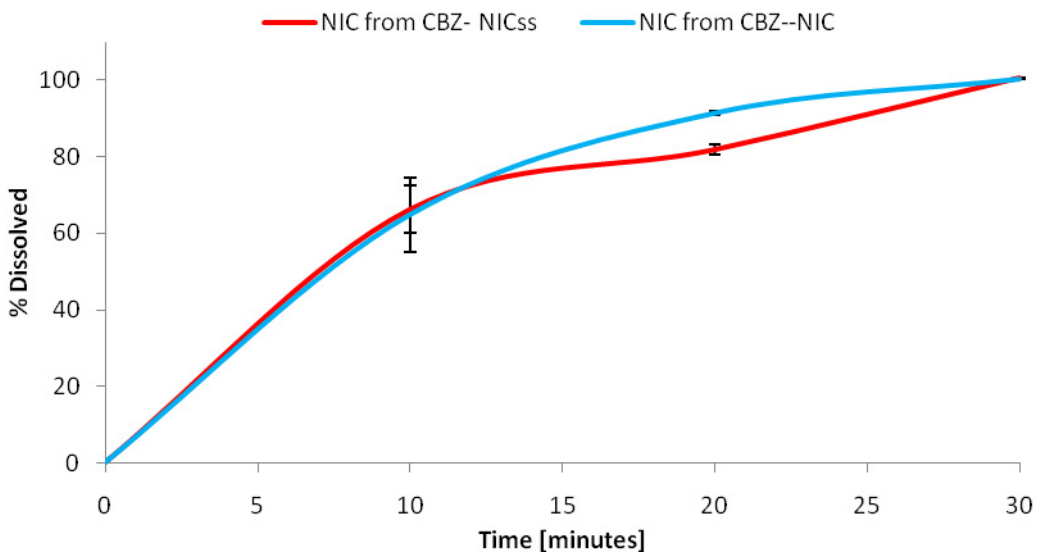

Figure 50. Mean % dissolved (± SD) of NIC from CBZ-NIC_{ss} cocrystal and physical blend formulations.

According to Figure 50, NIC from both cocrystal and physical blends dissolved within the first 30 minutes.

Dissolution of NIC is three times faster than for previously mentioned SAC. This could related to the solubility properties of the coformers used (NIC 1000 mg/mL; SAC 3.45 mg/mL) (74).

It can be clearly seen that dissolution of CBZ from cocrystal strongly depends on the solubility properties of the coformer. SAC dissolves slowly which allows water to be present for longer between CBZ particles, while NIC is rapidly dissolved and CBZ could not benefit from the presence of water.

Qiao *et al*. investigated the intrinsic dissolution rates of CBZ-NIC cocrystals and physical blends and its ability to transform to a dihydrate form of CBZ (316). According to these studies, the initial (at 3 min) intrinsic dissolution rate of CBZ--NIC physical mixture is much higher (0.0248 mg/min/cm^2) than for cocrystal (0.0123 mg/min/cm^2) and API (0.0103 mg/min/cm^2). After 35 minutes, the intrinsic dissolution rate of physical mixture decreased to values of CBZ dihydrate form (0.0080 mg/min/cm^2), while the intrinsic dissolution rate of cocrystal remained stable.

5.7.2 Indomethacin case

5.7.2.1 USP apparatus 1

The dissolution profile of Indomethacin from 25mg Indocid® capsules was determined in compendial media (SGF and SIF) using USP apparatus 1. Indomethacin is a weak acid (pKa 4.3) which is characterised by limited solubility in an acidic environment and high solubility in a basic environment. This trend can be clearly seen in Figure 51. 85% of IND dissolved within twenty minutes in SIF, whereas only three percent of Indomethacin dissolved within one hour.

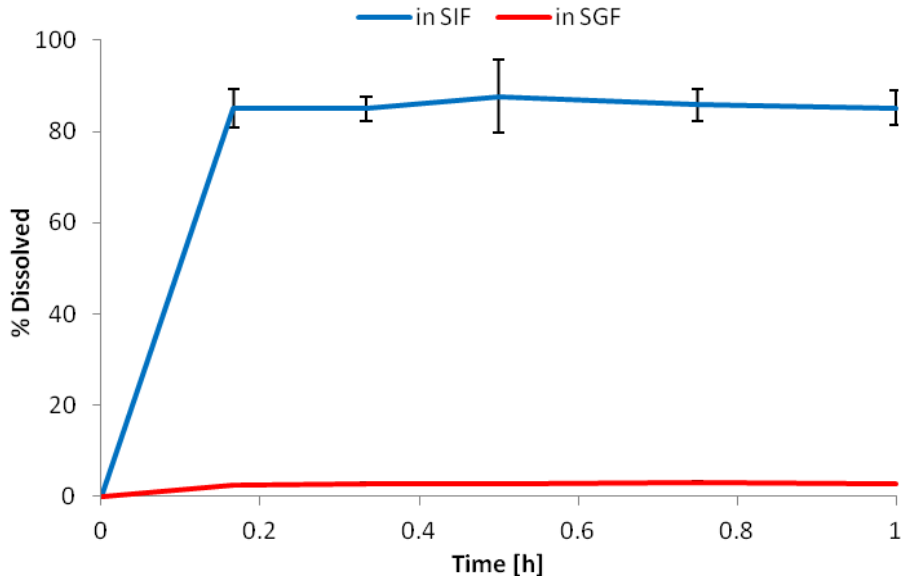

Figure 51. Mean % dissolved (± SD) of IND from 25 mg Indocid® in compendial media using USP apparatus 1 (100 rpm).

Dissolution of IND from 25 mg Indocid® capsules follows first-order kinetics (Table 59). R^2 and *AIC* values indicate that the dissolution profile in SGF can be slightly better described by 3-parameters Weibull function. However, $\beta > 1$ indicates that the dissolution profile of IND from 25 mg Indocid® capsules in SIF has sigmoidal shape. This may be misleading as whole 1 hour profile was consider for Weibull fitting, whereas the plateau was reached within 20 minutes.

Table 59. Dissolution kinetic parameters (± SD) of Indocid® capsule profiles.

Parameters	Zero-order kinetics	
	SGF	SIF
$k_0 [h^{-1}]$	-	-
R^2	-	-
AIC	-	-
First-order kinetics		
W_{max} [%]	10.88 ± 1.70	85.91± 4.48
$k_1 [h^{-1}]$	2.95 ± 0.11	32.03 ± 11.76
R^2	0.97 ± 0.02	1.00 ± 0.00
AIC	-12.73 ± 8.92	12.87 ± 12.88
3-parameter Weibull function		
W_{max} [%]	3.10 ± 0.10	-
α [h]	3.10 ± 0.65	-
β	2.12 ± 0.90	-
R^2	0.98 ± 0.02	-
AIC	-17.22 ± 17.25	-

Similar dissolution profiles were observed for Indocid® capsule that had similar composition to the conventional formulation (310). Around 10% of the drug dissolved in SGF and 85% in SIF within the first hour. The performance in SIF was slower reaching 60% drug dissolved at 20 minutes but still meeting the one hour specification for IR formulation. The discrepancies in the profiles could be related to formulation and methodology (USP 2, 100rpm, 900 mL). Bijanzadeh *et al.* tested 25 mg Indocid® capsules supplied by MSD according to USP monograph (USP 1, 750 mL, pH 7.2, 100rpm) and reported 90% of the IND dissolved within 10 minutes (317). This is in agreement with findings reported in Figure 51.

Due to the fact that Indocid® dissolves rapidly in basic conditions, this dissolution method will not be discriminative enough to characterise the dissolution profile of IND cocrystals. Further experiments were performed using flow-through cell dissolution apparatus.

5.7.2.2 USP apparatus 4

5.7.2.2.1 Dissolution studies of commercial formulation

Indomethacin IR and PR conventional formulations were withdrawn from the market and are no longer available in UK. They were known under the brand name Indocid® and have been manufactured by MSD. Currently in UK, Indocid® is available as 100 mg suppositories. Indocid® capsules that were used for these studies were supplied by MSD (Australia). Dissolution profiles of 25 mg Indocid® IR capsules were tested using USP apparatus 4.

5.7.2.2.1.1 Indocid® IR capsules

Indocid® capsule is a complete formulation that contains excipients such as lactose, lecithin and silica – colloidal anhydrous, which aid the dissolution of poorly soluble Indomethacin. Figure 52 illustrates the dissolution profiles of Indocid® capsules tested in various conditions. A similar trend to the USP apparatus 1 experiment was observed during the first hour of the test, during which Indomethacin was exposed to media that simulate gastric conditions: only 4% of Indomethacin dissolved, followed by rapid dissolution in intestinal conditions.

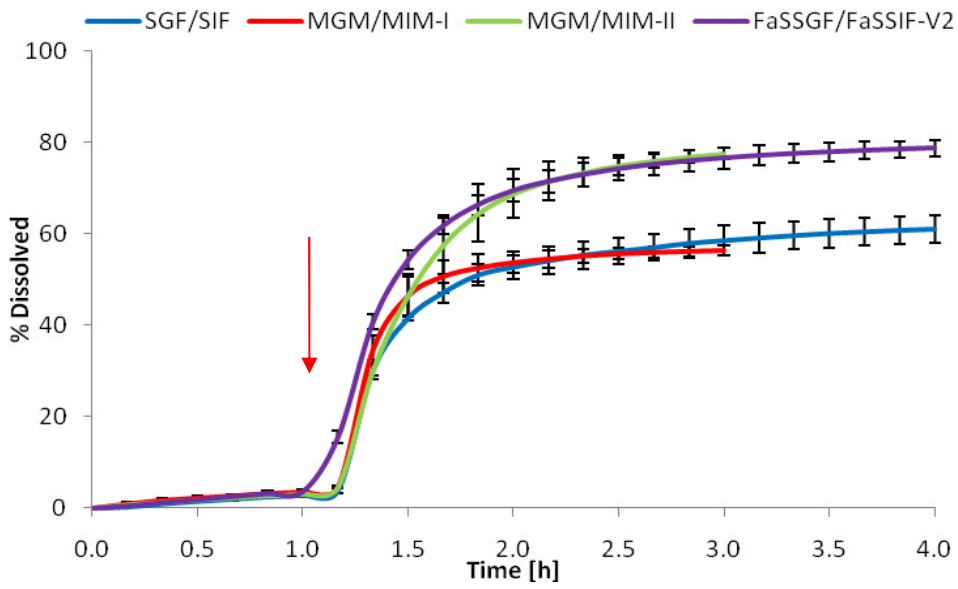

Figure 52. Mean % dissolved (± SD) of IND from 25 mg Indocid® capsules in various media using USP apparatus 4. [Red arrow indicates media change].

The dissolution profile of Indocid® capsule in compendial media is similar to that in MGM/MIM-I ($f_{1,\ area}$: 0.05) (Table 60). However, the precipitation percentage in compendial media is highly statistically significant ($p < 0.001$) when compared to MGM/MIM-I (Figure 54). There is also no significant difference between dissolution profiles in MGM/MIM-II and biorelevant media ($f_{1,area}$: 0.06). It looks that the species (Phosphate salts *vs* Maleic acids) present in MIM-I and MIM-II buffers have significant effect on dissolution ($f_{1,area}$: 0.05; 0.27). Performing dissolution of ionic compounds in one medium may not be sufficient to predict what happens *in vivo*. This can be clearly seen based on Indocid® formulation. Considered separately, minimal dissolution in gastric fluids and maximum in intestinal fluids, do not reflect the real nature of *in vivo* precipitation. Thus, there is a need for an *in vitro* technique that would be able to closely mimic this process. USP apparatus 4 offers the benefit of changing the dissolution environment, but the extent of precipitation strongly depends on the composition of the selected media (Figure 54). For instance, biorelevant media causes the smallest fraction of the dose to precipitate (Figure 54). Schamp *et al*. claim that inhibited precipitation may occur due to fact that dissolving drug is automatically interpolated in the micelles, which protects it from nucleation and subsequent precipitation (318). Biorelevant media consider drug solubilisation in mixed micelles; therefore, they mimic the physiological situation better than buffer solutions (319, 320).

Table 60. Summary of *f1, area* values comparing dissolution profiles of Indocid® capsules in various media.

SGF/SIF (as reference)	**25 mg Indocid® capsules**		
	MGM/MIM-I	**MGM/MIM-II**	**FaSSGF/FaSSIF-V2**
$f_{1,\ area}$	0.05	0.27	0.32

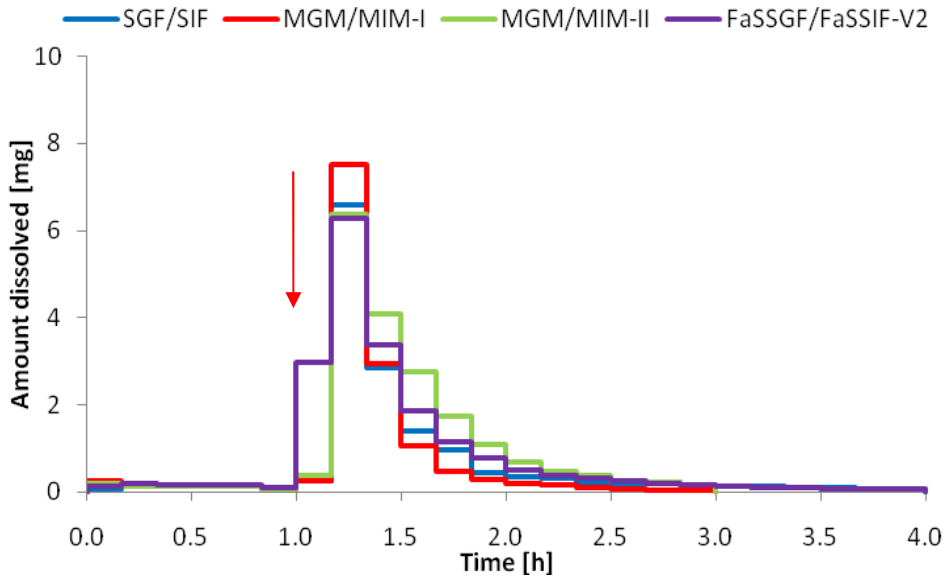

Figure 53. Non-cumulative profile of mean amount of IND dissolved from 25 mg Indocid® capsules in various media using USP apparatus 4. [Red arrow indicates media change].

Non-cumulative interpretation of the amount of the IND dissolved from Indocid® capsule allows confirmation that the fastest dissolution profile obtained in biorelevant media is due to the highest amount of IND dissolved (~ 3 mg) after the media change (Figure 53) and the least % of the dose precipitated (Figure 54).

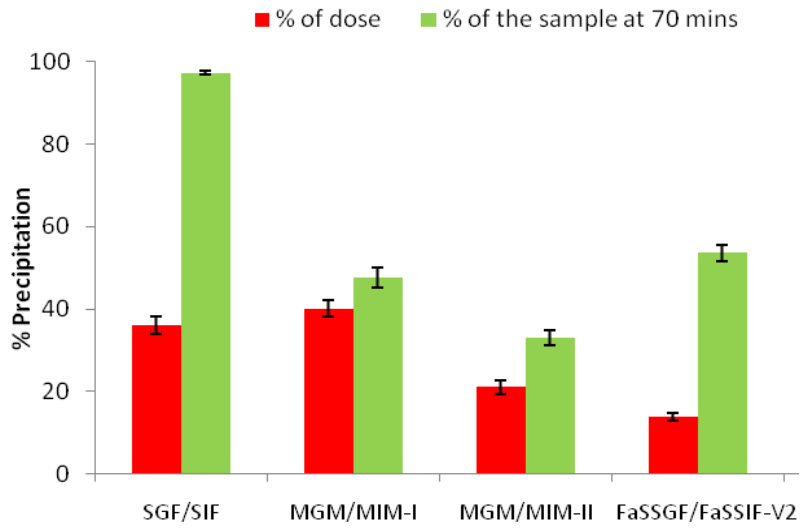

Figure 54. Percent (± SD) of dose and sample collected at 70 min of Indocid® precipitated in various media.

Due to the solubility pH-dependent nature of IND, fitting zero and first-order kinetics to the whole profile was not achievable. Thus, zero- and first-order kinetics were applied separately

to the profiles pre (up to 1h) and post media change (after 1h) (Table 61). Weibull function was fitted using the whole data profile.

According to the data presented in Table 61, dissolution of IND from 25 mg Indocid® capsules in gastric stage follows zero-order kinetics in compendial and biorelevant media. On the other hand, dissolution kinetics in modified media can be better characterised by a first-order equation. Rapid onset after media change in all the media can be described by first-order kinetics. The W_{max} value and S-shape ($\beta > 1$) of the dissolution curve can be successfully captured using 3-parameters Weibull function.

Table 61. Dissolution kinetic parameters (± SD) of Indocid® capsules profiles.

Parameters		**Gastric phase**			
		SGF/SIF	**MGM/MIM-I**	**MGM/MIM-II**	**FaSSGF/FaSSIF-V2**
Zero-order kinetics	$k_0 [h^{-1}]$	2.92 ± 0.51	3.95 ± 0.38	3.33 ± 0.31	3.75 ± 0.63
	R^2	0.99 ± 0.01	0.97 ± 0.01	0.97 ± 0.04	0.99 ± 0.01
	AIC	-18.92 ±7.07	-4.04 ± 8.00	-10.73 ± 7.68	-12.98 ± 5.08
		Intestinal phase			
	$k_0 [h^{-1}]$	27.85 ± 1.39	38.59 ± 1.04	50.49 ± 1.96	36.35 ± 1.00
	R^2	0.04 ± 0.09	0.28 ± 0.14	0.65 ± 0.10	-0.15 ± 0.11
	AIC	166.43 ± 1.38	107.24 ± 3.07	106.27 ± 4.82	177.47 ± 1.68
		Gastric phase			
First -order kinetics	W_{max} [%]	-	5.79 ± 1.88	6.75 ± 2.52	-
	$k_1 [h^{-1}]$	-	1.22 ± 0.69	0.80 ± 0.52	-
	R^2	-	1.00 ± 0.00	1.00 ± 0.01	-
	AIC	-	21.29 ± 4.30	-23.38 ± 10.29	-
		Intestinal phase			
	W_{max} [%]	60.50 ± 3.48	58.14 ± 1.33	84.32 ± 1.93	78.23 ± 2.35
	$k_1 [h^{-1}]$	1.97 ± 0.14	2.48 ± 0.34	1.54 ± 0.25	2.15 ± 0.14
	R^2	0.96 ± 0.01	0.94 ± 0.02	0.98 ± 0.01	0.99 ± 0.00
	AIC	105.70 ± 2.88	77.15 ± 4.27	76.89 ± 6.45	88.26 ± 2.96
		Gastric/intestinal phases			
3-parameter Weibull function	W_{max} [%]	57.47 ± 3.21	54.26 ± 1.29	74.41 ± 1.44	75.45 ± 2.23
	α [h]	11.73 ± 1.97	102.34 ± 79.26	12.97 ± 3.38	7.20 ± 0.34
	β	6.41 ± 0.89	14.23 ± 5.95	5.82 ± 1.19	5.13 ± 0.20
	R^2	0.98 ± 0.00	0.99 ± 0.00	0.99 ± 0.00	0.99 ± 0.00
	AIC	144.29 ± 2.01	95.12 ± 7.23	105.30 ± 5.41	144.22 ± 3.15

5.7.2.2.1 Pharmaceutical cocrystals

Indomethacin cocrystals were tested under the same conditions as Indocid® commercial formulations. IND_{sp} samples were used as a control formulation.

5.7.2.2.1.1 IND_{sp} samples

Dissolution of IND_{sp} in various media was presented in Figure 55. In all cases IND_{sp} significantly benefited from the presence of the single or mixed surfactants present in the media.

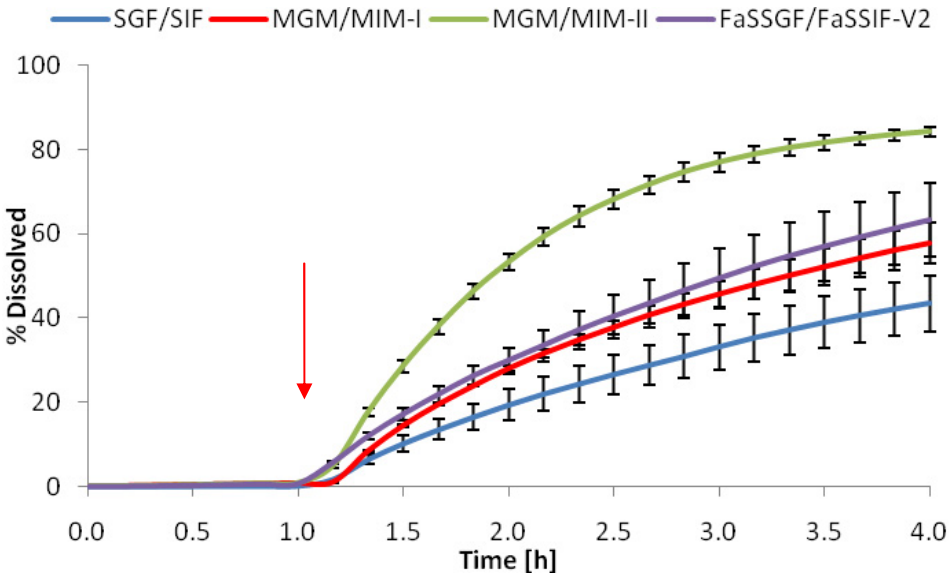

Figure 55. Mean % dissolved (± SD) of IND_{sp} in various media using USP apparatus 4. [Red arrow indicates media change].

The greatest dissolution enhancement ($f_{1,\ area}$: 1.35) was obtained when IND_{sp} samples were tested in MGM/MIM-II media (Table 62). This was confirmed with the findings that in this case larger amounts of IND were dissolved between 70 to 140 minutes of the test when compared with other non-cumulative profiles (Figure 56).

Table 62. Summary of $f_{1,\ area}$ values comparing dissolution profiles of IND_{sp} formulations in various media.

SGF/SIF (as reference)	IND_{sp}		
	MGM/MIM-I	MGM/MIM-II	FaSSGF/FaSSIF-V2
$f_{1,\ area}$	0.38	1.35	0.51

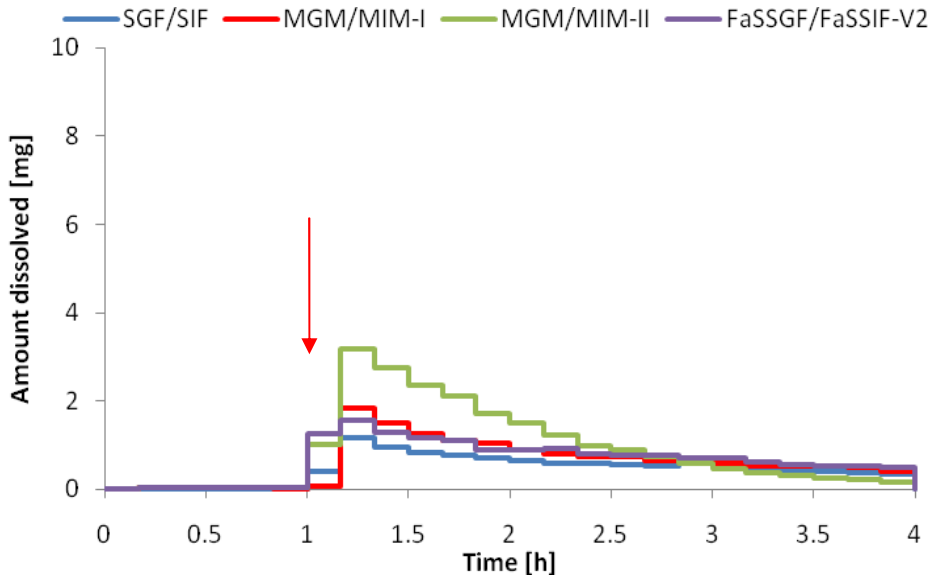

Figure 56. Non – cumulative profiles of mean amounts of IND_{sp} dissolved in various media using USP apparatus 4. [Red arrow indicates media change].

As in the Indocid® case, biorelevant media inhibited the precipitation of the dose. Overall, smaller proportions of the IND_{sp} dose were prone to precipitation in comparison to Indocid® capsules (Figure 57). It seems that precipitation was more likely to occur with the excipients used in the Indocid® formulation. Consequently, greater precipitation from Indocid® capsules than from IND_{sp} samples *in vivo* could reduce the amount of the IND arriving at the absorption site.

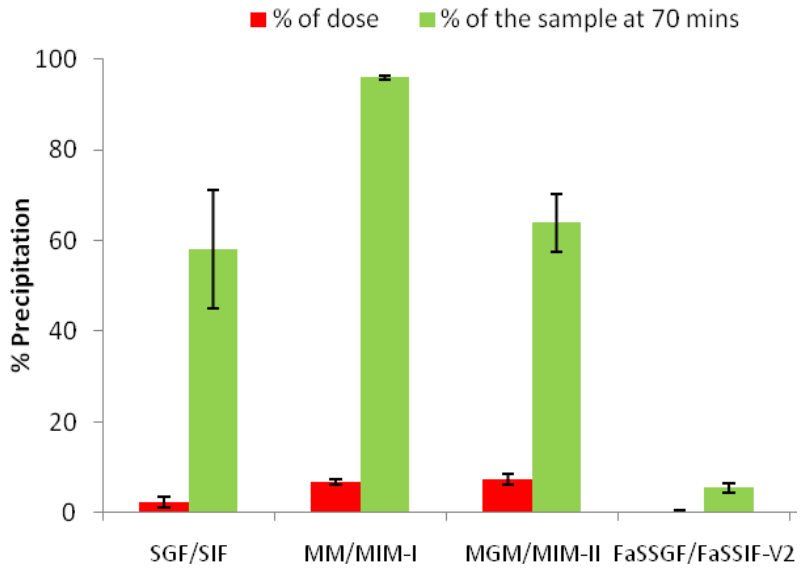

Figure 57. Percent (± SD) of dose and sample collected at 70 min of IND_{sp} precipitated in various media.

Dissolution of IND_{sp} in all media followed zero-order kinetics within the first hour and then upon the change of the media, the kinetics altered to first-order dissolution kinetics as presented in Table 63. Whole dissolution profiles of IND_{sp} can be well described using Weibull function according to which $\beta > 1$ indicated that all the curves had S-shape (Table 63).

Table 63. Dissolution kinetic parameters (± SD) of IND_{sp} profiles.

Parameters		**Gastric phase**			
		SGF/SIF	**MGM/MIM-I**	**MGM/MIM-II**	**FaSSGF/FaSSIF-V2**
Zero-order kinetics	$k_0 [h^{-1}]$	0.18 ± 0.14	0.69 ± 0.13	0.74 ± 0.05	0.65 ± 0.04
	R^2	0.97 ± 0.03	0.98 ± 0.00	0.97 ± 0.01	0.97 ± 0.01
	AIC	-53.81 ± 3.66	-33.30 ± 2.51	-26.49 ± 2.42	-29.96 ± 1.55
		Intestinal phase			
	$k_0 [h^{-1}]$	15.99 ± 2.57	21.82 ± 1.50	35.46 ± 0.78	23.70 ± 3.24
	R^2	0.97 ± 0.01	0.94 ± 0.00	0.78 ± 0.03	0.94 ± 0.02
	AIC	89.79 ± 11.03	113.49 ± 4.66	154.39 ± 2.63	116.09 ± 2.36
		Gastric phase			
First-order kinetics	W_{max} [%]	31.18 ± 50.81	-	-	-
	$k_1 [h^{-1}]$	0.33 ± 0.49	-	-	-
	R^2	0.97 ± 0.03	-	-	-
	AIC	-54.55 ± 3.01	-	-	-
		Intestinal phase			
	W_{max} [%]	75.21 ± 10.13	84.82 ± 16.53	95.24 ± 3.15	89.92 ± 20.29
	$k_1 [h^{-1}]$	0.29 ± 0.05	0.40 ± 0.10	0.80 ± 0.06	0.42 ± 0.06
	R^2	1.00 ± 0.00	1.00 ± 0.00	0.99 ± 0.00	1.00 ± 0.00
	AIC	31.20 ± 13.52	66.19 ± 1.38	92.47 ± 6.93	29.16 ± 14.85
		Gastric/Intestinal phases			
3-parameter Weibull function	W_{max} [%]	43.79 ± 6.22	56.09 ± 5.59	80.86 ± 1.55	63.12 ± 9.15
	α [h]	12.29 ± 0.89	11.55 ± 1.25	10.31 ± 0.79	9.88 ± 1.04
	β	2.66 ± 0.03	2.81 ± 0.02	3.36 ± 0.13	2.54 ± 0.09
	R^2	0.99 ± 0.00	0.99 ± 0.00	0.99 ± 0.00	0.99 ± 0.00
	AIC	100.71 ± 10.09	122.73 ± 0.87	140.81 ± 3.16	117.94 ± 2.53

5.7.2.2.1.2 IND-SAC$_{ss}$ samples

Dissolution of IND from IND-SAC$_{ss}$ cocrystal samples was determined in compendial, modified and biorelevant media (Figure 58). Dissolution of IND-SAC$_{ss}$ in both modified and biorelevant media greatly enhanced the dissolution profile of IND cocrystal (Table 64). The fact that the enhancement in dissolution is due to presence of single or mixed type of micelles in the composition of those media indicate that dissolution of IND is driven by solubilisation mechanism. This is in agreement with its high *logP* value of 4.27 (290). It has been reported previously that for compounds with low *logP* values (1-2) wettability is the predominant mechanism, whereas in the case of drugs with high *logP* values, solubilisation accounts for increased powder dissolution rate (320). In addition, dissolution profiles of IND from IND-SAC$_{ss}$ cocrystals in MIM-II and FaSSIF-V2 resulted in similar dissolution profiles ($f_{1,\ area}$: 0.07), which indicate that blank FaSSIF with SLS (MIM-II) could be potentially used to mimic dissolution behaviour of IND formulations to the same extent as biorelevant media.

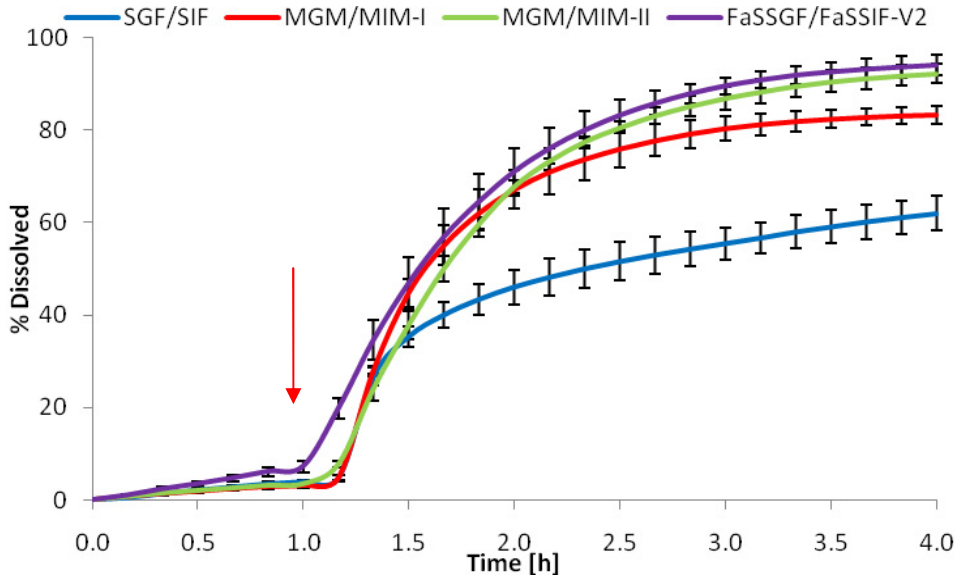

Figure 58. Mean % dissolved (± SD) of IND from IND-SAC$_{ss}$ in various media using USP apparatus 4. [Red arrow indicates media change].

Table 64. Summary of $f_{1,\ area}$ values comparing dissolution profiles of CBZ-SAC$_{ss}$ in various media.

SGF/SIF (as reference)	IND-SAC$_{ss}$		
	MGM/MIM-I	MGM/MIM-II	FaSSGF/FaSSIF-V2
$f_{1,\ area}$	0.40	0.48	0.57

A closer look at the amount of IND dissolved over the time, shows that despite those cumulative profiles in MGM/MIM-II and FaSSGF/FaSSIF-V2 are similar ($f_{1,area}$: 0.07) the amount of IND that dissolves after 70 minutes is slightly higher in modified media (Figure 59). The similarity observed in cumulative profiles is compensated by the fact that IND-SAC_{ss} precipitated upon the change of media by a significantly greater extent in MGM/MIM-II ($p < 0.001$).

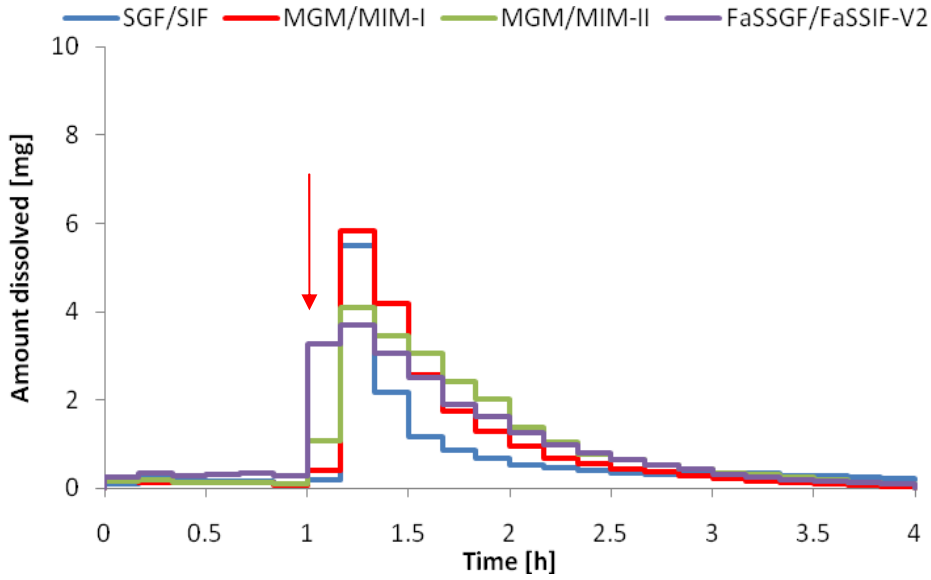

Figure 59. Non-cumulative profiles of mean amounts of IND dissolved from IND-SAC_{ss} samples in various media using USP apparatus 4. [Red arrow indicates media change].

According to Figure 60, the smallest fraction of the dose precipitated in biorelevant media, which was over 30 times smaller than compendial media.

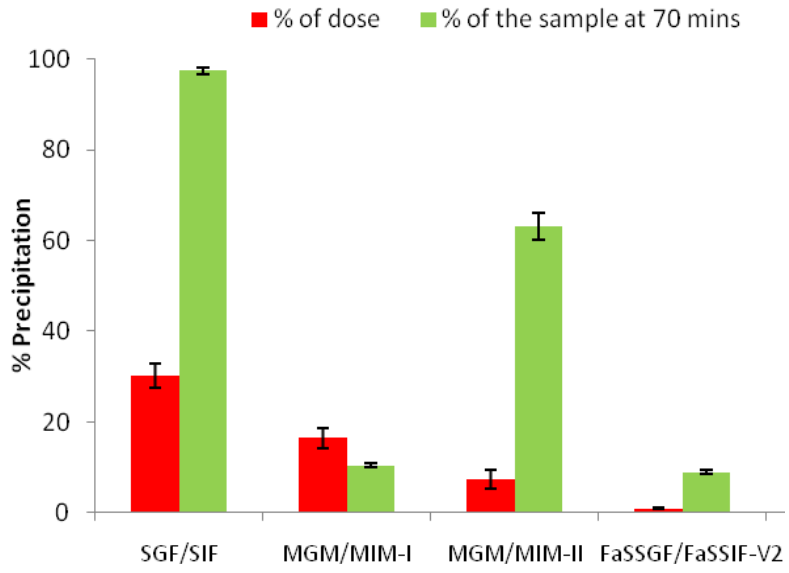

Figure 60. Percent (± SD) of dose and sample at 70 min of IND-SAC_{ss} precipitated in various media.

Dissolution of IND-SAC$_{ss}$ in all media simulating gastric conditions followed zero-order kinetics, whereas upon the change of the media, dissolution kinetics can be better characterised by first-order kinetics (Table 65). Predicted Weibull parameters characterise the whole dissolution profiles of IND-SAC$_{ss}$ indicating that dissolution profile has S-shape (β > 1).

Table 65. Dissolution kinetic parameters (± SD) of IND-SAC$_{ss}$ profiles.

Parameters		**Gastric phase**			
		SGF/SIF	**MGM/MIM-I**	**MGM/MIM-II**	**FaSSGF/FaSSIF-V2**
Zero-order kinetics	$k_0 [h^{-1}]$	3.98 ± 0.65	3.38 ± 0.48	3.68 ± 0.08	7.21 ± 1.12
	R^2	0.99 ± 0.01	0.97 ± 0.02	0.98 ± 0.01	0.99 ± 0.00
	AIC	-10.89 ± 4.61	-10.88 ± 6.95	-11.91 ± 4.00	-5.18 ± 1.90
		Intestinal phase			
	$k_0 [h^{-1}]$	26.64 ± 1.71	37.49 ± 1.28	40.35 ± 0.75	41.70 ± 0.74
	R^2	0.37 ± 0.07	0.39 ± 0.10	0.60 ± 0.07	0.39 ± 0.24
	AIC	157.43 ± 3.76	171.54 ± 3.88	167.94 ± 1.89	172.84 ± 5.51
		Gastric phase			
First -order kinetics	W_{max} [%]	-	6.49 ± 1.33	8.46 ± 3.17	-
	$k_1 [h^{-1}]$	-	0.75 ± 0.36	0.61 ± 0.25	-
	R^2	-	1.00 ± 0.00	1.00 ± 0.00	-
	AIC	-	-25.10 ± 4.38	-29.97 ± 8.86	-
		Intestinal phase			
	W_{max} [%]	60.12 ± 3.72	85.64 ± 2.09	97.94 ± 4.98	96.51 ± 4.14
	$k_1 [h^{-1}]$	1.47 ± 0.10	1.42 ± 0.14	1.09 ± 0.12	1.37 ± 0.33
	R^2	0.98 ± 0.00	0.98 ± 0.01	0.99 ± 0.00	1.00 ± 0.00
	AIC	97.84 ± 1.77	106.80 ± 8.08	100.73 ± 4.89	44.71 ± 13.67
		Gastric/Intestinal phase			
3-parameter Weibull function	W_{max} [%]	57.09 ± 3.42	79.95 ± 2.07	88.45 ± 2.73	91.43 ± 2.39
	α [h]	5.68 ± 1.03	9.34 ± 1.94	9.26 ± 0.82	5.64 ± 0.56
	β	3.37 ± 0.60	4.37 ± 1.94	3.72 ± 0.07	3.12 ± 0.37
	R^2	0.99 ± 0.00	0.99 ± 0.00	0.99 ± 0.00	0.99 ± 0.00
	AIC	152.80 ± 2.27	152.60 ± 4.18	143.24 ± 3.85	135.22 ± 2.87

5.7.2.2.1.3 IND-SAC$_{sd}$ samples

Dissolution of IND-SAC$_{sd}$ cocrystal samples was examined in various media using USP apparatus 4 (Figure 61). Samples of IND-SAC$_{sd}$ were produced during the first step of preparation of IND and SAC cocrystals by the UMAX process. Thus, it was very interesting to test the performance of the intermediate form to see if UMAX technology provides any advantages. Presence of the surfactants in the media led to a significant enhancement in dissolution rate of IND-SAC$_{sd}$ cocrystal samples (Table 66). Greatest enhancement in comparison to reference profile (SGF/SIF) was achieved in MGM/MIM-I ($f_{1,\ area}$: 0.39), that contains the highest concentration of SLS (0.2%). This enhancement corresponded to the fact that in this media, the precipitated sample collected after media change at 70 minutes was significantly lower ($p < 0.001$) than in the other media (Figure 63). This was confirmed by observation from the graph that illustrates the amount of the IND dissolved from IND-SAC$_{sd}$ cocrystal samples at certain time intervals (Figure 62). It can be clearly seen that up to 30 minutes after media change, significant amounts of IND were dissolved when tested in MIM-I.

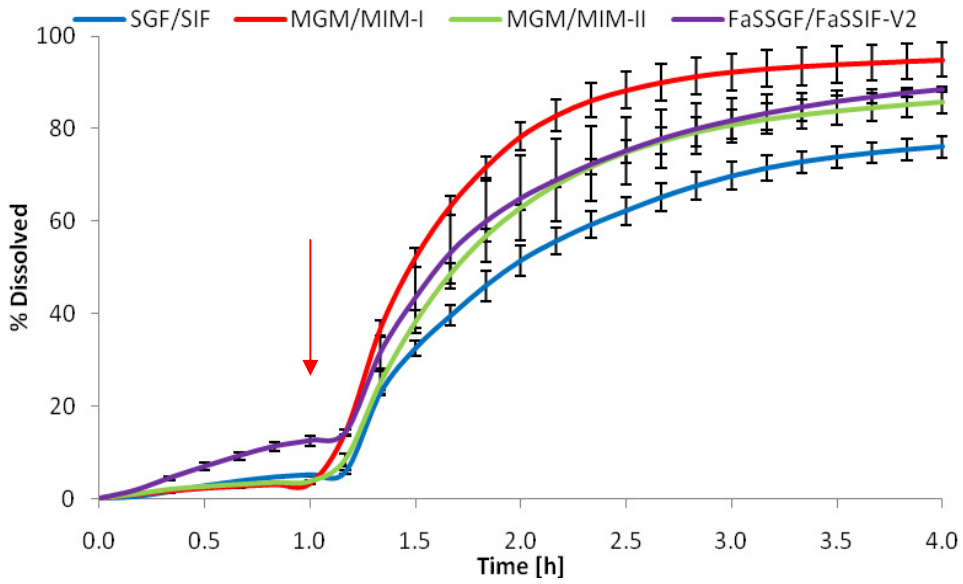

Figure 61. Mean % dissolved (± SD) of IND from IND-SAC$_{sd}$ in various media using USP apparatus 4. [Red arrow indicates media change].

Table 66. Summary of $f_{1,\ area}$ values comparing dissolution profiles of CBZ-SAC$_{sd}$ in various media.

SGF/SIF (as reference)	IND-SAC$_{sd}$		
	MGM/MIM-I	MGM/MIM-II	FaSSGF/FaSSIF-V2
$f_{1,\ area}$	0.39	0.18	0.24

Dissolution of IND-SAC$_{sd}$ in all media simulating gastric conditions followed first-order kinetics, and continue to be dissolved with the same kinetics after the media change (Table 67). Predicted Weibull parameters characterised the whole dissolution profiles of IND-SAC$_{sd}$ indicating that all profiles has sigmoidal shape ($\beta > 1$).

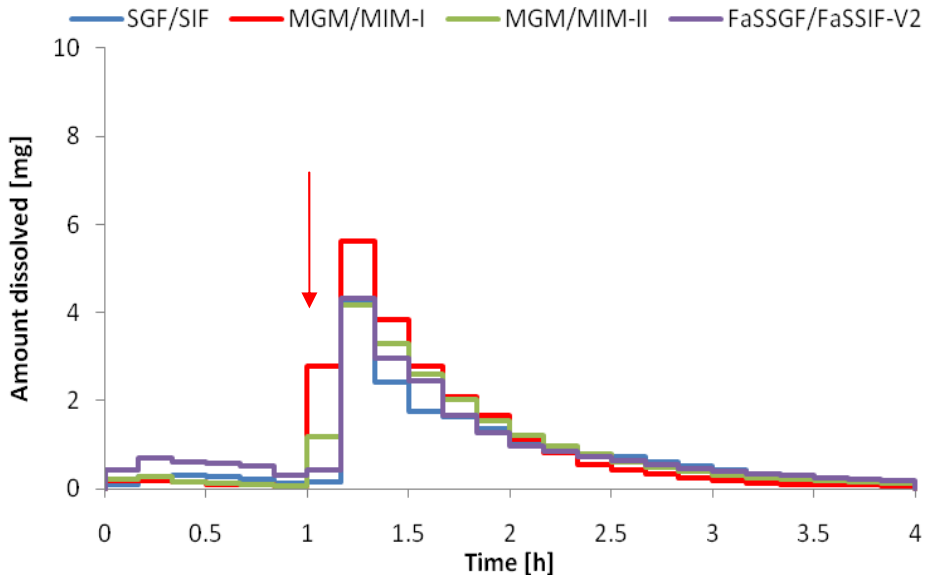

Figure 62. Non-cumulative profiles of mean amounts of IND dissolved from IND-SAC$_{sd}$ samples in various media using USP apparatus 4. [Red arrow indicates media change].

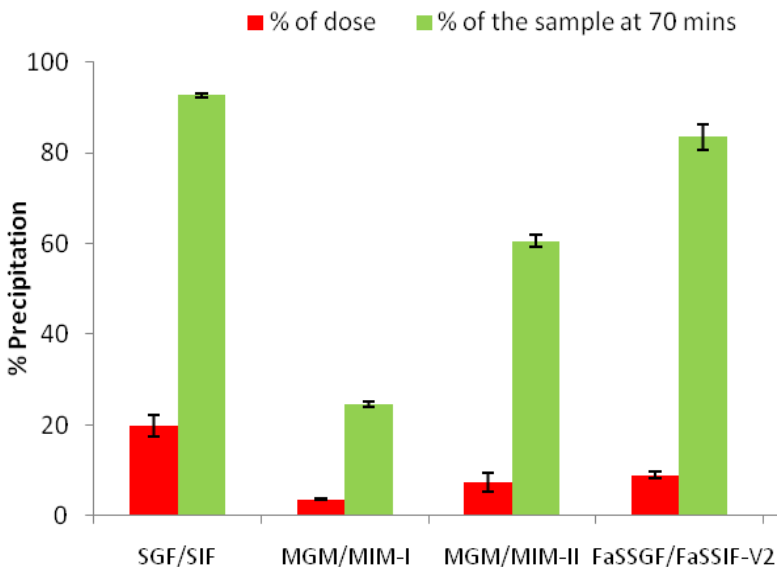

Figure 63. Percent (± SD) of dose and sample at 70 min of IND-SAC$_{sd}$ precipitated in various media.

Interestingly, cocrystals made by the spray-drying method significantly reduced the fraction of the dose that precipitated in MGM/MIM-I ($_{sd}$: 3.61%; $_{ss}$: 16.45%) and compendial media in comparison to cocrystal made by sonic-slurry ($_{sd}$: 19.85%; $_{ss}$: 30.25%) (Figure 63).

Table 67. Dissolution kinetic parameters (± SD) of IND-SAC$_{sd}$ profiles.

Parameters		Gastric phase			
		SGF/SIF	**MGM/MIM-I**	**MGM/MIM-II**	**FaSSGF/FaSSIF-V2**
Zero-order kinetics	k_0 [h^{-1}]	5.27 ± 0.13	3.61 ± 0.24	4.21 ± 0.35	13.21 ± 1.14
	R^2	0.98 ± 0.01	0.93 ± 0.03	0.92 ± 0.03	0.99 ± 0.00
	AIC	-1.98 ± 1.65	-2.64 ± 4.20	1.01 ± 1.31	3.15 ± 3.24
		Intestinal phase			
	k_0 [h^{-1}]	32.46 ± 1.22	43.13 ± 1.74	37.60 ± 1.08	38.50 ± 1.97
	R^2	0.67 ± 0.04	0.27 ± 0.08	0.55 ± 0.09	0.46 ± 0.24
	AIC	156.10 ± 3.27	178.45 ± 1.39	166.36 ± 1.58	167.93 ± 9.00
		Gastric phase			
First -order kinetics	W_{max} [%]	-	4.48 ± 0.48	4.88 ± 0.84	83.37 ± 40.96
	k_1 [h^{-1}]	-	1.35 ± 0.36	1.49 ± 0.26	0.23 ± 0.18
	R^2	-	1.00 ± 0.00	1.00 ± 0.00	0.99 ± 0.00
	AIC	-	-25.63 ± 3.01	-18.08 ± 2.57	3.09 ± 1.91
		Intestinal phase			
	W_{max} [%]	80.68 ± 2.30	96.75 ± 4.71	89.73 ± 5.41	90.35 ± 0.46
	k_1 [h^{-1}]	0.99 ± 0.07	1.57 ± 0.11	1.17 ± 0.14	1.29 ± 0.34
	R^2	1.00 ± 0.00	0.99 ± 0.00	0.99 ± 0.00	1.00 ± 0.00
	AIC	77.61 ± 3.22	89.03 ± 4.36	89.31 ± 7.95	74.91 ± 10.15
		Gastric/Intestinal phases			
3-parameter Weibull function	W_{max} [%]	73.32 ± 2.10	91.80 ± 4.10	82.26 ± 3.43	86.73 ± 0.27
	α [h]	6.76 ± 0.17	7.51 ± 0.37	7.95 ± 0.95	4.75 ± 0.39
	β	2.94 ± 0.13	4.09 ± 0.12	3.54 ± 0.02	2.92 ± 0.64
	R^2	0.99 ± 0.00	0.99 ± 0.00	0.99 ± 0.00	0.99 ± 0.00
	AIC	140.16 ± 2.58	147.49 ± 2.30	142.84 ± 5.83	141.23 ± 4.00

5.7.2.2.1.4 IND-SAC$_{umax}$ samples

Dissolution of IND-SAC$_{umax}$ cocrystal samples was studied in a range of compendial, modified and biorelevant media (Figure 64). Dissolution patterns are similar to those presented for IND-SAC$_{sd}$ (Figure 61). Micelles present in the media significantly enhance the dissolution of IND-SAC$_{umax}$ (Table 68). MGM/MIM-II generated a similar profile ($f_{1,area}$: 0.07) to that in FaSSGF/FaSSIF-V2. Dissolution in MGM/MIM-I is faster than in biorelevant and MIM-II media. Consistency with the results observed for IND-SAC$_{sd}$ proved that both dissolution profiles of IND-SAC$_{sd}$ and IND-SAC$_{umax}$ in MIM-I were actual and the greater enhancement in dissolution in MIM-I might be due to the interactions between IND-SAC and SLS.

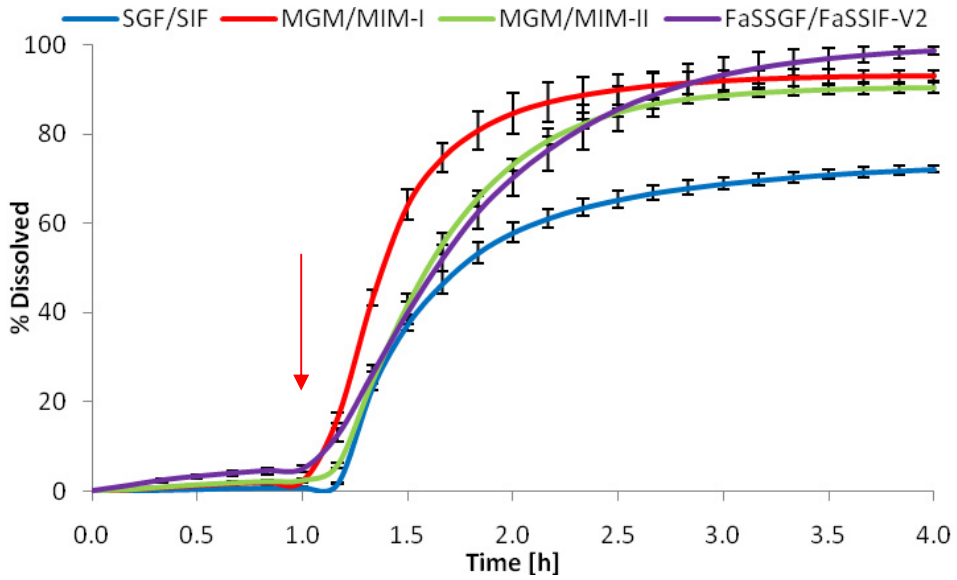

Figure 64. Mean % dissolved (+/- SD) of IND from IND-SAC$_{umax}$ in various media using USP apparatus 4. [Red arrow indicates media change].

Table 68. Summary of $f_{1,\ area}$ values comparing dissolution profiles of CBZ-SAC$_{umax}$ in various media.

SGF/SIF (as reference)	IND-SAC$_{umax}$		
	MGM/MIM-I	MGM/MIM-II	FaSSGF/FaSSIF-V2
$f_{1,\ area}$	0.41	0.27	0.32

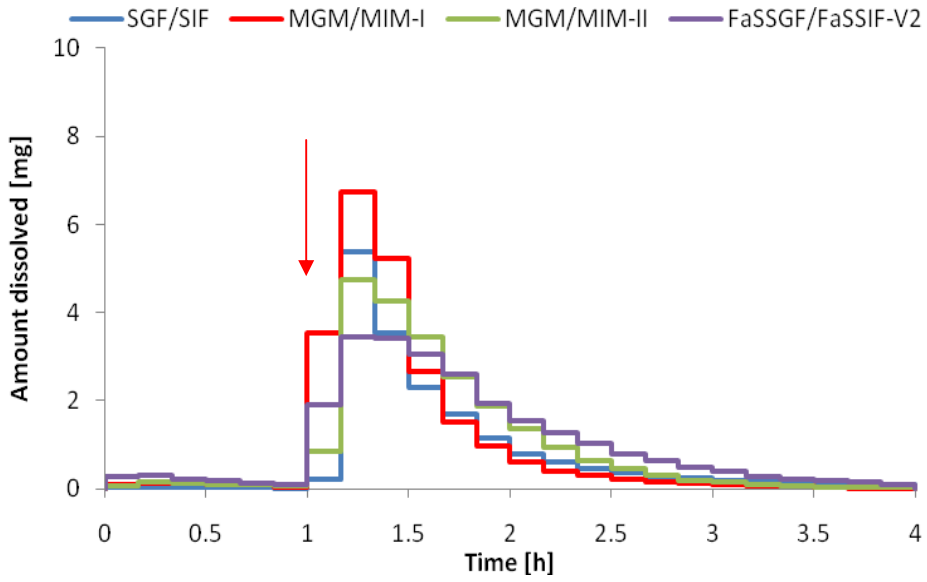

Figure 65. Non-cumulative profiles of mean amounts of IND dissolved from IND-SAC$_{umax}$ samples in various media using USP apparatus 4. [Red arrow indicates media change].

Processing IND-SAC$_{sd}$ cocrystals with UMAX technology did not change the trend previously seen in Figure 62. The highest amount of IND dissolved within first 30 minutes after media change when tested in MIM-I (Figure 65).

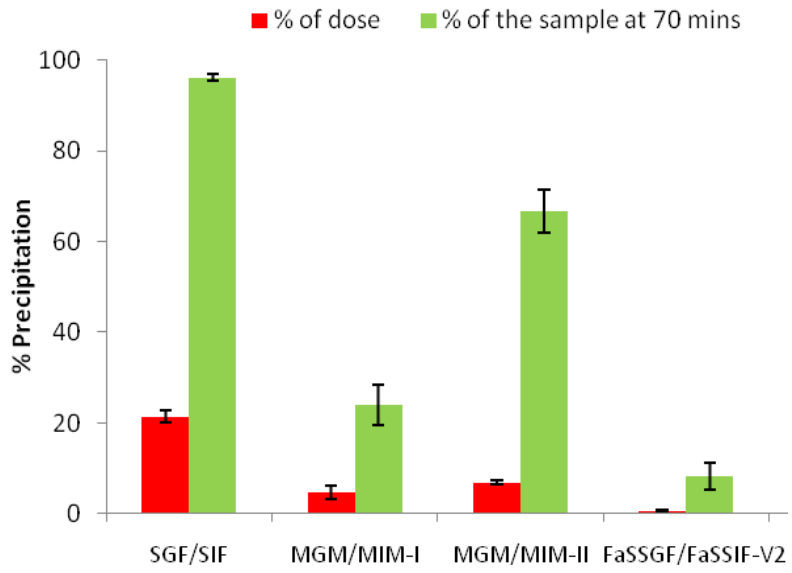

Figure 66. Percent (± SD) of dose and sample at 70 min of IND-SAC$_{umax}$ precipitated in various media.

Presence of the micelles in the media significantly reduces ($p < 0.001$) the percentage of the dose that precipitates upon changing media (Figure 66). Thus, testing formulations in biorelevant media is very important to aid better understanding of formulation and closely mimic *in vivo* performance. Investigating dissolution in just compendial media can lead to overestimated precipitation values. From the pharmacokinetic point of view, the less drug that precipitates, the greater the dose available at the absorption site. However, there are other factors that can affect the dose available at absorption site such as solubility.

Dissolution of IND-SAC_{umax} in compendial media simulating gastric conditions followed zero-order kinetics, whereas at the same stage in modified and biorelevant media, dissolution of IND followed first-order kinetics (Table 69). After changing the media, IND-SAC_{umax} dissolution can be characterised using first-order kinetics. Predicted Weibull parameters well characterised the whole dissolution profiles of IND-SAC_{umax}. Values of $\beta > 1$ indicate that all dissolution profiles of IND-SAC_{umax} have sigmoidal shape.

Table 69. Dissolution kinetic parameters (± SD) of IND-SAC$_{umax}$ profiles.

Parameters		Gastric phase			
		SGF/SIF	MGM/MIM-I	MGM/MIM-II	FaSSGF/FaSSIF-V2
Zero -order kinetics	k_0 [h^{-1}]	0.94 ± 0.14	2.48 ±0.46	2.44 ± 0.13	5.51 ± 0.87
	R^2	0.96 ± 0.03	0.98 ± 0.02	0.98 ± 0.00	0.99 ± 0.02
	AIC	-24.41 ± 6.37	-19.18 ± 9.38	-15.01 ± 0.38	2.32 ± 2.88
		Intestinal phase			
	k_0 [h^{-1}]	32.28 ± 0.68	43.48 ± 1.09	40.97 ± 0.34	43.06 ± 1.48
	R^2	0.43 ± 0.05	-0.11 ± 0.07	0.46 ± 0.06	0.62 ± 0.07
	AIC	165.46 ± 2.21	184.73 ± 2.22	173.84 ± 1.43	169.00 ± 4.48
		Gastric phase			
First -order kinetics	W_{max} [%]	-	7.88 ± 3.77	14.77 ± 9.16	7.09 ± 1.46
	k_1 [h^{-1}]	-	0.52 ± 0.4	0.23 ± 0.13	1.24 ± 0.22
	R^2	-	1.00 ± 0.00	0.98 ± 0.00	1.00 ± 0.00
	AIC	-	-24.62 ± 5.13	-14.00 ± 0.85	-19.09 ± 2.05
		Intestinal phase			
	W_{max} [%]	74.11 ± 0.85	94.02 ± 2.27	95.44 ± 2.12	105.44 ± 0.63
	k_1 [h^{-1}]	1.37 ± 0.07	2.10 ± 0.01	1.29 ± 0.09	1.05 ± 0.10
	R^2	0.98 ± 0.00	0.98 ± 0.01	0.98 ±0.00	0.99 ± 0.00
	AIC	106.98 ± 3.63	104.86 ± 7.68	115.50 ± 2.41	88.86 ± 9.09
		Gastric/Intestinal phases			
3-parameter Weibull function	W_{max} [%]	68.53 ± 1.06	90.44 ± 2.57	88.07 ± 1.12	95.71 ± 2.08
	α [h]	11.29 ± 1.12	9.63 ± 0.81	11.66 ± 0.71	7.88 ± 0.20
	β	4.75 ± 0.38	5.79 ± 0.33	4.54 ± 0.12	3.32 ± 0.19
	R^2	0.99 ± 0.00	0.99 ± 0.00	0.99 ± 0.00	0.99 ± 0.00
	AIC	148.96 ± 0.60	143.19 ± 12.77	140.53 ± 2.21	137.76 ± 7.39

5.7.2.2.1.5 IND-NIC$_{ss}$ samples

Dissolution of IND-NIC$_{ss}$ was determined in various media using USP apparatus 4 (Figure 67). Biorelevant media significantly ($f_{1,\ area}$: 0.28) enhanced dissolution of IND-NIC$_{ss}$ (Table 70). However, the dissolution of this formulation in MGM/MIM-II did not appear to have a similar profile ($f_{1,\ area}$: 0.15) to that in FaSSGF/FaSSIF-V2 which was seen in all previously tested IND formulations. This is probably due to the different effect of the single (in MIM-II) *versus* mixed (in FaSSIF-V2) micelles on NIC, which have solubilisation properties (299).

The fastest dissolution profile was observed in MGM/MIM-I, this is illustrated by the highest dissolution rate constant (k = 2.10) (Table 71).

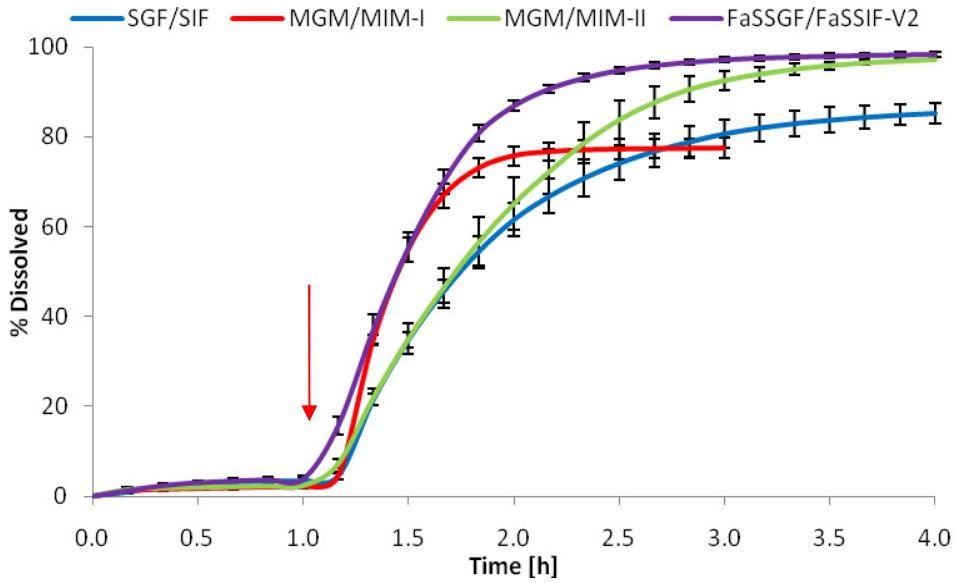

Figure 67. Mean % dissolved (± SD) of IND from IND-NIC$_{ss}$ in various media using USP apparatus 4. [Red arrow indicates media change].

Table 70. Summary of $f_{1,\,area}$ values comparing dissolution profiles of CBZ-NIC$_{ss}$ in various media.

SGF/SIF (as reference)	IND-NIC$_{ss}$		
	MGM/MIM-I	MGM/MIM-II	FaSSGF/FaSSIF-V2
$f_{1,\,area}$	0.18	0.12	0.28

The fastest dissolution profile in MGM/MIM-II can be supported with the fact that the greatest amount of IND dissolved for the first 20 minutes after the media change and formulation completely dissolved within three hours of the experiment (Figure 68).

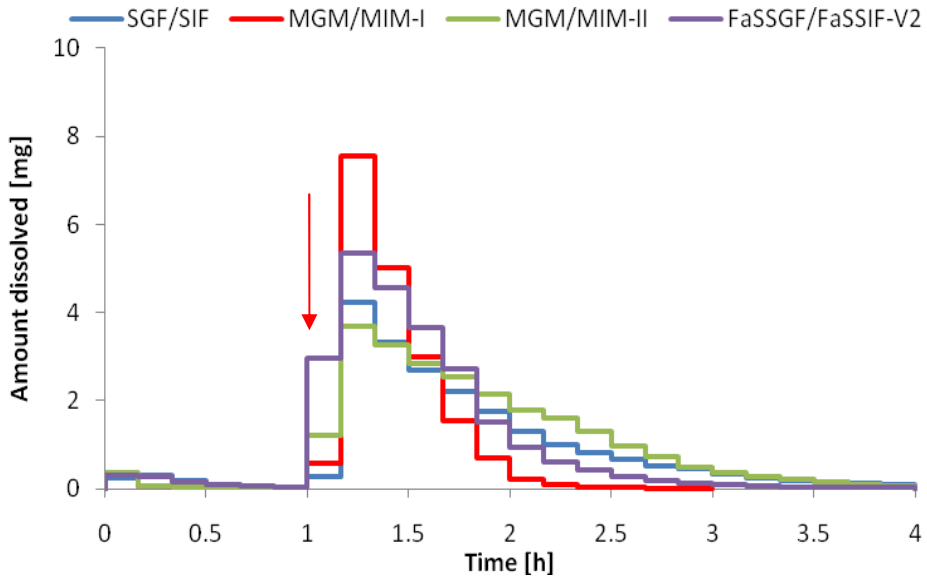

Figure 68. Non-cumulative profiles of mean amounts of IND dissolved from IND-NIC$_{ss}$ samples in various media using USP apparatus 4. [Red arrow indicates media change].

Furthermore, the complete dissolution of IND-NIC$_{ss}$ in MGM/MIM-I occurred faster due to the fact that 20% of the dose (5 mg) precipitated after the media change and less of the formulation remained for dissolution (Figure 69). As in previous formulations, biorelevant media resulted in the smallest fraction of the IND-NIC$_{ss}$ dose precipitating.

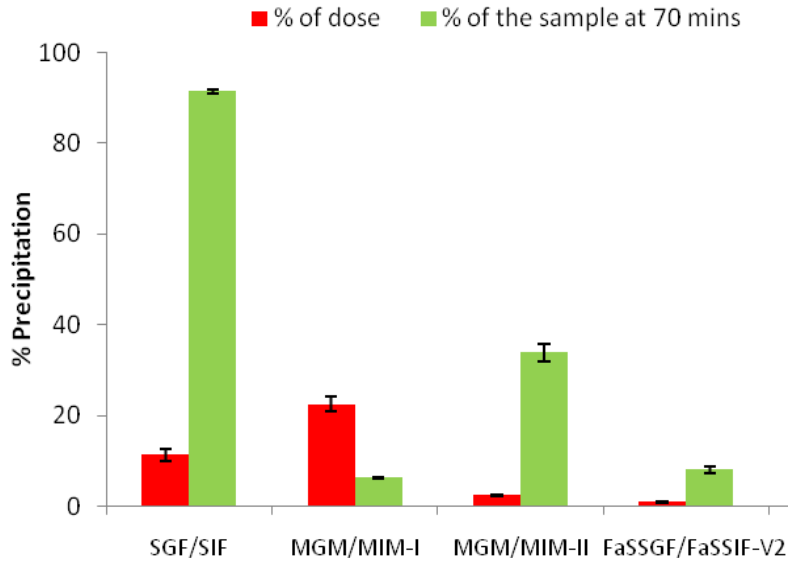

Figure 69. Percent (± SD) of dose and sample at 70 min of IND-NIC$_{ss}$ precipitated in various media.

Dissolution of IND-NIC$_{ss}$ followed first-order kinetics in the gastric and intestinal phases media (Table 71). Predicted Weibull parameters well characterised the whole dissolution profiles of IND-NIC$_{ss}$, indicating that all of them have S-shape.

Table 71. Dissolution kinetic parameters (± SD) of IND-NICss profiles.

Parameters		Gastric phase			
		SGF/SIF	**MGM/MIM-I**	**MGM/MIM-II**	**FaSSGF/FaSSIF-V2**
Zero-order kinetics	$k_0 [h^{-1}]$	4.24 ± 0.85	2.67 ± 0.65	2.97 ± 0.64	4.60 ± 0.79
	R^2	0.82 ± 0.04	0.54 ± 0.11	0.41 ± 0.10	0.82 ± 0.01
	AIC	6.26 ± 1.23	4.46 ± 5.05	7.66 ± 4.14	7.21 ± 1.98
		Intestinal phase			
	$k_0 [h^{-1}]$	37.27 ± 1.37	52.87 ± 1.55	42.14 ± 1.00	45.52 ± 0.38
	R^2	0.63 ± 0.06	0.47 ± 0.01	0.71 ± 0.09	0.16 ± 0.08
	AIC	164.00 ± 3.61	112.83 ± 1.04	164.71 ± 5.58	183.10 ± 1.25
		Gastric phase			
First-order kinetics	W_{max} [%]	4.08 ± 1.06	2.08 ± 0.44	2.24 ± 0.45	4.30 ± 0.79
	$k_1 [h^{-1}]$	2.21 ± 0.32	4.48 ± 0.87	5.71 ± 1.04	2.31 ± 0.08
	R^2	0.98 ± 0.01	0.98 ± 0.00	0.98 ± 0.00	1.00 ± 0.00
	AIC	-9.25 ± 2.20	-16.29 ± 5.01	-14.99 ± 3.66	-19.33 ± 2.63
		Intestinal phase			
	W_{max} [%]	91.46 ± 3.13	82.83 ± 2.29	108.95 ± 3.17	100.94 ± 0.09
	$k_1 [h^{-1}]$	1.05 ± 0.09	1.96 ± 0.03	0.90 ± 0.15	1.71 ± 0.11
	R^2	0.99 ± 0.00	0.95 ± 0.00	0.99 ± 0.00	0.99 ± 0.00
	AIC	101.46 ± 7.56	85.24 ± 1.82	105.68 ± 5.35	105.97 ± 5.18
		Gastric/Intestinal phases			
3-parameter Weibull function	W_{max} [%]	84.75 ± 2.20	76.14 ± 2.03	94.86 ± 0.67	96.27 ± 0.51
	α [h]	0.79 ± 0.09	20.11 ± 3.11	10.42 ± 0.52	8.94 ± 0.86
	β	1.34 ± 0.09	7.90 ± 0.51	3.55 ± 0.29	4.71 ± 0.04
	R^2	1.00 ± 0.00	0.99 ± 0.00	1.00 ± 0.00	1.00 ± 0.00
	AIC	72.12 ± 2.17	99.50 ± 0.94	136.81 ± 1.81	135.36 ± 3.13

Precipitation kinetics

The *in vitro* IND kinetics of the precipitation was determined using USP apparatus 4. USP apparatus 4 allows changing of the media during a continuous dissolution run, which closely mimics human gastrointestinal conditions. Due to the large differences in the solubility of IND in acidic and basic conditions, precipitation of IND occurred after media change. The

precipitated samples were treated according to the method described in section 4.4.11.1.1. However, it was observed that remaining precipitated samples left on the side of the bench salt-out further. Thus, it was important to treat the samples immediately after collection. The kinetics of the precipitation was determined using samples collected from dissolution experiments of IND-SAC_{ss} and IND-NIC_{ss} cocrystals in MGM/MIM-II media using USP apparatus 4.

Samples of IND-SAC_{ss} and IND-NIC_{ss} cocrystals collected after media change resulted in 85% of the sample precipitated 2 hours after collection (Figure 70). In contrast, when the sample was treated immediately 63 and 34% were reported for precipitated samples of IND-SAC_{ss} and IND-NIC_{ss} cocrystals, respectively. These findings proved that treatment of precipitated samples is a crucial step that should be performed immediately after collection. Delay in treatment of the precipitated samples may lead to misleading and overestimated value.

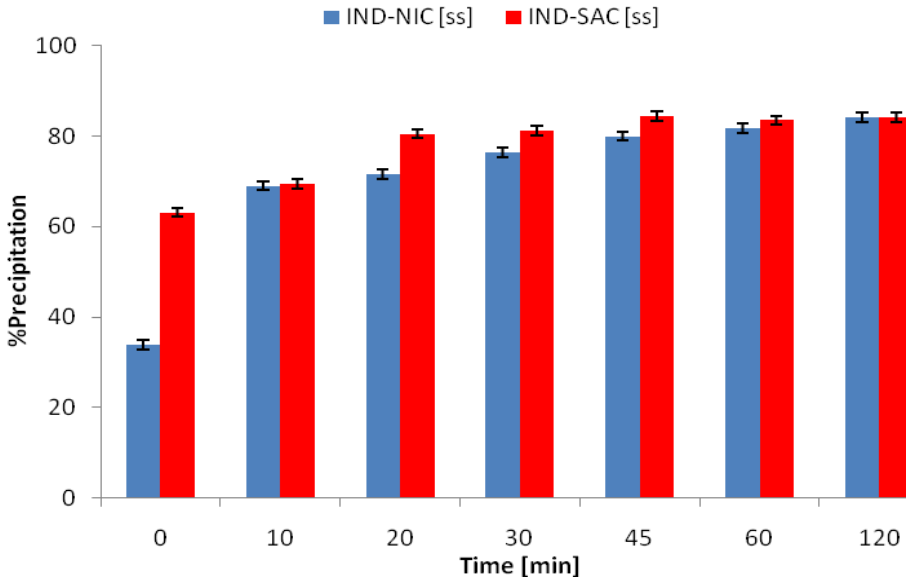

Figure 70. Kinetics of the precipitation (± SD) of IND-SAC_{ss} and IND-NIC_{ss} cocrystals. Precipitated samples obtained from dissolution experiments in MGM/MIM-II using USP apparatus 4.

5.7.2.2.2 Effect of type of coformer

Dissolution profiles of IND_{sp}, $IND\text{-}SAC_{ss}$, and $IND\text{-}NIC_{ss}$ in biorelevant media, were compared in order to verify which coformer type enhances dissolution of IND most efficiently (Figure 71). Dissolution profiles in biorelevant media were selected for comparison as the precipitation of the dose for all these formulations is lower than 1%. Both of the cocrystals made by sonic-slurrying demonstrated to significantly enhance the dissolution of IND. According to the difference factor $f_{1,area}$, Nicotinamide cocrystal of IND ($f_{1,area}$: 1.16) improves dissolution of IND more than the Saccharin cocrystal ($f_{1,\ area}$: 0.95). The difference between both cocrystals is also statistically significant ($f_{1,\ area}$: 0.19).

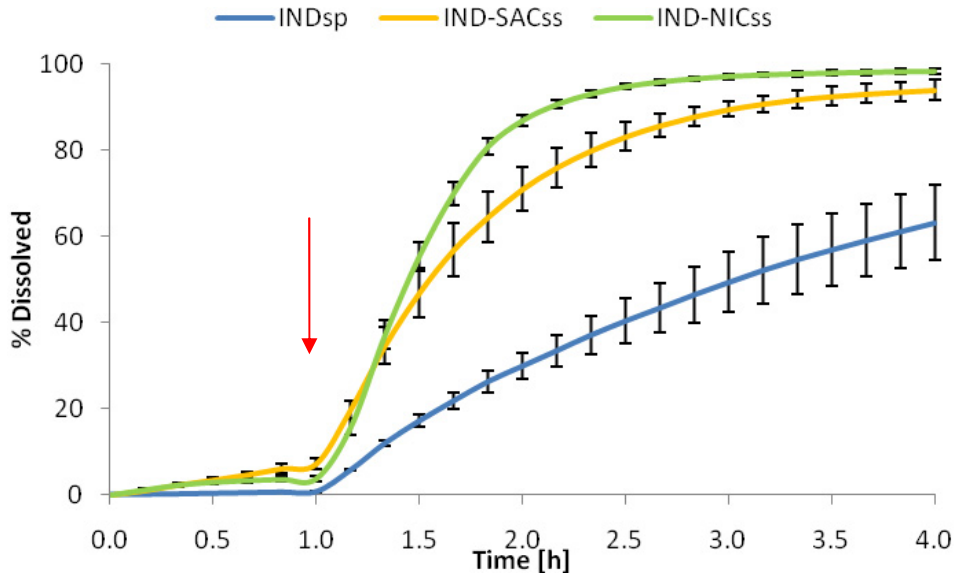

Figure 71. Mean % dissolved (± SD) of IND from cocrystals made by sonic-slurrying method and tested in biorelevant media using USP apparatus 4. INDsp samples were used as the control. [Red arrow indicates media change].

Interestingly, NIC cocrystals of CBZ did not demonstrate any dissolution enhancement of CBZ. Two observations could aid the understanding of this behaviour. Firstly, the dose of IND (25 mg) is eight times smaller than that of CBZ (200 mg). Thus, amounts of NIC in $CBZ\text{-}NIC_{ss}$ cocrystal may not be sufficient to impact its dissolution. Secondly, according to Hörter and Dressman, for compounds with high *logP*, solubilisation is the predominant mechanism (IND *logP* 4.27), whereas for compounds with low *logP* (CBZ *logP* 2.45), wettability is the mechanism which accounts for enhancement of the powder dissolution rate (320). It seems that it was easier to solubilise small amounts of IND than wet large amounts of CBZ.

5.7.2.2.3 Effect of method of preparation

Dissolution profiles of IND-SAC$_{ss}$, IND-SAC$_{sd}$ and IND-SAC$_{umax}$ in one of the modified media (MGM/MIM-II) were compared against dissolution of IND$_{sp}$ samples in order to assess which cocrystallisation method resulted in the highest improvement of dissolution (Figure 72). Dissolution profiles in modified media (MGM/MIM-II) were selected for comparisons, as the precipitation of the dose for all these formulations was similar and ranged from 6.8 to 7.4 %. $f_{1,\ area}$ values indicate that cocrystals made by sonic-slurrying and UMAX techniques significantly improved dissolution of poorly soluble IND$_{sp}$ samples (Table 72). Cocrystals made by UMAX technology provided the greatest enhancement of dissolution rate ($f_{1,\ area}$**:** 0.21).

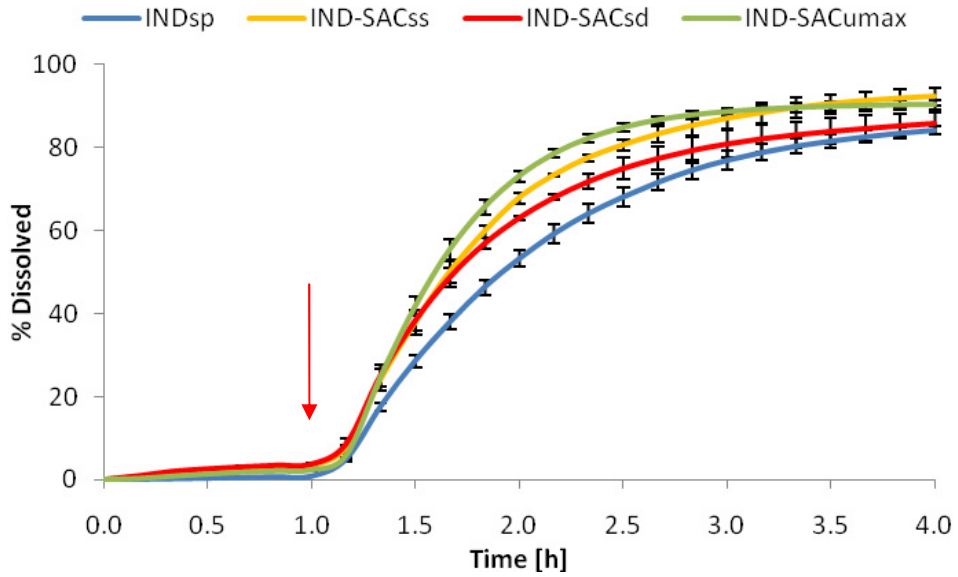

Figure 72. Mean % dissolved (± SD) of IND from IND-SAC cocrystals made by different cocrystallisation methods and tested in MGM/MIM-II media using USP apparatus 4. IND$_{sp}$ samples were used as control. [Red arrow indicates media change].

According to difference factor, spray-drying did not significantly improve the dissolution of IND$_{sp}$ ($f_{1,\ area}$**:** 0.11). This is due to the similarity in particle size between these two samples. The slightly faster dissolution profile of IND-SAC$_{sd}$ is due to the slightly smaller particle size (Table 73).

Table 72. Summary of $f_{1,\ area}$ values comparing dissolution profiles of different IND-SAC formulations in MGM/MIM-II.

IND_{sp} (as reference)	**MGM/MIM-II**		
	IND-SACss	**$IND\text{-}SAC_{sd}$**	**$CBZ\text{-}SAC_{umax}$**
$f_{1,\ area}$	0.18	0.11	0.21

Interestingly, despite having the largest particle size, $IND\text{-}SAC_{umax}$ cocrystals provided the greatest dissolution improvement. This indicates that UMAX technology may bring some additional benefits in terms of API and coformer packing and arrangement in cocrystals.

Table 73. Comparison of PSD (± SD) of IND_{sp} and IND-SAC cocrystals made by various cocrystallisation methods.

	D_{10} ± SD	**D_{50} ± SD**	**D_{90} ± SD**
IND_{sp}	4.74 ± 0.04 µm	24.86 ± 0.13 µm	55.21 ± 0.74 µm
$IND\text{-}SAC_{ss}$	1.89 ± 0.01 µm	15.40 ± 0.14 µm	57.45 ± 0.62 µm
$IND\text{-}SAC_{sd}$	3.27 ± 0.09 µm	22.63 ± 0.28 µm	49.59 ± 1.36 µm
$IND\text{-}SAC_{umax}$	5.89 ± 0.10 µm	32.27 ± 1.81 µm	67.34 ± 3.63 µm

5.7.2.2.4 Effect of cocrystal and its mechanism of dissolution

5.7.2.2.4.1 Saccharin types of IND cocrystals

Dissolution of the physical mixture of IND and SAC was performed in biorelevant media and its profile was compared against IND_{sp} and all IND-SAC cocrystals produced using various cocrystallisation methods (Figure 73). Physical blend of IND and SAC significantly improved dissolution of IND ($f_{1,\ area}$**:** 0.17); however to much smaller extent than all other IND-SAC cocrystals (Table 74). IND-SAC cocrystals made by sonic-slurrying and UMAX methods resulted in the fastest dissolution profiles reaching almost 100% within four hours. All samples apart from $IND\text{-}SAC_{sd}$ (8.88%) demonstrated precipitation of the dose below 1%. In all of the mentioned cases, IND benefited from the presence of SAC.

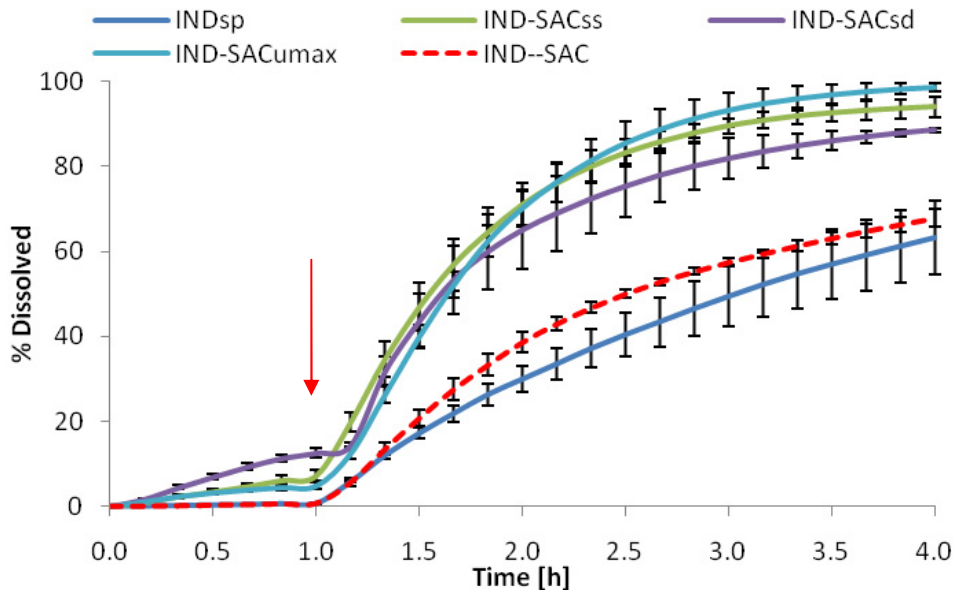

Figure 73. Mean % dissolved (± SD) of different IND-SAC formulations in biorelevant media. [Red arrow indicates media change].

Table 74. Summary of $f_{1,\ area}$ values comparing dissolution profiles of different IND-SAC formulations in biorelevant media.

IND_{sp} (as reference)	**FaSSGF/FaSSIF-V2**			
	IND - - SAC	**IND-SAC_{ss}**	**IND-SAC_{sd}**	**IND-SAC_{umax}**
$f_{1,\ area}$	0.17	0.95	0.83	0.96

In order to gain understanding of the mechanism by which SAC improves dissolution of IND, IND-SAC_{ss} cocrystals were selected to study the dissolution of SAC from the cocrystal. Closer investigation showed that SAC from IND-SAC_{ss} cocrystal dissolved at a slower rate than SAC from the physical blend (Figure 74) despite the fact that both SAC dissolved within the first 2 hours of the experiment. A similar trend was observed during examination of SAC formulations of CBZ (*Saccharin types of CBZ cocrystals* section 5.7.1.2.6.1). The packing and arrangement of the SAC and IND in both the physical blend and cocrystal plays an important role in the enhancement of dissolution of IND.

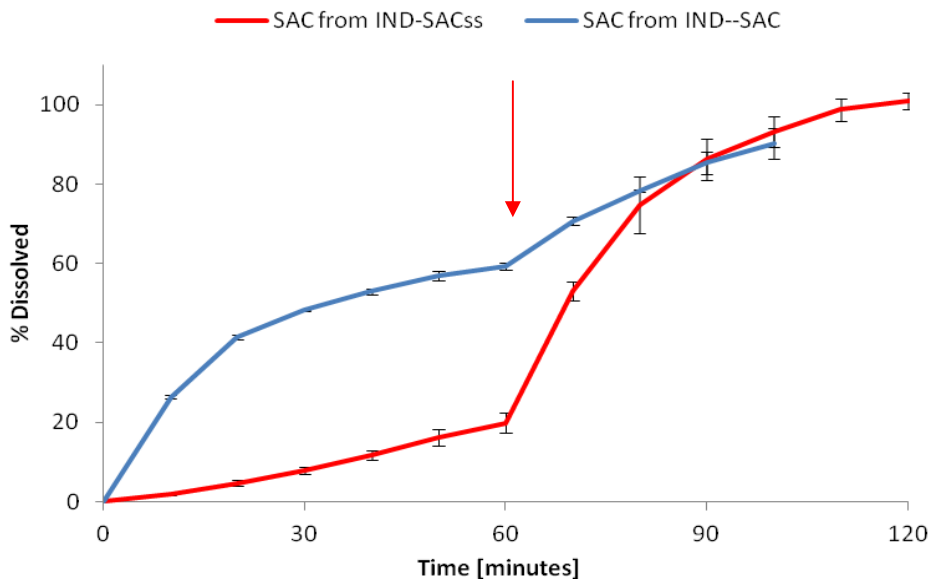

Figure 74. Mean % dissolved (± SD) of SAC from different IND-SAC formulations.

Dissolution of Saccharin from the cocrystal form follows a zero-order kinetics pattern in FaSSGF and it is much slower than that from the physical blend, which follows first-order kinetics in both media. After the change of media, dissolution of SAC from cocrystal seems to follow first-order characteristics. This could be due to solubilisation of SAC by bile salts present in FaSSIF-V2.

5.7.2.2.4.2 Nicotinamide types of IND cocrystals

Dissolution of the physical blend of IND and NIC was performed in biorelevant media and its profile was compared against IND_{sp} and all IND-NIC cocrystals produced using the sonic-slurrying method (Figure 75). The dissolution profile of the physical blend was significantly slower than IND-NIC_{ss} cocrystals ($f_{1,\ area}$**:** 0.41) but significantly faster ($f_{1,\ area}$**:** 0.53) than dissolution of IND_{sp} samples. IND-NIC_{ss} cocrystal provided the greatest dissolution enhancement of IND ($f_{1,\ area}$**:** 1.16).

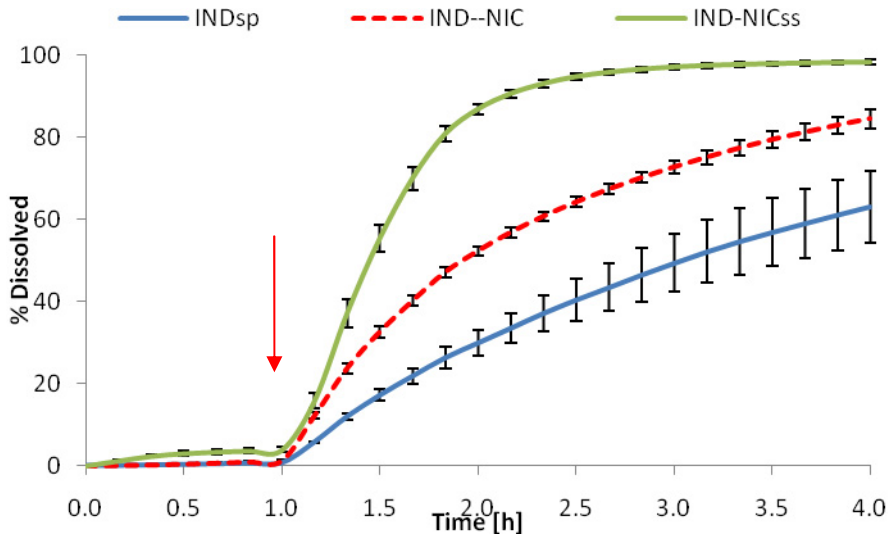

Figure 75. Mean % dissolved (± SD) of IND from different IND-NIC formulations in biorelevant media.

According to Figure 76, NIC from both the cocrystal and the physical blend dissolved within the first 30 minutes. These dissolution profiles of NIC were measured simultaneously with dissolution of IND. Despite the fact that the dissolution of NIC from cocrystal is as fast as from the physical blend; this still leads to a discrepancy between cumulative dissolution profiles of IND-NIC_{ss} and IND--NIC. This leads to the conclusion that it might be the packing and arrangement of the NIC and IND in both the physical blend and cocrystal that plays an important role in the enhancement of dissolution of IND.

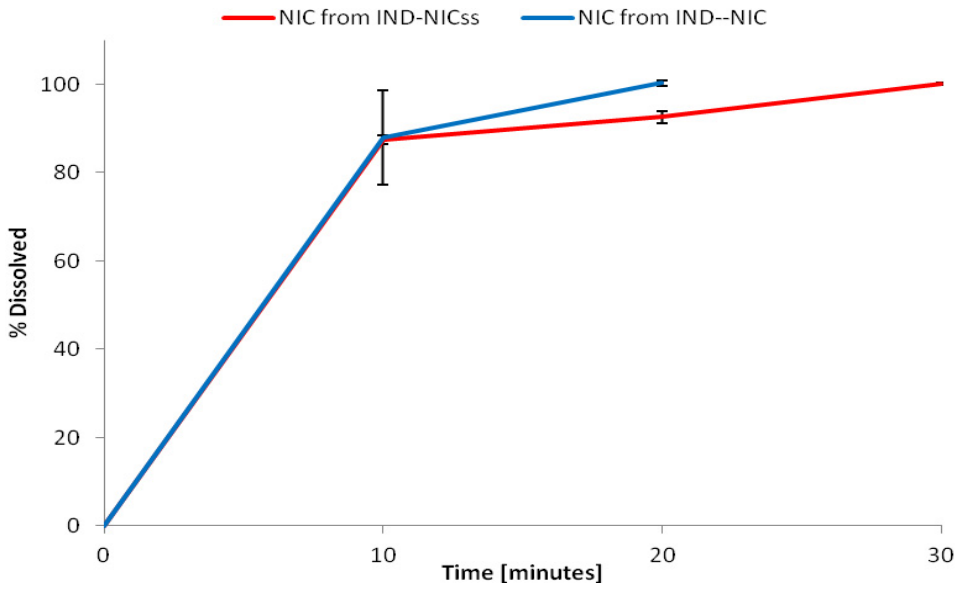

Figure 76. Mean % dissolved (± SD) of NIC from different IND-NIC formulations.

5.7.2.2.5 Effect of media on IND precipitation

Indomethacin precipitation depends on the medium used and type of formulation investigated. According to Figure 77, species that are present in SGF and SIF provoke precipitation of samples collected at 70 minutes, resulting in higher percentage of the dose precipitated. On the other hand, biorelevant media inhibited sample precipitation.

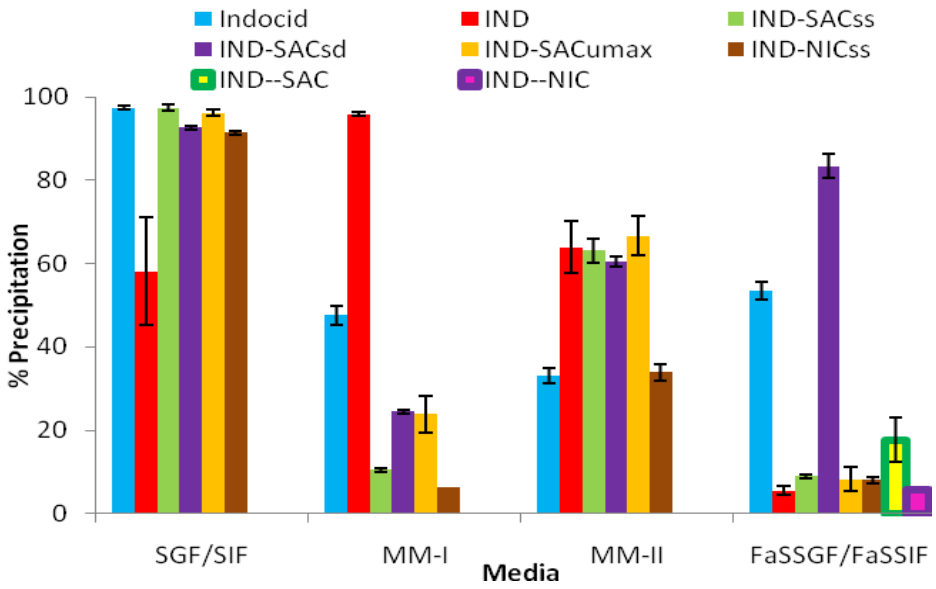

Figure 77. % precipitated (± SD) of the sample collected at 70min during dissolution of different IND formulations in various media.

Overall, the largest fraction of the Indocid® dose precipitated across all investigated media, whereas the smallest fraction of dose precipitated from IND_{sp} formulations (Figure 78). This might lead to the conclusion that excipients and coformers present in Indocid® formulation contribute to the extent of precipitation.

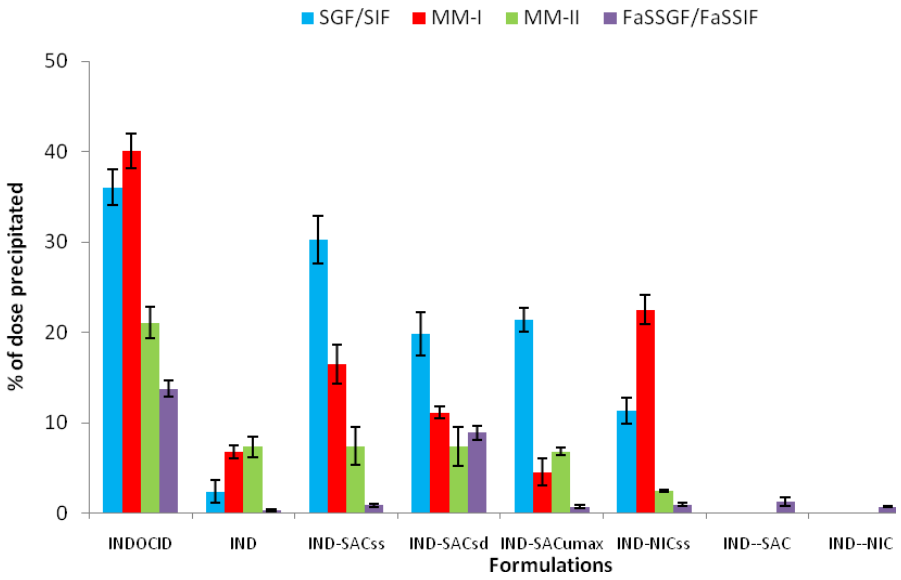

Figure 78. % of dose precipitated (± SD) during dissolution of different IND formulations in various media

6 Development of IVIVC

6.1 Carbamazepine case

6.1.1 Model-dependent approach

Intravenous and oral solution CBZ formulations are not available on the market, hence it was not possible to perform numerical deconvolution technique (226). When the drug follows a one-compartmental model and its elimination obeys first-order kinetics, then Wagner-Nelson deconvolution can be applied (243, 321). However, the CBZ follows a two-compartmental model; deconvolution technique for Tegretol® IR and PR formulations were still implemented with care. Deconvoluted profiles using Wagner-Nelson method for IR Tegretol® tablets are presented in Figure 79 .

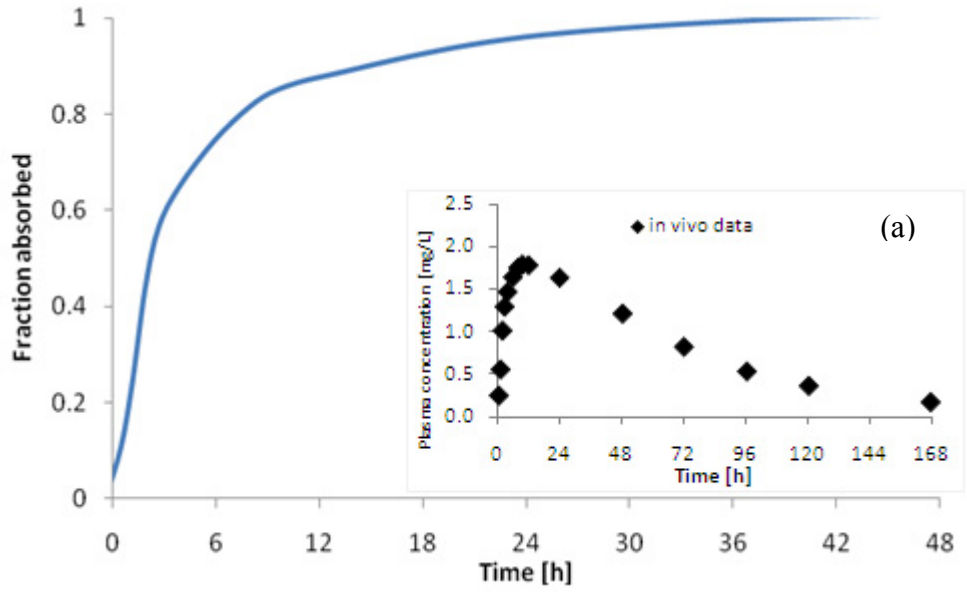

Figure 79. Mean *in vivo* absorption of CBZ from Tegretol® IR tablets obtained using Wagner-Nelson method. (a) Original *in vivo* data extracted from Meyer *et al*.(286).

According to Figure 79, 80% of CBZ is absorbed within 8 hours. *In vivo* fraction absorbed was compared with fractions dissolved obtained from experiments using USP apparatus 1 and USP apparatus 4. Volumes of the media used in USP apparatus 1 were not able to provide sink conditions. Thus, the plateau of the dissolution profile for Tegretol® IR was reached at 50%. Attempts at developing point-to-point Level A IVIVC using original and normalised (*) dissolution data were made and are presented in Figure 80.

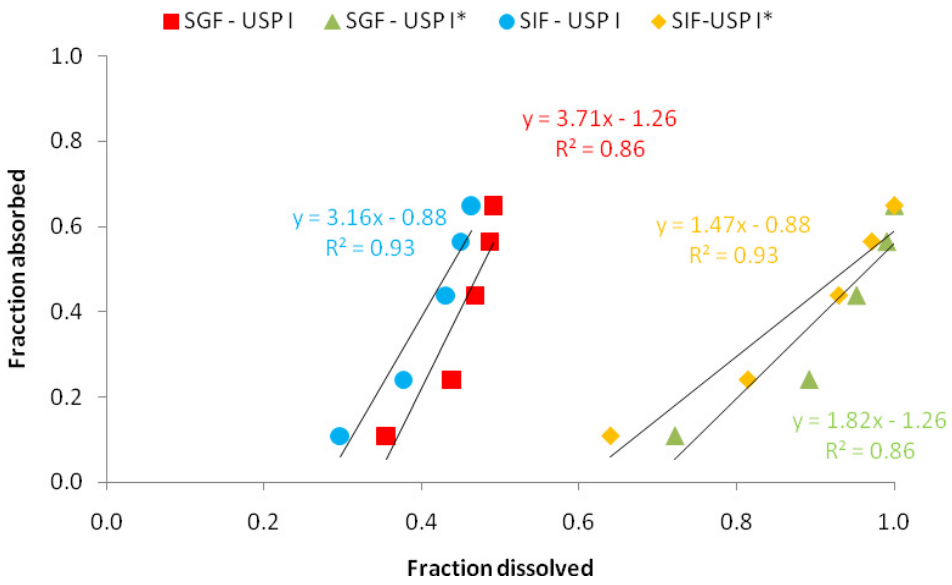

Figure 80. IVIVC of Tegretol® IR formulation using dissolution data obtained USP apparatus 1 experiments.* indicates normalised data.

Poor ($R^2 \leq 0.93$) IVIVC correlation was obtained using USP 1 dissolution data despite the normalisation (Figure 80). Dissolution profiles from USP 1 experiments were faster than absorption, which enabled 1:1 correlation.

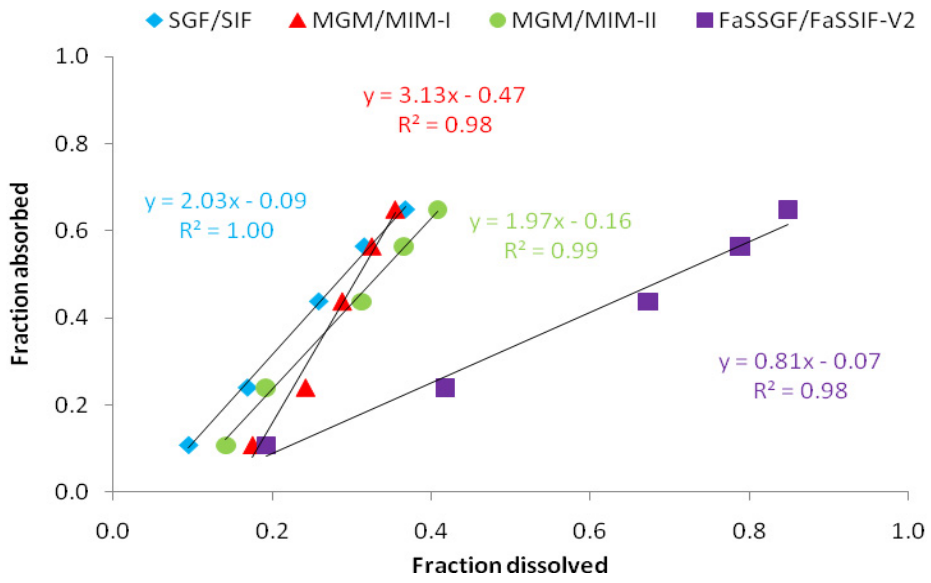

Figure 81. IVIVC of Tegretol® IR formulation using dissolution data obtained from USP apparatus 4 experiments.

Successful point-to-point Level A IVIVC was obtained using *in vitro* data tested in biorelevant media (Figure 81). The intercept of this linear regression is close to zero (-0.07)

together with a slope value close to 1 (0.81) and goodness of fit (R^2: 0.98) indicates good *in vitro-in vivo* correlation.

Deconvolution of the oral plasma concentration curve of 400 mg PR Tegretol® formulation using Wagner-Nelson method is presented in Figure 82. 80 % CBZ is absorbed within 14 hours.

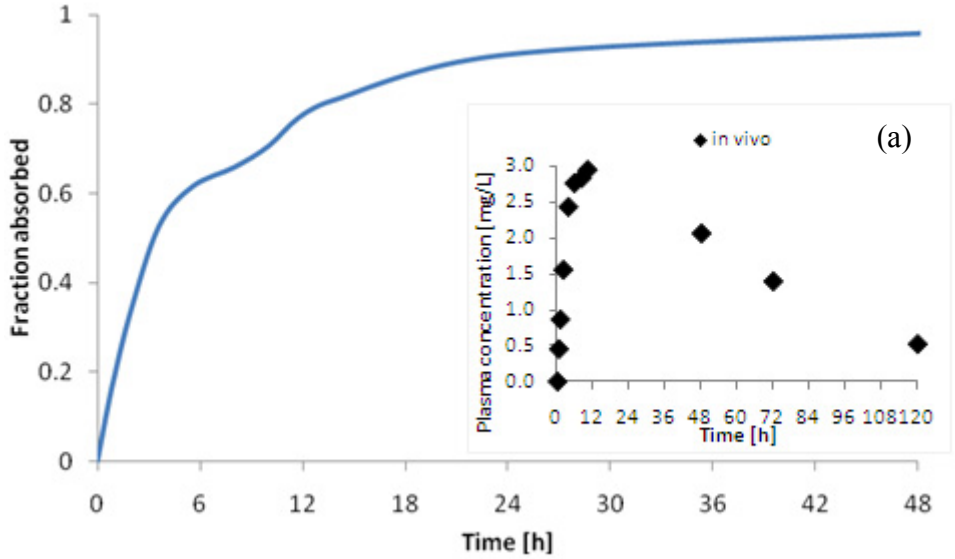

Figure 82. Mean *in vivo* absorption of CBZ from Tegretol® PR tablets using Wagner - Nelson method. (a) Original *in vivo* data extracted from Kovacevic *et al.* (82).

Fractions absorbed *in vivo* were related to fractions of CBZ dissolved *in vitro* by fitting linear regression model to the data (Figure 83). Correlations were performed using mean dissolution data tested using flow-through cell dissolution apparatus. Dissolution data for 400 mg Tegretol® PR tablets had similar dissolution profiles, thus correlations resulted in similar regression parameters. Dissolution data in biorelevant media (FaSSGF/FaSSIF-V2/FaSSCoF) allowed development of point-to-point Level A IVIVC. Goodness of fit value (R^2: 0.99) is close to one, intercept parameter (0.03) close to zero together with slope value (1.01) close to 1 indicate the desired method specifications that can be used to facilitate product development and serve as quality control tool during the manufacture process.

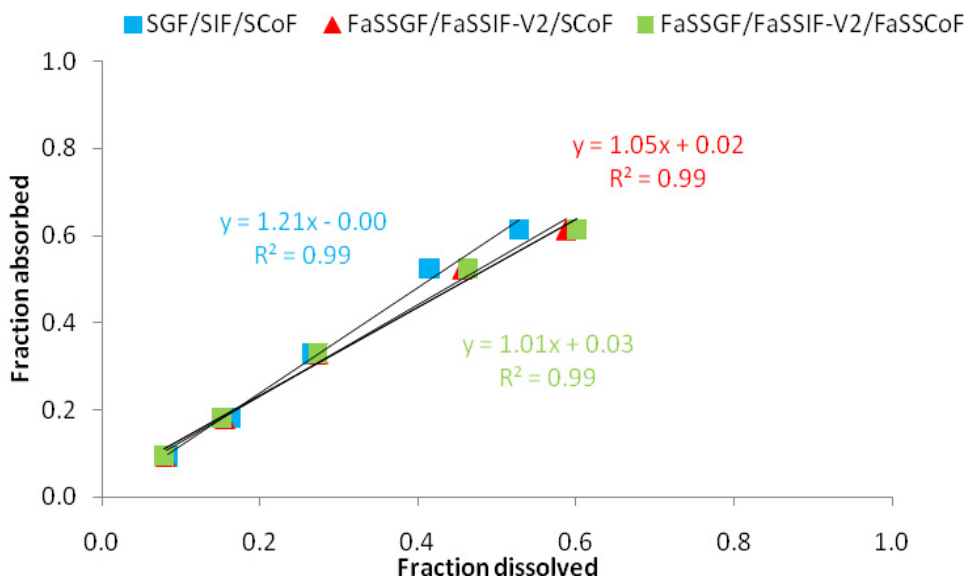

Figure 83. IVIVC of Tegretol® IR formulation using dissolution data obtained from USP apparatus 4 experiments.

6.1.2 PBPK model

6.1.2.1 IR formulation (200 mg Tegretol® tablets)

Physiological, physicochemical, pharmacokinetic and formulation parameters of Tegretol® (CBZ) were inserted into the Simcyp® software. The ability of Simcyp® software to predict dissolution data using solubility and particle size data was investigated. The dissolution data were predicted using the Wang-Flanagan (WF) equation. The predicted dissolution profiles aided then the prediction of Tegretol® *in vivo* performance (Figure 84). In comparison to existing *in vivo* data from Meyer *et al.* (283), the predicted plasma concentration profiles were overestimated (Table 75). The reason for overestimation could be due to the fact that WF approach does not take into the consideration formulation properties, which are essential for absorption modelling. Thus, an attempt to develop PBPK model using raw dissolution data from previously performed *in vitro* experiments was made.

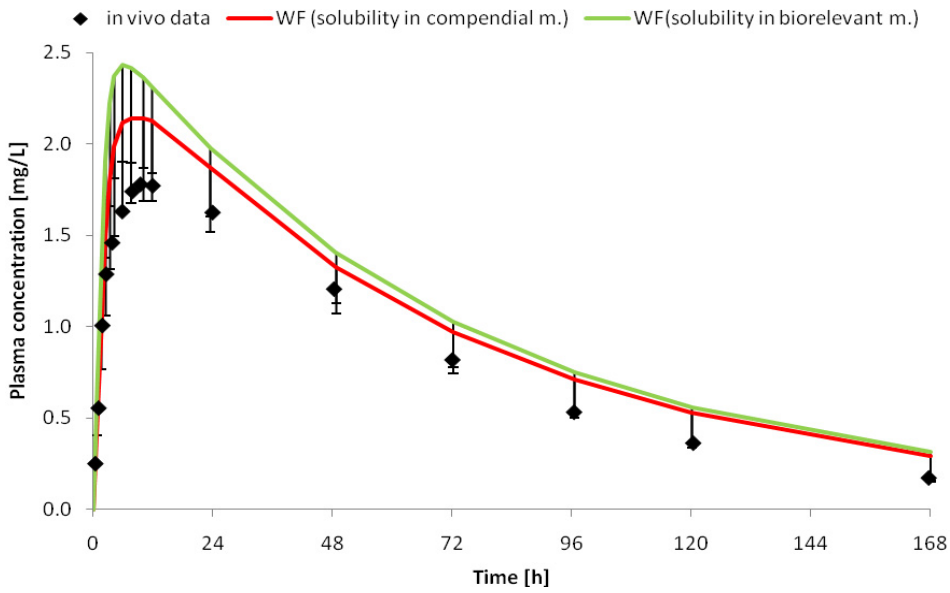

Figure 84. Mean (+ SD) simulated plasma concentration time profiles of PBPK IR Tegretol® model using predicted dissolution profile obtained by the Wang-Flanagan equation.

Table 75. Summary of indices for a PBPK IR Tegretol® model using predicted dissolution profiles obtained by the WF equation.

	f_1 (*in vivo* data as reference)
WF-compendial	25.63
WF-biorelevant	40.62

Prediction of plasma concentration time profiles of PBPK Tegretol® model using dissolution data was attempted. The same physiological, physicochemical, pharmacokinetic parameters as in WF approach were used in this model. Different type of dissolution data were used to predict *in vivo* behaviour of Tegretol® IR tablets. Figure 85 compares predicted plasma concentration profile from raw dissolution data obtained using USP apparatus 1 with observed *in vivo* profile reported by Meyer *et al.* (283). This predicted profile using USP apparatus 1 data is significantly slower (f_1: 35.44), and its C_{max}, T_{max} and AUC values are much lower than that reported for the observed profile (Table 77). Underestimation could be due to failure of providing sink conditions for CBZ in USP apparatus 1.

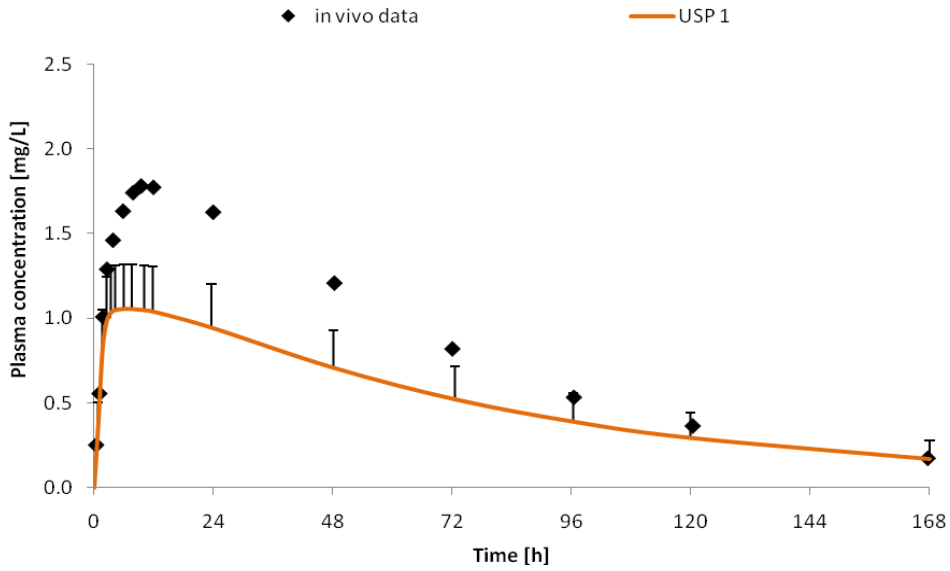

Figure 85. Mean (+ SD) simulated plasma concentration time profiles of PBPK IR Tegretol® model using dissolution profile obtained using USP apparatus 1. [*in vivo* data extracted from Meyer *et al*.(1992) (286)]

Predicted plasma concentration profiles using raw dissolution data of Tegretol® IR formulations tested using USP apparatus 4 are shown in Figure 86. As can be seen from Table 77, predicted plasma concentration time profiles that used dissolution data obtained from flow-though cell dissolution apparatus tested in compendial (f_1: 33.68) and both modified conditions (MGM/MIM-I f_1: 45.24; MGM/MIM-II f_1: 37.69) resulted in similar f_1 values to that in USP apparatus 1 (f_1: 35.44), despite the fact that USP apparatus 4 provided sink conditions. Also, plasma concentration time profiles predicted using dissolution data in compendial (C_{max}: 1.12; AUC: 95.15) and both modified conditions (MGM/MIM-I: C_{max}: 0.95; AUC: 81.98; MGM/MIM-II: C_{max}: 1.10; AUC: 94.10) resulted in similar ($p > 0.05$) C_{max} and AUC values (C_{max}: 1.02; AUC: 83.99) to data obtained using USP apparatus 1 (Appendix 8). It can be clearly seen from Figure 86 that dissolution in biorelevant media resulted in the best prediction (f_1: 6.94) of *in vivo* performance of 200 mg IR Tegretol® tablets (Table 77). Despite discrepancies in C_{max} and T_{max} values, the predicted profile resulted in similar AUC values (Table 76). The successful IVIVC was developed with the PBPK model using raw dissolution data tested in biorelevant media using flow-through cell dissolution apparatus.

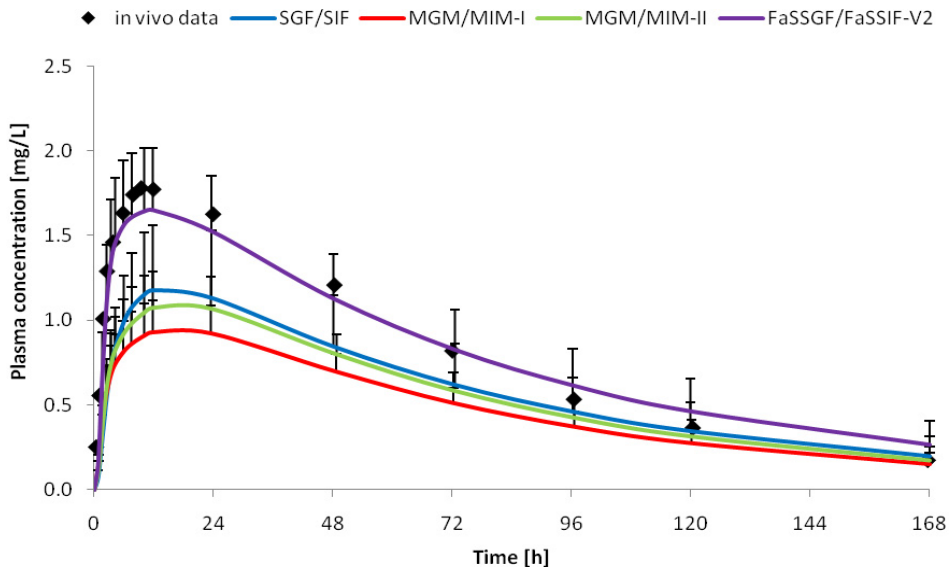

Figure 86. Mean (+ SD) simulated plasma concentration time profiles of PBPK IR Tegretol® model using dissolution profiles obtained using USP apparatus 4. [*in vivo* data extracted from Meyer *et al*.(1992) (283)]

Table 76. Mean simulated CBZ pharmacokinetic parameters for PBPK IR Tegretol® model.

	C_{max} [mg/L]	T_{max} [h]	*AUC* [mg/L.h]
In vivo	1.89	15.90	134.80
USP 1_{sim}	1.02	8.40	83.99
SGF/SIF_{sim}	1.12	17.68	95.15
MGM/MIM-I_{sim}	0.95	16.83	81.98
MGM/MIM-II_{sim}	1.10	16.82	94.10
FaSSGF/FaSSIF-$V2_{sim}$	1.57	10.96	127.88

Table 77. f_1 values comparing *in vivo* plasma concentration time profile with simulated plasma concentration time profiles of PBPK IR Tegretol® model using different dissolution profiles.

	f_1 (*in vivo* data as reference)
USP 1_{sim}	35.44
SGF/SIF_{sim}	33.68
MGM/MIM-I_{sim}	45.24
MGM/MIM-II_{sim}	37.69
FaSSGF/FaSSIF-$V2_{sim}$	6.94

According to the literature, the bioavailability of CBZ following oral administration is slow reaching approximately 70-90 % of CBZ being absorbed (322). The slow absorption of CBZ has been attributed to slow dissolution rate of CBZ in the GI tract in contrast to rapid GI transit time (323). Thus, CBZ absorption is primarily dissolution-rate limited (324, 325). The successful PBPK model resulted in an average 71 % of the CBZ absorbed, which is in agreement with reported values from the literature (Figure 87). Most of the CBZ was absorbed within 12 hours of oral administration. The absorption constant of k_a 0.37 h^{-1} was estimated using first-order kinetics.

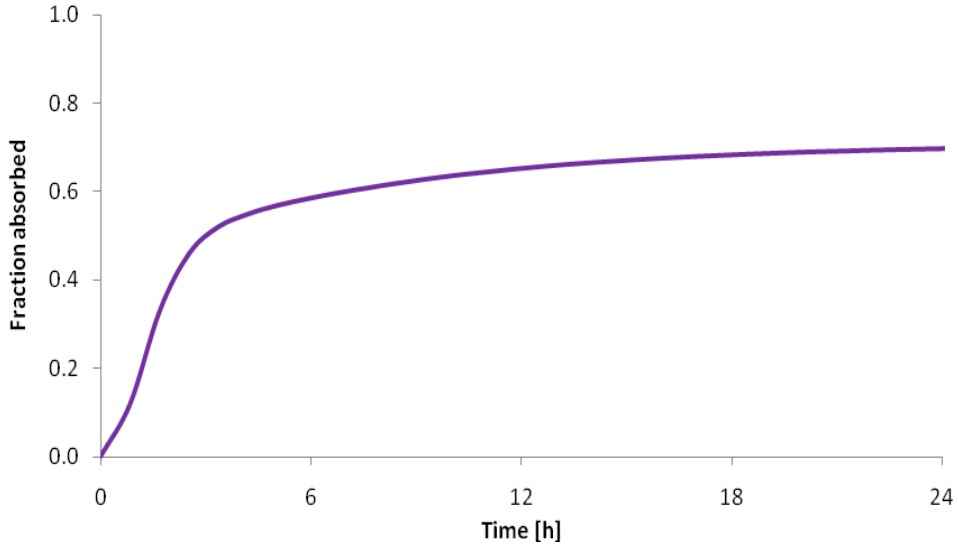

Figure 87. Mean predicted cumulative fraction of CBZ absorbed from Tegretol® IR tablets predicted using successful PBPK model.

Further examination of the Tegretol® IR PBPK model indicates that a large percentage (18%) of CBZ is absorbed from the colon (Figure 88). A similar value (25%) was reported for CBZ IR formulations under fasted state using ACAT model (248). The overall trend in the regional absorption was the same, however, some small differences in values were observed. These discrepancies could be due to discrepancies between PK parameters used for model development, quality of *in vitro* data used and features related to integrated ACAT and ADAM models.

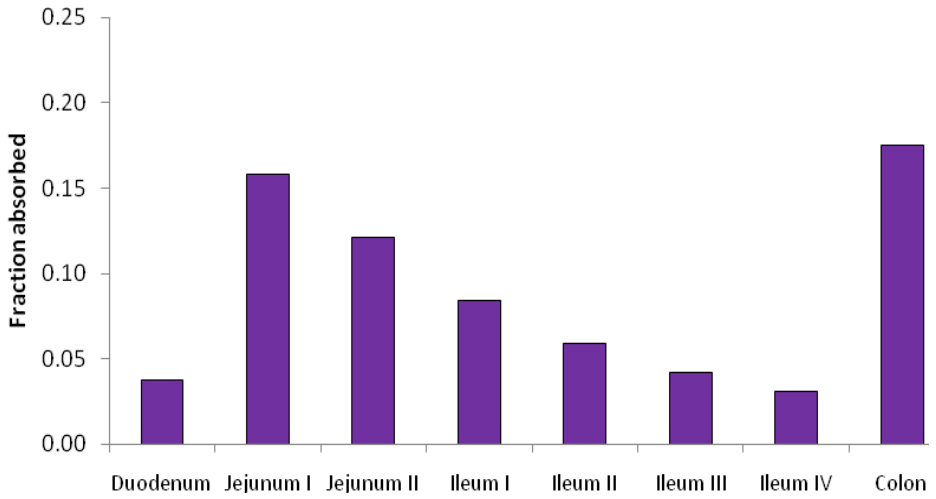

Figure 88. Mean predicted regional distribution of the fraction of the CBZ dose absorbed from 200 mg Tegretol® IR formulation.

6.1.2.2 PR formulation (400 mg Tegretol® tablets)

The same pharmacokinetic and physiological parameters were further used to develop the PBPK model for 400 mg PR Tegretol® tablets. 400 mg PR Tegretol® tablets were selected for these simulations for which two sets of clinical data were found (Figure 89) (82, 284).

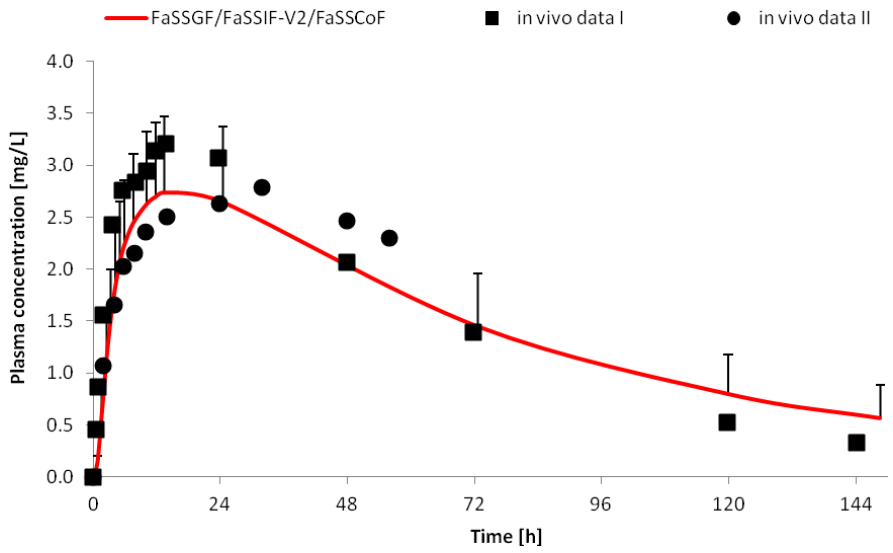

Figure 89. Mean (+ SD) predicted plasma concentration time profile of 400 mg PR Tegretol® tablets using the PBPK model for CBZ after oral administration of an IR Tegretol® tablets. [*in vivo* data extracted from Kovacevic *et al*. (82) and Larkin *et al*. (284)]

Dissolution profile performed in the biorelevant media (FaSSGF/FaSSIF-V2/FaSSCoF) was used to develop the PBPK model for 400 mg PR Tegretol® tablets. Predicted plasma concentration profiles of 400 mg PR Tegretol® tablets were similar to observed profiles obtained from two separate clinical studies (*in vivo* data II: f_1: 9.46 and *in vivo* data I: 18.91). The predicted mean plasma concentration profile of PR Tegretol® formulation is more significantly similar (f_1: 9.46) to the observed profiles reported by Larkin *et al.* (*in vivo* data II) (284). However, the comparison with this profile was only performed until 56 hours. Thus, comparison with *in vivo* I data may be more reliable.

The ADAM model was also used to predict the regional absorption of CBZ from 400 mg Tegretol® PR tablets (Figure 90). PR formulation might have a significant impact on the regional absorption. In previously examined IR formulation, CBZ was to the same extent absorbed in the jejunum and colon, whereas in the case of PR formulation there was more than 2.5 times increase in absorption in the colon compared to the jejunum. One quarter of the dose was absorbed in the colon resulting in the overall absorption around 60 %.

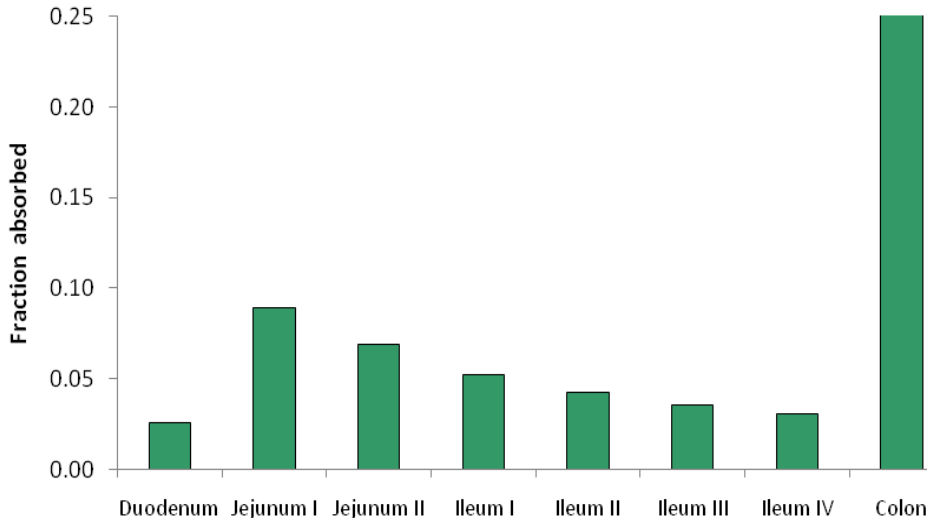

Figure 90. Mean predicted regional distribution of the fraction of the CBZ dose absorbed from 400 mg Tegretol® PR formulation.

The ACAT model developed by Zhang *et al*. showed that up to 50 % of 400 mg Tegretol XR formulation can be absorbed in the colon (248). The colon is considered as an important absorption site for CR formulations and often it can be referred as targeted drug delivery. An extensive study of 42 compounds in human showed that BCS class I drugs were well

absorbed in the colon (326). Thus, understanding of the impact of solubility and dissolution rate on the absorption in the colon is essential.

6.1.2.3 Sensitivity analysis

6.1.2.3.1 Sensitivity analysis for PBPK model after administration of IR Tegretol® tablets.

Sensitivity analysis was performed for two types of parameters. The first group was related to absorption processes and include parameters such as solubility, particle size, *logP* and human effective permeability (P_{eff}). The second group consists of parameters that describe the distribution of the drug in the human body such as volume of distribution (V_d) and clearance after oral administration (CL_{po}). Increasing solubility by 10 folds would have a minimal effect on the C_{max} and T_{max} (Table 78). However, if CBZ would be less soluble (by 10 folds) then there would be significant reduction in AUC and C_{max}. Time to reach T_{max} would be twice as long as that at the current solubility. Micronisation of the API will slightly enhance C_{max} and AUC. On the other hand, 10 times larger particle size would result in lower AUC and C_{max} and significantly delayed T_{max} (nearly 2 fold). Lipophilicity of the CBZ was insensitive to any changes (Figure 91). Human effective permeability may affect the PBPK model if lower values than 3.1 x 10^{-4} cm/s would be selected. CBZ belongs to BCS class II drugs which are characterised by high permeability, thus it was unlikely that human permeability will be sensitive to changes. The human permeability value of 4.3 x 10^{-4} cm/s was determined using very accurate regional human jejunal perfusion technique. It is worth of noting that too fast dissolution rate may cause saturation process, which may affect rate of permeation.

Table 78. Sensitivity analysis of absorption related parameters of Tegretol® IR PBPK model.

	AUC [mg*h/L]	C_{max} [mg/mL]	T_{max} [h]
Control	177.08	2.43	5.90
Solubility x10	182.73	2.57	5.05
Solubility / 10	53.10	0.58	10.93
PS x10	155.99	1.98	10.11
PS / 10	181.39	2.55	5.88

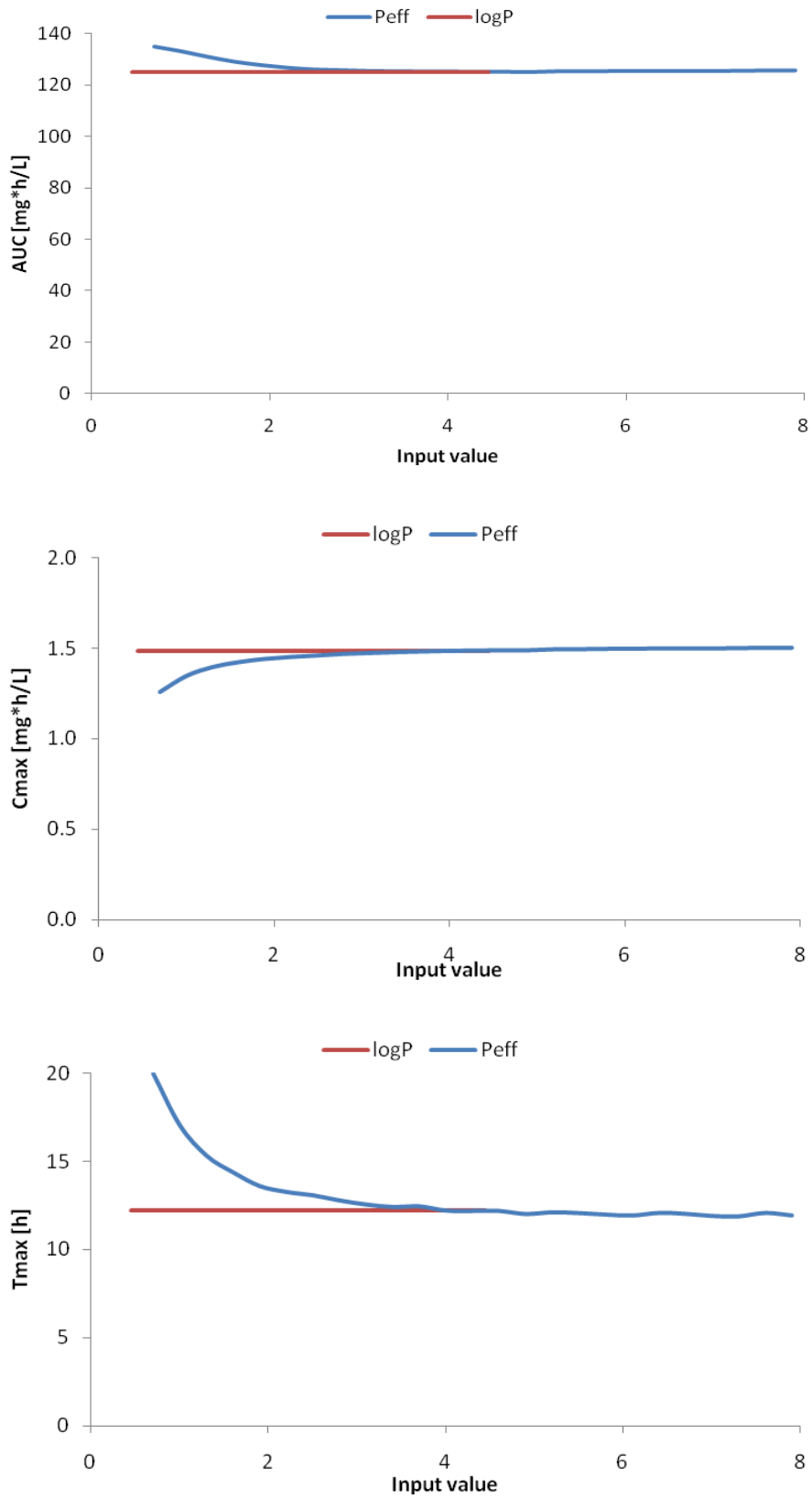

Figure 91. Sensitivity analysis of absorption parameters: *logP* (unitless) and P_{eff} (x 10^{-4} cm/s).

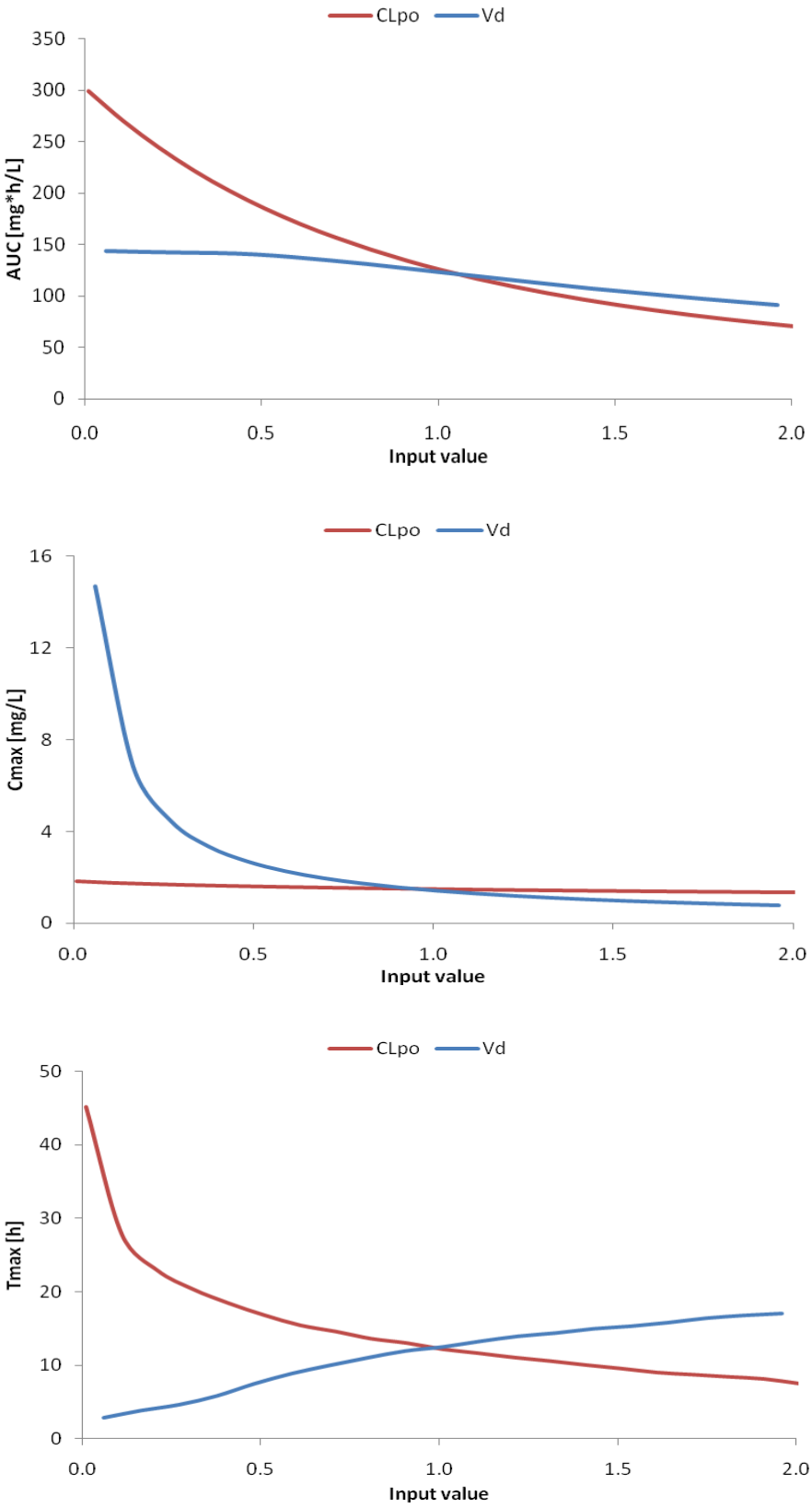

Figure 92. Sensitivity analysis of distribution parameters: V_d (L/kg) and Cl_{po} (L/h).

Figure 92 illustrates that clearance and volume of distributions are the two parameters that are the most susceptible to any changes. For instance, small changes in the clearance value will cause significant changes in *AUC* and T_{max} levels. However, it will have only minimal effect on the C_{max} value. Similarly to clearance parameter, V_d value will affect the T_{max} and *AUC* levels the most and it will have the least impact on C_{max}.

6.1.2.4 Reported IVIVC for CBZ

Several studies have been conducted in order to develop IVIVC of Carbamazepine products. In 1984, Kaneniwa *et al*. found a correlation between *in vitro* time required for 30, 50, 60 and 80% to be dissolved and the *in vivo* absorption rate constant by using two liters of gastric fluid as dissolution media and 100rpm (327). A year later, Neuvonen reported a good agreement between *in vitro* release of Carbamazepine in 1L of 0.1M HCl using USP apparatus 1 at 100rpm and the absorption profile *in vivo* (328). The similar dissolution specifications (0.1M HCl, 100rpm) using paddle instead of basket apparatus allowed Hartley *et al*. to assess the bioavailability of two formulations in epileptic children at steady state (329) .

Moreover, Meyer *et al*. developed an IVIVC using three generic 200 mg tablets products and innovator product using 900 mL of water containing 1% SLS stirred at 75 rpm in paddle apparatus. The relationship between the percentage dissolved during the first 45 minutes and the C_{max} and *AUC* values was found to be more useful in predicting the bioequivalence of CBZ (Multiple Level C) (330). The same group attempted to establish Level A IVIVC for three generic CBZ formulations and reformulated innovator product, which was shown to be approximately 6% more bioavailable than the old formulation (331). They have failed to establish Level A IVIVC but again successfully developed Multiple C correlation. This time they found a correlation between T_{max} and C_{max} and percentage dissolved *in vitro* at 5, 10, 15, 20 and 30 minutes using the same dissolution method (paddle, 900 mL, 75 rpm, water containing 1% SLS).

Jung *et al*. failed to find Level A IVIVC using the same dissolution method but have achieved linear correlation between *AUC* and percentage drug dissolved of four formulations at 45, 60 and 90 minutes in intestinal medium (Level C) (332). Another Level C correlation was established by Lake *et al*. who obtained linear relationships between C_{max} values of four formulations and percentage dissolved *in vitro* at 20, 40 and 50 minutes in water containing

1% SLS (paddle, 900 mL, 75 rpm) (240). In 2000, Veng-Pedersen *et al*. successfully developed Level A IVIVC using a scaled convolution based predictive approach using data from four CBZ formulations (331). In this case, dissolution data in water containing 1% SLS (paddle, 900 mL, 75 rpm) were convoluted by a single exponential and the estimated unit impulse response function and time scaled and mapped with drug concentration data.

Kovacevic *et al*. established successful Level A IVIVC for immediate (IR) and controlled (CR) release CBZ formulations using Physiologically Based Pharmacokinetic (PBPK) modeling (82). To achieve this gastrointestinal simulation based on the advanced compartmental absorption and transit (ACAT) model built – in GastroPlus® software was used. The *in vivo* drug absorption and disposition was simulated based on CBZ physicochemical and pharmacokinetic properties and drug dissolution kinetics observed *in vitro*. Also, in this case, the dissolution method used water containing 1%SLS (paddle, 900 mL, 75 rpm) resulted in the best prediction. Despite the proven effectiveness of this medium, the physiological relevance of this dissolution method can be questioned.

6.2 Indomethacin case

6.2.1 Model-independent approach

Numerical deconvolution of the Indomethacin *in vivo* data using PCDCON resulted in the profile presented in Figure 93. It can be clearly seen that the absorption of IND is delayed and only around 20 mg of Indomethacin was absorbed within four hours. Incomplete absorption supports the findings that were observed during dissolution using USP apparatus 4 that relates to low solubility in acidic pH and the precipitation upon media change. Also, it may be concluded that due to the fact that solubility of IND is very low in acidic environment, gastric emptying may be responsible for slower initial absorption onset. Possibly Indomethacin precipitated *in vivo* after GE which resulted in lower amounts absorbed (20 mg within 4 h). This may indicate that probably 20% (remaining 5 mg of the dose) of the IND precipitated, and this is in agreement with *in vitro* studies performed. According to the dissolution studies of IND, 15% of Indocid® dose precipitated in biorelevant media. Some discrepancies could be due to variability of *in vivo* data.

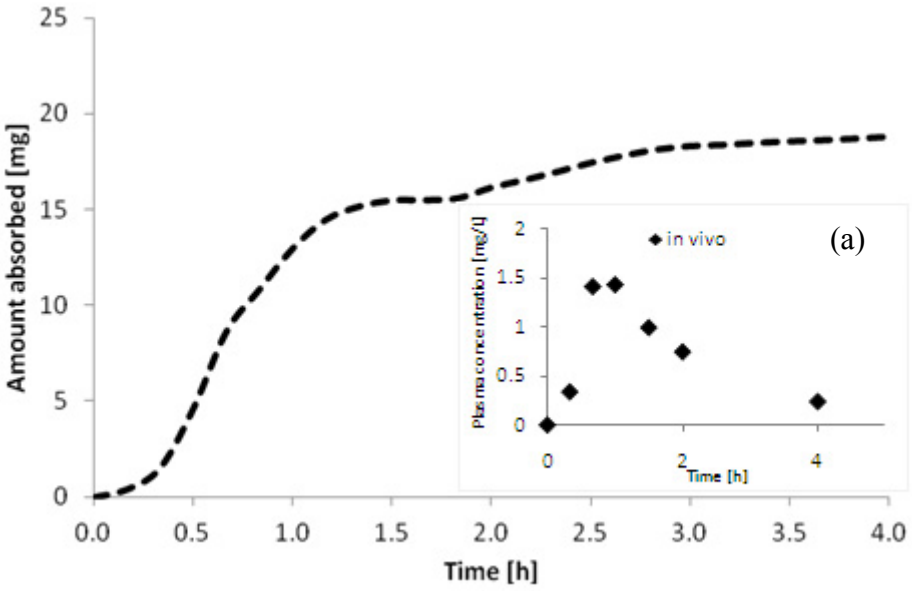

Figure 93. Mean *in vivo* absorption profile after oral administration of 25 mg Indocid® capsules.
(a) Original *in vivo* data extracted from Yeh *et al*. (285).

Dissolution data in various media were then compared with *in vivo* absorption Indocid® data (Figure 94) and Level A IVIVC were made. Level A IVIVC was not achievable with the original dissolution data obtained from USP apparatus 4 presented as cumulative amount dissolved (Figure 95). Time at which media were changed (1 h) limited the comparison with *in vivo* absorption of Indomethacin data and resulted in non-linear correlation (Figure 95). This indicated that the absorption is faster than dissolution, thus dissolution in gastric conditions is a rate limiting step. Thus, attempts to correlate only dissolution data from an intestinal part were made (Figure 96). It is worth noting that due to precipitation that was measured *in vitro*, the dissolution profiles reached plateau at around one and a half hours of experiment. Taking into consideration the values after the plateau is reached will result in many points close to each other at the terminal part of the correlation (as seen in Figure 95). Terminal points from dissolution profiles (after plateau) will affect the goodness of fit of the linear regression. Thus for the further correlations *in vivo* and *in vitro* data until two hours were used.

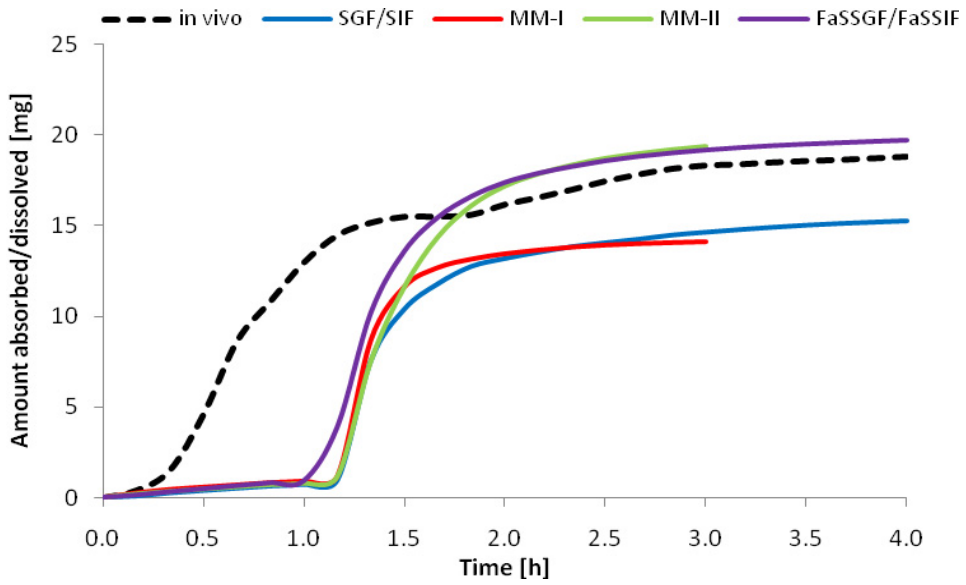

Figure 94. Mean i*n vivo* amount absorbed and *in vitro* amount dissolved data of Indocid® IR capsules.

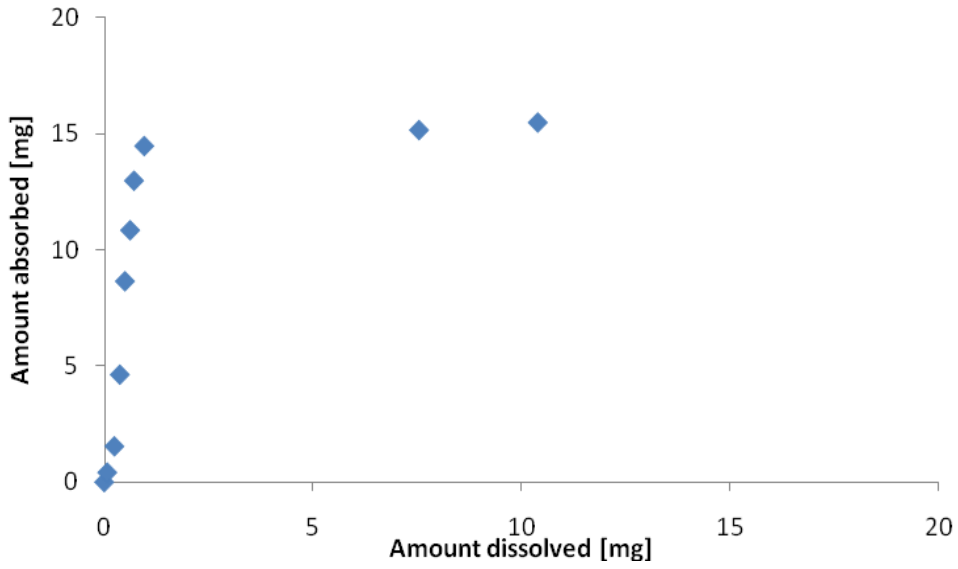

Figure 95. Mean i*n vivo* amount absorbed *versus in vitro* amount dissolved for Indocid® IR capsules.

Using dissolution profiles from the part of profile that was performed using simulated intestinal media resulted in non-linear correlation (R^2 0.73 – 0.91) indicating that dissolution occurred faster than absorption (Figure 96).

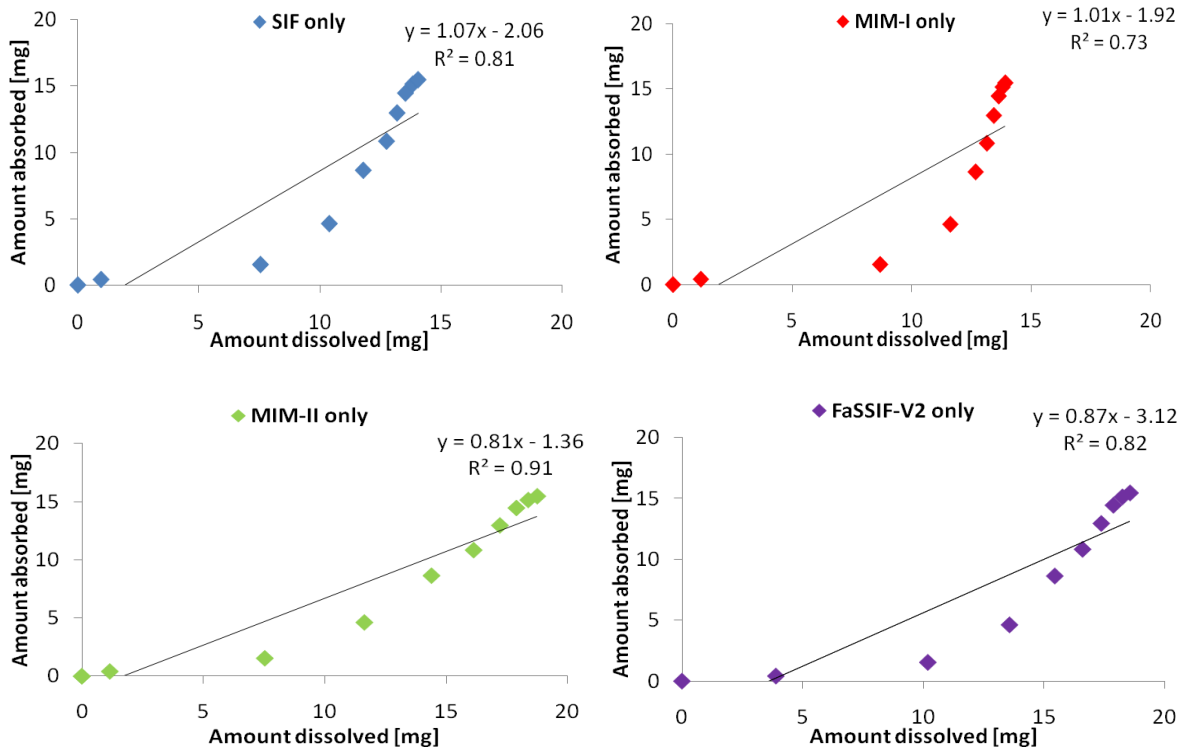

Figure 96. Level A IVIVC using dissolution data simulating only intestinal conditions using USP apparatus 4.

As IND absorbed faster than dissolved, thus time scaling using Levy's plot was applied (Figure 96).

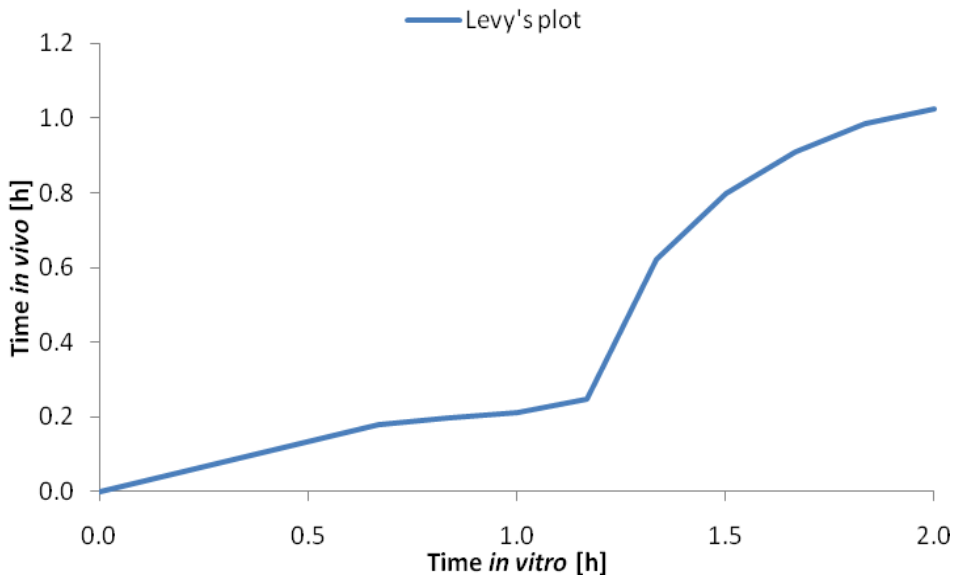

Figure 97. Levy's plot.

Levy's plot was not a straight line thus the scaling factor was not clearly calculated; however, observed rupture in the Levy's plot denotes at which time the *in vitro* and *in vivo* processes

diverged (Figure 97). At the turning point, amount absorbed at 0.25 hour (15 min) corresponds to amount dissolved at 1.17 h (70 minutes). The time 0.25 hour indicates the time shifting required for development of linear correlation. Since, minimal dissolution (3%) of IND was observed up to the first hour, the *in vitro* data were handled in order to mimic the dissolution experiment with media change occuring at an earlier time point than the one hour performed (Figure 98). The *in vitro* dissolution data for Indocid® capsules tested in various media using USP apparatus 4, where shifted this way to simulate media change occuring at 20 minutes. The shifted profiles were then correlated with amount absorbed *in vivo* (Figure 98).

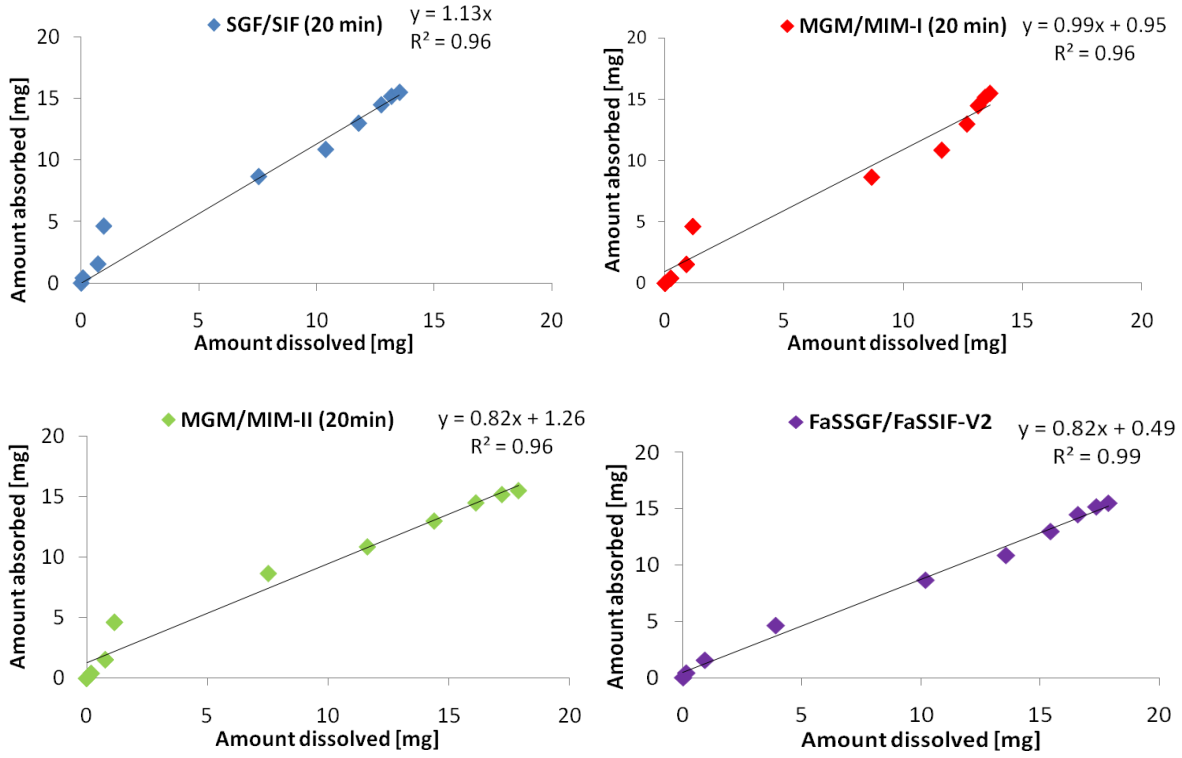

Figure 98. Level A IVIVC using time scaled dissolution data at 20 min in all media using USP apparatus 4.

For all correlations, the extent of fit (R^2) of linear regression is in the range of 0.96 – 0.99 which indicates that very good correlations were made. According to the R^2 values, dissolution data in biorelevant media tested using USP apparatus 4 provided the best IVIVC correlations. Time scaling that was applied highlights the fact that more attention should be paid to parameters such as GE time and media change as they may have crucial impact on the quality of IVIVC obtained.

6.2.2 PBPK modelling

6.2.2.1 IR formulation (25 mg Indocid® capsules)

Physiological, physicochemical, pharmacokinetic and formulation parameters of Indocid® (IND) were inserted into the Simcyp® software. The ability of Simcyp® software to predict dissolution data using solubility and particle size data was investigated. The dissolution data were predicted using the Wang-Flanagan (WF) equation. The predicted dissolution profiles were then used for the prediction of Indocid® *in vivo* performance (Figure 99). When the Wang-Flanagan equation was used to predict *in vivo* behaviour of IND, it was found that gastric emptying (GE) time became a crucial parameter. Initially, GE time was set up at 1 hour, in accordance with a change of media during dissolution experiments using USP apparatus 4. The commercial formulation of Indomethacin, Indocid®, is available in a capsule form. According to Kaus *et al*. gastric emptying time of Perspex non-disintegrating radiolabelled capsules ranges between 15-197 min, and strongly depends on the migrating motor complex (MMC) (333). Simulation with GE time at 1 h resulted in a lower C_{max} and delayed T_{max} (Figure 99). GE time in Simcyp® software is set to 20 minutes (0.4 h) as a default value; therefore, attempts at simulation using a shorter GE time was made. The predicted profile with GE time set up to 0.4 hour provided better similarity (f_1: 22.86) to the observed data than that with GE occurring at 1 hour (Table 79). As can be seen from Figure 99, simulations resulted in a closer C_{max} value and T_{max} was reached faster. Thus for further predictions GE time was set to 0.4 hour default value in Simcyp® software

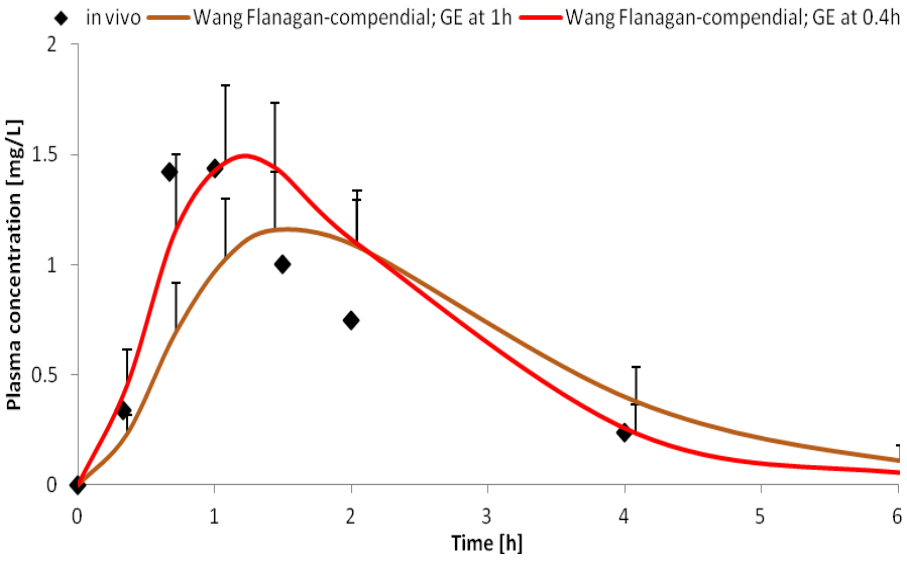

Figure 99. Mean (+ SD) simulated plasma concentration time profiles of PBPK Indocid® model using predicted dissolution profile obtained by the Wang-Flanagan equation. [*in vivo* data extracted from Yeh *et al*. 1982 (285)]

Table 79. Indices for a PBPK Indocid® model using predicted dissolution profiles obtained by the Wang-Flanagan equation at different GE time.

	f_1 (*in vivo* data as reference)
WF – compendial – GE at 0.4 h	22.86
WF – compendial – GE at 1 h	36.20

According to Figure 100, when the Wang-Flanagan approach was supported with solubility values of IND in compendial and biorelevant media, the simulated profile similar to the observed *in vivo* data (Table 80) and no difference was observed between the two simulated profiles (f_1: 0.03). The slight insignificant decrease was probably due to some discrepancies in solubility of IND in these two types of media. This model predicted better absorption phase than distribution and elimination phases. More care should be taken when selecting distribution and clearance parameters for a PBPK model development of IND.

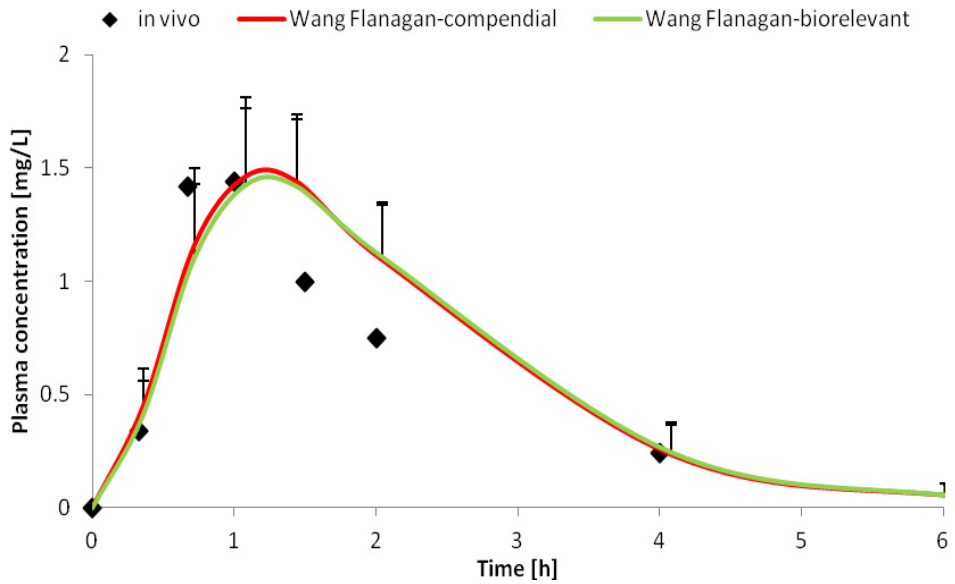

Figure 100. Mean (+ SD) simulated plasma concentration time profiles of PBPK Indocid® model using predicted dissolution profile obtained by the Wang-Flanagan equation. [*in vivo* data extracted from Yeh *et al.* 1982 (285)]

Table 80. Indices for a PBPK Indocid® model using predicted dissolution profiles obtained by the Wang-Flanagan equation.

	f_1 (*in vivo* data as reference)
WF - compendial	22.86
WF - biorelevant	22.83

According to the literature, the absorption of IND following oral administration is fast and complete. The successful PBPK model resulted in an average of 100 % IND absorption, which is in agreement with reported values from the literature (Figure 101). IND was absorbed within 3 hours of oral administration. The absorption constant of k_a 0.97 h^{-1} was estimated using first-order kinetics.

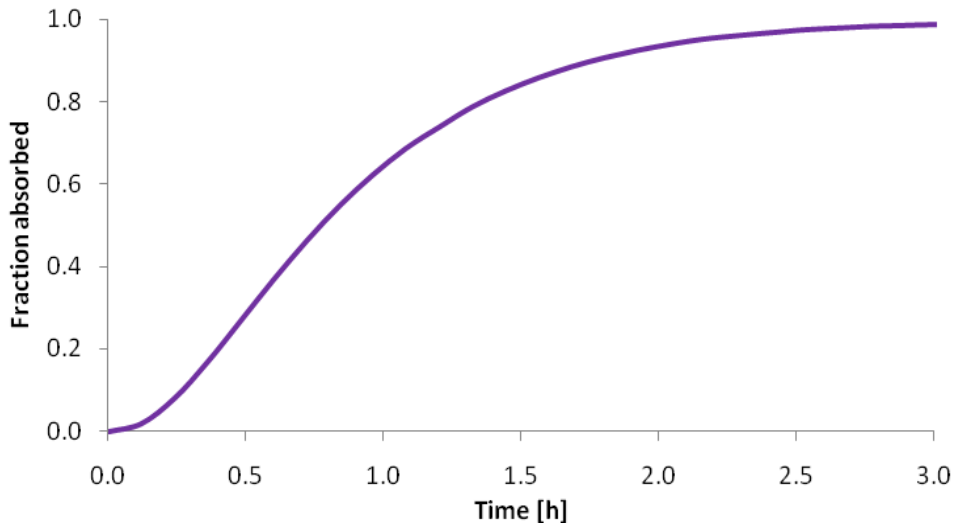

Figure 101. Mean predicted cumulative fraction of IND absorbed from Indocid® IR capsules predicted using predicted dissolution data using the Wang-Flanagan equation.

According to predicted regional fraction absorbed presented in Figure 102, a quarter of the dose was absorbed in duodenum, and around 64 % of the IND dose was absorbed in both compartments of the jejunum. A smaller fraction of the drug was absorbed in the duodenum than in the jejunum due to relatively short transit times, which are 14 and 71 minutes, respectively (174).

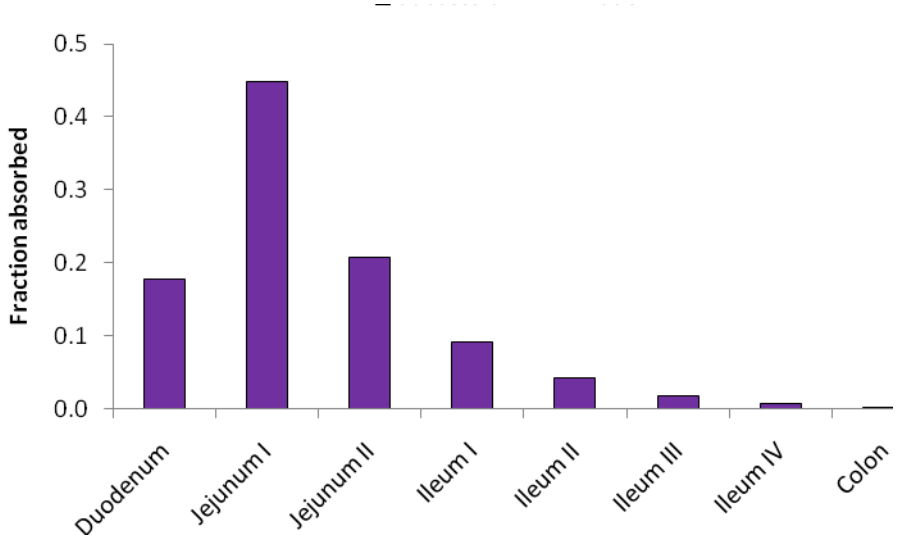

Figure 102. Mean predicted regional distribution of the fraction of the IND dose absorbed from 25 mg Indocid® IR formulation.

Despite small discrepancies between T_{max} and AUC values of predicted and observed data; it seems that point-to-point Level A IVIVC was developed with the PBPK model using predicted dissolution data.

Furthermore, the ability of Simcyp® software to predict dissolution data using raw dissolution data was investigated (Figure 103). All simulations using dissolution data tested using USP apparatus 1 were under-predicted. However, simulations using dissolution profiles in SIF resulted in better predictions than when both media SGF and SIF were considered. Indomethacin is a weak acid (pKa 4.3) which characterises low solubility in an acidic environment and high solubility in a basic environment. This trend was also present when data from USP apparatus 4 were used (Figure 104). Simulated C_{max} and AUC were significantly lower and T_{max} had delayed onset. The attempt of simulating *in vivo* profiles using only data extracted from intestinal part of the USP apparatus 4 was made (data not shown). The simulated profiles were improved in comparison to those profiles presented in Figure 104; however, they were still under-predicted.

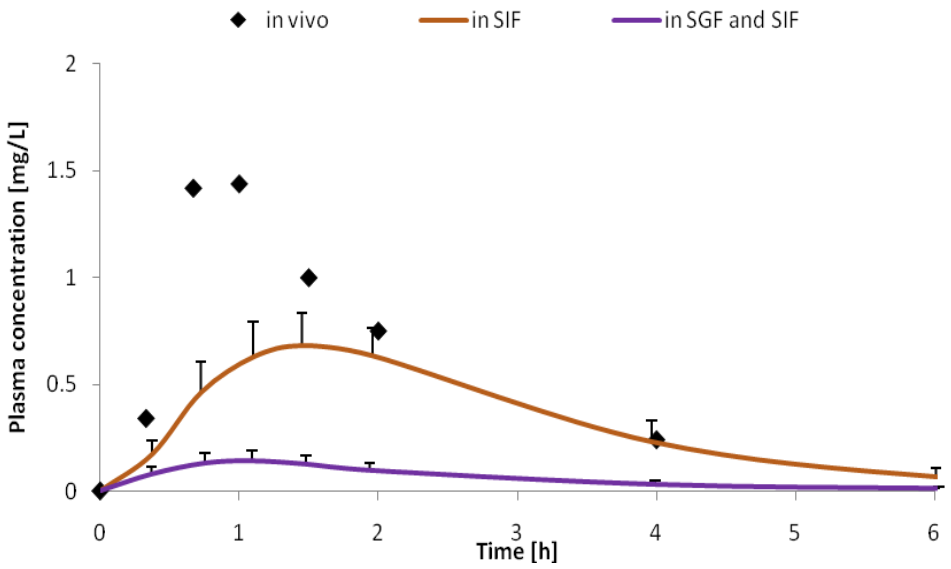

Figure 103. Mean (+ SD) simulated plasma concentration time profiles of PBPK Indocid® model using dissolution profiles tested in USP apparatus 1.

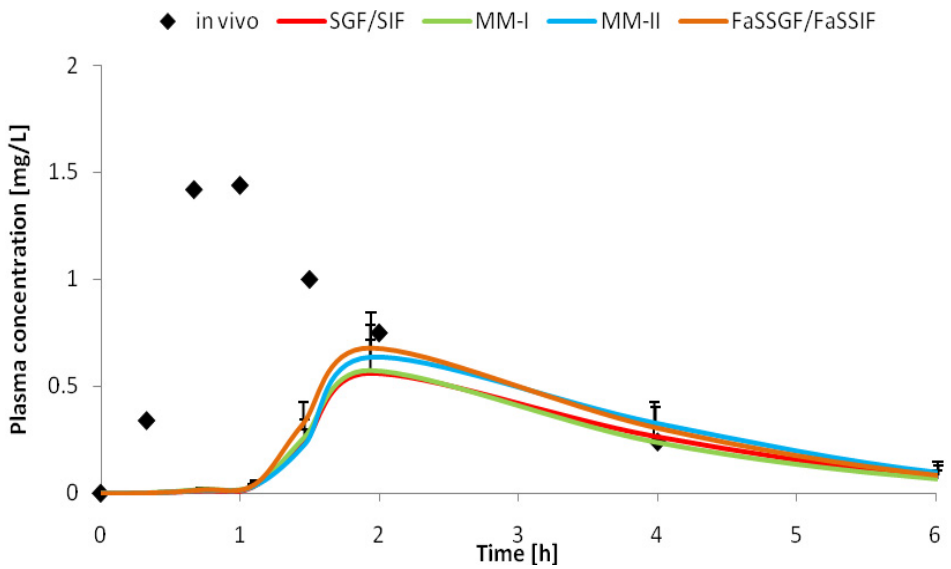

Figure 104. Mean (+ SD) simulated plasma concentration time profiles of PBPK Indocid® model using dissolution profiles tested in USP apparatus 4.

It was not possible to develop IVIVC for Indocid® capsules using PBPK model developed with raw dissolution data. This could be due to the fact that *in vivo* precipitation was not adequately characterised by the in vitro experiment. WF approach at least simulated absorption phase of IND from Indocid® capsules. Also, Indocid® capsules were withdrawn

from many countries including the UK. Therefore, availability of other than 25 mg Indocid® capsules formulations was restricted.

6.2.3 Sensitivity analysis

Sensitivity analysis was performed for three types of parameters. The first group was related to absorption process and included parameters such as solubility, particle size, *logP* and apparent permeability coefficient. P_{app} value was selected for sensitivity studies due to absence of *in vivo* human jejunal permeability data. Therefore, P_{eff} value was predicted using apparent permeability coefficient obtained from Caco-2 *in vitro* experiment. The second group consisted of parameters that describe the distribution of drug in the human body such as volume of distribution (V_d) and clearance after oral administration (CL_{po}). The third group related to physiological parameters, such as gastric emptying time that is a crucial parameter especially for ionisable drugs. Increasing or decreasing solubility by 10 fold will not affect the *AUC* (Table 81). Decreased solubility resulted in a lower C_{max} value. Interestingly, improving solubility of IND would result in similar *in vivo* performance when micronising the drug to a tenth of the size. On the other hand, decreasing solubility (by 10 fold) would result in similar *in vivo* performance to that when larger particles would be tested. Lipophilicity of the IND was insensitive to any changes (Figure 105). Also, apparent permeability coefficient was not sensitive to any alterations in the tested range 210 - 300 x 10^{-6} cm/s.

Table 81. Sensitivity analysis of absorption related parameters of Indocid® IR PBPK model.

	***AUC* [mg*h/L]**	**C_{max} [mg/mL]**	**T_{max} [h]**
Control	3.66	1.52	1.09
Solubility x10	3.63	1.45	1.23
Solubility / 10	3.63	1.32	1.32
PS x10	3.62	1.36	1.32
PS / 10	3.63	1.45	1.22

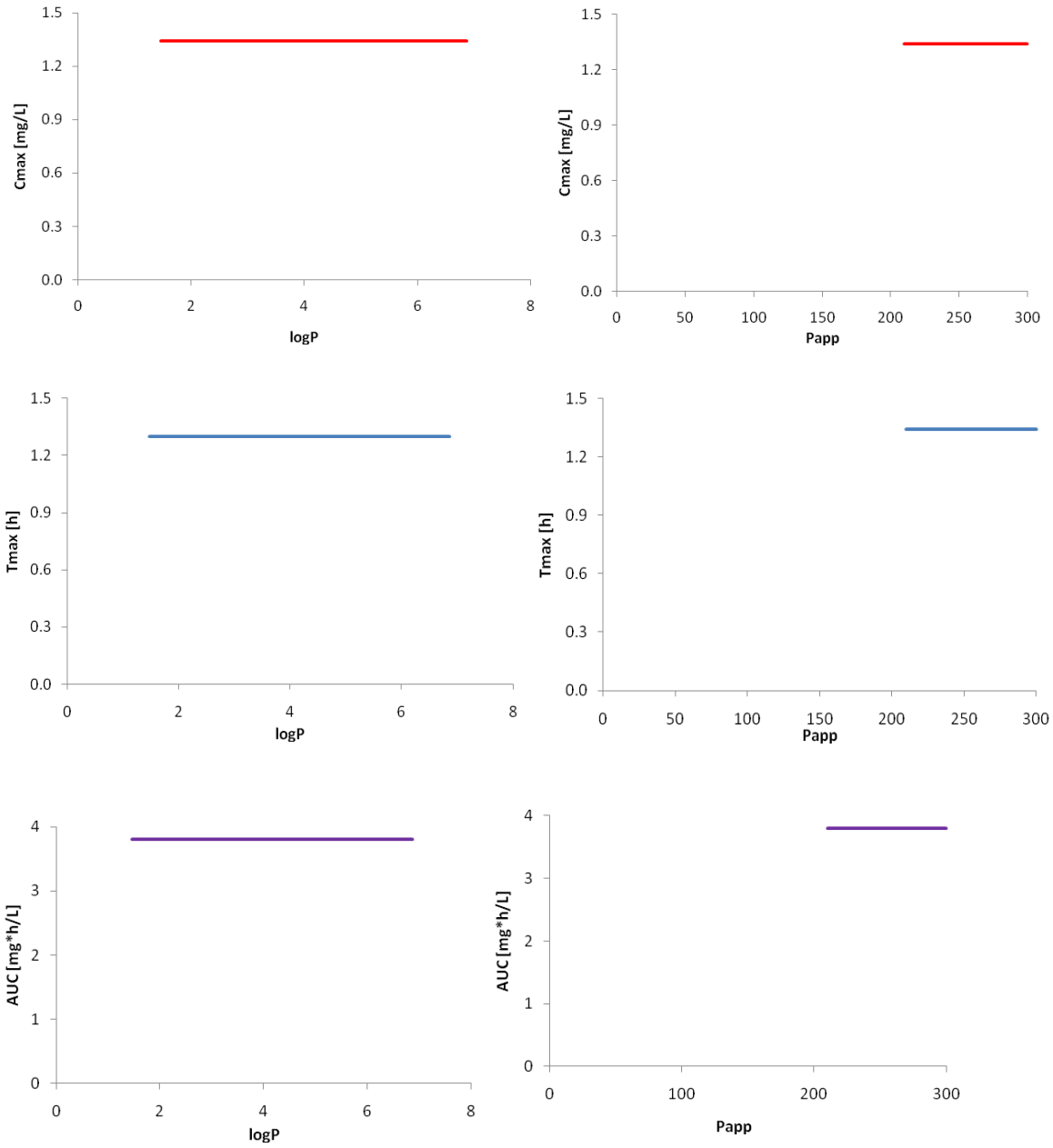

Figure 105. Sensitivity analysis of absorption parameters: *log P* (unitless) and P_{app} (x10^{-6} cm/s).

Likewise, in the case of the PBPK model for Tegretol®, clearance and volume of distribution affected the model the most. Higher clearance resulted in lower C_{max}, T_{max} and AUC values (Figure 106). The volume of distribution did not affect AUC, but had impact on T_{max} and C_{max}. Failure of predicting well IND distribution and elimination phases during WF approach could be due to inappropriate selection of clearance and volume of distribution parameters.

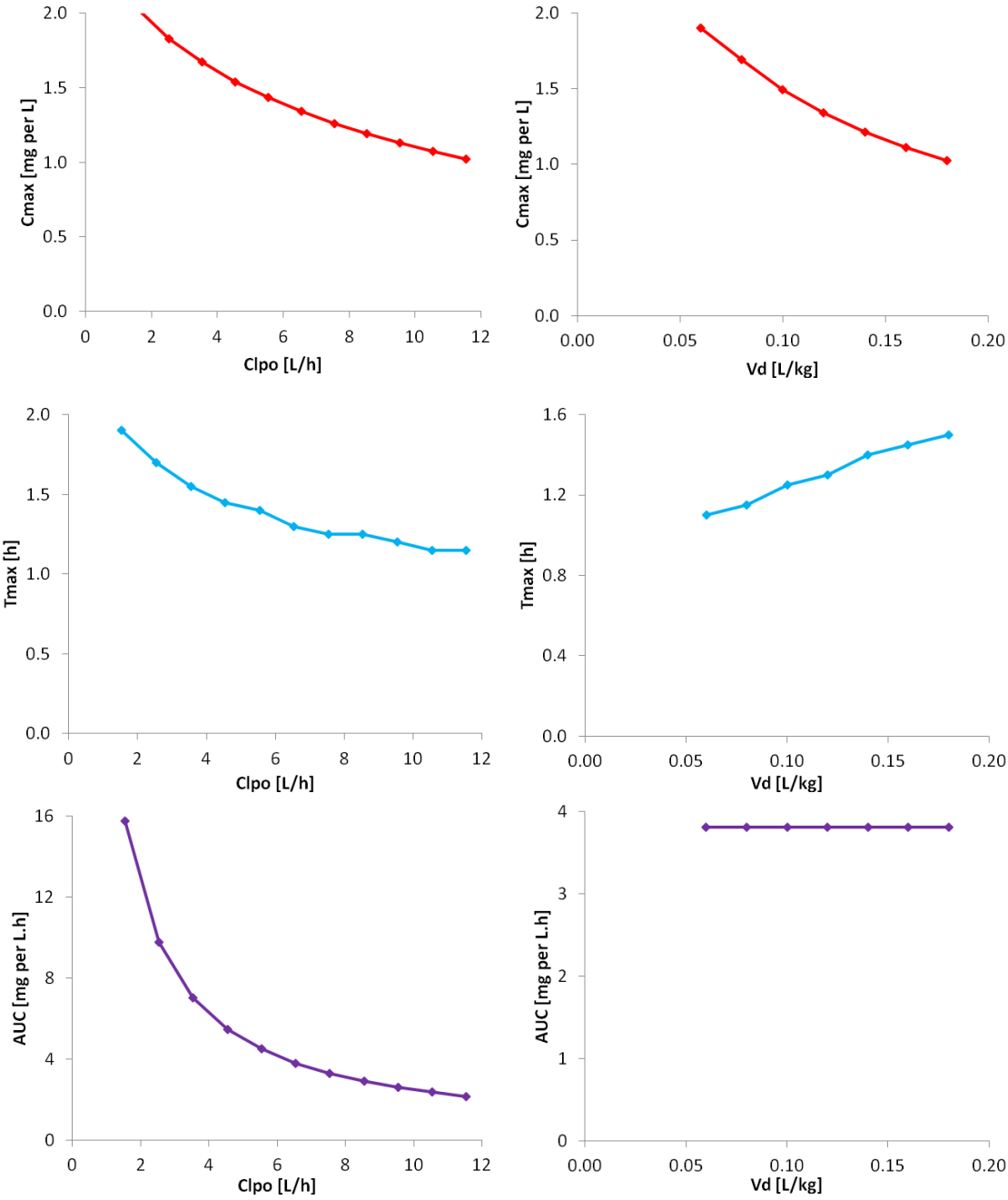

Figure 106. Sensitivity analysis of distribution parameters.

In the case, when ionisable compounds are subject to *in vivo* performance, changing of the pH in the GI environment will be one of the most important parameters that may define the overall performance. GE time does not have any influence on the *AUC*, but the faster the GE, the higher C_{max} can be reached within a shorter time (Figure 107).

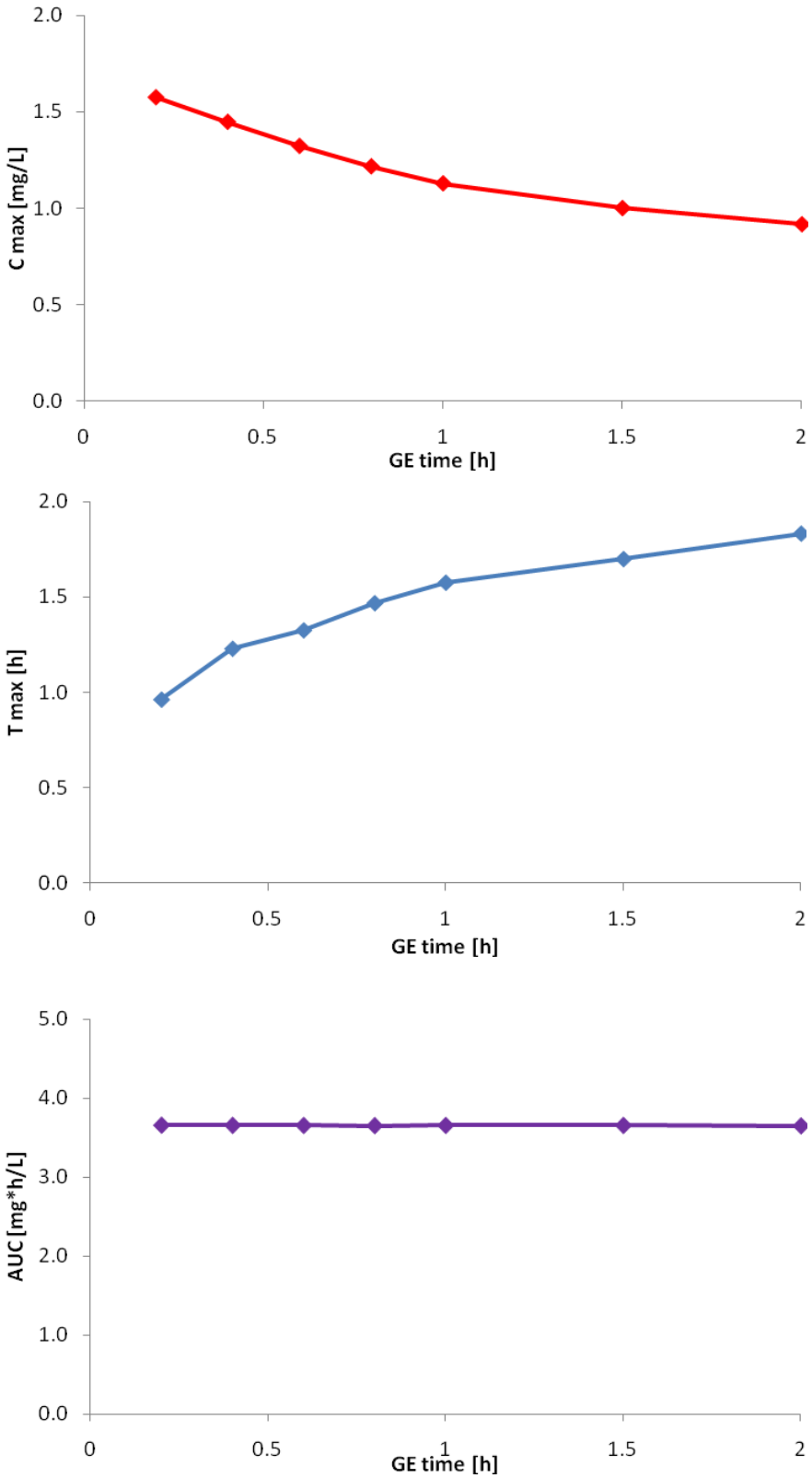

Figure 107. Sensitivity analysis of physiological parameters.

7 Predictions of absorption of cocrystals

7.1 Carbamazepine case

Tegretol® PBPK models were used to predict absorption of cocrystals based on their dissolution data. Both models were developed for commercial formulations which contained various excipients that aid dissolution. Thus, in order to avoid misleading interpretations, the CBZ_{sp} profile in biorelevant media was used as the control.

It was found that overall bioavailability of CBZ from CBZ cocrystals did not increase dramatically. An overall 2 % increment was observed when compared against the CBZ_{sp} sample (Table 83). However, the rate of absorption for CBZ-SAC_{ss} samples was significantly faster (f_1: 15.47) than the rate of CBZ_{sp} absorption (Table 82). This was confirmed by a higher value of the absorption constant (k_a: 0.26) for CBZ-SAC_{ss} when compared to that of the CBZ_{sp} control profile (k_a: 0.16). Further comparison of fraction absorbed in individual GI segments was performed (Figure 109). Both CBZ-SAC cocrystals ($_{ss}$ and $_{umax}$) absorbed larger fractions of the dose in the first three segments of the GI tract responsible for absorption (duodenum, jejunum I and jejunum II) when compared with the CBZ_{sp} performance. However, this resulted in a lower fraction of the dose absorbed in the colon. Hence, overall absorption did not increase significantly.

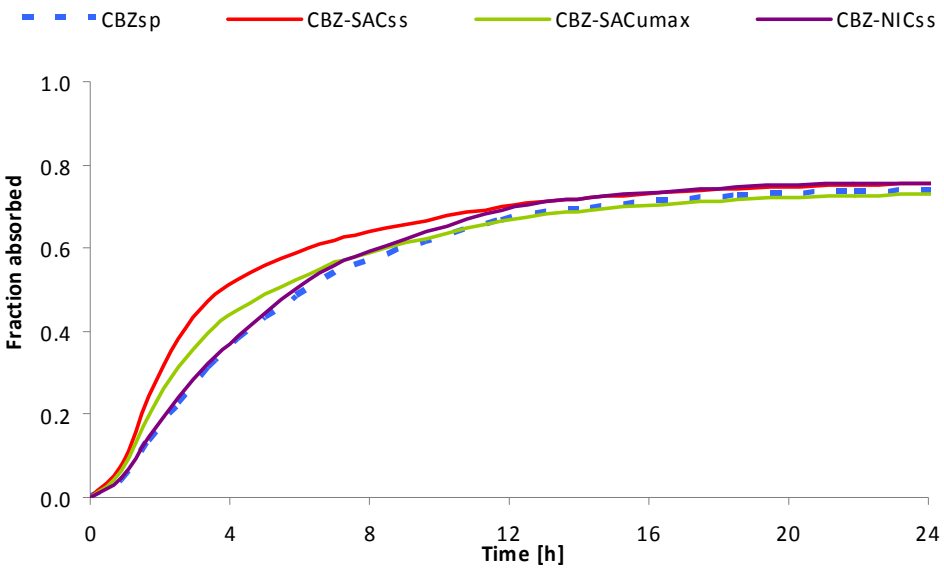

Figure 108. Mean predicted cumulative fraction of CBZ absorbed from different formulations.

Table 82. Summary of f_1 valuescomparing fraction absorbed of CBZ from different CBZ formulations.

Formulations	f_1 CBZ_{sp} (as a reference)
CBZ-SAC_{ss}	15.47
CBZ-SAC_{umax}	7.18
CBZ-NIC_{ss}	3.31

Table 83. Absorption constants (k_a) and overall *in vivo* absorption for different CBZ formulations.

Formulations	Absorption constant k_a [h^{-1}]	Absorption [%]
CBZ_{sp}	0.16	74
CBZ-SAC_{ss}	0.26	76
CBZ-SAC_{umax}	0.21	73
CBZ-NIC_{ss}	0.16	76

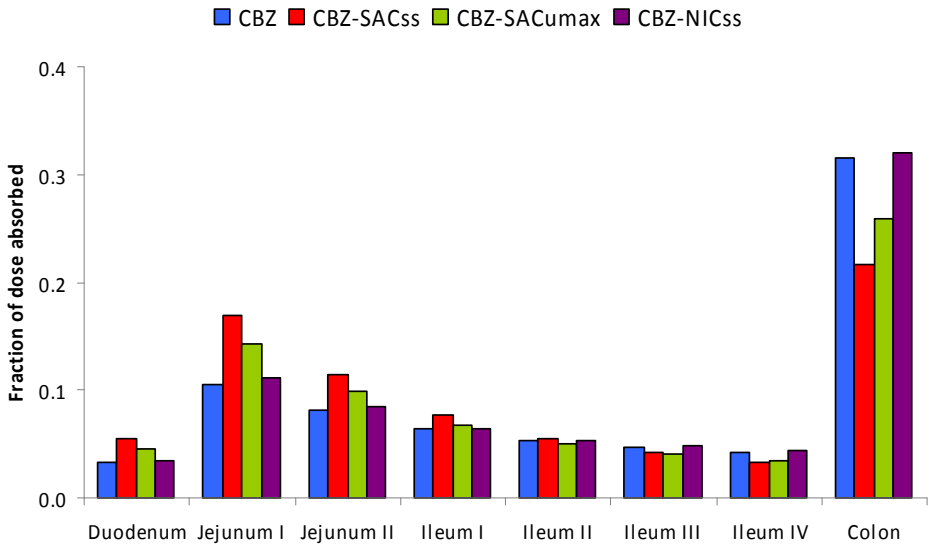

Figure 109. Mean predicted regional distribution of the fraction of the CBZ dose absorbed for different CBZ formulations.

7.2 Indomethacin case

All formulations of IND completely absorbed within 3 hours, and IND-NIC_{ss} cocrystal absorbed slightly faster than the others (Table 85). % absorbed of IND from IND-NIC_{ss} cocrystal was 8% higher at 1 h in comparison to IND_{sp} (Figure 110). However, overall the improvement was not statistically significant ($f_1 \leq 4.72$) (Table 84).

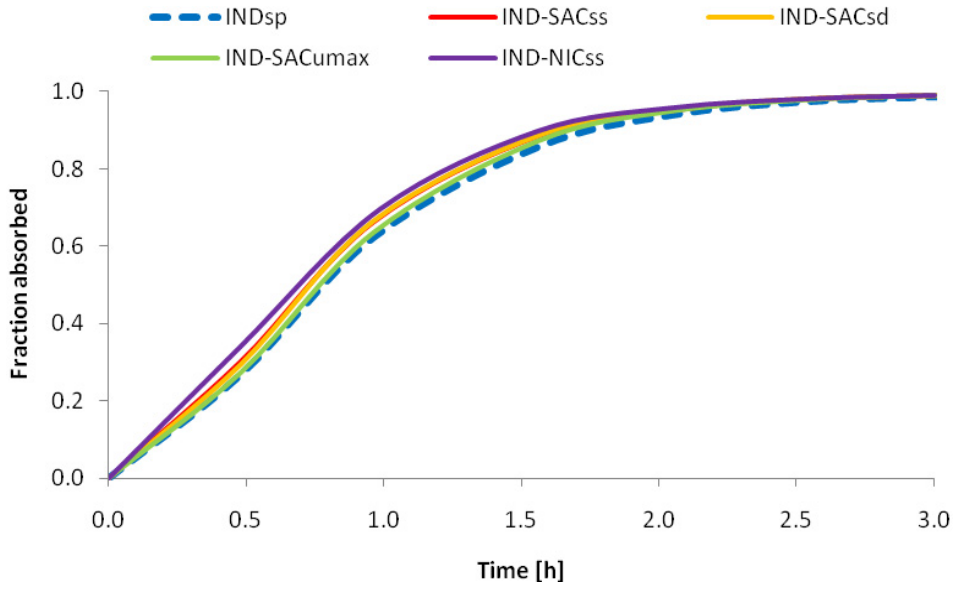

Figure 110. Mean predicted cumulative fraction absorbed of IND from different IND formulations.

Table 84. Summary of f_1 values comparing cumulative fraction absorbed of IND from different IND formulations.

Formulations	f_1 IND_{sp} (as a reference)
IND-SAC_{ss}	2.61
IND-SAC_{sd}	2.66
IND-SAC_{umax}	0.96
IND-NIC_{ss}	4.72

Table 85. Absorption constants (k_a) and overall *in vivo* absorption for different IND formulations.

Formulations	Absorption constant k_a [h^{-1}]	Absorption [%]
IND_{sp}	0.80	99
IND-SAC_{ss}	0.91	99
IND-SAC_{sd}	0.90	99
IND-SAC_{umax}	0.83	99
IND-NIC_{ss}	1.01	99

A similar trend was observed when fractions absorbed of the IND dose in different GI tract segments were compared. According to Figure 111, slightly larger fractions of the IND were absorbed from IND-NIC_{ss} in the duodenum when compared with IND formulation. Around 70 % of the dose was absorbed in the jejunum segment.

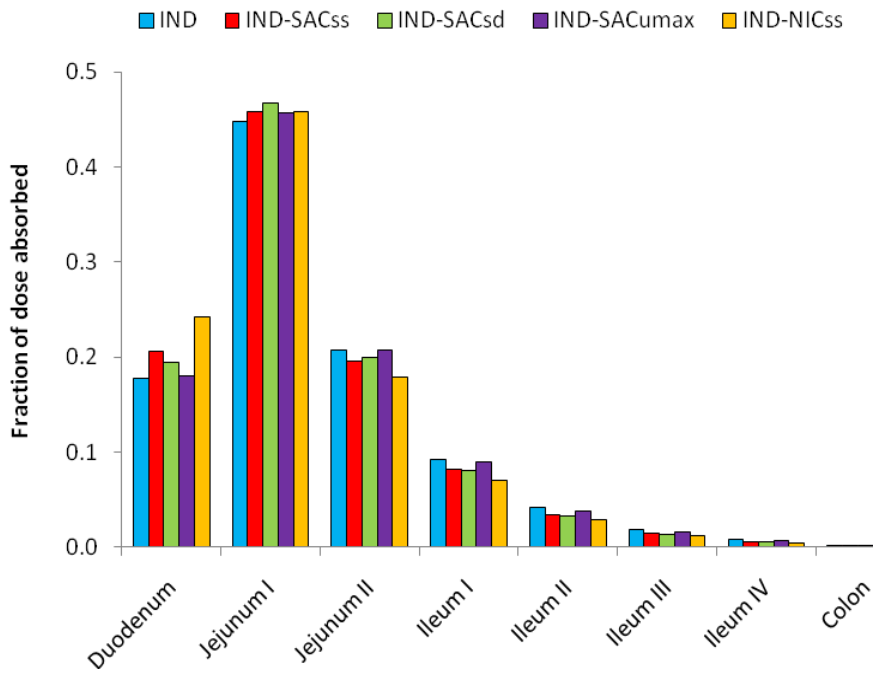

Figure 111. Mean predicted regional distribution of the fraction of the IND dose absorbed for different IND formulations.

8 Conclusions and future work

Conventional dissolution apparatus (USP apparatus 1) was not adequate to characterise *in vitro* performance of poorly soluble drugs. In the case of Tegretol® tablets, sink conditions were not provided, resulting in dissolving only 50 % of the formulation. Whereas, in the case of pH-dependent solubility IND compound present in Indocid® capsules, around 3 % of the IND dissolved in gastric conditions. Rapid dissolution of this formulation within five minutes occurred in SIF (pH 6.8). This method was unable to characterise dissolution of cocrystals.

Flow-through cell dissolution (USP apparatus 4) provides infinite sink conditions and allowed the change of media, which helped to mimic the *in vivo* environments closely. USP apparatus 4 allowed discrimination between performances in different media. Dissolution of Tegretol® tablets in biorelevant media resulted in the greatest enhancement by 1.5 fold due to the presence of bile salts. SAC cocrystals of CBZ significantly improved dissolution of poorly soluble CBZ. SAC cocrystals made by sonic-slurrying method resulted in two - fold higher dissolution than cocrystals made using UMAX technology when compared against dissolution of CBZ_{sp} samples.

Moreover, it was found that physical blends of CBZ and SAC (CBZ--SAC) significantly enhanced dissolution of CBZ. Statistical analysis between blend (CBZ--SAC) and cocrystals indicated that only dissolution performance of cocrystal made by sonic-slurrying proved to make a complex compound that enhanced dissolution better than the physical blends of the two components. Further investigation showed that SAC from CBZ-SAC_{ss} cocrystal was dissolving at a slower rate than SAC from the physical blend, despite the fact that both SAC dissolved within the first 90 minutes of the experiment. It was hypothesised that upon contact with water, weak hydrogen bonds between hydrophobic CBZ and the highly soluble coformer SAC immediately broke down. The SAC from the cocrystal was available for water to dissolve and thus allowing water to penetrate between poorly soluble CBZ at the same time, leading to dissolution enhancement of CBZ. The findings that the same ratio of API and coformer (depending if formed as cocrystal or physical blend) can lead to different dissolution performance led to the conclusion that crystal packing and arrangement in these two formulations are different and thus packing and arrangement play an important role in enhancement of dissolution by cocrystals. In order to fully understand and confirm the hypothesis of packing and arrangements in cocrystals, further examination of these cocrystals may be beneficial such as single X-ray diffraction, nuclear magnetic resonance (NMR), or

thermogravimetric analysis (TGA). Also, it may be interesting to investigate in future studies the effect of micelles on the dissolution of SAC itself, in order to gain understanding of whether the dissolution enhancement is due to solubilisation of an API or SAC or both components together.

Interestingly, NIC cocrystals of CBZ did not demonstrate any dissolution enhancement. Two observations could aid the understanding of this behaviour. Firstly, the dose of IND (25 mg) is eight times smaller than that of CBZ (200 mg). Thus, amounts of NIC in CBZ-NIC_{ss} cocrystal may not be sufficient to impact its dissolution. Secondly, according to Hörter and Dressman, for compounds with high *logP*, solubilisation is the predominant mechanism (IND *logP* 4.27), whereas for compounds with lower *logP* (CBZ 2.45) wettability is the mechanism which accounts for enhancement of powder dissolution rate (324). It seems that it was easier to solubilise small amounts of IND than wet large amounts of CBZ.

In the case of Indomethacin and its cocrystals, USP apparatus 4 allowed quantification of the precipitation of the samples upon the media change. This phenomenon is known to occur *in vivo*; however its process is not fully understood yet. It has been observed that biorelevant media resulted in the smallest fraction of the dose precipitating, whereas compendial media led to the greatest fraction of IND precipitated in all formulations (control, commercial and cocrystal formulations). This could be explained by the fact that bile salts present in biorelevant media inhibited precipitation of IND. Overall, the largest fraction of the Indocid® dose precipitated across all investigated media, whereas the smallest fraction of dose precipitated form IND_{sp} formulations. This led to the conclusion that excipients and coformers present in Indocid® formulations contributed to the extent of precipitation.

Among SAC cocrystals, those made by UMAX technology provided the greatest enhancement of dissolution rate. Moreover, the dissolution profile of the physical blend was significantly slower than IND-SAC cocrystals but slightly faster than dissolution of IND_{sp} samples**.** Both, SAC and NIC cocrystals made by sonic-slurrying demonstrated to significantly enhance the dissolution of IND. Nicotinamide cocrystal of IND improves dissolution of IND greater than Saccharin cocrystal. Also, the dissolution profile of the physical blend of IND and NIC was significantly slower than IND-NIC_{ss} but significantly faster than dissolution of IND_{sp} samples. Further investigation of the dissolution mechanism of NIC from cocrystal and physical blend revealed that NIC from both the cocrystal and the physical blend dissolved within the first 30 minutes. This led to the conclusion that it might

be the packing and arrangement of the NIC and IND in both physical blend and cocrystal that plays an important role in the enhancement of dissolution of IND.

Successful IVIVC for Tegretol® tablets and Indocid® capsules were established using both traditional and PBPK approaches. Successful point-to-point Level A IVIVC for IR Tegretol® tablets was obtained using *in vitro* dissolution data tested in biorelevant media using USP apparatus 4. Also, dissolution data of PR Tegretol® tablets in biorelevant media (FaSSGF/FaSSIF-V2/FaSSCoF) allowed development of 1:1 *in vitro – in vivo* correlations. Successful point-to-point Level A IVIVC for Indocid® capsules was developed using numerical deconvolution method. Dissolution profiles obtained by testing formulations in biorelevant media using USP apparatus 4 provided the best IVIVC correlations. Development involved time scaling using Levy's plot technique.

Successful PBPK models were developed for IR and PR formulations of Tegretol® tablets using dissolution data (USP apparatus 4) tested in biorelevant media. The simulations using predicted dissolution profiles using the Wang-Flanagan equation were overestimated when compared against *in vivo* observed data. The reason for overestimation could be attributed to the limitations of Wang-Flanagan approach, which do not consider formulation properties. Also, inadequately measured values of particle size of CBZ could led to over-prediction. It seems that the particle size of CBZ in Tegretol® tablets is much larger than that measured using laser diffraction. Sonication process that samples were exposed to could break down the primary particle size further.

When the Wang Flanagan equation was used to predict *in vivo* behaviour of Indocid® capsules, it was found that gastric emptying (GE) time became a crucial parameter. This is expected for ionisable compounds. The predicted profile with GE time set up to 0.4 hour was more similar to the observed data than that with GE occurring at 1 hour. When the Wang-Flanagan approach was supported with solubility values of IND in biorelevant media, the profiles were similar to when using compendial media. On the other hand, it was not possible to develop IVIVC for Indocid® capsules using the PBPK model developed with raw dissolution data. Several factors affect the absorption modelling, it seems that not all of them were investigated.

Development of the PBPK model for the neutral compound, CBZ was possible using raw dissolution data tested in biorelevant media using USP apparatus 4. Unfortunately, this was not the case when pH-solubility dependent drug, Indomethacin was investigated. In the case

of this compound, prediction using the Wang-Flanagan equation was able to predict absorption phase successfully.

The successfully developed PBPK models were used further to predict *in vivo* performance of pharmaceutical cocrystals. It was found that predicted cumulative fraction absorbed of CBZ from CBZ cocrystals did not increase dramatically. An overall 2 % increment was observed when compared against the CBZ_{sp} sample. The rate of absorption for CBZ-SAC_{ss} samples was significantly faster than the rate of CBZ_{sp} absorption. Among IND cocrystals, IND-NIC_{ss} cocrystal was predicted to absorb slightly faster than other IND-SAC cocrystals. Predicted cumulative fraction absorbed of IND-NIC_{ss} was 8% higher at 1 h in comparison to IND_{sp}. Overall the improvement was not statistically significant.

References

1. G.L. Amidon, H. Lennernas, V.P. Shah, and J.R. Crison. A theoretical basis for a biopharmaceutic drug classification: the correlation of in vitro drug product dissolution and in vivo bioavailability. Pharm. Res. 12: 413-420 (1995).

2. T. Takagi, C. Ramachandran, M. Bermejo, S. Yamashita, L.X. Yu, and G.L. Amidon. A provisional biopharmaceutical classification of the top 200 oral drug products in the United States, Great Britain, Spain, and Japan, Mol. Pharm. 3: 631 (2006).

3. D.J. Good and N. Rodríguez-Hornedo. Solubility advantage of pharmaceutical cocrystals. Cryst. Growth Des. 9: 2252-2264 (2009).

4. N. Blagden, M. de Matas, P.T. Gavan, and P. York. Crystal engineering of active pharmaceutical ingredients to improve solubility and dissolution rates. Adv. Drug Del. Rev. 59: 617-630 (2007).

5. P. Kahela, R. Aaltonen, E. Lewing, M. Anttila, and E. Kristoffersson. Pharmacokinetics and dissolution of two crystalline forms of carbamazepine. Int. J. Pharm. 14: 103-112 (1983).

6. A. Ainouz, J.R. Authelin, P. Billot, and H. Lieberman. Modeling and prediction of cocrystal phase diagrams. Int. J. Pharm. 374: 82-89 (2009).

7. F. Wöhler. Justus Lieb Ann Chem. 51: 153 (1844).

8. J.D. Dunitz. Crystal and co-crystal: a second opinion. Cryst. Eng. Comm. 5: 506 (2003).

9. G.R. Desiraju. Crystal and co-crystal. Cryst. Eng. Comm. 5: 466-467 (2003).

10. A.D. Bond. What is a co-crystal? Cryst. Eng. Comm. 9: 833-834 (2007).

11. C.B. Aakeröy, M.E. Fasulo, and J. Desper. Cocrystal or salt: Does it really matter? Mol. Pharm. 4: 317-322 (2007).

12. Ö. Almarsson and M.J. Zaworotko. Crystal engineering of the composition of pharmaceutical phases. Do pharmaceutical co-crystals represent a new path to improved medicines? Chem. Commun. 7: 1889-1896 (2004).

13. S.L. Childs, L.J. Chyall, J.T. Dunlap, V.N. Smolenskaya, B.C. Stahly, and G.P. Stahly. Crystal engineering approach to forming cocrystals of amine hydrochlorides with organic acids. Molecular complexes of fluoxetine hydrochloride with benzoic, succinic, and fumaric acids. J. Am. Chem. Soc. 126: 13335-13342 (2004).

14. S.L. Childs, G.P. Stahly, and A. Park. The salt−cocrystal continuum: The influence of crystal structure on ionization state. Mol. Pharm. 4: 323-338 (2007).

15. P. Vishweshwar, J.A. McMahon, J.A. Bis, and M.J. Zaworotko. Pharmaceutical cocrystals. J. Pharm. Sci. 95: 499-516 (2006).

16. K.G. Wilson. Columbia Guide to Standard American English, MJF Books, 1998.

17. C.B. Aakeröy and D.J. Salmon. Building co-crystals with molecular sense and supramolecular sensibility. Cryst. Eng. Comm. 7: 439-448 (2005).

18. F. Lara-Ochoa and G. Espinosa-Pérez. Cocrystals definitions. Supramol. Chem. 19: 553-557 (2007).

19. Z. Li, B.-S. Yang, M. Jiang, M. Eriksson, E. Spinelli, N. Yee, and C. Senanayake. A practical solid form screen approach to identify a pharmaceutical glutaric acid cocrystal for development. Org. Proc. Res. Dev. 13: 1307-1314 (2009).

20. S. Goyal, M.R. Thorson, G.G.Z. Zhang, Y. Gong, and P.J.A. Kenis. Microfluidic approach to cocrystal screening of pharmaceutical parent compounds. Cryst. Growth Des. 12: 6023-6034 (2012).

21. J.H. ter Horst, M.A. Deij, and P.W. Cains. Discovering new co-crystals. Cryst. Growth Des. 9: 1531-1537 (2009).

22. G. He, C. Jacob, L. Guo, P.S. Chow, and R.B.H. Tan. Screening for cocrystallisation tendency: The role of intermolecular interactions. J. Phys. Chem. B. 112: 9890-9895 (2008).

23. A. Jayasankar, L. S. Reddy, S.J. Bethune and N. Rodríguez -Hornedo. Role of cocrystal and solution chemistry on the formation and stability of cocrystals with different stoichiometry. Cryst. Growth Des.. 9: 889-897 (2009).

24. H.M. Powell. The structure of molecular compounds. Part IV. Clathrate compounds. J Chem Soc: 61-73 (1948).

25. G.P. Stahly. Diversity in single- and multiple-component crystals. The search for and prevalence of polymorphs and cocrystals. Cryst. Growth Des. 7: 1007-1026 (2007).

26. N. Takata, K. Shiraki, R. Takano, Y. Hayashi, and K. Terada. Cocrystal screening of stanolone and mestanolone using slurry crystallization. Cryst. Growth Des. 8: 3032-3037 (2008).

27. FDA GRAS Notice Inventory; http://accessdata.fda.gov (Accessed 21/02/2013).

28. N. Blagden, D.J. Berry, A. Parkin, H. Javed, A. Ibrahim, P.T. Gavan, L.L. De Matos, and C.C. Seaton. Current directions in co-crystal growth. New J. Chem. 32: 1659-1672 (2008).

29. G.R. Desiraju. Supramolecular synthons in crystal engineering—A new organic synthesis. Angew. Chem. Int. Ed. Eng. 34: 2311-2327 (1995).

30. M.C. Etter. Encoding and decoding hydrogen-bond patterns of organic compounds. Acc. Chem. Res. 23: 120-126 (1990).

31. T.R. Shattock, K.K. Arora, P. Vishweshwar, and M.J. Zaworotko. Hierarchy of supramolecular synthons: Persistent carboxylic acid···pyridine hydrogen bonds in cocrystals that also contain a hydroxyl moiety. Cryst. Growth Des. 8: 4533-4545 (2008).
32. L.S. Reddy, N.J. Babu, and A. Nangia. Carboxamide-pyridine N-oxide heterosynthon for crystal engineering and pharmaceutical cocrystals. Chem. Comm. 1369-1371 (2006).
33. J.A. Bis and M.J. Zaworotko. The 2-Aminopyridinium-carboxylate supramolecular heterosynthon: A robust motif for generation of multiple-component crystals. Cryst. Growth Des. 5: 1169-1179 (2005).
34. S.L. Childs and M.J. Zaworotko. The reemergence of cocrystals: The crystal clear writing is on the wall introduction to virtual special issue on pharmaceutical cocrystals. Cryst. Growth & Des. 9: 4208-4211 (2009).
35. P.H. Stahl and C.G. Wermuth. Handbook of pharmaceutical salts: Properties, selection and use. (2002).
36. B.R. Bhogala, S. Basavoju, and A. Nangia. Tape and layer structures in cocrystals of some di- and tricarboxylic acids with 4,4[prime or minute]-bipyridines and isonicotinamide. From binary to ternary cocrystals. Cryst. Eng. Comm. 7: 551-562 (2005).
37. A.N. Sokolov, T. Friščić, and L.R. MacGillivray. Enforced face-to-face stacking of organic semiconductor building blocks within hydrogen-bonded molecular cocrystals. J. Am. Chem. Soc. 128: 2806-2807 (2006).
38. G.P. Stahly. A Survey of cocrystals reported prior to 2000. Cryst. Growth Des. 9: 4212-4229 (2009).
39. D. Braga, G. Palladino, M. Polito, K. Rubini, F. Grepioni, M.R. Chierotti, and R. Gobetto. Three polymorphic forms of the co-crystal 4,4'-bipyridine/pimelic acid and their structural, thermal, and spectroscopic characterization. Chem. 14: 10149- 10159 (2008).
40. A. Bak, A. Gore, E. Yanez, M. Stanton, S. Tufekcic, R. Syed, A. Akrami, M. Rose, S. Surapaneni, T. Bostick, A. King, S. Neervannan, D. Ostovic, and A. Koparkar. The co-crystal approach to improve the exposure of a water-insoluble compound: AMG 517 sorbic acid co-crystal characterization and pharmacokinetics. J. Pharm. Sci. 97: 3942-3956 (2008).
41. C.C. Seaton, A. Parkin, C.C. Wilson, and N. Blagden. Controlling the formation of benzoic acid: isonicotinamide molecular complexes. Cryst. Growth Des. 9: 47-56 (2009).
42. A. Jayasankar, D.J. Good, and N. Rodríguez-Hornedo. Mechanisms by which moisture generates cocrystals. Mol. Pharm. 4: 360-372 (2007).

43. A.V. Trask, W.D.S. Motherwell, and W. Jones. Pharmaceutical cocrystallization: Engineering a remedy for caffeine hydration. Cryst. Growth Des. 5: 1013 (2005).
44. Z.Q. Yu, P.S. Chow, and R.B.H. Tan. Operating regions in cooling cocrystallization of caffeine and glutaric acid in acetonitrile. Cryst. Growth Des. 10: 2382 (2010).
45. S.G. Fleischman, S.S. Kuduva, J.A. McMahon, B. Moulton, R.D. Bailey Walsh, N. Rodríguez-Hornedo, and M.J. Zaworotko. Crystal engineering of the composition of pharmaceutical phases: Multiple-component crystalline solids involving carbamazepine. Cryst. Growth Des. 3: 909-919 (2003).
46. M.B. Hickey, M.L. Peterson, L.A. Scoppettuolo, S.L. Morrisette, A. Vetter, H. Guzmán, J.F. Remenar, Z. Zhang, M.D. Tawa, S. Haley, M.J. Zaworotko, and Ö.Almarssön. Performance comparison of a co-crystal of carbamazepine with marketed product. Eur. J. Pharm. Biopharm. 67: 112-119 (2007).
47. K. Seefeldt, J. Miller, F. Alvarez-Núñez, and N. Rodríguez-Hornedo. Crystallization pathways and kinetics of carbamazepine–nicotinamide cocrystals from the amorphous state by in situ thermomicroscopy, spectroscopy, and calorimetry studies. J. Pharm. Sci. 96: 1147-1158 (2007).
48. J.F. Remenar, M.L. Peterson, P.W. Stephens, Z. Zhang, Y. Zimenkov, and M.B. Hickey. Celecoxib:nicotinamide dissociation: Using excipients to capture the cocrystal's potential. Mol. Pharm. 4: 386-400 (2007).
49. K. Shiraki, N. Takata, R. Takano, Y. Hayashi, and K. Terada. Dissolution improvement and the mechanism of the improvement from cocrystallization of poorly water-soluble compounds. Pharm. Res. 25: 2581-2592 (2008).
50. S. Basavoju, D. Boström, and S.P. Velaga. Indomethacin-saccharin cocrystal: design, synthesis and preliminary pharmaceutical characterization. Pharm. Res. 25: 530-541(2008).
51. A.V. Yadav, A.S. Shete, A.P. Dabke, P.V. Kulkarni, and S.S. Sakhare. Co-crystals: a novel approach to modify physicochemical properties of active pharmaceutical ingredients. Ind. J. Pharm. Sci. 71: 359-370 (2009).
52. B. Puschner, R.H. Poppenga, L.J. Lowenstine, M.S. Filigenzi, and P.A. Pesavento. Assessment of melamine and cyanuric acid toxicity in cats. J. Vet. Diagn. Invest. 19: 616-624 (2007).

53. A.M. Chen, M.E. Ellison, A. Peresypkin, R.M. Wenslow, N. Variankaval, C.G. Savarin, T.K. Natishan, D.J. Mathre, P.G. Dormer, D.H. Euler, R.G. Ball, Z. Ye, Y. Wang, and I. Santos. Development of a pharmaceutical cocrystal of a monophosphate salt with phosphoric acid. Chem. Comm. 0: 419-421 (2007).

54. S. Basavoju, D. Boström, and S.P. Velaga. Pharmaceutical cocrystal and salts of Norfloxacin. Cryst. Growth Des. 6: 2699-2708 (2006).

55. P. Vishweshwar, J.A. McMahon, M.L. Peterson, M.B. Hickey, T.R. Shattock, and M.J. Zaworotko. Crystal engineering of pharmaceutical co-crystals from polymorphic active pharmaceutical ingredients. Chem. Comm. 0: 4601-4603 (2005).

56. P.M. Bhatt, N.V. Ravindra, R. Banerjee, and G.R. Desiraju. Saccharin as a salt former. Enhanced solubilities of saccharinates of active pharmaceutical ingredients. Chem. Comm. 28: 1073-1075 (2005).

57. Zegarac M. Pharmaceutically acceptable co crystalline forms of sildenafil. WO080362 A1. (2007).

58. S. Zhang and A.C. Rasmuson. The theophylline-oxalic acid cocrystal system: solid phases, thermodynamics and crystallisation. Cryst. Eng. Comm. 14: 4644-4655 (2012).

59. A.V. Trask, W.D.S. Motherwell, and W. Jones. Physical stability enhancement of theophylline via cocrystallization. Int. J. Pharm. 320: 114-123 (2006).

60. G. Bettinetti, M.R. Caira, A. Callegari, M. Merli, M. Sorrenti, and C. Tadini. Structure and solid-state chemistry of anhydrous and hydrated crystal forms of the trimethoprim-sulfamethoxypyridazine 1:1 molecular complex. J. Pharm. Sci. 89: 478-489 (2000).

61. J. Broadhead, S.K.E. Rouan, and C.T. Rhodes. The spray-drying of pharmaceuticals. Drug Dev. Ind. Pharm. 18: 1169-1206 (1992).

62. A. Y. Sheikh, S. A. Rahim, R. B. Hammond and K. J. Roberts. Scalable solution cocrystallization: case of carbamazepine-nicotinamide I. Cryst. Eng. Comm. 11: 501-509 (2009).

63. M.R. Caira, L.R. Nassimbeni, and A.F. Wildervanck. Selective formation of hydrogen bonded cocrystals between a sulfonamide and aromatic carboxylic acids in the solid state. J. Chem. Soc., Perkin Trans. 2. 0: 2213-2216 (1995).

64. G. Bruni, M. Maietta, V. Berbenni, M. Bini, S. Ferrari, D. Capsoni, M. Boiocchi, C. Milanese and A. Marini. Preparation and characterization of carprofen co-crystals. Cryst. Eng. Comm. 14: 435-445 (2012).

65. I. Tomaszewska, S. Karki, J. Shur, R. Price, and N. Fotaki, Pharmaceutical characterisation and evaluation of cocrystals: Importance of in vitro dissolution conditions and type of coformer. Int. J. Pharmaceut. 453: 380-388 (2013).
66. A. Alhalaweh and S.P. Velaga. Formation of cocrystals from stoichiometric solutions of incongruently saturating systems by spray drying. Cryst. Growth Des. 10: 3302-3305 (2010).
67. G. Reucroft, D. Parikh, and D. Hipkiss. Vol. WO 2010/007447.
68. G. Reucroft, D. Parikh, and D. Hipkiss. Vol. WO 2010/007446.
69. D.P. McNamara, S.L. Childs, J. Giordano, A. Iarriccio, J. Cassidy, M.S. Shet, R. Mannion, E. O'Donnell, and A. Park. Use of a glutaric acid cocrystal to improve oral bioavailability of a low solubility API. Pharm. Res. 23: 1888-1897 (2006).
70. N. Schultheiss and A. Newman. Pharmaceutical cocrystals and their physicochemical properties. Cryst. Growth Des. 9: 2950-2967 (2009).
71. A. Alhalaweh, A. Sokolowski, N. Rodríguez-Hornedo, and S.P. Velaga. Solubility behavior and solution chemistry of indomethacin cocrystals in organic solvents. Cryst. Growth Des. 11: 3923–3929 (2011).
72. M.L. Cheney, D.R. Weyna, N. Shan, M. Hanna, L. Wojtas, and M.J. Zaworotko. Coformer selection in pharmaceutical cocrystal development: a case study of a meloxicam aspirin cocrystal that exhibits enhanced solubility and pharmacokinetics. J. Pharm. Sci. 100: 2172-2181 (2011).
73. Z. Rahman, C. Agarabi, A.S. Zidan, S.R. Khan, and M.A. Khan. Physico-mechanical and stability evaluation of carbamazepine cocrystal with nicotinamide. AAPS Pharm. Sci. Tech. 12: 693-704 (2011).
74. M.L. Cheney, N. Shan, E.R. Healey, M. Hanna, L. Wojtas, M.J. Zaworotko, V. Sava, S. Song, and J.R. Sanchez-Ramos. Effects of crystal form on solubility and pharmacokinetics: A crystal engineering case study of lamotrigine. Cryst. Growth Des. 10: 394-405 (2009).
75. J.F. Remenar, S.L. Morissette, M.L. Peterson, B. Moulton, J.M. MacPhee, H.R. Guzmán, and Ö. Almarsson. Crystal engineering of novel cocrystals of a triazole drug with 1,4-dicarboxylic acids. J. Am. Chem. Soc. 125: 8456-8457 (2003).
76. J. Lu and S. Rohani. Preparation and characterization of theophylline-nicotinamide cocrystal. Org. Proc. Res. Dev. 13: 1269-1275 (2009).

77. M.S. Jung, J.S. Kim, M.S. Kim, A. Alhalaweh, W. Cho, S.J. Hwang, and S.P. Velaga. Bioavailability of indomethacin-saccharin cocrystals. J. Pharm. Pharmacol. 62: 1560-1568 (2010).

78. N. Rodríguez-Hornedo and D. Murphy. Surfactant-facilitated crystallization of dihydrate carbamazepine during dissolution of anhydrous polymorph. J. Pharm. Sci. 93: 449-460 (2004).

79. Y. Kobayashi, S. Ito, S. Itai, and K. Yamamoto. Physicochemical properties and bioavailability of carbamazepine polymorphs and dihydrate. Int. J. Pharm. 193: 137-146 (2000).

80. A.L. Grzesiak, M. Lang, K. Kim, and A.J. Matzger. Comparison of the four anhydrous polymorphs of carbamazepine and the crystal structure of form I. J. Pharm. Sci. 92: 2260-2271 (2003).

81. D. Murphy, F. Rodríguez-Cintron, B. Langevin, R.C. Kelly, N. Rodríguez-Hornedo, Solution-mediated phase transformation of anhydrous to dihydrate carbamazepine and the effect of lattice disorder, Int. J. Pharm. 246: 121–134 (2002).

82. I.Kovacević, J. Parojcić, I. Homsek, M. Tubić-Grozdanis and P. Langguth. Justification of biowaiver for carbamazepine, a low soluble high permeable compound, in solid dosage forms based on IVIVC and gastrointestinal simulation. Mol. Pharm. 6: 40-47 (2008).

83. R. Banerjee, P. M. Bhatt, N. V. Ravindra, and G. R. Desiraju. Saccharin salts of active pharmaceutical ingredients, their crystal structures, and increased water solubilities. Cryst. Growth Des. 5: 2299–2309 (2005).

84. W.W. Porter III, S.C. Elie, and A.J. Matzger. Polymorphism in carbamazepine cocrystals. Cryst. Growth Des. 8: 14-16 (2008).

85. J. Truelove, R. Bawarshi-Nassar, N.R. Chen, and A. Hussain. Solubility enhancement of some developmental anti-cancer nucleoside analogs by complexation with nicotinamide. Int. J. Pharmaceut.19: 17-25 (1984).

86. V.R. Hathwar, R. Pal, and T.N. Guru Row. Charge density analysis of crystals of nicotinamide with salicylic acid and oxalic acid: An insight into the salt to cocrystal continuum. Cryst. Growth Des. 10: 3306-3310 (2010).

87. H.M. Ratajczak, I. Bryndal, I. Ledoux-Rak and A. J. Barnes. Search for molecular crystals with NLO properties: 3-Nitrophenol with nicotinamide and isonicotinamide. J. Mol. Struct. 1047: 310–316 (2013).

88. M.B. Fawzi, E. Davison, and M.S. Tute. Rationalization of drug complexation in aqueous solution by use of Hückel frontier molecular orbitals. J. Pharm. Sci. 69: 104-106 (1980).
89. S. Bogdanova, D. Sidzhakova, V. Karaivanova, and S. Georgieva. Aspects of the interactions between indomethacin and nicotinamide in solid dispersions. Int. J. Pharmaceut. 163: 1-10 (1998).
90. N. Ahuja, O. P. Katare, B. Singh. Studies on dissolution enhancement and mathematical modelling of drug release of a poorly water-soluble drug using water-soluble carriers. Eur. J. Pharmaceut.Biopharm.65: 26–38 (2007).
91. J.R. DiPalma. Basic pharmacology in medicine, Medical Surveillance Inc., (1994).
92. M.A. Khan, A.A. Karnachi, V. Agarwal, S.R. Vaithiyalingam, S. Nazzal, and I.K. Reddy. Stability characterization of controlled release coprecipitates and solid dispersions. J. Cont. Rel. 63: 1-6 (2000).
93. P.A. Slavin, D.B. Sheen, E.E.A. Shepherd, J.N. Sherwood, N. Feeder, R. Docherty, and S. Milojevic. Morphological evaluation of the γ-polymorph of indomethacin. J. Cryst. Growth. 237: 300-305 (2002).
94. M.A. Amiji and B.J. Sandmann. Applied physical pharmacy, McGraw-Hill Companies, USA (2003).
95. G. Singhvi and M. Singh. Review: In-vitro drug release characterization models. Int. J. Pharm. Studies Res. 2: 77-84 (2011).
96. E. Brunner. Reaktionsgeschwindigkeit in heterogenen systemen. Z. Phys.Chem. 43: 56-102 (1904).
97. A. Dokoumetzidis and P. Macheras. A century of dissolution research: from Noyes and Whitney to the biopharmaceutics classification system. Int. J. Pharm. 321: 1-11 (2006).
98. M. Wilderman. Über die geschwindigkeit molekularer und chemischer reaktionen in heterogenen systemen. Erster Teil. Z. Phys. Chem. 66:445-495 (1909).
99. P. Danckwerts. Significance of liquid-film coefficients in gas absorption. Ind. Eng. Chem. 43: 1460-1467 (1951).
100. U.V. Banaker. Pharmaceutical dissolution testing, Marcel Dekker, Inc.: New York (1992).
101. F.D.A. U.S. Department of Health and Human Services, Center for Drug Evaluation and Research. Dissolution testing of immediate release dosage forms: Guidance for industry, US Government Printing Office, Rockville MD (1997).

102. R.J. Babu and J. K. Pandit. Effect of aging on the dissolution stability of glibenclamide/ b-cyclodextrin complex. Drug Dev. Ind. Pharm. 25: 1215–1219 (1999).
103. N. L. Gonzalez Vidal, M.I.V. Brevedan, M. A. Varillas, L.D. Simionato and M.T. Pizzorno. Effect of accelerated-aging conditions on the dissolution stability of ciprofloxacin tablets. Dissolution Tech. February (2010).
104. C.J. Taborsky-Urdinola, V.A. Gray and L.T. Grady. Effects of packaging and storage on the dissolution of model prednisone tablets. Am. J. Health-Syst. Pharm. 38: 1322-1327 (1981).
105. S. Haidar, B. Davit, M.L. Chen, D. Conner, L. Lee, Q. Li, R. Lionberger, F. Makhlouf, D. Patel, D. Schuirmann, and L. Yu. Bioequivalence approaches for highly variable drugs and drug products. Pharm. Res. 25: 237-241 (2008).
106. C.L. Cheng, L.X. Yu, H.L. Lee, C.Y. Yang, C.S. Lue, and C.H. Chou. Biowaiver extension potential to BCS Class III high solubility-low permeability drugs: bridging evidence for metformin immediate-release tablet. Eur. J. Pharm. Sci. 22: 297-304 (2004).
107. F.D.A. U.S. Department of Health and Human Services, Center for Drug Evaluation and Research. Waiver of in vivo bioavailability and bioequivalency studies for immediate-release solid dosage forms based on a Biopharmaceutics Classification System. Guidance for industry. US Government Printing Office, Rockville MD, (2000).
108. The United State Pharmacopeia. (USP 32) United States Pharmacopeial Convention, Inc: Rockville MD (2009).
109. L. Shargel, S. Wu-Pong, and A.B.C. Yu. Applied biopharmaceutics & pharmacokinetics, Appleton & Lange Reviews/McGraw-Hill, Medical Pub. Division, New York (2005).
110. The United State Pharmacopeia. United States Pharmacopeial Convention, Inc: Rockville MD (1970).
111. B.R. Rohrs. Dissolution method development for poorly soluble compounds. Dissolution Tech. August: 1-5 (2001).
112. S. Klein and V.P. Shah. A standardized mini paddle apparatus as an alternative to the standard paddle. AAPS Pharm. Sci. Tech, 9, 1179-1184 (2008).
113. G. B. Crist. Trends in small-volume dissolution apparatus for low-dose compounds. Dissolution Tech. February: 19-22 (2009).

114. E. Scheubel, M. Lindenberg, E. Beyssac, and J.-M. Cardot. Small volume dissolution testing as a powerful method during pharmaceutical development. Pharmaceut. 2: 351-363 (2010).
115. J. Kramer and E. Stippler. Experiences with USP apparatus 4 calibration. Dissolution Tech. 12: 33-39 (2005).
116. Reynolds, W.C. Fundamentals of turbulence for turbulence modeling and simulation. Lecture Notes for Von Karman Institute, Agard Report No. 755. (1987).
117. J. Dressman and J. Kramer. Pharmaceutical dissolution testing, Taylor & Francis Group, US, (2005).
118. B. Abrahamsson, A. Pal, M. Sjoberg, M. Carlsson, E. Laurell, and J.G. Brasseur. A novel in vitro and numerical analysis of shear-induced drug release from extended release tablets in the fed stomach. Pharm. Res. 22: 1215-1226 (2005).
119. M. McAllister. Dynamic dissolution: A step closer to predictive dissolution testing? Mol. Pharmaceut. 7: 1374-1387 (2010).
120. S.M. Diebold. Physiological parameters relevant to dissolution testing: hydrodynamic considerations. In Pharmaceutical dissolution; Dressman, J.B., Kramer, J., Taylor & Francis, London, U.K., (2005).
121. D.M. D'Arcy, O.I. Corrigan, A.M. Healy. Evaluation of hydrodynamics in the basket dissolution apparatus using computational fluid dynamics—Dissolution rate implications. Eur. J. Pharm. Sci. 27: 259-267 (2006).
122. B. Crist and D. Spisak. Evaluation of induced variance of physical parameters on the calibrated USP dissolution apparatus 1 and 2. Dissolution Tech. Feb: 28-31 (2005).
123. FIP guidelines for dissolution testing of solid oral products, Pharm. Ind. 59: 760-760 (1997).
124. Z. Gao. Mathematical modeling of variables involved in dissolution testing. J. Pharm. Sci. 100: 4934-4942 (2011).
125. Z. Gao. In vitro dissolution testing with flow-through method: A technical note. AAPS Pharm. Sci. Tech. 10: 1401-1405 (2009).
126. L.H. Emara, N.F. Taha, and N.M. Mursi. Investigation of the effect of different flow-through cell designs on the release of diclofenac sodium SR tablets. Dissolution Tech. 16: 23-31 (2009).
127. N. Fotaki. Flow-through cell apparatus (USP apparatus 4): Operation and features. Dissolution Tech 18: 46-49 (2011).

128. F. Langenbucher, D. Benz, W. Kurth, H. Moller, and M. Otz. Standardized flow-cell method as an alternative to existing pharmacopoeial dissolution testing. Pharm Ind. 51: 1276-1281 (1989).
129. F. Langenbucher. In vitro assessment of dissolution kinetics: Description and evaluation of a column-type method. J. Pharm. Sci. 58: 1265- 1272 (1969).
130. N. Fotaki and C. Reppas. The flow-through cell methodology in the evaluation of intralumenal drug release characteristics. Dissolution Tech. 17-21 (2005).
131. Q. Wang, N. Fotaki, and Y. Mao. Biorelevant dissolution: Methodology and application in drug development. Dissolution Tech. August: 6-12 (2009).
132. W. Brown. Apparatus 4 flow-through cell: Some thoughts on operational characteristics. Dissolution Tech. 12: 28-30 (2005).
133. U.S. Food and Drug Administration Dissolution Method database http://www.accessdata.fda.gov/scripts/cder/dissolution/dsp_SearchResults_Dissolutions.cfm?PrintAll=1 [Accessed 15/05/13].
134. USP. The United States Pharmacopeia (USP 36), Pharmacopeial Convention, Inc, Rockville MD, (2013).
135. I. Singh and H.Y. Aboul-Enein. Advantages of USP apparatus IV (flow-through cell apparatus) in dissolution studies. JICS. 3: 220-222 (2006).
136. L. Kalantzi, E. Nicolaides, R.C., Page, G.A Digenis and C.Reppas. Prediction of the average plasma profile after oral administration of cross-linked capsules of amoxicillin, International Symposium on scientific and regulatory aspects of dissolution and bioequivalence, Athens, (2002).
137. Zolnik B.S., Raton J-L., and Burgess D.J. Application of USP Apparatus 4 and in situ fiber optic analysis to microsphere release testing. Dissolution Tech. 12: 11-14 (2005).
138. L.H. Emara, B.S. El-Menshawi, and M.Y. Estefan. In vitro-in vivo correlation and comparative bioavailablity of vincamine in prolonged-release preparations. Drug Dev. Ind. Pharm. 26: 243-251 (2000).
139. R. Dunn, H. Reimers, L. Ward, and J. Chapman. Suppository dissolution utilizing USP Apparatus 4. Dissolution Tech. 3: 18-19 (1996).
140. J. Hu, A. Kyad, V. Ku, P. Zhou, and N. Cauchon. A comparison of dissolution testing on lipid soft gelatin capsules using USP Apparatus 2 and Apparatus 4. Dissolution Tech. 12: 6-9 (2005).

141. Y. Wu and E.S. Ghaly. Effect of hydrodynamic environment on tablet dissolution using flow-through dissolution apparatus. P. R. Health Sci. J., 25: 75-83 (2006).
142. T.J. Looney. USP Apparatus 4 [Flow-through method] primer. Dissolution Tech. 3: 10-12 (1996).
143. M. Kakhi. Classification of the flow regimes in the flow-through cell. Eur. J. Pharm. Sci. 37: 531-544 (2009).
144. G.H. Zhang, W.A. Vadino, T.T. Yang, W.P. Cho, and I.A. Chaudry. Evaluation of the flow-through cell dissolution apparatus: effects of flow rate, glass beads and tablet position on drug release from different type of tablets. Drug Dev. Ind. Pharm. 20: 2063-2078 (1994).
145. G. Shiko, L.F. Gladden, A.J. Sederman, P.C. Connolly, and J.M. Butler. MRI studies of the hydrodynamics in a USP 4 dissolution testing cell. J. Pharm. Sci. 100: 976-991 (2011).
146. B. Wennergren, J. Lindberg, M. Nicklasson, G. Nilsson, G. Nyberg, R. Ahlgren, C. Persson, and B. Palm. A collaborative in vitro dissolution study: comparing the flow-through method with the USP paddle method using USP prednisone calibrator tablets. Int.J. Pharmaceut. 53: 35-41 (1989).
147. J.W. Eaton, D. Tran, W.W. Hauck, and E.S. Stippler. Development of a performance verification test for USP apparatus 4. Pharm. Res. 29: 345-351 (2012).
148. L. Kalantzi, K. Goumas, V. Kalioras, B. Abrahamsson, J.B. Dressman, and C. Reppas. Characterization of the human upper gastrointestinal contents under conditions simulating bioavailability/bioequivalence studies. Pharm. Res. 23: 165-176 (2006).
149. A. Diakidou, M. Vertzoni, K. Goumas, E. Söderlind, B. Abrahamsson, J. Dressman, and C. Reppas. Characterization of the contents of ascending colon to which drugs are exposed after oral administration to healthy adults. Pharm. Res. 26: 2141-2151 (2009).
150. L. Kalantzi, E. Persson, B. Polentarutti, B. Abrahamsson, K. Goumas, J.B. Dressman, and C. Reppas. Canine intestinal contents vs. simulated media for the assessment of solubility of two weak bases in the human small intestinal contents. Pharm. Res. 23: 1373-1381 (2006).
151. F. H. Pennings, B. L. S. Kwee, and H. Vromans. Influence of enzymes and surfactants on the disintegration behavior of cross-linked hard gelatin capsules during dissolution. Drug Dev. Ind. Pharm. 32: 33-37 (2006).
152. M. Vertzoni, J. Dressman, J. Butler, J. Hempenstall, and C. Reppas. Simulation of fasting gastric conditions and its importance for the in vivo dissolution of lipophilic compounds. Eur. J. Pharm. Biopharm. 60: 413-417 (2005).

153. J.B. Dressman, G.L. Amidon, C. Reppas, and V.P. Shah. Dissolution testing as a prognostic tool for oral drug absorption: immediate release dosage forms. Pharm. Res. 15: 11-22 (1998).

154. R. Takano, K. Sugano, A. Higashida, Y. Hayashi, M. Machida, Y. Aso and S. Yamashita. Oral absorption of poorly water-soluble drugs: Computer simulation of fraction absorbed in humans from a miniscale dissolution test. Pharm. Res. 23: 1144-1156 (2006).

155. E. Söderlind, E. Karlsson, A. Carlsson, R. Kong, A. Lenz, S. Lindborg and J.J. Sheng. Simulating fasted human intestinal fluids: Understanding the roles of lecithin and bile acids. Mol .Pharm. 7: 1498–1507 (2010).

156. E. Jantratid, N. Janssen, C. Reppas, and J.B. Dressman. Dissolution media simulating conditions in the proximal human gastrointestinal tract: an update. Pharm. Res. 25:1663-1676 (2008).

157. E. Jantratid and J.B. Dressman. Biorelevant dissolution media simulating the proximal human gastrointestinal tract: An update. Dissolution Tech. Aug. 21-25 (2009).

158. N. Fotaki, M. Symillides, and C. Reppas. In vitro versus canine data for predicting input profiles of isosorbide-5-mononitrate from oral extended release products on a confidence interval basis. Eur. J. Pharm. Sci. 24: 115-122 (2005).

159. M. Vertzoni, A. Diakidou, M. Chatzilias, E. Söderlind, B. Abrahamsson, J.B. Dressman, and C. Reppas. Biorelevant media to simulate fluids in the ascending colon of humans and their usefulness in predicting intracolonic drug solubility. Pharm. Res. 27: 2187-2196 (2010).

160. J.W. Moore and H.H. Flanner. Mathematical comparison of curves with an emphasis on in vitro dissolution profiles. Pharm. Tech. 20: 64-74 (1996).

161. H.L. Ju and S.J. Liaw. On the assessment of similarity of drug dissolution profiles—A simulation study. Drug Inf. J. 31: 1273-1289 (1997).

162. J.P. Liu, M.C. Ma, and S.C. Chow. Statistical evaluation of similarity factor f2 as a criterion for assessment of similarity between dissolution profiles. Drug Inf. J. 31: 1255-1271 (1997).

163. Y. Tsong, T. Hammerstrom, and J.J. Chen. Multipoint dissolution specification and acceptance sampling rule based on profile modeling and principal component analysis. J. Biopharm. Stat. 7: 423-439 (1997).

164. V.P. Shah, Y. Tsong, P. Sathe, and J.P. Liu. In vitro dissolution profile comparison-statistics and analysis of the similarity factor, f2. Pharm. Res. 15: 889-896 (1998).

165. C. Reppas and E. Nicolaides. Analysis of drug dissolution data. In Oral drug absorption; Dressman J.B., Lennernaes, H., Marcel Dekker, New York, (2000).
166. P. Costa and J.M. Sousa Lobo. Modeling and comparison of dissolution profiles. Eur. J. Pharm. Sci. 13: 123-133 (2001).
167. M. Vertzoni, M. Symillides, A. Iliadis, E. Nicolaides, and C. Reppas. Comparison of simulated cumulative drug versus time data sets with indices. Eur. J. Pharm. Biopharm. 56: 421-428 (2003).
168. J. Siepmann and F. Siepmann. Mathematical modeling of drug delivery. Int. J. Pharm. 364: 328-343 (2008).
169. T. Soni and N. Chotai. Assessment of dissolution profile of marketed aceclofenac formulations. J. Young. Pharm. 2: 21-26 (2010).
170. J.B. Dressman and H. Lennernas. Oral drug absorption: Prediction and assessment, Taylor & Francis, (2000).
171. S. Pundir, A. Badola and D. Sharma. Sustained release matrix technology and recent advance in matrix drug delivery system: A review. Int. J. Drug Res.Tech. 3: 12-20 (2013).
172. V. Papadopoulou, K. Kosmidis, M. Vlachou, and P. Macheras. On the use of the Weibull function for the discernment of drug release mechanisms. Int. J. Pharm. 309: 44-50 (2006).
173. F. Langenbucher. Letters to the Editor: Linearization of dissolution rate curves by the Weibull distribution. J. Pharm. Pharmacol. 24: 979-981 (1972).
174. L.X. Yu, E. Lipka, J.R. Crison, and G.L. Amidon. Transport approaches to the biopharmaceutical design of oral drug delivery systems: prediction of intestinal absorption. Adv. Drug Deliv. Rev. 19: 359-376 (1996).
175. B. Agoram, W.S. Woltosz, and M.B. Bolger. Predicting the impact of physiological and biochemical processes on oral drug bioavailability. Adv. Drug Deliv. Rev. 1: 41-67 (2001).
176. N.N.Songa, S.Y.Zhang, and C.X. Liu. Overview of factors affecting oral drug absorption. Asian J. Drug Metab. Pharmacokinetics. 4: 167-176 (2004).
177. K.A. Hasselbalch. Die berechnung der wasserstoffzahl des blutes aus der freien und gebundenen kohlensäure desselben, und die sauerstoffbindung des blutes als funktion der wasserstoffzahl, Julius Springer, Berlin, (1916).
178. M.A. Hedaya. Basic pharmacokinetics. CRC Press, Taylor & Francis Group, US, (2012).

179. D.B. Warren, H. Benameur, C.J. Porter, and C.W. Pouton. Using polymeric precipitation inhibitors to improve the absorption of poorly water-soluble drugs: A mechanistic basis for utility. J. Drug Target. 18: 704-731 (2010).
180. Z. Liu, S. Wang, and M. Hu. Chapter 11 - Oral absorption basics: Pathways, physico-chemical and biological factors affecting absorption. In Q. Yihong, C. Yisheng, G.G.Z. Zhang, L. Liu, W.R. Porter. Developing Solid Oral Dosage Forms, Academic Press, San Diego, 263-288 (2009).
181. E. Kerns, L. Di. Drug-like properties: Concepts, structure design and methods: from ADME to toxicity optimization. In Permeability. Academic Press 86-99 (2010).
182. P. Stenberg, K. Luthman, P. Artursson. Virtual screening of intestinal drug permeability. J. Cont. Rel. 65: 231–243 (2000).
183. G. Chawla, P. Gupta, V. Koradia, and A.K. Bansal. Gastroretention. A means to address regional variability in intestinal drug absorption. Pharmaceutical tech. (2003).
184. D.M. Mudie, G.L. Amidon, and G.E. Amidon. Physiological parameters for oral delivery and in vitro testing. Mol. Pharm. 7: 1388-1405 (2010).
185. A.S. Dahan and G.L. Amidon. Gastrointestinal dissolution and absorption of class II drugs. Drug bioavailability, Wiley-VCH Verlag GmbH & Co. KGaA, 33-51 (2009).
186. H.A. Schmidt, G. Fritzlar, W. Dolle, and H. Goebell. Comparative studies on the histamine and insulin stimulated acid pepsin secretion in patients suffering from ulcus duodeni and control persons. Dtsch. Med. Wochenschr. 95: 2011-2016 (1970).
187. R. Lambert, F. Martin, and M. Vagne. Relationship between hydrogen ion and pepsin concentration in human gastric secretion. Digestion. 1: 65-77 (1968).
188. M. Armand, P. Borel, B. Pasquier, C. Dubois, M. Senft, M. Andre, J. Peyrot, J. Salducci, and D. Lairon. Physicochemical characteristics of emulsions during fat digestion in human stomach and duodenum. Am. J. Physiol. 271: 172-183 (1996).
189. M. Vertzoni, H. Archontaki, and C. Reppas. Determination of intralumenal individual bile acids by HPLC with charged aerosol detection. J. Lipid Res. 49: 2690-2695 (2008).
190. J. Rhodes, D.E. Barnardo, S.F. Phillips, R.A. Rovelstad, and A.F. Hofmann. Increased reflux of bile into the stomach in patients with gastric ulcer. Gastroenterology. 57: 241-252 (1969).
191. M. Kristensen. Titration curves for gastric secretion. A study on duodenal ulcer and gastric ulcer with particular reference to the effect of glycopyrronium. Scand. J. Gastroenterol. Suppl. 32: 11-144 (1975).

192. W.D.W. Rees, D. Botham, and L.A. Turnberg. A demonstration of bicarbonate production by the normal human stomach in vivo. Digest. Dis. Sci. 27: 961-966 (1982).
193. S. Clarysse, J. Tack, F. Lammert, G. Duchateau, C. Reppas, P. Augustijns. Postprandial evolution in composition and characteristics of human duodenal fluids in different nutritional states. J. Pharm. Sci. 98: 1177–1192 (2009).
194. J. Brouwers, J. Tack, F. Lammert, and P. Augustijns. Intraluminal drug and formulation behavior and integration in in-vitro permeability estimation: a case study with amprenavir. J. Pharm. Sci. 95: 372-383 (2006).
195. T.C. Northfield and I. McColl. Postprandial concentrations of free and conjugated bile acids down the length of the normal human small intestine. Gut. 14: 513-518 (1973).
196. S.D. Ladas, P.E. Isaacs, G.M. Murphy, and G.E. Sladen. Comparison of the effects of medium and long chain triglyceride containing liquid meals on gall bladder and small intestinal function in normal man. Gut. 25: 405-411 (1984).
197. L.C. McGee and A.B. Hastings. The carbon dioxide tension and acid-base balance of jejunal secretions in man. J. Biol. Chem. 142: 893–904 (1942).
198. A. White, P. Handler, E.L. Smith. Principles of biochemistry. 4. McGraw-Hill; New York: Specialized Extracellular Fluids: 806-827 (1968).
199. J.G. Banwell, S.L. Gorbach, N.F. Pierce, R. Mitra, A. Mondal. Acute undifferentiated human diarrhea in tropics 2. Alterations in intestinal fluid and electrolyte movements. J. Clin. Invest. 50: 890–900 (1971).
200. C.G.Wilson. Gastrointestinal transit and drug absorption; J.B. Dressman, H. Lennernaes. Marcel Dekker, New York, (2000).
201. S.S. Ozturk, B.O. Palsson, and J.B. Dressman. Dissolution of ionizable drugs in buffered and unbuffered solutions. Pharm. Res. 5: 272-282 (1988).
202. J.J. Sheng, D.P. McNamara, and G.L. Amidon. Toward an in vivo dissolution methodology: a comparison of phosphate and bicarbonate buffers. Mol. Pharm. 6: 29-39 (2009).
203. S. Li, P. Doyle, S. Metz, A.E. Royce, and A.T.M. Serajuddin. Effect of chloride ion on dissolution of different salt forms of haloperidol, a model basic drug. J. Pharm. Sci. 94: 2224-2231 (2005).
204. C.L. Lim, C. Byrne, and J.K. Lee. Human thermoregulation and measurement of body temperature in exercise and clinical settings. Ann. Acad. Med. Singapore. 37: 347-353 (2008).

205. D.F. Evans, G. Pye, R. Bramley, A.G. Clark, T.J. Dyson, and J.D. Hardcastle. Measurement of gastrointestinal pH profiles in normal ambulant human subjects. Gut. 29: 1035-1041 (1988).

206. A. Lindahl, A.L. Ungell, L. Knutson, and H. Lennernas. Characterization of fluids from the stomach and proximal jejunum in men and women. Pharm. Res. 14: 497-502 (1997).

207. P. Kumar and B. Mishra. Colon targeted drug delivery systems-an overview. Curr. Drug Deliv. 5: 186-198 (2008).

208. J.B. Dressman, R.R. Berardi, L.C. Dermentzoglou, T.L. Russell, S.P. Schmaltz, J.L. Barnett, and K.M. Jarvenpaa. Upper gastrointestinal (GI) pH in young, healthy men and women. Pharm. Res. 7: 756-761 (1990).

209. J.D. Maxwell, A. Ferguson, W.C. Watson. The effect of gastric secretory status on jejunal pH measured by radiotelemetering. Digestion. 4: 345–352 (1971).

210. C. A. Youngberg, R. R. Berardi, W.F. Howatt, M. L. Hyneck, G. L. Amidon, J. H. Meyer, J. B. Dressman. Comparison of gastrointestinal pH in cystic-fibrosis and healthy subjects. Dig. Dis. Sci. 32: 472–480 (1987).

211. B. W. Watson, S. J. Meldrum, H. C. Riddle, R. L. Brown, G. E. Sladen. pH Profile of gut as measured by radiotelemetry capsule. Br. Med. J. 2: 104–106 (1972).

212. L. Ovesen, F. Bendtsen, U. Tage-Jensen, N.T. Pedersen, B. R. Gram, S. J. Rune. Intraluminal pH in the stomach, duodenum, and proximal jejunum in normal subjects and patients with exocrine pancreatic insufficiency. Gastroenterol. 90: 958–962 (1986).

213. R. L. Bown, G. E. Sladen, M. L. Clark, A. M. Dawson. The production and transport of ammonia in the human colon. Gut.12: 863 (1971).

214. C.V. Gisolfi, R.W. Summers, G.P. Lambert, and T. Xia. Effect of beverage osmolality on intestinal fluid absorption during exercise. J. App. Phys. 85: 1941-1948 (1998).

215. Davenport, HW. Physiology of the digestive tract. Year Book Medical Publishers, Inc; Chicago: 101-178 (1982).

216. B. Pedersen, A. Müllertz, H. Brøndsted, and H. Kristensen. A comparison of the solubility of danazol in human and simulated gastrointestinal fluids. Pharm. Res. 17: 891-894 (2000).

217. A. W. Basit and E. L. McConnell. Drug delivery to the colon. In Controlled release in oral drug delivery C.G. Wilson, P. J. Crowley. Springer (2011).

218. E. Persson, A.-S. Gustafsson, A. Carlsson, R. Nilsson, L. Knutson, P. Forsell, G. Hanisch, H. Lennernäs, and B. Abrahamsson. The effects of food on the dissolution of poorly soluble drugs in human and in model small intestinal fluids. Pharm. Res. 22: 2141-2151 (2005).

219. S. Lartigue, Y. Bizais , S. B. Des Varannes , A. Murat , B. Pouliquen , J. Galmiche. Inter- and intrasubject variability of solid and liquid gastric emptying parameters. A scintigraphic study in healthy subjects and diabetic patients. Dig. Dis. Sci.39:109-115 (1994).

220. F. Podczeck, N. C. Course, J. M. Newton and M. B. Short. The influence of non-disintegrating tablet dimensions and density on their gastric emptying in fasted volunteers. J.Pharm. Pharmacol. 59: 23-27 (2007).

221. R. Khosla and S.S. Davis, The effect of tablet size on the gastric emptying of non-disintegrating tablets, Int. J. Pharm. 62**:** 9–11 (1990).

222. United State Pharmacopoeia. In vitro and in vivo evaluations of dosage forms, Mack Publishing, Easton, PA, (2004).

223. U.S. Department of Health and Human Services, Food and Drug Administration, and CDER. Guidance for Industry. Extended release oral dosage forms: Development, evaluation, and application of in vitro/in vivo correlations (1997).

224. J.G. Wagner. Application of the Wagner-Nelson absorption method to the two-compartment open model. J Pharmacokinet. Biopharm. 2: 469-486 (1974).

225. J.C. Loo and S. Riegelman. New method for calculating the intrinsic absorption rate of drugs. J. Pharm. Sci. 57: 918-928 (1968).

226. K.C. Yeh, D.J. Holder, G.A. Winchell, L.A. Wenning, and T. Prueksaritanont. An extended point-area deconvolution approach for assessing drug input rates. Pharm. Res. 18: 1426-1434 (2001).

227. J. Emami. In vitro - in vivo correlation: from theory to applications. J. Pharm. Pharm. Sci. 9: 169-189 (2006).

228. R.J. Rackley. In vitro-in vivo correlation for controlled-release dosage forms, Dissolution Tech. Feb: 12-17 (1996).

229. S. Takka, A. Sakr and A. Goldberg. Development and validation of an in vitro-in vivo correlation for buspirone hydrochloride extended release tablets. J. Cont. Rel. 88: 147-157 (2003).

230. G. Balan, P.Timmins, D.S. Greene and P.H. Marathe. In-vitro in-vivo correlation models for glibenclamide after administration of metformin/glibenclamide tablets to healthy human volunteers. J. Pharm. Pharmacol. 52: 831-8 (2000).

231. J.M. Cardot, E. Beyssac, and M. Alric. In vitro-in vivo correlation: Importance of dissolution in IVIVC. Dissolution tech. 14: 15-19 (2007).

232. Y. Qiu, Y. Chen, G.G.Z. Zhang, L. Liu, and W. Porter. Developing solid oral dosage forms. Pharmaceutical Theory & Practice., Elsevier, U.S., (2008).

233. H. J. Shah, G. Subbaiah, D. M. Patel and C.N. Patel. In-vitro in-vivo correlation of modified release dosage form of Lamotrigine. Biopharm. Drug Dispos.30: 524-531 (2009).

234. A. Bose and W.T. Wui. Convolution and validation of in vitro-in vivo correlation of water-insoluble sustained-release drug (domperidone) by first-order pharmacokinetic one-compartmental model fitting equation. Eur. J. Drug Metab. Pharmacokinet. 23: 23 (2012).

235. M. Dey, R. Enever, M. Marino, J. Michelucci, D. Smith, R. Warner, and R. Weierstall. Sustained-release etodolac bioavailability and dose proportionality: correlation between in vivo and in vitro performance. Int. J. Pharmaceut. 49: 121-128 (1989).

236. S.S. Hwang, W. Bayne, and F. Theeuwes. In vivo evaluation of controlled-release products. J. Pharm. Sci. 82: 1145-1150 (1993).

237. N. Katori, K. Okudaira, N. Aoyagi, Y. Takeda, and M. Uchiyama. In vitro and in vivo correlation for controlled-release formulation of d-chlorpheniramine maleate. J. Pharmacobiodyn. 14: 567-575 (1991).

238. P. Buch, P. Holm, J.Q. Thomassen, D. Scherer, R. Branscheid, U. Kolb, and P. Langguth. IVIVC for fenofibrate immediate release tablets using solubility and permeability as in vitro predictors for pharmacokinetics. J. Pharm. Sci. 99: 4427-4436 (2010).

239. J. Radovanovic, Z. Duric, M. Jovanovic, S. Ibric, and M. Petrovic. An attempt to establish an in vitro-in vivo correlation: case of paracetamol immediate-release tablets. Eur. J. Drug Metab. Pharmacokinet. 23: 33-40 (1998).

240. O.A. Lake, M. Olling, and D.M. Barends. In vitro/in vivo correlations of dissolution data of carbamazepine immediate release tablets with pharmacokinetic data obtained in healthy volunteers. Eur. J. Pharm. Biopharm. 48: 13-19 (1999).

241. J. Devane, and J. Butler. The impact of in vitro-in vivo relationships on product. Pharm. Tech. 21: 146-159 (1997).

242. A. Dahan, J. M. Miller, and G.L. Amidon. Prediction of solubility and permeability class membership: provisional BCS classification of the world's top oral drugs. AAPS J. 11: 740–746 (2009).
243. J.G. Wagner. Pharmacokinetics for the pharmaceutical scientist, Technomic Publishing Company (1993).
244. E. Demirturk and L. Oner. In vitro-in vivo correlations. J. Pharm. Sci. 28: 215-224 (2003).
245. W.R. Gillepsie. PCDCON: Deconvolution for pharmacokinetic applications. University of Texas, Austin, TX (1992).
246. J.M. Cardot and B.M. Davit. In vitro-in vivo correlations: tricks and traps. AAPS J. 14: 491-499 (2012).
247. G. Levy. Effect of dosage form on drug absorption: a frequent variable in clinical pharmacology. Arch. Int. Pharmacodyn. Ther. 152: 59–68 (1964).
248. X. Zhang, R.A. Lionberger, B.M. Davit, and L.X. Yu. Utility of physiologically based absorption modeling in implementing Quality by Design in drug development. AAPS J. 13: 59-71 (2011).
249. W. Huang, S.L. Lee, and L.X. Yu. Mechanistic approaches to predicting oral drug absorption. AAPS J. 11: 217-224 (2009).
250. M. Jamei, D. Turner, J. Yang, S. Neuhoff, S. Polak, A. Rostami-Hodjegan, and G. Tucker. Population-based mechanistic prediction of oral drug absorption. AAPS J. 11: 225-237 (2009).
251. L. X. Yu and G. L. Amidon. A compartmental absorption and transit model for estimating oral drug absorption. Int. J. Pharmaceut. 186: 119–125 (1999).
252. M. Jamei, S. Marciniak, K. Feng, A. Barnett, G. Tucker, and A. Rostami-Hodjegan. The Simcyp population-based ADME simulator. Exp. Opin Drug Metab. Toxicol. 5: 211-223 (2009).
253. J. Wang and D.R. Flanagan. General solution for diffusion-controlled dissolution of spherical particles. 1. Theory. J. Pharm. Sci. 88: 731-738 (1999).
254. A. A. Noyes and W. R. Whitney. The rate of solution of solid substances in their own solutions. J. Am. Chem. Soc. 19: 930–934 (1897).
255. Yang J, M. Jamei, K.R. Yeo, G.T. Tucker, A. Rostami-Hodjegan. Prediction of intestinal first-pass drug metabolism. Curr. Drug Metab. 8: 676–84 (2007).

256. H.J. Clewell, 3rd, P.R. Gentry, T.R. Covington, and J.M. Gearhart. Development of a physiologically based pharmacokinetic model of trichloroethylene and its metabolites for use in risk assessment. Environ. Health Perspect. 2: 283-305 (2000).
257. H.M. Jones, M. Dickins, K. Youdim, J.R. Gosset, N.J. Attkins, T.L. Hay, I.K. Gurrell, Y.R. Logan, P.J. Bungay, B.C. Jones, and I.B. Gardner. Application of PBPK modelling in drug discovery and development at Pfizer. Xenobiotica. 42: 94-106 (2012).
258. Y. Nakajima, K. Hattori, M. Shinsei, N. Matsunaga, H. Iizasa, H. Sasabe, H. Akiyama, G. Miyanmoto, and E. Nakashima. Physiologically-based pharmacokinetic analysis of grepafloxacin. Biol. Pharm. Bull. 23: 1077-1083 (2000).
259. K.K. Manuilov, S.M. Navashin, and S.E. Kuleshov. Use of gentamicin physiologically-based model for individual dosing. Int. J. Clin. Pharmacol. Res. 13: 59-63 (1993).
260. C.R. Kirman, S.M. Hays, G.L. Kedderis, M.L. Gargas, and D.E. Strother. Improving cancer dose-response characterization by using physiologically based pharmacokinetic modeling: an analysis of pooled data for acrylonitrile-induced brain tumors to assess cancer potency in the rat. Risk Anal. 20: 135-151 (2000).
261. R. Kawai, D. Mathew, C. Tanaka, and M. Rowland. Physiologically based pharmacokinetics of cyclosporine A: extension to tissue distribution kinetics in rats and scale-up to human. J. Pharmacol. Exp. Ther. 287: 457-468 (1998).
262. F.Y. Bois. Physiologically based modelling and prediction of drug interactions. Basic & Clin. Pharm. Toxicol. 106: 154-161 (2010).
263. T.N. Johnson and A. Rostami-Hodjegan. Resurgence in the use of physiologically based pharmacokinetic models in pediatric clinical pharmacology: parallel shift in incorporating the knowledge of biological elements and increased applicability to drug development and clinical practice. Paediatr. Anaesth. 21: 291-301 (2011).
264. F. Bouzom and B. Walther. Pharmacokinetic predictions in children by using the physiologically based pharmacokinetic modelling. Fundam. Clin. Pharmacol. 22: 579-587 (2008).
265. H.M. Jones, N. Parrott, G. Ohlenbusch, and T. Lave. Predicting pharmacokinetic food effects using biorelevant solubility media and physiologically based modelling. Clin. Pharmacokinet. 45: 1213-1226 (2006).

266. S.M. Hays, B.A. Elswick, G.M. Blumenthal, F. Welsch, R.B. Conolly, and M.L. Gargas. Development of a physiologically based pharmacokinetic model of 2- methoxyethanol and 2 methoxyacetic acid disposition in pregnant rats. Toxicol. Appl. Pharmacol. 163: 67-74 (2000).

267. A.N. Edginton and S. Willmann. Physiology-based simulations of a pathological condition: prediction of pharmacokinetics in patients with liver cirrhosis. Clin. Pharmacokinet. 47: 743-752 (2008).

268. H.J. Clewell, P.R. Gentry, J.M. Gearhart, T.R. Covington, M.I. Banton, and M.E. Andersen. Development of a physiologically based pharmacokinetic model of isopropanol and its metabolite acetone. Toxicol. Sci. 63: 160-172 (2001).

269. H.A. El-Masri and E.M. Kenyon. Development of a human physiologically based pharmacokinetic (PBPK) model for inorganic arsenic and its mono- and di-methylated metabolites. J. Pharmacokinet. Pharmacodyn. 35: 31-68 (2008).

270. M. Efentakis and J.B. Dressman. Gastric juice as a dissolution medium: Surface tension and pH. Eur. J. Drug Metab. Pharmacokinet. 23: 97-102 (1998).

271. M. Gibaldi and S. Feldman. Mechanisms of surfactant effects on drug absorption. J. Pharm. Sci. 59: 579-589 (1970).

272. S. Solvang and P. Finholt. Effect of tablet processing and formulation factors on dissolution rate of the active ingredient in human gastric juice. J. Pharm. Sci. 59: 49-52 (1970).

273. A. Aburub, D.S. Risley, and D. Mishra. A critical evaluation of fasted state simulating gastric fluid (FaSSGF) that contains sodium lauryl sulfate and proposal of a modified recipe. Int. J. Pharm. 347: 16-22 (2008).

274. C. Long, K. Tang, H. Chokshi, and N. Fotaki. Investigation on the physiological relevant amount of surfactant in simulated gastric fluids for in vitro solubility and dissolution studies, International conference and exhibition on pharmaceutical, nutraceutical and cosmeceutical technology, Kuala Lumpur, Malaysia, (2012).

275. J.R. Crison, N.D. Weiner, and G.L. Amidon. Dissolution media for in vitro testing of water-insoluble drugs: Effect of surfactant purity and electrolyte on in vitro dissolution of carbamazepine in aqueous solutions of sodium lauryl sulfate. J. Pharm. Sci. 86: 384-388 (1997).

276. M.H. Ropers, G. Czichocki, and G. Brezesinski. Counterion Effect on the thermodynamics of micellization of alkyl sulfates. J. Phys. Chem. B. 107: 5281-5288 (2003).

277. R.R.J. Beynon and J.J.S. Easterby. Buffer solutions, IRL Press at Oxford University Press, (1996).

278. USP. The United States Pharmacopeia (USP 29), Pharmacopeial Convention, Inc, Rockville MD, (2006).

279. D.D. Van Slyke. On the measurement of buffer values and on the relationship of buffer to the dissociation constant of the buffer and the concentration and reaction and reaction of the buffer solution. J. Biol. Chem. 52: 525-570 (1922).

280. M. Vertzoni, C. Reppas and H.A. Archontaki. Sensitive and simple liquid chromatographic method with ultraviolet detection for the determination of nifedipine in canine plasma. Anal. Chim. Acta. 573-574: 298-304 (2006).

281. M.A. Al Za'abi, G.H. Dehghanzadeh, R.L. Norris, and B.G. Charles. A rapid and sensitive microscale HPLC method for the determination of indomethacin in plasma of premature neonates with patent ductus arteriousus. J Chromatogr. B Analyt. Technol. Biomed. Life Sci. 830: 364-367 (2006).

282. A. Glomme, J. Marz, and J.B. Dressman. Comparison of a miniaturized shake-flask solubility method with automated potentiometric acid/base titrations and calculated solubilities. J. Pharm. Sci. 94: 1-16 (2005).

283. M.C. Meyer, A.B. Straughn, E.J. Jarvi, G.C. Wood, F.R. Pelsor, and V.P. Shah. The bioinequivalence of carbamazepine tablets with a history of clinical failures. Pharm. Res. 9: 1612-1616 (1992).

284. J.G. Larkin, A. McLellan, A. Munday, M. Sutherland, E. Butler and M.J. Brodie. A double-blind comparison of conventional and controlled-release carbamazepine in healthy subjects. Br. J. Clin. Pharmacol. 27: 313-322 (1989).

285. K.C. Yeh, E.T. Berger, G.O. Breault, B.W. Lei, and F.G. McMahon. Effect of sustained release on the pharmacokinetic profile of indomethacin in man. Biopharm. Drug Dispos. 3: 219-230 (1982).

286. S. Winiwarter, N.M. Bonham, F. Ax, A. Hallberg, H. Lennernäs, and A. Karlén. Correlation of human jejunal permeability (in vivo) of drugs with experimentally and theoretically derived parameters. A multivariate data analysis approach. J. Med. Chem. 41: 4939-4949 (1998).

287. H. Lennernäs, O. Ahrenstedt, R. Hallgren, L. Knutson, M. Ryde, and L.K. Paalzow. Regional jejunal perfusion, a new in vivo approach to study oral drug absorption in man. Pharm. Res. 9: 1243-1251 (1992).

288. W.D. Hooper, D.K. Dubetz, F. Bochner, L.M. Cotter, G.A. Smith, M.J. Eadie and J.H. Tyrer. Plasma protein binding of carbamazepine. Clin. Pharmacol. Ther. 17: 433-440 (1975).
289. P.L. Morselli and A. Frigerio. Metabolism and pharmacokinetics of carbamazepine. Drug Metab. Rev. 4: 97-113 (1975).
290. L.M. Cotter, M.J. Eadie, W.D. Hooper, C.M. Lander, G.A. Smith, and J.H. Tyrer. The pharmacokinetics of carbamazepine. Eur. J. Clin. Pharmacol. 12: 451-456 (1977)
291. G. Bouchard, P.A. Carrupt, B. Testa, V. Gobry, and H.H. Girault. Lipophilicity and solvation of anionic drugs. Chemistry. 8: 3478-3484 (2002).
292. M.A Strafford, A. Avdeef, P. Artursson, C.A.S. Johansson, K. Luthman, C.R. Brownell, R. Lyon, Am. Assoc. Pharm. Sci. Ann Mtng. Poster presentation (2000).
293. S. Sung, H. Yang, K. Uryu, E. B. Lee, L. Zhao, D. Shineman, J.Q. Trojanowski, V.M. Lee and D. Pratico. Modulation of nuclear factor-κβ activity by indomethacin influences Aβ levels but not Aβ precursor protein metabolism in a model of Alzheimer's disease. Am. J. Pathol. 165: 2197–2205 (2004).
294. N. Seedher and M. Kanojia. Micellar solubilization of some poorly soluble antidiabetic drugs: a technical note. AAPS Pharm. Sci. Tech. 9: 431-436 (2008).
295. T. Taupitz and S. Klein. Can biorelevant media be simplified by using SLS and Tween 80 to replace bile compounds? Open Drug Del. J. 4: 30-37 (2010).
296. D. Attwood and A.T. Florence. Physical pharmacy [electronic resource], Pharmaceutical Press, (2008).
297. C.O. Rangel-Yagui, A. Pessoa, and L.C. Tavares. Micellar solubilization of drugs. J. Pharm. Pharm. Sci. 8: 147-165 (2005).
298. S. Klein. Biorelevant dissolution test methods for modified release dosage forms, Johann Wolfgang Goethe University of Frankfurt am Main, (2005).
299. T. Zoeller and S. Klein. Simplified biorelevant media for screening dissolution performance of poorly soluble drugs. Dissolution Tech. 14: 8-13 (2007).
300. E. Stippler, S. Kopp, J. B. Dressman. Comparison of US pharmacopeia simulated intestinal fluid TS (without pancreatin) and phosphate standard buffer pH 6.8, TS of the international pharmacopoeia with respect to their use in in-vitro dissolution testing. Dissolution tech. 6-10 (2004).
301. S. Klein. The use of biorelevant dissolution media to forecast the in vivo performance of a drug. AAPS J. 12: 397-406 (2010).

302. D.D. Perrin and B. Dempsey. Practical limitations in the use of buffers. Buffers for pH and metal ion control, Springer Netherlands, 55-61 (1979).
303. F. Liu, H.A. Merchant, R.P. Kulkarni, M. Alkademi, and A.W. Basit. Evolution of a physiological pH 6.8 bicarbonate buffer system: Application to the dissolution testing of enteric coated products. Eur. J. Pharm. Biopharm. 78: 151-157 (2011).
304. H.M. Fadda, H.A. Merchant, B.T. Arafat, and A.W. Basit. Physiological bicarbonate buffers: stabilisation and use as dissolution media for modified release systems. International J. Pharm. 382: 56-60 (2009).
305. D.P. McNamara, K.M. Whitney, and S.L. Goss. Use of a physiologic bicarbonate buffer system for dissolution characterization of ionizable drugs. Pharm. Res. 20: 1641-1646 (2003).
306. G. Garbacz, B. Kołodziej, M. Koziolek, W. Weitschies, and S. Klein. An automated system for monitoring and regulating the pH of bicarbonate buffers. AAPS Pharm. Sci. Tech. 14: 517-522 (2013).
307. M.P.d.l.C. Moreno, M. Oth, S. Deferme, F. Lammert, J. Tack, J. Dressman, and P. Augustijns. Characterization of fasted-state human intestinal fluids collected from duodenum and jejunum. J. Pharm. Pharmacol. 58: 1079-1089 (2006).
308. Z. Rahman, R. Samy, V.A. Sayeed, and M.A. Khan. Physicochemical and mechanical properties of carbamazepine cocrystals with saccharin. Pharm. Dev. Technol. 17: 457-465 (2012).
309. N.J. Babu and A. Nangia. Solubility advantage of amorphous drugs and pharmaceutical cocrystals. Cryst. Growth Des. 11: 2662-2679 (2011).
310. A. Nokhodchi, Y. Javadzadeh, M.R. Siahi-Shadbad, and M. Barzegar-Jalali. The effect of type and concentration of vehicles on the dissolution rate of a poorly soluble drug (indomethacin) from liquisolid compacts. J. Pharm. Pharm. Sci. 8: 18-25 (2005).
311. M.A. EL-Massik, O.Y. Abdallah, S. Galal, and N.A. Daabis. Towards a universal dissolution medium for carbamazepine. Drug Dev. Ind. Pharm. 32: 893-905 (2006).
312. A. R. Patel and V. Y. Joshi. Evaluation of SLS: APG mixed surfactant systems as carrier for solid dispersion. AAPS Pharm. Sci. Tech. 9: 583–590 (2008).
313. J.R. Medina, D.K. Salazar, M. Hurtado, A.R. Cortés, and A.M. Domínguez-Ramírez. Comparative in vitro dissolution study of carbamazepine immediate-release products using the USP paddles method and the flow-through cell system. Saudi Pharmaceut. J. 1-7 (2013).
314. J.Y. Kim, S. Kim, M. Papp, K. Park, and R. Pinal. Hydrotropic solubilization of poorly water-soluble drugs. J. Pharm. Sci. 99: 3953-3965 (2010).

315. Y. Gao, H. Zu, and J. Zhang. Enhanced dissolution and stability of adefovir dipivoxil by cocrystal formation. J. Pharm. Pharmacol. 63: 483-490 (2011).
316. N. Qiao, K. Wang, W. Schlindwein, A. Davies, and M. Li. In situ monitoring of carbamazepine–nicotinamide cocrystal intrinsic dissolution behaviour. Eur. J. Pharmaceut. Biopharm. 83: 415-426 (2013).
317. M.Bijanzadeh, M. Mahmoudian, M.E. Zolfaghari, M.M.Gouya, T.Khazinia, and A.Khosravi. The influence of particle size and dissolution rate on bioavailabilty of two indomethacine capsules. DARU J. Pharm. Sci. 5: 51-61 (1995).
318. K. Schamp, S.-A. Schreder, and J. Dressman. Development of an in vitro/in vivo correlation for lipid formulations of EMD 50733, a poorly soluble, lipophilic drug substance. Eur. J. Pharmaceut. Biopharm. 62: 227-234 (2006).
319. Y.E. Arnold, G. Imanidis, and M.T. Kuentz. Advancing in-vitro drug precipitation testing: new process monitoring tools and a kinetic nucleation and growth model. J. Pharm. Pharmacol. 63: 333-341 (2011).
320. D. Hörter and J.B. Dressman. Influence of physicochemical properties on dissolution of drugs in the gastrointestinal tract. Adv. Drug Del. Rev. 46: 75-87 (2001).
321. J.G. Wagner. Pharmacokinetic absorption plots from oral data alone or oral/intravenous data and an exact Loo–Riegelman equation. J. Pharmaceut. Sci. 72: 838-842 (1983).
322. J.R. White, M.W. Garrison, and M.A. Koda-Kimble. Basic clinical pharmacokinetics handbook, Applied Therapeutics, Inc., 1994.
323. W.J. Taylor and A.L. Finn. Individualizing drug therapy: Carbamazepine. Ethosuximide. Phenobarbital, Gross, Townsend, Frank, 1981.
324. D.M. Woodbury, J.K. Penry, and R.P. Schmidt. Antiepileptic drugs, Raven Press, 1972.
325. B. Widdop. Therapeutic drug monitoring, Churchill Livingstone, 1985.
326. C. Tannergren, A. Bergendal, H. Lennernas, and B. Abrahamsson. Toward an increased understanding of the barriers to colonic drug absorption in humans: implications for early controlled release candidate assessment. Mol. Pharm. 6: 60-73 (2009).
327. N. Kaneniwa, O. Umezawa, N. Watari, K. Kawakami, H. Asami, and M. Sumi. [Bioavailability and dissolution test of commercial carbamazepine tablets]. Yakugaku Zasshi. 104: 83-90 (1984).
328. P.J. Neuvonen. Bioavailability and central side effects of different carbamazepine tablets. Int. J. Clin. Pharmacol. Ther. Toxicol. 23: 226-232 (1985).

329. R. Hartley, J. Aleksandrowicz, C.J. Bowmer, A. Cawood, and W.I. Forsythe. Dissolution and relative bioavailability of two carbamazepine preparations for children with epilepsy. J. Pharm. Pharmacol. 43: 117-119 (1991).
330. M.C. Meyer, A.B. Straughn, R.M. Mhatre, V.P. Shah, R.L. Williams, and L.J. Lesko. The relative bioavailability and in vivo-in vitro correlations for four marketed carbamazepine tablets. Pharm. Res. 15: 1787-1791 (1998).
331. P. Veng-Pedersen, J.V. Gobburu, M.C. Meyer, and A.B. Straughn. Carbamazepine level-A in vivo-in vitro correlation (IVIVC): a scaled convolution based predictive approach. Biopharm. Drug Dispos. 21: 1-6 (2000).
332. H. Jung, R.C. Milán, M.E. Girard, F. León, and M.A. Montoya. Bioequivalence study of carbamazepine tablets: In vitro/in vivo correlation. Int. J.Pharmaceut. 152: 37-44 (1997).
333. L.C. Kaus, J.T. Fell, H. Sharma, and D.C. Taylor. On the intestinal transit of a single non-disintegrating object. Int. J. Pharmaceut. 20: 315-323 (1984).

Appendix 1

Detailed calculations for CBZ-SAC and CBZ-NIC cocrystals

MW of CBZ = 236.27g/mol

MW of SAC = 183.18g/mol

MW of NIC = 122.12g/mol

Amount of CBZ in Tegretol tablet = 200mg = 0.2g

Amount of CBZ moles in 200mg

$$n = \frac{m}{M}$$

where n – number of moles [mol];

m - mass of compound [g]

M – molecular weight [g/mol]

$$n = \frac{0.2g}{236.27g/mol} = 8.47 \times 10^{-4} mol$$

$$n = 8.47x10^{-4} mol \times 1000 = 0.847mmol$$

The same molar amount of coformers (SAC; NIC) must be obtained in order to achieve 1:1 molar ratio of CBZ:SAC and CBZ:NIC. Thus, above equation needs to be converted to:

$$m = n \times M$$

Then amount of SAC and NIC can be calculated as follows:

SAC:

$$m_{SAC} = 8.47 \times 10^{-4} mol \times 183.18g/mol$$
$$m_{SAC} = 0.155g = 155mg$$

NIC:

$$m_{NIC} = 8.47 \times 10^{-4} mol \times 122.12g/mol$$
$$m_{NIC} = 0.103g = 103mg$$

Therefore total amount of cocrystal that is equivalent to 200mg of CBZ is estimated:

CBZ-SAC=200mg+155mg=355mg

CBZ-NIC=200mg+103mg=303mg

Appendix 2

CBZ-MCC

	WEIGHT [MG]	AREA
1	26.2	31517.70
2	26.2	31238.20
3	26.2	30530.40
4	26.4	32161.00
5	26.2	31138.20
6	26.3	31166.00
7	26.1	30952.50
8	26.3	30370.10
9	26.4	31231.60
10	26.2	30848.10
	MEAN	31115.38
	ST DEV	503.59
	CV	0.02
	%CV	**1.60**

CBZ-SAC$_{ss}$-MCC

	WEIGHT [MG]	AREA
1	41.5	30338.50
2	41.6	30108.90
3	41.6	30793.40
4	41.7	29585.20
5	41.4	29627.60
6	41.4	30955.70
7	41.7	30354.00
8	41.5	29992.50
9	41.5	30679.60
10	41.5	30128.80
	MEAN	30256.42

	ST DEV	462.64
	CV	0.02
	%CV	**1.52**

CBZ-NICss-MCC

	WEIGHT [MG]	**AREA**
1	36.2	29308.10
2	36.2	30044.80
3	36.2	30407.50
4	36.4	30211.70
5	36.4	31029.60
6	36.3	29916.70
7	36.4	30357.40
8	36.4	30129.00
9	36.4	30686.30
10	36.4	30897.30
	MEAN	30298.84
	ST DEV	503.99
	CV	0.02
	%CV	**1.72**

Appendix 3

Detailed calculations for IND-SAC and IND-NIC cocrystals

MW of IND = 357.79g/mol

MW of SAC = 183.18g/mol

MW of NIC = 122.12g/mol

Amount of IND in Indocid capsule = 25mg = 0.025g

Amount of IND moles in 25mg

$$n = \frac{m}{M}$$

where n – number of moles [mol];

m - mass of compound [g]

M – molecular weight [g/mol]

$$n = \frac{0.025g}{357.79g/mol} = 6.99 \times 10^{-5} mol$$

$$n = 6.99x10^{-5} mol \times 1000 = 0.0699mmol$$

The same molar amount of coformers (SAC; NIC) must be obtained in order to achieve 1:1 molar ratio of IND:SAC and IND:NIC. Thus, above equation needs to be converted to:

$$m = n \times M$$

Then amount of SAC and NIC can be calculated as follows:

SAC:

$$m_{SAC} = 6.99x10^{-5} mol \times 183.18g/mol$$
$$m_{SAC} = 0.0128g = 12.79mg$$

NIC:

$$m_{NIC} = 6.99 \times 10^{-5} mol \times 122.12g/mol$$
$$m_{NIC} = 0.00853g = 8.53mg$$

Therefore total amount of cocrystal that is equivalent to 25mg of IND is estimated:

IND-SAC=25mg+12.79mg=37.79mg

IND-NIC=25mg+8.53mg=33.53mg

Appendix 4

CBZ--SAC

	WEIGHT [MG]	AREA
1	35.62	3141.40
2	35.69	3175.30
3	35.51	3005.30
4	35.65	3024.97
5	35.47	3010.60
6	35.54	3069.69
7	35.48	3093.60
8	35.75	3041.84
9	35.62	3111.20
10	35.6	3131.60
	MEAN	3080.55
	ST DEV	59.31
	CV	0.02
	%CV	**1.93**

CBZ--NIC

	WEIGHT [MG]	AREA
1	35.86	3508.92
2	35.89	3536.52
3	35.9	3471.40
4	35.79	3517.50
5	35.78	3588.82
6	35.88	3578.22
7	35.75	3565.70
8	35.94	3514.96
9	35.88	3516.60
10	35.78	3470.10
	MEAN	3526.87
	ST DEV	40.87
	CV	0.01
	%CV	**1.16**

Appendix 5

Yeh *et al*. oral

0.17	4.39
0.33	3
0.5	2.01
0.75	1.4
1	1.06
1.25	1.83
1.5	0.64
2	0.45
4	0.12

Yeh *et al*. oral

0.33	0.34
0.67	1.43
1.00	1.45
1.50	1.01
2.03	0.77
4.00	0.25

Appendix 6

xm/µm	q3lg			
	CBZ	CBZ-SAC$_{ss}$	CBZ-SAC$_{umax}$	CBZ-NIC$_{ss}$
0.67	0.05	0.15	0.10	0.19
0.99	0.06	0.21	0.13	0.24
1.20	0.06	0.26	0.14	0.28
1.40	0.05	0.30	0.16	0.30
1.64	0.05	0.35	0.19	0.33
1.99	0.04	0.41	0.23	0.37
2.39	0.04	0.48	0.30	0.40
2.84	0.04	0.54	0.40	0.42
3.39	0.04	0.61	0.53	0.45
3.99	0.06	0.67	0.68	0.47
4.64	0.08	0.72	0.82	0.50
5.48	0.12	0.76	0.97	0.55
6.71	0.18	0.79	1.10	0.63
8.22	0.26	0.76	1.15	0.74
9.72	0.35	0.69	1.12	0.85
11.46	0.45	0.60	1.06	0.94
13.69	0.57	0.51	0.96	0.99
16.43	0.72	0.46	0.83	0.97
19.44	0.86	0.44	0.67	0.87
22.91	1.01	0.46	0.52	0.73
27.39	1.17	0.51	0.35	0.56
32.86	1.32	0.55	0.21	0.40
39.34	1.44	0.54	0.11	0.26
46.83	1.46	0.45	0.05	0.15
55.78	1.28	0.30	0.03	0.07
66.73	0.84	0.15	0.01	0.02
79.69	0.32	0.05	0.01	0.00
94.66	0.02	0.00	0.00	0.00

xm/才m	q3lg				
	IND	IND-SACss	IND-SACsd	IND-SAC$_{umax}$	IND-NICss
0.67	0.06	0.13	0.11	0.04	0.12
0.99	0.08	0.17	0.13	0.05	0.16
1.20	0.08	0.19	0.14	0.06	0.19
1.40	0.09	0.22	0.13	0.07	0.21
1.64	0.09	0.24	0.13	0.07	0.25
1.99	0.10	0.28	0.13	0.08	0.29
2.39	0.11	0.32	0.12	0.09	0.35
2.84	0.13	0.36	0.11	0.11	0.41
3.39	0.15	0.40	0.11	0.13	0.48
3.99	0.18	0.43	0.12	0.16	0.55
4.64	0.21	0.45	0.12	0.18	0.62
5.48	0.26	0.47	0.15	0.22	0.70
6.71	0.32	0.48	0.19	0.27	0.80
8.22	0.38	0.47	0.26	0.31	0.88
9.72	0.45	0.48	0.37	0.34	0.95
11.46	0.53	0.51	0.53	0.39	1.01
13.69	0.63	0.56	0.76	0.45	1.05
16.43	0.76	0.60	1.01	0.55	1.05
19.44	0.88	0.62	1.21	0.66	0.96
22.91	1.01	0.63	1.32	0.80	0.80
27.39	1.15	0.65	1.34	0.98	0.56
32.86	1.25	0.70	1.24	1.16	0.30
39.34	1.26	0.79	1.08	1.31	0.12
46.83	1.12	0.84	0.87	1.36	0.03
55.78	0.84	0.76	0.63	1.26	0.00
66.73	0.49	0.53	0.36	0.97	0.00
79.69	0.21	0.29	0.14	0.58	0.00
94.66	0.07	0.14	0.00	0.23	0.00
112.56	0.02	0.06	0.00	0.05	0.00
134.47	0.00	0.00	0.00	0.01	0.00

Appendix 7

Two Way Repeated Measures ANOVA (Two Factor Repetition) Wednesday, December 14, 2011, 12:12:17

Data source: Data 1 in CBZ-solubility data-TW AnovaRM across medium

Balanced Design

Dependent Variable: Solubility

Normality Test (Shapiro-Wilk) Passed (P = 0.600)

Equal Variance Test: Passed (P = 0.297)

Source of Variation	**DF**	**SS**	**MS**	**F**	**P**
Sample no	2	75.003	37.501		
Medium	4	81376.916	20344.229	338.917	<0.001
Medium x Sample no	8	480.218	60.027		
Formulation	3	113358.493	37786.164	267.943	<0.001
Formulation x Sample no	6	846.140	141.023		
Medium x Formulation	12	97507.867	8125.656	66.185	<0.001
Residual	24	2946.509	122.771		
Total	59	296591.145	5026.969		

Main effects cannot be properly interpreted if significant interaction is determined. This is because the size of a factor's effect depends upon the level of the other factor.

The effect of different levels of Medium depends on what level of Formulation is present. There is a statistically significant interaction between Medium and Formulation. (P = <0.001)

Power of performed test with alpha = 0.0500: for Medium : 1.000

Power of performed test with alpha = 0.0500: for Formulation : 1.000

Power of performed test with alpha = 0.0500: for Medium x Formulation : 1.000

Least square means for Medium :

Group	Mean
SGF	264.238
SIF	223.020

Std Err of LS Mean = 2.237

Least square means for Formulation :

Group	Mean
CBZ-MCC	284.531
CBZ-NIC-MCC	238.135
CBZ-SACss-MCC	237.830

Std Err of LS Mean = 3.066

Least square means for Medium x Formulation :

Group	Mean
SGF x CBZ-MCC	250.819
SGF x CBZ-NIC-MCC	208.116
SGF x CBZ-SACss-MCC	232.076
SIF x CBZ-MCC	199.523
SIF x CBZ-NIC-MCC	226.397
SIF x CBZ-SACss-MCC	210.054
SIF x CBZ-SACumax-MCC	256.104
FaSSGF x CBZ-MCC	416.517
FaSSGF x CBZ-NIC-MCC	258.011
FaSSGF x CBZ-SACss-MCC	197.166
FaSSGF x CBZ-SACumax-MCC	467.287
FaSSIF-V2 x CBZ-MCC	287.473
FaSSIF-V2 x CBZ-NIC-MCC	273.125
FaSSIF-V2 x CBZ-SACss-MCC	285.806
FaSSIF-V2 x CBZ-SACumax-MCC	324.318

Std Err of LS Mean = 6.397

All Pairwise Multiple Comparison Procedures (Bonferroni t-test):

Comparisons for factor: **Medium**

Comparison	**Diff of Means**	**t**	**P**	**P<0.050**
FaSSGF vs. SIF	111.726	35.323	<0.001	Yes
FaSSGF vs. SGF	70.507	22.291	<0.001	Yes
FaSSGF vs. acetate	69.086	21.842	<0.001	Yes
FaSSGF vs. FaSSIF-V2	42.065	13.299	<0.001	Yes
FaSSIF-V2 vs. SIF	69.661	22.024	<0.001	Yes
FaSSIF-V2 vs. SGF	28.442	8.992	<0.001	Yes
FaSSIF-V2 vs. acetate	27.021	8.543	<0.001	Yes
acetate vs. SIF	42.640	13.481	<0.001	Yes
acetate vs. SGF	1.422	0.449	1.000	No
SGF vs. SIF	41.218	13.031	<0.001	Yes

Comparisons for factor: **Formulation**

Comparison	**Diff of Means**	**t**	**P**	**P<0.050**
CBZ-SACumax- vs. CBZ-SACss-MC	105.947	24.433	<0.001	Yes
CBZ-SACumax- vs. CBZ-NIC-MCC	105.643	24.363	<0.001	Yes
CBZ-SACumax-MCC vs. CBZ-MCC	59.246	13.663	<0.001	Yes
CBZ-MCC vs. CBZ-SACss-MCC	46.701	10.770	<0.001	Yes
CBZ-MCC vs. CBZ-NIC-MCC	46.396	10.700	<0.001	Yes
CBZ-NIC-MCC vs. CBZ-SACss-MCC	0.305	0.0702	1.000	No

Comparisons for factor: **Formulation within SGF**

Comparison	**Diff of Means**	**t**	**P**	**P<0.05**
CBZ-SACumax- vs. CBZ-NIC-MCC	157.825	17.191	<0.001	Yes
CBZ-SACumax- vs. CBZ-SACss-MC	133.865	14.582	<0.001	Yes
CBZ-SACumax-MCC vs. CBZ-MCC	115.123	12.540	<0.001	Yes
CBZ-MCC vs. CBZ-NIC-MCC	42.703	4.651	<0.001	Yes

CBZ-MCC vs. CBZ-SACss-MCC	18.742	2.042	0.301	No
CBZ-SACss-MCC vs. CBZ-NIC-MCC	23.960	2.610	0.084	No

Comparisons for factor: **Formulation within acetate**

Comparison	**Diff of Means**	**t**	**P**	**P<0.05**
CBZ-SACumax- vs. CBZ-NIC-MCC	80.212	8.737	<0.001	Yes
CBZ-SACumax- vs. CBZ-SACss-MC	41.188	4.487	<0.001	Yes
CBZ-SACumax-MCC vs. CBZ-MCC	36.913	4.021	0.002	Yes
CBZ-MCC vs. CBZ-NIC-MCC	43.299	4.716	<0.001	Yes
CBZ-MCC vs. CBZ-SACss-MCC	4.275	0.466	1.000	No
CBZ-SACss-MCC vs. CBZ-NIC-MCC	39.024	4.251	0.001	Yes

Comparisons for factor: **Formulation within SIF**

Comparison	**Diff of Means**	**t**	**P**	**P<0.05**
CBZ-SACumax-MCC vs. CBZ-MCC	56.581	6.163	<0.001	Yes
CBZ-SACumax- vs. CBZ-SACss-MC	46.049	5.016	<0.001	Yes
CBZ-SACumax- vs. CBZ-NIC-MCC	29.707	3.236	0.018	Yes
CBZ-NIC-MCC vs. CBZ-MCC	26.874	2.927	0.039	Yes
CBZ-NIC-MCC vs. CBZ-SACss-MCC	16.343	1.780	0.511	No
CBZ-SACss-MCC vs. CBZ-MCC	10.531	1.147	1.000	No

Comparisons for factor: **Formulation within FaSSGF**

Comparison	**Diff of Means**	**t**	**P**	**P<0.05**
CBZ-SACumax- vs. CBZ-SACss-MC	270.121	29.423	<0.001	Yes
CBZ-SACumax- vs. CBZ-NIC-MCC	209.276	22.796	<0.001	Yes
CBZ-SACumax-MCC vs. CBZ-MCC	50.770	5.530	<0.001	Yes
CBZ-MCC vs. CBZ-SACss-MCC	219.350	23.893	<0.001	Yes
CBZ-MCC vs. CBZ-NIC-MCC	158.506	17.266	<0.001	Yes
CBZ-NIC-MCC vs. CBZ-SACss-MCC	60.845	6.628	<0.001	Yes

Comparisons for factor: **Formulation within FaSSIF-V2**

Comparison	**Diff of Means**	**t**	**P**	**P<0.05**
CBZ-SACumax- vs. CBZ-NIC-MCC	51.193	5.576	<0.001	Yes
CBZ-SACumax- vs. CBZ-SACss-MC	38.512	4.195	0.001	Yes
CBZ-SACumax-MCC vs. CBZ-MCC	36.845	4.013	0.002	Yes
CBZ-MCC vs. CBZ-NIC-MCC	14.348	1.563	0.772	No
CBZ-MCC vs. CBZ-SACss-MCC	1.667	0.182	1.000	Do Not Test
CBZ-SACss-MCC vs. CBZ-NIC-MCC	12.681	1.381	1.000	Do Not Test

Comparisons for factor: **Medium within CBZ-MCC**

Comparison	**Diff of Means**	**t**	**P**	**P<0.05**
FaSSGF vs. SIF	216.994	25.682	<0.001	Yes
FaSSGF vs. SGF	165.698	19.611	<0.001	Yes
FaSSGF vs. acetate	148.192	17.539	<0.001	Yes
FaSSGF vs. FaSSIF-V2	129.044	15.273	<0.001	Yes
FaSSIF-V2 vs. SIF	87.950	10.409	<0.001	Yes
FaSSIF-V2 vs. SGF	36.654	4.338	0.001	Yes
FaSSIF-V2 vs. acetate	19.148	2.266	0.308	No
acetate vs. SIF	68.802	8.143	<0.001	Yes
acetate vs. SGF	17.506	2.072	0.469	No
SGF vs. SIF	51.296	6.071	<0.001	Yes

Comparisons for factor: **Medium within CBZ-NIC-MCC**

Comparison	**Diff of Means**	**t**	**P**	**P<0.05**
FaSSIF-V2 vs. SGF	65.009	7.694	<0.001	Yes
FaSSIF-V2 vs. acetate	48.099	5.693	<0.001	Yes
FaSSIF-V2 vs. SIF	46.728	5.530	<0.001	Yes

FaSSIF-V2 vs. FaSSGF	15.114	1.789	0.837	No
FaSSGF vs. SGF	49.895	5.905	<0.001	Yes
FaSSGF vs. acetate	32.985	3.904	0.005	Yes
FaSSGF vs. SIF	31.614	3.742	0.008	Yes
SIF vs. SGF	18.281	2.164	0.386	No
SIF vs. acetate	1.371	0.162	1.000	Do Not Test
acetate vs. SGF	16.910	2.001	0.544	Do Not Test

Comparisons for factor: **Medium within CBZ-SACss-MCC**

Comparison	**Diff of Means**	**t**	**P**	**P<0.05**
FaSSIF-V2 vs. FaSSGF	88.639	10.491	<0.001	Yes
FaSSIF-V2 vs. SIF	75.751	8.965	<0.001	Yes
FaSSIF-V2 vs. SGF	53.730	6.359	<0.001	Yes
FaSSIF-V2 vs. acetate	21.756	2.575	0.152	No
acetate vs. FaSSGF	66.883	7.916	<0.001	Yes
acetate vs. SIF	53.995	6.391	<0.001	Yes
acetate vs. SGF	31.974	3.784	0.007	Yes
SGF vs. FaSSGF	34.910	4.132	0.003	Yes
SGF vs. SIF	22.022	2.606	0.141	No
SIF vs. FaSSGF	12.888	1.525	1.000	No

Comparisons for factor: **Medium within CBZ-SACumax-MCC**

Comparison	**Diff of Means**	**t**	**P**	**P<0.05**
FaSSGF vs. SIF	211.183	24.994	<0.001	Yes
FaSSGF vs. acetate	162.049	19.179	<0.001	Yes
FaSSGF vs. FaSSIF-V2	142.969	16.921	<0.001	Yes
FaSSGF vs. SGF	101.346	11.995	<0.001	Yes
SGF vs. SIF	109.837	13.000	<0.001	Yes
SGF vs. acetate	60.703	7.184	<0.001	Yes

SGF vs. FaSSIF-V2	41.624	4.926	<0.001	Yes
FaSSIF-V2 vs. SIF	68.214	8.073	<0.001	Yes
FaSSIF-V2 vs. acetate	19.080	2.258	0.314	No
acetate vs. SIF	49.134	5.815	<0.001	Yes

A result of "Do Not Test" occurs for a comparison when no significant difference is found between two means that enclose that comparison. For example, if you had four means sorted in order, and found no difference between means 4 vs. 2, then you would not test 4 vs. 3 and 3 vs. 2, but still test 4 vs. 1 and 3 vs. 1 (4 vs. 3 and 3 vs. 2 are enclosed by 4 vs. 2: 4 3 2 1). Note that not testing the enclosed means is a procedural rule, and a result of Do Not Test should be treated as if there is no significant difference between the means, even though one may appear to exist.

Appendix 8

Two Way Repeated Measures ANOVA (Two Factor Repetition) Wednesday, December 14, 2011, 12:26:08

Data source: Data 1 in Notebook3

Balanced Design

Dependent Variable: solubility

Normality Test (Shapiro-Wilk) Failed (P < 0.050)

Equal Variance Test: Passed (P = 0.278)

Source of Variation	DF	SS	MS	F	P
Sample no	2	6359.718	3179.859		
medium	4	11906067.398	2976516.850	2428.842	<0.001
medium x Sample no	8	9803.905	1225.488		
formulation	4	1038696.570	259674.142	150.404	<0.001
formulation x Sample no	8	13812.065	1726.508		
medium x formulation	16	2036485.716	127280.357	134.450	<0.001
Residual	32	30293.496	946.672		
Total	74	15041518.868	203263.768		

Main effects cannot be properly interpreted if significant interaction is determined. This is because the size of a factor's effect depends upon the level of the other factor.

The effect of different levels of medium depends on what level of formulation is present. There is a statistically significant interaction between medium and formulation. (P = <0.001)

Power of performed test with alpha = 0.0500: for medium : 1.000

Power of performed test with alpha = 0.0500: for formulation : 1.000

Power of performed test with alpha = 0.0500: for medium x formulation : 1.000

Least square means for medium :

Group	Mean
SGF	1.280
acetate	8.998
SIF	960.147
FaSSGF	1.864
FaSSIF-V2	610.675

Std Err of LS Mean = 9.039

Least square means for formulation :

Group	Mean
IND [sigma]	188.938
IND-NICss	526.766
IND-SACss	299.159
IND-SACumax	227.677
IND-SACsd	340.425

Std Err of LS Mean = 10.728

Least square means for medium x formulation :

Group	Mean
SGF x IND [sigma]	0.243
SGF x IND-NICss	1.414
SGF x IND-SACss	1.205
SGF x IND-SACumax	1.132
SGF x IND-SACsd	2.404
acetate x IND [sigma]	5.617
acetate x IND-NICss	9.361
acetate x IND-SACss	12.243

acetate x IND-SACumax	8.041
acetate x IND-SACsd	9.728
SIF x IND [sigma]	541.767
SIF x IND-NICss	1545.749
SIF x IND-SACss	903.582
SIF x IND-SACumax	582.657
SIF x IND-SACsd	1226.982
FaSSGF x IND [sigma]	0.988
FaSSGF x IND-NICss	1.731
FaSSGF x IND-SACss	2.272
FaSSGF x IND-SACumax	2.374
FaSSGF x IND-SACsd	1.957
FaSSIF-V2 x IND [sigma]	396.073
FaSSIF-V2 x IND-NICss	1075.574
FaSSIF-V2 x IND-SACss	576.494
FaSSIF-V2 x IND-SACumax	544.182
FaSSIF-V2 x IND-SACsd	461.052

Std Err of LS Mean = 17.764

All Pairwise Multiple Comparison Procedures (Bonferroni t-test):

Comparisons for factor: **medium**

Comparison	**Diff of Means**	**t**	**P**	**P<0.050**
SIF vs. SGF	958.868	75.013	<0.001	Yes
SIF vs. FaSSGF	958.283	74.967	<0.001	Yes
SIF vs. acetate	951.149	74.409	<0.001	Yes
SIF vs. FaSSIF-V2	349.472	27.339	<0.001	Yes
FaSSIF-V2 vs. SGF	609.395	47.673	<0.001	Yes
FaSSIF-V2 vs. FaSSGF	608.811	47.628	<0.001	Yes
FaSSIF-V2 vs. acetate	601.677	47.069	<0.001	Yes
acetate vs. SGF	7.718	0.604	1.000	No

acetate vs. FaSSGF	7.134	0.558	1.000	Do Not Test
FaSSGF vs. SGF	0.585	0.0457	1.000	Do Not Test

Comparisons for factor: **formulation**

Comparison	**Diff of Means**	**t**	**P**	**P<0.050**
IND-NICss vs. IND [sigma]	337.828	22.266	<0.001	Yes
IND-NICss vs. IND-SACumax	299.089	19.713	<0.001	Yes
IND-NICss vs. IND-SACss	227.607	15.001	<0.001	Yes
IND-NICss vs. IND-SACsd	186.341	12.282	<0.001	Yes
IND-SACsd vs. IND [sigma]	151.487	9.984	<0.001	Yes
IND-SACsd vs. IND-SACumax	112.748	7.431	<0.001	Yes
IND-SACsd vs. IND-SACss	41.266	2.720	0.263	No
IND-SACss vs. IND [sigma]	110.222	7.265	<0.001	Yes
IND-SACss vs. IND-SACumax	71.482	4.711	0.015	Yes
IND-SACumax vs. IND [sigma]	38.739	2.553	0.340	No

Comparisons for factor: **formulation within SGF**

Comparison	**Diff of Means**	**t**	**P**	**P<0.05**
IND-SACsd vs. IND [sigma]	2.161	0.0797	1.000	No
IND-SACsd vs. IND-SACumax	1.272	0.0469	1.000	Do Not Test
IND-SACsd vs. IND-SACss	1.199	0.0442	1.000	Do Not Test
IND-SACsd vs. IND-NICss	0.990	0.0365	1.000	Do Not Test
IND-NICss vs. IND [sigma]	1.171	0.0432	1.000	Do Not Test
IND-NICss vs. IND-SACumax	0.282	0.0104	1.000	Do Not Test
IND-NICss vs. IND-SACss	0.209	0.00773	1.000	Do Not Test
IND-SACss vs. IND [sigma]	0.962	0.0355	1.000	Do Not Test
IND-SACss vs. IND-SACumax	0.0723	0.00267	1.000	Do Not Test
IND-SACumax vs. IND [sigma]	0.889	0.0328	1.000	Do Not Test

Comparisons for factor: **formulation within acetate**

Comparison	Diff of Means	t	P	P<0.05
IND-SACss vs. IND [sigma]	6.625	0.244	1.000	No
IND-SACss vs. IND-SACumax	4.202	0.155	1.000	Do Not Test
IND-SACss vs. IND-NICss	2.882	0.106	1.000	Do Not Test
IND-SACss vs. IND-SACsd	2.515	0.0928	1.000	Do Not Test
IND-SACsd vs. IND [sigma]	4.110	0.152	1.000	Do Not Test
IND-SACsd vs. IND-SACumax	1.687	0.0622	1.000	Do Not Test
IND-SACsd vs. IND-NICss	0.367	0.0135	1.000	Do Not Test
IND-NICss vs. IND [sigma]	3.743	0.138	1.000	Do Not Test
IND-NICss vs. IND-SACumax	1.320	0.0487	1.000	Do Not Test
IND-SACumax vs. IND [sigma]	2.423	0.0894	1.000	Do Not Test

Comparisons for factor: **formulation within SIF**

Comparison	Diff of Means	t	P	P<0.05
IND-NICss vs. IND [sigma]	1003.983	37.030	<0.001	Yes
IND-NICss vs. IND-SACumax	963.093	35.522	<0.001	Yes
IND-NICss vs. IND-SACss	642.168	23.685	<0.001	Yes
IND-NICss vs. IND-SACsd	318.767	11.757	<0.001	Yes
IND-SACsd vs. IND [sigma]	685.216	25.273	<0.001	Yes
IND-SACsd vs. IND-SACumax	644.326	23.765	<0.001	Yes
IND-SACsd vs. IND-SACss	323.401	11.928	<0.001	Yes
IND-SACss vs. IND [sigma]	361.815	13.345	<0.001	Yes
IND-SACss vs. IND-SACumax	320.925	11.837	<0.001	Yes
IND-SACumax vs. IND [sigma]	40.890	1.508	1.000	No

Comparisons for factor: **formulation within FaSSGF**

Comparison	Diff of Means	t	P	P<0.05

IND-SACumax vs. IND [sigma]	1.386	0.0511	1.000	No
IND-SACumax vs. IND-NICss	0.643	0.0237	1.000	Do Not Test
IND-SACumax vs. IND-SACsd	0.416	0.0154	1.000	Do Not Test
IND-SACumax vs. IND-SACss	0.101	0.00374	1.000	Do Not Test
IND-SACss vs. IND [sigma]	1.285	0.0474	1.000	Do Not Test
IND-SACss vs. IND-NICss	0.542	0.0200	1.000	Do Not Test
IND-SACss vs. IND-SACsd	0.315	0.0116	1.000	Do Not Test
IND-SACsd vs. IND [sigma]	0.970	0.0358	1.000	Do Not Test
IND-SACsd vs. IND-NICss	0.227	0.00836	1.000	Do Not Test
IND-NICss vs. IND [sigma]	0.743	0.0274	1.000	Do Not Test

Comparisons for factor: **formulation within FaSSIF-V2**

Comparison	**Diff of Means**	**t**	**P**	**P<0.05**
IND-NICss vs. IND [sigma]	679.501	25.062	<0.001	Yes
IND-NICss vs. IND-SACsd	614.522	22.666	<0.001	Yes
IND-NICss vs. IND-SACumax	531.392	19.599	<0.001	Yes
IND-NICss vs. IND-SACss	499.079	18.408	<0.001	Yes
IND-SACss vs. IND [sigma]	180.421	6.655	<0.001	Yes
IND-SACss vs. IND-SACsd	115.442	4.258	0.001	Yes
IND-SACss vs. IND-SACumax	32.313	1.192	1.000	No
IND-SACumax vs. IND [sigma]	148.109	5.463	<0.001	Yes
IND-SACumax vs. IND-SACsd	83.130	3.066	0.040	Yes
IND-SACsd vs. IND [sigma]	64.979	2.397	0.217	No

Comparisons for factor: **medium within IND [sigma]**

Comparison	**Diff of Means**	**t**	**P**	**P<0.05**
SIF vs. SGF	541.524	20.948	<0.001	Yes
SIF vs. FaSSGF	540.779	20.919	<0.001	Yes
SIF vs. acetate	536.149	20.740	<0.001	Yes

SIF vs. FaSSIF-V2	145.694	5.636	<0.001	Yes
FaSSIF-V2 vs. SGF	395.830	15.312	<0.001	Yes
FaSSIF-V2 vs. FaSSGF	395.085	15.283	<0.001	Yes
FaSSIF-V2 vs. acetate	390.456	15.104	<0.001	Yes
acetate vs. SGF	5.374	0.208	1.000	No
acetate vs. FaSSGF	4.630	0.179	1.000	Do Not Test
FaSSGF vs. SGF	0.745	0.0288	1.000	Do Not Test

Comparisons for factor: **medium within IND-NICss**

Comparison	**Diff of Means**	**t**	**P**	**P<0.05**
SIF vs. SGF	1544.335	59.739	<0.001	Yes
SIF vs. FaSSGF	1544.019	59.727	<0.001	Yes
SIF vs. acetate	1536.389	59.432	<0.001	Yes
SIF vs. FaSSIF-V2	470.176	18.188	<0.001	Yes
FaSSIF-V2 vs. SGF	1074.160	41.551	<0.001	Yes
FaSSIF-V2 vs. FaSSGF	1073.843	41.539	<0.001	Yes
FaSSIF-V2 vs. acetate	1066.213	41.244	<0.001	Yes
acetate vs. SGF	7.947	0.307	1.000	No
acetate vs. FaSSGF	7.630	0.295	1.000	Do Not Test
FaSSGF vs. SGF	0.317	0.0122	1.000	Do Not Test

Comparisons for factor: **medium within IND-SACss**

Comparison	**Diff of Means**	**t**	**P**	**P<0.05**
SIF vs. SGF	902.377	34.906	<0.001	Yes
SIF vs. FaSSGF	901.309	34.865	<0.001	Yes
SIF vs. acetate	891.339	34.479	<0.001	Yes
SIF vs. FaSSIF-V2	327.087	12.653	<0.001	Yes
FaSSIF-V2 vs. SGF	575.290	22.254	<0.001	Yes
FaSSIF-V2 vs. FaSSGF	574.222	22.212	<0.001	Yes

FaSSIF-V2 vs. acetate	564.251	21.827	<0.001	Yes
acetate vs. SGF	11.038	0.427	1.000	No
acetate vs. FaSSGF	9.970	0.386	1.000	Do Not Test
FaSSGF vs. SGF	1.068	0.0413	1.000	Do Not Test

Comparisons for factor: **medium within IND-SACumax**

Comparison	**Diff of Means**	**t**	**P**	**P<0.05**
SIF vs. SGF	581.524	22.495	<0.001	Yes
SIF vs. FaSSGF	580.283	22.447	<0.001	Yes
SIF vs. acetate	574.616	22.228	<0.001	Yes
SIF vs. FaSSIF-V2	38.475	1.488	1.000	No
FaSSIF-V2 vs. SGF	543.049	21.007	<0.001	Yes
FaSSIF-V2 vs. FaSSGF	541.808	20.959	<0.001	Yes
FaSSIF-V2 vs. acetate	536.141	20.739	<0.001	Yes
acetate vs. SGF	6.909	0.267	1.000	No
acetate vs. FaSSGF	5.667	0.219	1.000	Do Not Test
FaSSGF vs. SGF	1.241	0.0480	1.000	Do Not Test

Comparisons for factor: **medium within IND-SACsd**

Comparison	**Diff of Means**	**t**	**P**	**P<0.05**
SIF vs. FaSSGF	1225.025	47.387	<0.001	Yes
SIF vs. SGF	1224.579	47.370	<0.001	Yes
SIF vs. acetate	1217.255	47.087	<0.001	Yes
SIF vs. FaSSIF-V2	765.930	29.628	<0.001	Yes
FaSSIF-V2 vs. FaSSGF	459.095	17.759	<0.001	Yes
FaSSIF-V2 vs. SGF	458.648	17.742	<0.001	Yes
FaSSIF-V2 vs. acetate	451.324	17.458	<0.001	Yes
acetate vs. FaSSGF	7.770	0.301	1.000	No
acetate vs. SGF	7.324	0.283	1.000	Do Not Test

SGF vs. FaSSGF	0.447	0.0173	1.000	Do Not Test

A result of "Do Not Test" occurs for a comparison when no significant difference is found between two means that enclose that comparison. For example, if you had four means sorted in order, and found no difference between means 4 vs. 2, then you would not test 4 vs. 3 and 3 vs. 2, but still test 4 vs. 1 and 3 vs. 1 (4 vs. 3 and 3 vs. 2 are enclosed by 4 vs. 2: 4 3 2 1). Note that not testing the enclosed means is a procedural rule, and a result of Do Not Test should be treated as if there is no significant difference between the means, even though one may appear to exist.

Appendix 8

Table Analyzed	Data 1			
Two-way ANOVA				
Source of Variation	% of total variation	P value		
Column Factor	2.27	0.4546		
Row Factor	93.27	< 0.0001		
Source of Variation	P value summary	Significant?		
Column Factor	ns	No		
Row Factor	***	Yes		
Source of Variation	Df	Sum-of-squares	Mean square	F
Column Factor	5	895.1	179.0	1.022
Row Factor	2	36718	18359	104.8
Residual	10	1752	175.2	
Number of missing values	0			
Bonferroni posttests				
In vivo vs USP 1sim				
Row Factor	In vivo	USP 1sim	Difference	95% CI of diff.
Cmax [mg/L]	1.890	1.020	-0.8700	-72.52 to 70.78
Tmax [h]	15.90	8.400	-7.500	-79.15 to 64.15
AUC [mg/L.h]	134.8	83.99	-50.81	-122.5 to 20.84
Row Factor	Difference	t	P value	Summary
Cmax [mg/L]	-0.8700	0.04647	P > 0.05	ns
Tmax [h]	-7.500	0.4006	P > 0.05	ns
AUC [mg/L.h]	-50.81	2.714	P > 0.05	ns
In vivo vs SGF/SIFsim				
Row Factor	In vivo	SGF/SIFsim	Difference	95% CI of diff.
Cmax [mg/L]	1.890	1.120	-0.7700	-72.42 to 70.88
Tmax [h]	15.90	17.68	1.780	-69.87 to 73.43
AUC [mg/L.h]	134.8	95.15	-39.65	-111.3 to 32.00
Row Factor	Difference	t	P value	Summary
Cmax [mg/L]	-0.7700	0.04113	P > 0.05	ns
Tmax [h]	1.780	0.09508	P > 0.05	ns
AUC [mg/L.h]	-39.65	2.118	P > 0.05	ns

In vivo vs MGM/MIM-Isim

Row Factor	In vivo	MGM/MIM-Isim	Difference	95% CI of diff.
Cmax [mg/L]	1.890	0.9500	-0.9400	-72.59 to 70.71
Tmax [h]	15.90	16.83	0.9300	-70.72 to 72.58
AUC [mg/L.h]	134.8	81.98	-52.82	-124.5 to 18.83

Row Factor	Difference	t	P value	Summary
Cmax [mg/L]	-0.9400	0.05021	P > 0.05	ns
Tmax [h]	0.9300	0.04968	P > 0.05	ns
AUC [mg/L.h]	-52.82	2.821	P > 0.05	ns

In vivo vs MGM/MIM-IIsim

Row Factor	In vivo	MGM/MIM-IIsim	Difference	95% CI of diff.
Cmax [mg/L]	1.890	1.100	-0.7900	-72.44 to 70.86
Tmax [h]	15.90	16.82	0.9200	-70.73 to 72.57
AUC [mg/L.h]	134.8	94.10	-40.70	-112.4 to 30.95

Row Factor	Difference	t	P value	Summary
Cmax [mg/L]	-0.7900	0.04220	P > 0.05	ns
Tmax [h]	0.9200	0.04914	P > 0.05	ns
AUC [mg/L.h]	-40.70	2.174	P > 0.05	ns

In vivo vs FaSSGF/FaSSIF-V2sim

Row Factor	In vivo	FaSSGF/FaSSIF-V2sim	Difference	95% CI of diff.
Cmax [mg/L]	1.890	1.570	-0.3200	-71.97 to 71.33
Tmax [h]	15.90	10.96	-4.940	-76.59 to 66.71
AUC [mg/L.h]	134.8	127.9	-6.920	-78.57 to 64.73

Row Factor	Difference	t	P value	Summary
Cmax [mg/L]	-0.3200	0.01709	P > 0.05	ns
Tmax [h]	-4.940	0.2639	P > 0.05	ns
AUC [mg/L.h]	-6.920	0.3696	P > 0.05	ns